Universitat de Girona

Methylome profiling of B and T cells along multiple sclerosis disease progression: a pilot study

Naiara Celarain Sanz

Universitat de Girona

DOCTORAL THESIS

Methylome profiling of B and T cells along Multiple Sclerosis disease progression: A pilot study

Naiara Celarain Sanz

2023

Universitat de Girona

DOCTORAL THESIS

Methylome profiling of B and T cells along Multiple Sclerosis disease progression: A pilot study

Naiara Celarain Sanz

2023

Doctoral Programme in Molecular Biology, Biomedicine and Health

Supervised by:

Jordi Tomàs-Roig, Ph. D

Lluís Ramió i Torrentà, Ph. D, M.D.

Tutor:

Xavier Xifró Collsamata, Ph. D

Presented to obtain the PhD degree at the University of Girona

This Doctoral Thesis contains 13 Annexes:

Annex I, II, III, IV, V, VI, VII, VIII, IX, X, XI, XII, XIII

We should appreciate what we are able to do,
and not feel bad about what we haven´t done
- Tulku Thondup

There is nothing permanent
except change
- Heraclitus

ACKNOWLEDGMENT

Lejos queda aquel verano del año 2017, cuando Jordi y Ester, me hicisteis la entrevista para ser parte de un proyecto sobre metilación en Esclerosis Múltiple. Mucho ha llovido desde entonces, y ahora que esta etapa llega a su recta final, echo la mirada hacia atrás, y siento un profundo agradecimiento por haber escogido este camino, así como por todas las personas con las que me he encontrado en ella. Todas me han dado una ayuda inestimable, que llevaré siempre conmigo, y que me han ayudado a crecer.

Lo primero de todo, quería agradecer a mi director de tesis, Jordi, por haberme acompañado durante todos estos años en este viaje. Aunque no ha sido un camino fácil, me alegro de que te hayas quedado hasta el final, y que al mirar atrás, podamos sentirnos orgullosos de todo lo que hemos alcanzado. He aprendido muchísimo, no solo en el trabajo, sino también a nivel personal, y siempre estaré agradecida por la paciencia y empatía que mostraste en los momentos en los que emocionalmente más vulnerable me encontraba. A nivel profesional, me has enseñado la perseverancia, y la importancia de moverse de aquí para allá para establecer colaboraciones, algo inestimable para el futuro.

A mi co-director Lluís, gracias por tu apoyo y tu esfuerzo para que me sintiera parte del equipo durante estos años. Ha sido un placer haber tenido la oportunidad de ser parte de esta unidad, donde he aprendido una manera más cercana y personal de tratar a los pacientes. Ester, gracias por haberme ayudado con la parte de los miRNA, sobre todo al comienzo, cuando no sabía muy bien ni por dónde empezar a estudiarlos. Siempre te has mostrado predispuesta a ayudar con una sonrisa, y eso siempre se agradece. También quería agradecer a Xavier Xifró, mi tutor de la UdG, por su disposición de ayudarme si alguna vez he necesitado algo.

También quería agradecer a los demás miembros del grupo UNIEM, pues gran parte de la tesis no habría sido posible sin vuestra ayuda. Desde enfermería, Micky y Marina, siempre dispuestos a ayudar con la recogida de las muestras; Pepi, ayudando y organizando el reclutamiento de pacientes y voluntarios; la unidad de neuropsicólogos, Claudia, Judit y Jordi G., realizando los test cognitivos a los pacientes; los neurólogos Lluís, René, Gary y Héctor, que durante las visitas hicieron posible que los pacientes conocieran éste proyecto y accedieran a participar en él; María, por haber ayudado a rescatar una de las muestras llevándome al IGTP *in extremis*, y por la ayuda con los miRNAs; y también a Txell, aunque sólo pudimos coincidir en la última etapa del proyecto. También quería

agradecer a los pacientes de la unidad y a los voluntarios que accedieron a ser parte de este proyecto, pues sin vuestra voluntad altruista esta tesis no habría empezado siquiera.

También ha habido muchos profesionales de otros ámbitos y centros de investigación que con su ayuda y colaboración nos permitieron seguir adelante con el proyecto. María Buxó, gracias por tu ayuda durante el análisis estadístico de los resultados. La estadística puede ser una área intimidante, al menos para mí, y agradezco que respondieras a mis preguntas básicas con mucha paciencia. Dra. Eva Martínez Cáceres, gracias por habernos dado apoyo durante el procesamiento de las muestras de sangre. Nos dejaste un hueco en tu laboratorio, y siempre mostraste predisposición para que nuestra estancia en el IGTP fuera lo más cómoda posible. Dr. Marco Antonio Fernández y Gerard Requena, gracias por vuestro soporte y conocimiento durante la citometría y el sorting de las células. Sé que algunas de nuestras muestras fueron complicadas de procesar, y agradezco vuestra paciencia. Dr. Simon Heath, thank you for your invaluable support during the bioinformatic analysis of the sequencing results. Your knowledge have been essential for the completion of this doctoral thesis. Aida Valls y Dra. Carolina Sanz, gracias por vuestra ayuda durante todo el proceso de NanoString.

Ya en el labo, fueron muchas las personas que hicieron mi estancia en IDIBGI un lugar donde daba gusto ir a trabajar. Imma, mi gran compañera de ordenador durante tantos años, que me ha enseñado de lo que es esforzarse de verdad por aquello que deseas, y junto a Neus, Laia, Mireia, Mar, Alba, Isabel, Raquel, Vero, Paula, fue un placer estar junto a todas vosotras en nuestra U del fondo del laboratorio, cuando aun no sabíamos lo que era el covid. Tengo muy gratos recuerdos de aquellos años que aún ahora, me hacen sonreír. Adri y Marina, gracias por todas las conversaciones que me alegraron el día, fue un placer entrar en vuestro territorio y reconquistar la poyata nada vez que tenía que realizar un experimento. Albert y Ana, me alegro mucho de haberos conocido y de haber compartido parte del camino, aunque fue breve el tiempo que pudimos coincidir. Bet, Sara, Rocío, Gerard, gracias por hacer que mi estancia en el labo fuera más agradable y ameno. Rebecca, gracias por ser una de las pocas personas con las que pude hablar sobre nuestra pasión compartida de los videojuegos. Mel·lina, gracias por haberme ayudado con el HOMER. Y gracias también al resto de grupos de investigación y personal del IDIBGI con los que conviví todos éstos años, que de un modo u otro, han perfilado los recuerdos que tengo durante mi estancia allí.

También quería dar las gracias a las personas que fuera del ámbito del trabajo me apoyaron e hicieron que mi estancia en Girona fuera una de las mejores experiencias que he tenido en mi vida.

Pep, desde el fondo de mi corazón, gracias. Sé que no estaría aquí, siendo la persona que soy ahora, si no te hubiera conocido. Todo lo que he aprendido en este camino, todo lo que he experimentado, lo llevaré para siempre conmigo como un tesoro invaluable. Me has enseñado a crecer, y has sido el apoyo con el que he podido andar hasta donde estoy ahora. Aunque todo avanza, y todo cambia; mis recuerdos y mi aprendizaje perdurarán. Miriam, y a los demás parentesians, gracias por ser un grupo tan cálido y comprensivo, me he sentido como en casa desde el principio. Marien, siempre sonrío cuando veo las fotos de nuestros planes. Estos cinco años dan para mucho, y he perdido la cuenta de la cantidad de tazas y creps de chocolate que nos hemos comido. Mi estancia en Girona no habría sido lo mismo si no hubieras estado allí. Anna, tu vitalidad, actitud positiva, y tu alegría me han servido de apoyo cuando mi ánimo flaqueaba. Gerard, y a los demás miembros del club de Kendo Girona, gracias por vuestra amistad todos estos años, tanto dentro del dojo y como fuera de él. Ha sido un placer ir al entrenamiento con los ánimos bajos, y volver a casa renovada y con una sonrisa de oreja a oreja. Arigato gozaimasu.

Y por supuesto, nada de esto habría podido ser posible sin mi querida familia. Aita, Ama, y Oihane (nere lapasista!), gracias por haber estado siempre a mi lado, dándome todo el apoyo que podíais durante estos arduos años, escuchando mis frustraciones en las etapas más bajas, cuando la motivación era mínima y no sabía cómo acabaría todo; pero celebrando también cada pequeño avance como si fuera vuestro. Urte hauetan zehar, jakitea hor zeundetela, urruti fisikoki baina gertu aldi berean, lasaitasuna eman nau. Asko pozten naiz nere familia zaretelako. Bihotzez maite zaituztet. Nere lapasista maitiari, eskerrik asko nere ahizpatxita maitia izateagatik. Izeba Pili, tesi hau zuri ere dedikatu nahi dizut. Espero det nitaz harro sentitzea. Beti izango zaitut gogoan. Goian bego.

Eskerrik asko denoi.

ABBREVIATIONS

µL	Microliter
5-meC	5-methylcytosine
Ab	Antibody
Ag	Antigen
APC	Antigen presenting cell
Amp_Score	Amplification score
ASC	Antibody secreting cell
BAI	Indexed file for BAM
BAM	Binary alignment/map
BBB	Blood brain barrier
BCR	B cell receptor
BDNF	Brain derived neurotrophic factor
BED	Browser extensible data
Bmem	Memory B
bp	Base pair
cDNA	Complementary DNA
CH3	Methyl group
CI	Confidence interval
CIS	Clinically isolated syndrome
CGI	CpG island
CNS	Central nervous system
Cq	Quantification cycle
Cq_conf	Calculated confidence of the Cq value
Chr	Chromosome
CRISPR	Clustered regularly interspaced short palindromic repeats
CSF	Cerebrospinal fluid
CTCF	CCCTC-binding factor
CTDSPL	CTD Small Phosphatase Like
DC	Dendritic cell

DMF	Dimethyl fumarate
DMG	Differentially methylated gene
DMR	Differentially methylated region
DNA	Deoxyribonucleic acid
DNAme	DNA methylation
DNMT	DNA methyltransferase
DIT	Dissemination in time
DIS	Dissemination in space
EAE	Experimental autoimmune encephalomyelitis
EBV	Epstein-Barr virus
ECEL1	Endothelin converting enzyme like 1
ECEL1P2	Endothelin converting enzyme like 1 pseudogene 2
ECM	Extracellular matrix
EDS	Electronic data sheet
EDSS	Expanded disability status scale
ER	Endoplasmic reticulum
ERV	Endogenous retrovirus
FBS	Fetal bovine serum
FC	Fold change
FDR	False discovery rate
GC	Germinal center
Gd+	Gadolinium-enhanced
GH	GeneHancer
GN	Global normalization
GO	Gene ontology
Hg38	Genome Reference Consortium Human Build 38
HLA	Human leukocyte antigen
HOMER	Hypergeometric optimization of motif enrichment
Hypo	Hypomethylated
Hyper	Hypermethylated

Ig	Immunoglobulin
IFN-γ	Interferon-gamma
IL	Interleukin
IL21R	Interleukin 21 Receptor
IP	Immunoprecipitation
IQR	Interquartile range
Kb	Kilobase
KEGG	Kyoto Encyclopedia of Genes and Genomes
LINE	Long-interspersed nuclear element
log_2FC	Fold change in logarithmic base 2
LTR	Long terminal repeat
MALDI-TOF	Matrix-assisted laser desorption/ionization-time of flight
MapQ	Mapping quality
MBD	Methyl-CpG binding domain
MBP	Myelin basic protein
MeDIP	Methylated DNA immunoprecipitation
MeDIP-seq	Methylated DNA immunoprecipitation followed by sequencing
MHC I	Class I major histocompatibility complex
MHC II	Class II major histocompatibility complex
miRNA	microRNA
mM	Millimolar
mL	Milliliters
MOG	Myelin oligodendrocyte glycoprotein
mRNA	Messenger RNA
MRI	Magnetic resonance imaging
MS	Multiple Sclerosis
MS-MLPA	Methylation-specific multiplex ligation-dependent probe amplification
MS-qPCR	Methylation-specific quantitative polymerase chain reaction
NANOS3	Nanos C2HC-type zinc finger 3
NAWM	Normal appearing white matter

NF-kB	Nuclear factor kappa B
ng	Nanogram
NGS	Next-generation sequencing
nL	Nanoliter
nM	Nanomolar
NMO	Neuromyelitis optica
NO	Nitric oxide
NOS	Nitric oxide synthases
NOS1	Nitric oxide synthase 1
non-LTR	non-long terminal repeat
OSBP2	Oxysterol Binding Protein 2
PBMC	Peripheral blood mononuclear cell
PBS	Phosphate-buffered saline
PCR	Polymerase chain reaction
PPMS	Primary-progressive multiple sclerosis
pre-miRNA	Precursor miRNA
pri-miRNA	Primary miRNA transcript
PTEN	Phosphatase and tensin homolog
PTGFR	Prostaglandin F2 Receptor
PTGFRN	Prostaglandin F2 Receptor Inhibitor
PGF2-α	Prostaglandin F2-alpha
Q1-Q3	First quartile-Third quartile
qPCR	Quantitative polymerase chain reaction
RE	Relative expression
Redox	Reduction-oxidation
rho	Spearman's test rho value
RISC	RNA-induced silencing complex
RNA	Ribonucleic acid
RISC	RNA-induced silencing complex
rpkm	Reads per kilobase per million
RRMS	Relapsing-remitting multiple sclerosis

ROS	Reactive oxygen species
RT	Room temperature
SAM	Sequence alignment/map
SFMC	Synovial fluid mononuclear cell
SINE	Small-interspersed nuclear element
SNP	Single nucleotide polymorphism
SOP	Standard operating procedure
SPMS	Secondary-progressive multiple sclerosis
SPSS	Statistical Package for the Social Sciences
STD	Standard
SVA	SINE-R-VNTR-Alu
Tc	Cytotoxic T
TCR	T cell receptor
TGF	Transforming growth factor
TET	Ten-eleven translocation
TLR	Toll-like receptors
Th	Helper T
THBS3-AS1	THBS3 antisense RNA 1
TMM	Trimmed mean of M-values
Treg	Regulatory T
TSS	Transcription start site
TTS	Transcription termination site
UPR	Unfolded protein response
UTR	Untranslated region
YY1	Ying yang 1

LIST OF FIGURES

Figure 1. Worldwide MS prevalence per 100,000 population in 2020…….……...10
Figure 2. Phenotypes of MS…….……12
Figure 3. Activation, maduration, and differentiation undergone by B cells…….……..14
Figure 4. Activation, maduration, and differentiation undergone by T cells…….……..16
Figure 5. Hypothetical molecular mechanisms involved in MS upon recognition of the MBP autoantigen…….……....18
Figure 6. Epigenetic mechanisms……..……....20
Figure 7. Methylation and demethylation of the cytosine nucleotide…….……..21
Figure 8. Biogenesis of miRNAs…….…….24
Figure 9. Gating strategy used for the isolation of memory B cells and regulatory T cells derived from whole peripheral blood…….36
Figure 10. Summary of the MeDIP protocol……....37
Figure 11. Flowchart of the sequencing and the bioinformatics analysis…….40
Figure 12. NanoString nCounter® Elements™ XT technology……...42
Figure 13. A Taqman® OpenArray™ plate…….….44
Figure 14. Flowchart followed during the differential expression analysis of miRNAs…….….46
Figure 15. Description of the DMRs determined in MS patients at the diagnosis (RRMS vs control) and at later stages of clinical course (SPMS vs RRMS) in memory B and regulatory T cells……..54
Figure 16. Number of common DMGs in memory B and regulatory T cells resulting from the comparison between controls, RRMS and SPMS patients..……...…56
Figure 17. Number of common differentially methylated miRNA genes in memory B and regulatory T cells resulting from the comparison between controls, RRMS and SPMS patients…..57
Figure 18. Candidate genes showing differential expression between RRMS patients and controls in memory B and regulatory T cells…….…….…….61
Figure 19. Description of the genomic location, methylation profile, and mRNA expression of *PTGFRN* in memory B cells of RRMS patients and controls. ……..……..……..…64
Figure 20. Description of the genomic location, methylation profile, and mRNA expression of *IL21R* in memory B cells of RRMS patients and controls. ……..……..…...66
Figure 21. Description of the genomic location, methylation profile, and mRNA expression of *OSBP2* in memory B cells of RRMS patients and controls…….……..68
Figure 22. Description of the genomic location, methylation profile, and mRNA expression of *NOS1* in memory B cells of RRMS patients and controls……70

Figure 23. Description of the genomic location, methylation profile, and mRNA expression of *ECEL1P2* in regulatory T cells of RRMS patients and controls. ……..……...73
Figure 24. Scatter plot and correlation coeficient between the Cq values of both replicates for all detectable miRNAs in memory B and regulatory T cells…….…….82
Figure 25. Candidate miRNAs showing differential expression between the groups of study in memory B cells…….…….83
Figure 26. Scatter plot and correlation coeficient between the relative expression of miR-181c-5p in memory B cells and the number of Gd+ lesions in RRMS patients……..……....85
Figure 27. Description of the genomic location, methylation profile, and relative expression of *MIR181C* in memory B cells of RRMS patients……..……..……...86
Figure 28. Description of the genomic location, methylation profile, and relative expression of *MIR29A* in memory B cells of MS patients……88
Figure 29. Description of the genomic location, methylation profile, and relative expression of *MIR26A1* in memory B cells of MS patients.……..…..90
Figure 30. Description of the genomic location, methylation profile, and relative expression of *MIR150* in memory B cells of MS patients. ……..92
Figure 31. Description of the genomic location, methylation profile, and relative expression of *MIR193A* in memory B cells of MS patients.…….93
Figure 32. Description of the genomic location, methylation profile, and relative expression of *MIR30D* in memory B cells of MS patients.……..94
Figure 33. Description of the genomic location, methylation profile, and relative expression of *MIR92B* in memory B cells of MS patients.…….…..96
Figure 34. Common predicted targets for miR-26a-5p, miR-29a-3p and miR-30d-3p…….98
Figure 35. KEGG pathway analysis for the dysregulated miRNAs……..99
Figure 36. Electrophoresis in an agarose gel (1.5%) of the sonicated DNA after 10 cycles of sonication in the Bioruptor® Pico instrument……..……150

LIST OF TABLES

Table 1. Methylation studies in MS…….…….26
Table 2. Summary of demographic, clinical, and radiological data collected from controls, RRMS patients, and SPMS patients…….……..51
Table 3. List of candidate genes selected for the transcriptome analysis by NanoString nCounter® Elements™ XT.……..58
Table 4. Location of the DMRs within the candidate gene sequence in memory B and regulatory T cells when comparing RRMS with their controls.……..59
Table 5. List of detected and undetected candidate genes in memory B and regulatory T cells when mRNA was studied using the NanoString nCounter® Elements™ XT.…….……60
Table 6. Differentially expressed candidate genes in memory B and regulatory T cells of RRMS vs controls…….…..61
Table 7. Biological mechanisms and pathways associated with *PTGFRN, IL21R, OSBP2, NOS1* and *ECEL1*……...62
Table 8. Distribution of the DMRs related to candidate miRNA genes in memory B cells……..…75
Table 9. Distribution of the DMRs related to candidate miRNA genes in regulatory T cells……...77
Table 10. Classification of candidate miRNAs based on their detectability among samples in memory B cells..……..…….……..80
Table 11. Classification of candidate miRNAs based on their detectability among samples in regulatory T cells.……...…….……...81
Table 12. Relative expression of candidate miRNAs showing significant differences between the groups of study in memory B cells...…….……84
Table 13. Number of predicted targets for the dysregulated candidate miRNAs based on miRDB and targetScan databases.……...97

TABLE OF CONTENTS

ACKNOWLEDGEMENTS ……i
ABBREVIATIONS……....v
LIST OF FIGURES ……...…….xi
LIST OF TABLES ……....…..xiii
SUMMARY …….…....1
RESUMEN ……...3
RESUM ……..5
1. INTRODUCTION ……8
1.1. MULTIPLE SCLEROSIS…….9
1.1.1. Introduction to multiple sclerosis…….…….…9
1.1.2. Epidemiology……10
1.1.3. Diagnostic criteria…….11
1.1.4. Clinical course……..11
1.1.5. Pathogenesis of MS……..12
1.1.5.1. Immune system……...……12
1.1.5.2. Immune system dysfunction in MS……...……16
1.1.6. Risk factors……...19
1.1.6.1. Genetic factors.……..……..19
1.1.6.2. Environmental factors……...……...19
1.2. EPIGENETIC MECHANISMS……..19
1.2.1. DNA methylation……..20
1.2.1.1. Mechanism of action……...…….20
1.2.1.2. Distribution of DNA methylation throughout the genome……..21
1.2.1.3. DNA methylation and miRNAs……...22
1.2.1.4. Contribution of DNA methylation to MS pathology……...25

2. HYPOTHESIS AND OBJECTIVES……...……...29
2.1. HYPOTHESIS……...……..30
2.2. OBJECTIVES…….……30

3. PATIENTS AND METHODS……..32
3.1. PATIENTS…….……..33
3.1.1. Design of the study……...……33
3.1.2. Recruitment of the subjects of the study…….……33

3.1.2.1. Criteria of inclusion and exclusion……..……...33
3.1.2.2. Ethical Statement…….……...33
3.1.3. Variables of study……34
3.2. METHODS……34
3.2.1. Collection of fresh whole peripheral blood…….……34
3.2.2. Flow citometry and cell sorting……...…35
3.2.3. DNA and RNA extraction……...….37
3.2.4. Immunoprecipitation of methylated DNA (MeDIP)……37
3.2.5. Next-generation sequencing and bioinformatics……...…38
3.2.6. Gene ontology, KEGG pathway and miRNA targets…….…..41
3.2.7. Transcriptome of candidate DMGs……..…….41
3.2.7.1. NanoString nCounter® Elements™ XT ……...…...41
3.2.7.1.a. Procedure……..41
3.2.7.1.b. Expression analysis of candidate genes……...43
3.2.7.2. Taqman® OpenArray™ Human Advanced microRNA panel……..…...43
3.2.7.2.a. Procedure……...…..44
3.2.7.2.b. Quality control and pre-processing of the amplification curves…….….45
3.2.7.2.c. Data normalization…….…..45
3.2.7.2.d. Expression analysis of candidate miRNAs……..46
3.3. STATISTICAL ANALYSIS……47
3.3.1. Genome wide methylation differences between the groups of study……...…47
3.3.2. Expression analysis of candidate genes……47
3.3.3. Expression analysis of candidate miRNAs……...47
3.3.4. Relation between methylation and expression of candidate genes……...47
3.3.5. Relation between methylation and expression of candidate miRNAs……..48
3.3.6. Relation between candidate genes expression and clinical, radiological and neuropsychological variables……..48
3.3.7. Relation between candidate miRNAs expression and clinical, radiological and neuropsychological variables……..48

4. RESULTS……..50
4.0. SUBJECTS OF STUDY…….....51
4.1. STUDY OF THE WHOLE GENOME METHYLOME PROFILE……52
4.1.1. Samples…….....52

4.1.2. Genome-wide methylation differences among the groups of study……..……..52
4.1.2.1. Description of differentially methylated regions……..…..52
4.1.2.2. Description of differentially methylated genes……..….55
4.1.3. Summary……..57
4.2. VALIDATION STUDY AT RNA LEVEL: CANDIDATE GENES……...…58
4.2.1. List of studied candidate genes…….58
4.2.2. Methylation profile of the candidate genes……..59
4.2.3. Transcriptome of candidate genes…….....……...59
4.2.3.1. Samples…….……..59
4.2.3.2. Performance of the NanoString nCounter® Elements™ XT…….…….60
4.2.3.3. Differential mRNA expression between RRMS patients and controls...60
4.2.3.4. Biological role and gene ontology analysis……62
4.2.4. Relation between mRNA expression and clinical, radiological, and neuropsychological variables in RRMS patients……62
4.2.5. Study of the methylation profile and mRNA expression in candidate genes…...62
4.2.5.1. PTGFRN……..63
4.2.5.2. IL21R…….…….65
4.2.5.3. OSBP2……...…..67
4.2.5.4. NOS1……..…….69
4.2.5.5. ECEL1P2……72
4.2.6. Summary……...74
4.3. VALIDATION STUDY AT RNA LEVEL: CANDIDATE miRNA GENES…..…..……74
4.3.1. List of studied candidate miRNAs……...……74
4.3.2. Methylation profile of the studied miRNA genes……..……...74
4.3.3. Transcriptome of candidate miRNA genes…….....……..80
4.3.3.1. Samples……...……80
4.3.3.2. Performance of the Taqman® OpenArray™ Human Advanced microRNA panel……..……..……..……..80
4.3.3.3. Quality control and pre-processing of the amplification curves…….81
4.3.3.4. Differential miRNA expression among the groups of study……..…….82
4.3.4. Relation between the relative expression of miRNA and the clinical, radiological, and neuropsychological variables in MS patients……..84
4.3.5. Study of the methylation profile and relative expression of candidate miRNA genes……..…….85
4.3.5.1. miR-181c-5p……..……..85

4.3.5.2. miR-29a-3p……..……...87
4.3.5.3. miR-26a-5p……..…..89
4.3.5.4. miR-150-5p…….……..……..91
4.3.5.5. miR-193a-5p…….……..92
4.3.5.6. miR-30d-3p…….……94
4.3.5.7. miR-92b-3p……..…95
4.3.6. miRNA targets and KEGG enrichment analysis……..97
4.3.7. Summary……..99

5. DISCUSSION……..……101
5.1. The importance of DNA methylation in MS…….……102
5.2. Genome-wide methylome profile of MS patients……103
5.3. Relation between DNA methylation and RNA expression in immune cells of MS patients and controls……105
5.3.1. At the onset of disease……106
5.3.2. Later stages of the disease……..110
5.4. Relation between miR-181c expression and Gd+ lesions in RRMS patients……...113
5.5. Future perspectives for (de)methylation therapies in MS……114
5.6. Limitations of study……..116

6. CONCLUSIONS…….…….……...119
7. REFERENCES…….……..122
8. ANNEX I. Protocol – Isolation of PBMCs from whole peripheral blood……..…….147
9. ANNEX II. Protocol – MeDIP……...……..……...149
10. ANNEX III. Script in R – Differential methylation analysis (MEDIPS).…….……157
11. ANNEX IV. Protocol – NanoString nCounter® Elements™ XT……..……...…….160
12. ANNEX V. Protocol - TaqMan® Advanced miRNA Assay and Taqman® Open Array™ Human Advanced microRNA panel…….……...……..162
13. ANNEX VI. Detailed demographic, clinical, radiological, and experimental data for each participant of the study…….167
14. ANNEX VII. List of studied mature miRNAs using the Taqman® OpenArray™ Human advanced microRNA panels…….…168
15. ANNEX VIII. Association analysis between Cq_conf, Amp_Score and Cq values in memory B cells.……...……..169
16. ANNEX IX. Association analysis between Cq_conf, Amp_Score and Cq values in regulatory T cells ……..170

17. ANNEX X. Candidate miRNAs showing differential expression between the groups of study in memory B cells_second replicate…….……...171
18. ANNEX XI. Correlation between the relative expression of miR-181c-5p in memory B cells and the number of Gd+ lesions in RRMS patients_second replicate…….....173
19. ANNEX XII. Association analysis between relative expression el miRNAs and the normalized methylation values in DMRs_second replicate.…….……....174
20. ANNEX XIII. List of miRNA targets common for miRDB and TargetScan databases…….…….…….175

SUMMARY

Multiple sclerosis (MS) is a chronic, inflammatory, autoimmune and neurodegenerative disease characterized by the infiltration of autoreactive immune cells (including B and T cells) into the central nervous system that leads to axonal damage, demyelination, and ultimately, neurodegeneration. MS is the most frequent cause of non-traumatic injury in young adults, and it is estimated that 2.8 million people worldwide have been diagnosed with MS.

The aetiology of MS is still unknown, but strong scientific evidence points to a complex interaction between genetic and environmental factors mediated by epigenetics. One of the most studied epigenetic mechanisms is the methylation of DNA, which consists of adding a methyl group to a naked cytosine. DNA methylation fulfils many vital functions like the regulation of gene expression or the silencing of transposable elements of the genome. Alterations in the DNA methylation profile have been associated with pathogenic events, including MS. Methylation studies in MS have been mainly focused on distinct tissues presenting cell heterogeneity, such as peripheral blood mononuclear cells. However, each cell population has a unique and distinctive DNA methylation pattern, which should be taken into consideration when studying the pathophysiology of the disease.

This doctoral thesis studies the complete methylome of two immune cells closely involved in MS, memory B cells and regulatory T cells. These two cell types were collected from the peripheral blood of MS patients at the diagnosis and progressive stages of the disease. The complete methylome of the DNA was obtained by the immunoprecipitation of the methylated DNA followed by high throughput sequencing. In addition, the transcriptome of genes showing methylation differences among the groups of study was analysed, and the transcriptome of differentially methylated genes encoding for microRNAs was also studied.

In summary, recently diagnosed MS patients displayed global DNA hypomethylation in both immune cells, while MS patients at later stages of the disease exhibited a remarkable global DNA hypermethylation. Among the differentially methylated genes studied, *PTGFRN, IL21R, NOS1, OSBP2*, and *MIR181C* showed changes at the RNA level in memory B cells at diagnosis, while *ECEL1P2* did so in regulatory T cells. At later stages of the disease, differential expression of *MIR29A, MIR30D, MIR26A1, MIR92B, MIR150* and *MIR193A* was

detected in memory B cells. Due to their neuroprotective role in MS, miR-29a, miR-30d and miR-26a qualify as promising candidates for future epigenetic interventions.

RESUMEN

La Esclerosis Múltiple (EM) es una enfermedad crónica, inflamatoria, neurodegenerativa, y de naturaleza autoinmune caracterizada por la infiltración de células inmunitarias autorreactivas (como las células B y T) en el sistema nervioso central que desencadenan daño axonal, desmielinización, y finalmente, neurodegeneración. La EM es la principal causa de discapacidad no-traumática entre la población joven, con un cómputo global de 2.8 millones de personas afectadas a nivel mundial.

A pesar de que la etiología de la EM es aún desconocida, fuertes indicios indican que se debe a una compleja interacción entre factores genéticos y ambientales mediados por la epigenética. Uno de los mecanismos epigenéticos más estudiados es la metilación de ADN, que consiste en la adición de un grupo metilo a una citosina. Este mecanismo epigenético interviene en múltiples funciones vitales como la regulación de la expresión génica o el silenciamiento de elementos transponibles del genoma. Alteraciones en el perfil de metilación del genoma han sido asociadas a procesos patogénicos, incluyendo la EM. La mayoría de los estudios de metilación realizados en EM se han centrado en tejidos con una población celular heterogénea, tales como las células mononucleares de sangre periférica. En la actualidad, hay evidencia científica que atribuye a cada población celular un perfil de metilación único y distintivo, hecho que debe tenerse en cuenta en el estudio patofisiológico de la enfermedad.

Esta tesis doctoral se ha centrado en el estudio del perfil completo de metilación del ADN de dos poblaciones celulares estrechamente implicadas en la EM, las células B de memoria y las células T reguladoras. Estos dos tipos celulares se han obtenido a partir de sangre periférica de pacientes recién diagnosticados y en estadíos progresivos de la enfermedad. Para la obtención del metiloma completo se ha utilizado la tecnología basada en la inmunoprecipitación del ADN metilado seguido de su secuenciación. En segunda instancia, se ha estudiado el transcriptoma de genes que muestran regiones diferencialmente metiladas entre los grupos de estudio. Además, se ha estudiado el transcriptoma de genes diferencialmente metilados que codifican para microRNAs.

En resumen, se ha encontrado que los pacientes recién diagnosticados muestran una hipometilación global del ADN en ambos tipos celulares, mientras que pacientes en estadíos progresivos muestran una marcada hipermetilación del ADN. Entre los genes diferencialmente metilados estudiados, *PTGFRN, IL21R, NOS1, OSBP2* y *MIR181C*

mostraron cambios significativos a nivel de ARN en células B de memoria en el momento del diagnóstico, mientras que *ECEL1P2* lo hizo en las células T reguladoras. En estadíos progresivos de la enfermedad, se observó una expresión diferencial de *MIR29A, MIR26A1, MIR150, MIR193A, MIR30D, y MIR92B* en las células B de memoria. Entre ellos, por su naturaleza neuroprotectora, miR-29a, miR-30d, y miR-26a se postulan como candidatos prometedores para futuras terapias epigenéticas.

RESUM

L'Esclerosi Múltiple (EM) és una malaltia crònica, inflamatòria, de naturalesa autoimmune caracteritzada per la infiltració de cèl·lules immunitàries autoreactives (com les cèl·lules B i T), que desencadenen dany axonal, desmielinització, i finalment, neurodegeneració. La EM és la principal causa de discapacitat no-traumàtica entre la població jove, amb un balanç global de 2.8 milions de persones afectades a nivell mundial.

A pesar que l'etiologia de la EM és encara desconeguda, forts indicis indiquen que es deu a una complexa interacció entre factors genètics i ambientals mediats per l'epigenètica. Un dels mecanismes epigenètics més estudiats és la metilació d'ADN, que consisteix en l'addició d'un grup metil a una citosina. Aquest mecanisme epigenètic intervé en múltiples funcions vitals com la regulació de l'expressió gènica o el silenciament d'elements retrotransposables del genoma. Alteracions en el perfil de metilació del genoma han estat associades a processos patogènics, incloent la EM. Els estudis de metilació realitzats en EM s'han centrat en teixits amb una població cel·lular heterogènia, com ara les cèl·lules mononuclears de sang perifèrica. En l'actualitat, hi ha evidència científica que atribueix a cada població cel·lular un perfil de metilació únic i distintiu, fet que ha de tenir-se en compte en l'estudi patofisiológic de la malaltia.

Aquesta tesi doctoral s'ha centrat en l'estudi del perfil complet de metilació de l'ADN de les cèl·lules B de memòria i les cèl·lules T reguladores. Aquests dos tipus cel·lulars s'han obtingut a partir de sang perifèrica de pacients recentment diagnoticats i en estadis progressius de la malaltia. Per a l'obtenció del metiloma complet s'ha utilitzat la tecnologia basada en la inmunoprecipitació de l'ADN metilat seguit per la seva seqüenciació. En segona instància, s'ha caracteritzat el transcriptoma de gens que mostren regions diferencialment metilades entre els diferents grups d'estudi. A més, s'ha estudiat el transcriptoma d'aquells gens diferencialment metilats que codifiquen per microRNAs.

En resum, els pacients recentment diagnosticats mostren una hipometilació global de l'ADN en els dos tipus cel·lulars, mentre que pacients en estadis més progressius mostren una marcada hipermetilació de l'ADN. Després d'analitzar el transcriptoma de gens diferencialment metilats, s'ha observat que a l'inici de la malaltia els pacients EM mostren canvis significatius a nivell d'RNA dels gens *PTGFRN, IL21R, NOS1, OSBP2* i *MIR181C* en les cèl·lules B de memòria, i de *ECEL1P2* en les cèl·lules T reguladores. En els pacients EM

en estadis progressius de la malaltia, en canvi, s'ha detectat una expressió diferencial dels gens *MIR29A, MIR26A1, MIR150, MIR193A, MIR30D,* i *MIR92B* en les cèl·lules B de memòria. Entre ells, per la seva naturalesa neuroprotectora, miR-29a, miR-30d, i miR-26a esdevenen prometedors candidats per a futures teràpies epigenètiques.

1. Introduction

1.1. MULTIPLE SCLEROSIS

1.1.1. Introduction to multiple sclerosis

Understanding how neurons develop, interact and function has a direct influence in the aetiology of neurological disorders. Neurons represent the dominant cell type in the central nervous system (CNS). With the assistance of glial cells, neurons form synapses that allow effective communication within the organism (Allen and Lyons, 2018). Oligodendrocytes are a class of glial cells responsible for producing large amounts of myelin that wrap axons contributing to the myelination process (Baumann and Dinh, 2001). The myelin sheath protects and insulates axons, enabling a rapid propagation of action potentials. Some types of lesions in the CNS resulted in axonal demyelination, causing severe neurological impairments (Filippi M., 2003; Waxman SG., 2006). Demyelination compromises the integrity of the myelin sheath, and consequently, impairs communication between the nervous system and the rest of the body (Love S., 2006).

Multiple sclerosis (MS) is a chronic, neurological, inflammatory, progressive and autoimmune disease of the CNS (Coles et al., 1999; Goldenberg MM., 2012) characterized by the infiltration of proinflammatory and autoreactive immune cells through the blood-brain barrier (BBB) into the CNS (Claudio et al., 1995; Kirk et al., 2003), causing demyelination (Lubetzki and Stankoff, 2014), axonal damage (Filippi M., 2003) and ultimately, death of the CNS neurons (Compston and Coles, 2008). MS is a disorder where inflammatory and neurodegenerative mechanisms converge to trigger a progressive neurodegeneration characterized by both physical and cognitive disability (Jongen et al., 2012; Kister et al., 2013).

MS is the most frequent cause of non-traumatic neurological disability in young adults in western countries (Compston and Confavreux, 2006). It is usually diagnosed between the ages of 20 and 40, causing great health, social and economic burden (Compston and Confavreux, 2006; Wallin et al., 2019). Patients with MS display a great variety of symptoms as a result of demyelinating lesions and neurodegeneration in different areas of the CNS (Pirko and Noseworthy, 2007). These dysfunctions comprise motor alterations, spasticity, paraesthesia, vision disturbances, loss of coordination and balance, urination disorders, sexual dysfunction, pain, fatigue, as well as cognitive and affective disorders (Levin MC., 2021).

Furthermore, patients with MS can also display comorbidities (Marrie RA., 2017) that might affect the diagnosis aggravating the disability and the quality of life (Marck et al., 2016; Marrie et al., 2015).

1.1.2. Epidemiology

There are approximately 2.8 million people worldwide affected with MS (Multiple Sclerosis International Federation – Atlas of MS – 3rd Edition, September 2020). The highest prevalence has been reported in North America, while Oceania exhibits the lowest number of cases (Figure 1). A total of 80 to 180 cases per 100,000 inhabitants have been reported in Spain (Perez-Carmona et al., 2019), and in particular, 9000 out of 55,000 Spanish cases are in Catalonia (MS Barometer, 2020; Multiple Sclerosis Foundation of Catalonia, retrieved from https://www.fem.es/es/). The prevalence of the disease has significantly risen in the last decades affecting especially women (Perez-Carmona et al., 2019), who have a two to three fold increased risk of developing MS (Harbo et al., 2013). Distance from equator (latitude) has also been correlated with incidence of MS, with the highest number of cases in areas located far from this latitude (Simpson et al., 2019) (Figure 1).

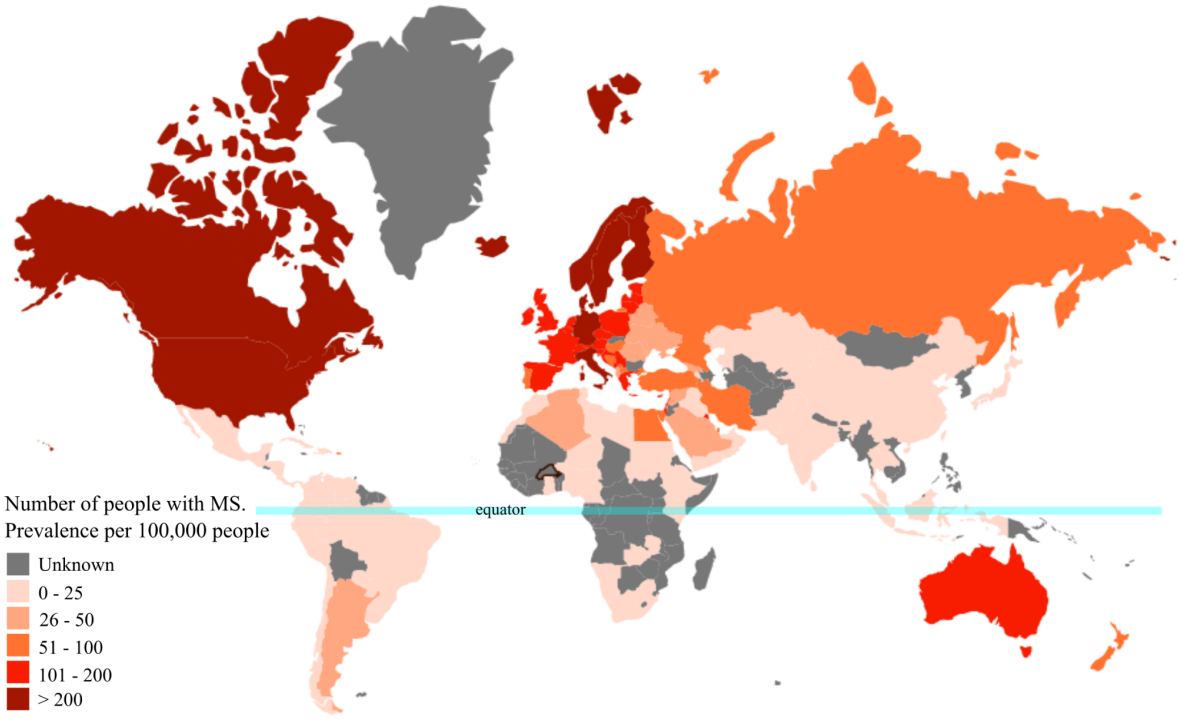

Figure 1. Worldwide MS prevalence per 100,000 population in 2020. The blue line represents the equator. Figure modified from Multiple Sclerosis International Federation – Atlas of MS, 3rd Edition, September 2020; retrieved from www.atlasofms.org. *MS: multiple sclerosis.*

1.1.3. Diagnostic criteria

In recent decades, the diagnostic criteria for MS have been based on the dissemination in space (DIS) and the dissemination in time (DIT) of CNS lesions. The first approximation was described by Allison and Millar (1953), and then revised by Poser (1983), who established common worldwide diagnostic criteria for the following 20 years. Later, Ian McDonald elaborated a newly updated diagnostic criteria for MS which has been subjected to three revisions since 2001. The last revision occurred in 2017 and included both the measurement of cerebrospinal fluid oligoclonal bands and cortical magnetic resonance imaging (MRI) lesions to determine DIS (Thompson et al., 2018).

1.1.4. Clinical course

MS can be classified into four different clinical phenotypes depending on the clinical activity and the progression of the disease (Lublin et al., 2014): clinically isolated syndrome (CIS), relapsing-remitting MS (RRMS), secondary-progressive MS (SPMS) and primary-progressive MS (PPMS) (Figure 2).

In about 85% of MS patients, the disease first manifests itself as a single clinical episode (CIS) characterized by inflammatory demyelinated lesions in the CNS with no signs of DIT. Patients diagnosed with CIS may eventually develop RRMS, which is the most common form of MS and is characterized by a relapsing phase (formation of new lesions) followed by a remitting phase (partial or total recovery of clinical manifestations), with no disease progression between the relapses. Among RRMS patients, around half of them convert to the SPMS phenotype within 10 to 20 years, showing an ongoing disability in the absence of clinical episodes. Lastly, 15% of MS patients develop the clinical form of PPMS, characterized by a progressive accumulation of disability right from the onset of disease, without any sign of recovery (Lublin et al., 2014).

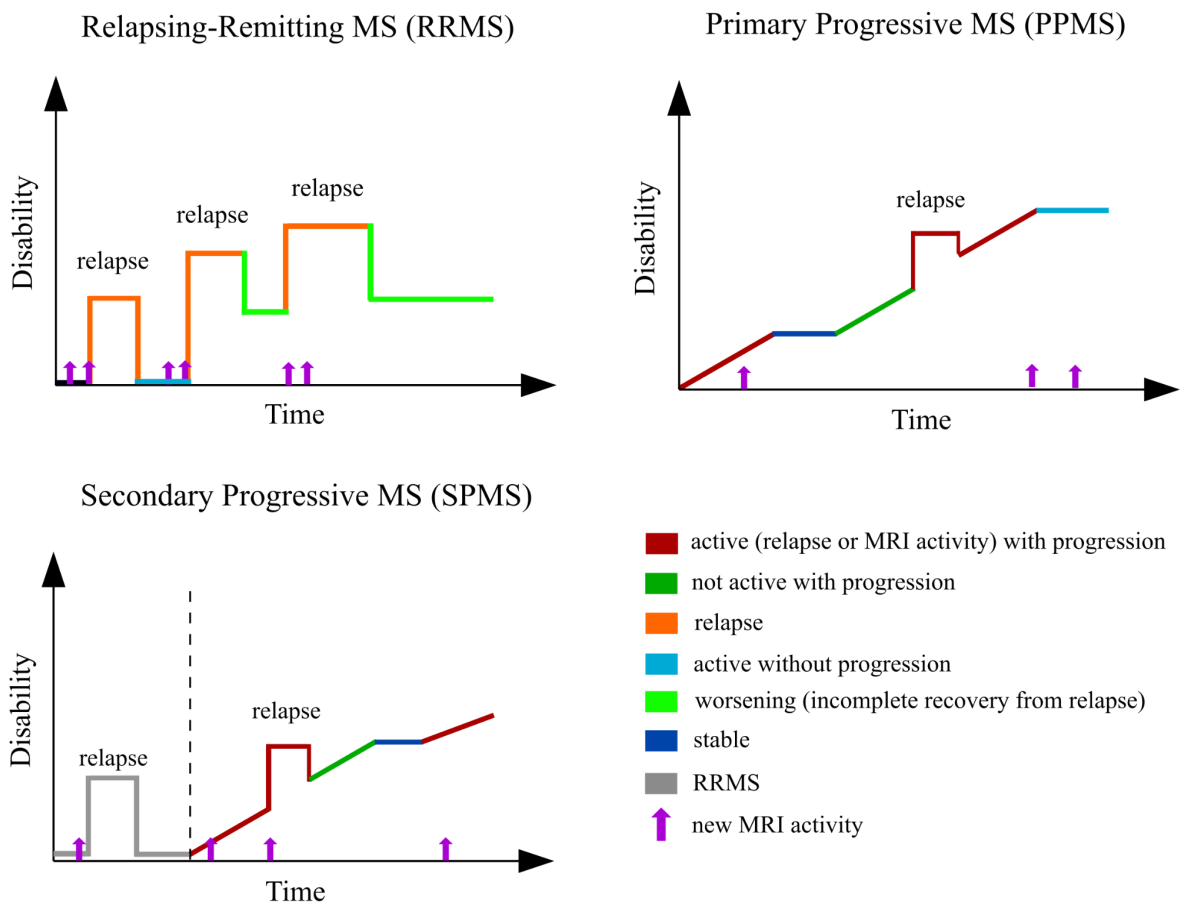

Figure 2. Phenotypes of MS. Figure modified from National Multiple Sclerosis Society, 2013; retrieved from: www.nationalmssociety.org. *MRI: magnetic resonance imaging; RRMS: relapsing-remitting multiple sclerosis.*

1.1.5. Pathogenesis of MS

Patients with MS display an over-stimulated inflammatory response along with cumulative neurodegeneration caused by demyelination, axonal damage, and death of CNS cells (Hauser and Oksenberg, 2006; Kutzelnigg et al. 2005; Sospedra and Martin, 2005; Wu and Alvarez, 2011). In all of these events, the immune system plays a key role (Sospedra and Martin, 2005).

1.1.5.1. Immune system

The immune system is a complex network composed of chemicals, proteins, white blood cells, tissues and organs that protects the organism from harmful substances and pathogens (Abbas et al., 2020). The CNS damage in MS is related with dysfunctions in immune-mediated processes including components of the innate and the adaptive immune system. Innate immunity is the first and non-specific immune response, while adaptive

immunity is a specific mechanism of defence that exponentially increases upon repeated exposure to an unchanging stimulus (Abbas et al., 2020).

The *innate immune system* is the first line of defence mediated by sentinel cells such as macrophages, dendritic cells and natural killer cells (Turvey and Broide, 2010). The innate immune response is mainly directed against microbial and viral pathogens (Turvey and Broide, 2010). All sentinel cells display toll-like receptors (TLRs) on their cell surface that recognize structurally-conserved pathogenic molecules known as antigens (El-Zayat et al. 2019). The immediate host immune response against specific molecular patterns promotes the release of cytokines and chemokines, which favours the recruitment of adaptive immune cells to the target site (Turvey and Broide, 2010).

The *adaptive immune system* is a highly specialized immune response responsible for long-term memory immunity (Netea et al., 2019). The adaptive immune system has two different mechanisms of action: cell-mediated immune response driven by T-lymphocytes, and humoral immune response mediated by B-lymphocytes (Chaplin DD., 2010). Chemokines and cytokines released by the innate system facilitate the migration of both T and B cells from circulating blood to the site of infection (Iwasaki and Medzhitov, 2015). Once they reach the target area, they induce cell-mediated lysis of target cells and promote antibody secretion.

B-lymphocytes or B cells are generated in the bone marrow and matured in germinal centres (GCs) of secondary lymphoid organs (i.e. lymph nodes, spleen) (Mauri and Bosma, 2012). The main role of B cells is to secrete antibodies that recognize specific antigens, but they can also serve as professional antigen presenting cells (APCs) (Cyster and Allen, 2019) together with dendritic cells and macrophages from the innate immune system. Naïve B cells have a B cell receptor (BCR) on the cell surface that recognizes a specific antigen (Yang and Reth, 2015). When an antigen is recognized by the BCR, it is internalized, processed and later presented on the cell surface via class II major histocompatibility complex (MHC II) molecules to CD4+ helper T cells (Barroso et al. 2015) (Figure 3). When a helper T (Th) cell recognizes the antigen/MHC II complex, it releases several cytokines that activate the B cells (Barroso et al. 2015). Activated B cells then travel to GCs to undergo proliferation, clonal expansion, somatic mutations, affinity maturation, and finally differentiation into two main cell types: plasma cells and memory B cells (Yam-Puc et al., 2018) (Figure 3). Plasma cells

are terminally differentiated antibody-secreting cells (ASCs) responsible for producing large amounts of antibodies similar to the BCR that has recognized the antigen (Nutt et al., 2015). Antibodies exert their effector functions by either blocking the ligand-receptor interaction, opsonizing antigens for macrophage-mediated phagocytosis or activating the complement system-induced inflammation (Yu et al., 2020). Memory B (Bmem) cells, on the other hand, are long-lived quiescent cell reservoirs that express specific immunoglobulin (Ig) molecules on their cell surface, contributing to a rapid and efficient immune response in case of antigen re-exposure. Once activated, Bmem cells re-enter the GCs to acquire the antibody secreting phenotype, differentiating into plasmablast and long-lived plasma cells (Kurosaki et al., 2015).

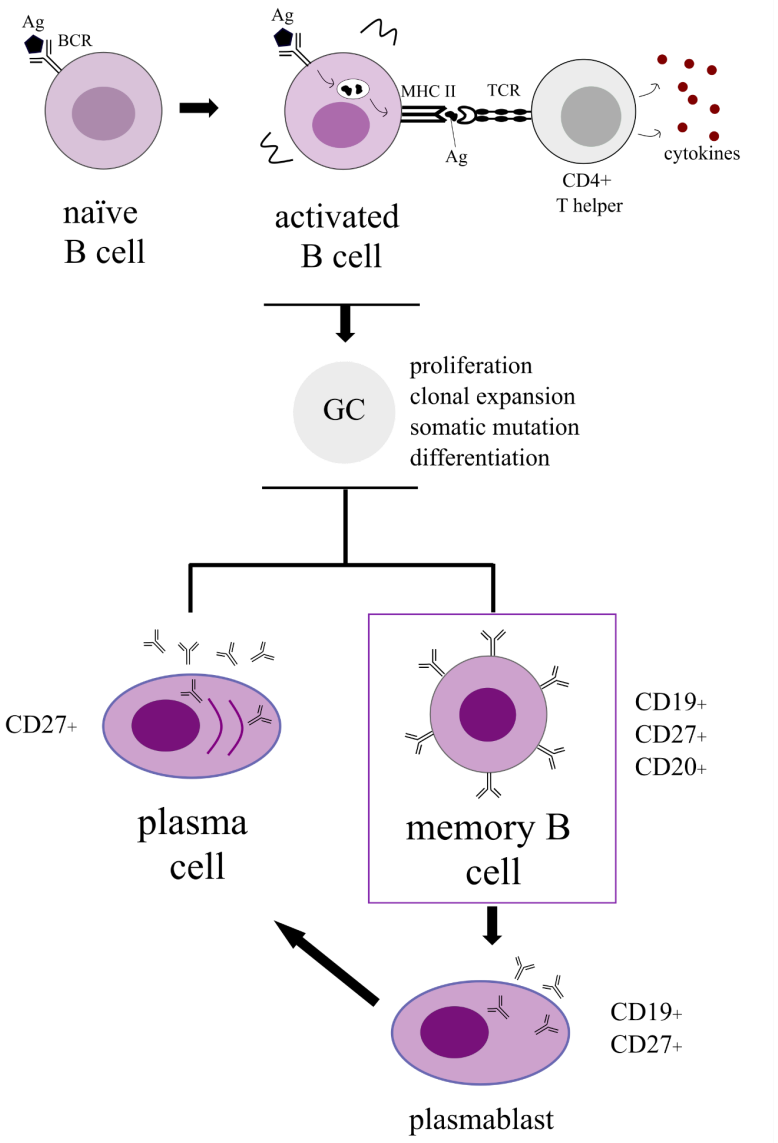

Figure 3. Activation, maturation, and differentiation undergone by B cells. Figure source: own elaboration. *Ag: antigen; BCR: B cell receptor; GC: germinal centre; MHC II: class II major histocompatibility complex; TCR: T cell receptor.*

T-lymphocytes or T cells originate in the bone marrow and mature in the thymus (Kumar et al., 2018). These cells have a T cell receptor (TCR) on their surface that recognizes a specific antigen displayed by the MHC II molecules of the APCs (Sundberg et al., 2007) (Figure 4). Once activated, T cells differentiate into three main cell types: CD4+ Th cells, CD8+ cytotoxic T (Tc) cells or regulatory T (Treg) cells (Figure 4). Once differentiated, they are released into the blood and lymphatic system, or remain in peripheral tissues in case of infection (Kumar et al., 2018). Each type of T cell has a different mechanism of action. Th cells release chemokines and cytokines into the target site stimulating the phagocytic function of macrophages, the secretion of antibodies by plasma B cells and the activation of Tc cells (Alberts et al., 2015). Tc cells recognize and release noxious cytokines to lyse the infected cells (Andersen et al., 2006). Treg cells, on the other hand, are regulatory agents responsible for maintaining immune homeostasis and peripheral tolerance (Vignali et al., 2008; Zozulya et al., 2008). The main mechanism of action of Treg cells is the release of inhibitory cytokines that suppress the deleterious activity of autoreactive immune cells (Figure 4). Furthermore, Treg cells can regulate the maturation and function of dendritic cells, and inhibit the macrophage-mediated inflammation by releasing granzymes and perforins that cause the cytolysis of APCs (Vignali et al., 2008) (Figure 4). Therefore, an imbalance in the number and activity of Treg cells might result in the development of autoimmune diseases (Sakaguchi et al., 2008; Schildknecht et al., 2009).

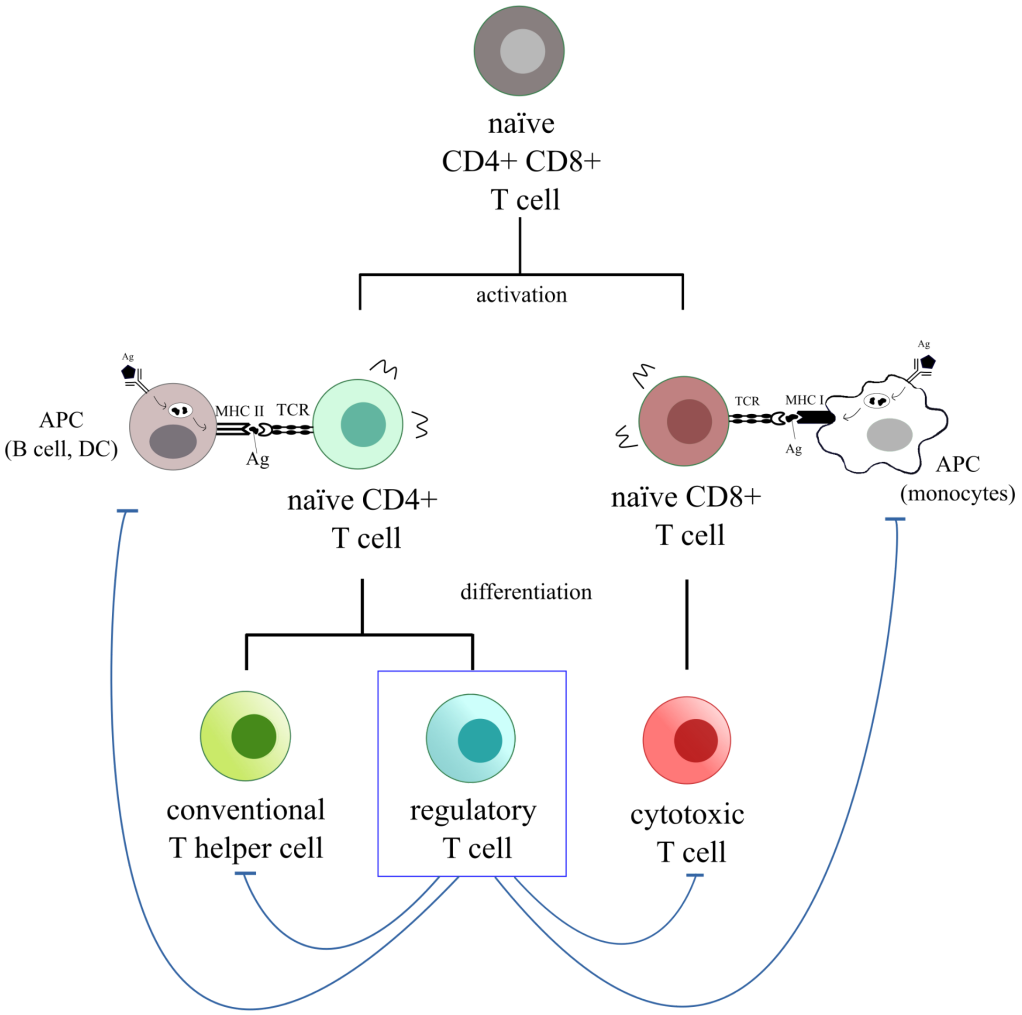

Figure 4. Activation, maturation, and differentiation undergone by T cells. The blunt end arrow coming from the regulatory T cell indicates a suppressive function. Figure source: own elaboration. *Ag: antigen; APC: antigen presenting cell; DC: dendritic cell; MHC I: class I major histocompatibility complex; MHC II: class II major histocompatibility complex; TCR: T cell receptor.*

1.1.5.2. Immune system dysfunctions in MS

Until recently, MS was considered a T cell-driven inflammatory disease; however, the success of immunomodulatory drugs targeting B cells (Baker et al., 2017) and the discovery of oligoclonal bands in the cerebrospinal fluid (CSF) of MS patients (Villar et al., 2005) have underpinned the importance of B cells in the development and progression of the disease. In recent years, it has been proposed that the interaction between B cells and T cells is what drives the development of the disorder (van Langelaar et al., 2020). Due to the autoimmune nature of the disease, it has been suggested that MS may be the consequence of autoreactive immune cells recognizing antigens of the body (autoantigens) and later attacking and destroying CNS tissues (Mirshafiey and Kianiaslani, 2013; Riedhammer and Weissert, 2015).

Several autoantigens have been suggested to trigger the autoimmune response. The main candidates are the myelin-related proteins, especially myelin basic protein (MBP) and myelin oligodendrocyte glycoprotein (MOG) (Riedhammer and Weissert, 2015). The hypothetical MS onset pathway involving MBP, which is widely supported by the bibliography, is described in Figure 5.

Abnormalities in the B and T cell populations have also been reported in MS. Autoreactive B cells of MS patients can cross back and forth between the CNS and the periphery passing through the BBB (von Büdingen et al., 2012). Moreover, aberrant lymphoid follicles resembling GC-like structures containing B, T and plasma cells have been found in the meninges of SPMS patients (Serafini et al., 2004). This suggests that autoreactive B cells might proliferate and differentiate within the CNS into resident autoreactive memory B and plasma cells, aggravating the course of the disease. Similarly, alterations in T cells including the Treg subset have also been described in MS. In contrast to healthy individuals, Treg cells from MS patients cannot properly cross the BBB (Danikowski et al., 2017), hindering their role as proinflammatory cell suppressors during the disease. Furthermore, Treg cells isolated from MS patients exhibit defective suppressive functions, as they are unable to inhibit both the proliferation of autoreactive effector T cells and the release of proinflammatory cytokines (Bell et al., 2020; Costantino et al., 2008).

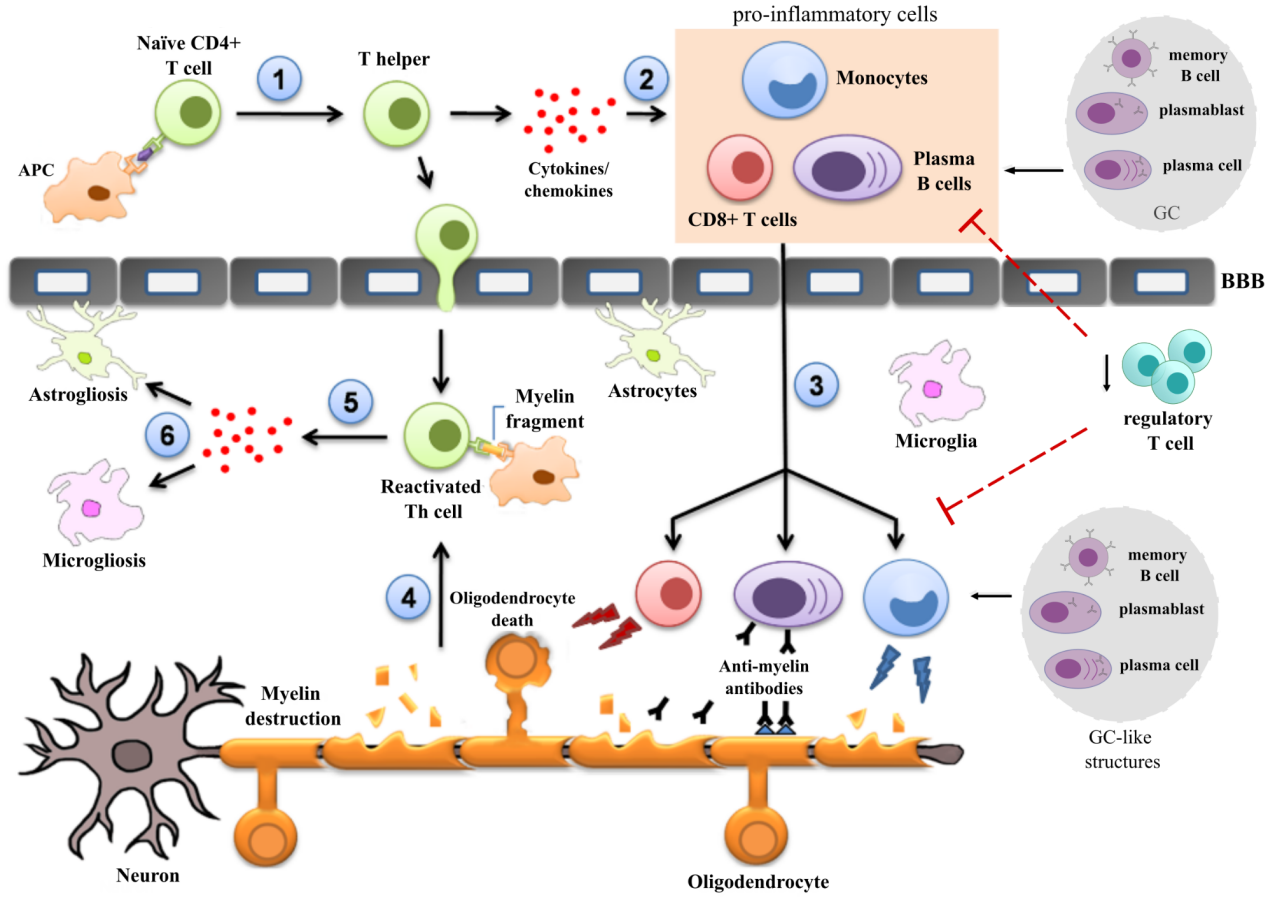

Figure 5. Hypothetical molecular mechanisms involved in MS upon recognition of the MBP autoantigen. **STEP 1.** Peripheral APCs (i.e. naïve B cells) recognize an antigen similar to the MBP and present it to autoreactive naïve CD4+ T cells via MHC II molecules. **STEP 2.** Activated naïve CD4+ T cells differentiate into Th cells, which participate in the production of chemokines that favours the recruitment of inflammatory cells such as CD8+ T cells, macrophages, and B cells to the target site. Activated naïve B cells, on the other hand, migrate to GCs to undergo differentiation into autoreactive plasma cells and memory B cells. Memory B cells remain as a reservoir of B cells, and are activated and differentiated to plasma cells upon re-exposure to the previously recognized autoantigen. Plasma cells secrete antibodies targeting the autoantigen. Abnormalities in the regulatory T cell population fail to suppress autoreactive cells, aggravating the inflammatory response and compromising the CNS homeostasis. **STEP 3.** Proinflammatory immune cells including B cells, T cells and monocytes enter the CNS through the BBB, exacerbating the inflammatory response. CD8+ T cells attack and destroy oligodendrocytes, causing neuronal death. B cells form ectopic GC-like structures within the CNS, where memory B cells are reactivated and differentiated into antibody secreting cells. Antibodies, in combination with the complement system, lead to myelin destruction and axonal damage. **STEP 4.** As a result of demyelination and axonal disruption, new fragments of myelin (autoantigen) are generated. **STEP 5**. APCs residing in the CNS present the autoantigen to autoreactive CD4+ Th cells promoting a feedback loop of inflammatory response. **STEP 6.** Chemokines released by reactivated CD4+ Th cells lead to astrogliosis and microgliosis aggravating the CNS neurodegeneration. Figure modified from Celarain and Tomas-Roig, 2020. *APC: antigen presenting cell; BBB: blood-brain barrier; CNS: central nervous system; GC: germinal centre; MBP: myelin basic protein; MHC: major histocompatibility complex; MS: multiple sclerosis; Th: helper T.*

1.1.6. Risk factors

MS is a complex disorder where genetic variants, environmental factors and epigenetic modifications are risk factors that contribute to the pathophysiology of the disease.

1.1.6.1. Genetic factors

Approximately 1% of the whole genome displays genetic variations between human populations (Shastry BS., 2002). Among them, single nucleotide polymorphism (SNP) comprises a variation in a single nucleotide that might lead to changes in the amino acid sequence, increasing the risk for developing diseases, including MS (Shastry BS., 2002; Wang and Moult, 2001). Indeed, there is strong evidence that the SNP HLA-DRB1*15:01, which is located in the human leukocyte antigen (HLA) locus that codifies for MHC II molecules (Oksenberg et al., 2008), increases susceptibility to MS by three fold (Ramagopalan et al., 2009; Simmonds and Gough, 2007).

1.1.6.2. Environmental factors

The existing literature points out key environmental factors related to MS. These include smoking, Epstein-Barr virus (EBV) infection, vitamin D deficiency and to a lesser extent, obesity, salt intake, gut microbiota, and exposure to long term stress (Ascherio and Munger, 2007; Celarain and Tomas-Roig, 2020; Olsson et al., 2016). All these factors can alter the methylation pattern of the genome (Fetahu et al., 2014; Godderis et al., 2012; Rawson et al., 2012; Robertson et al., 1995; Strickland et al., 2013; Zeilinger et al., 2013), enhancing both neuroinflammatory and neurodegenerative mechanisms associated with greater risk of MS (Al-Hajri and Del Bigio, 2010; Cepok et al., 2005; Inestrosa et al., 2014; Kitamura and Kasai, 2007; Sternberg et al., 2008; Quintana FJ., 2013).

1.2. EPIGENETIC MECHANISMS

Epigenetics can be defined as reversible modifications of the deoxyribonucleic acid (DNA) that does not involve an alteration of its sequence. Epigenetic mechanisms include DNA methylation (DNAme), microRNAs (miRNAs) and histone modifications (Figure 6) (Allis and Jenuwein, 2016; Yao et al., 2019). Herein, we have focused our efforts on understanding the contribution of DNAme to the pathophysiology of the disease.

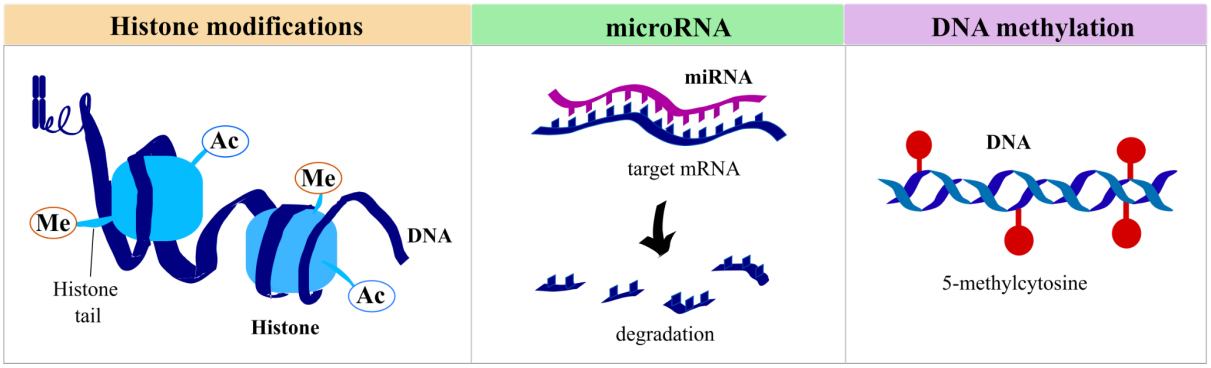

Figure 6. Epigenetic mechanisms. Figure source: own elaboration. *Me: methylation; Ac: acetylation; miRNA: microRNA.*

1.2.1. DNA methylation

DNAme is an epigenetic mark with an essential role in regulating gene expression (Razin and Cedar, 1991). It also has a major role in maintaining the homeostasis of the genome transcription keeping highly repetitive sequences and transposable elements silenced (Jansz N., 2019), allowing the inheritance of the genomic imprinting during replication and cell division (Elhamamsy AR., 2017), and along with other epigenetic mechanisms, acting as an intermediate between environmental stimulus and gene expression, allowing organisms to adapt to the environment (Celarain and Tomas-Roig, 2019; Law and Holland, 2019).

1.2.1.1. Mechanism of action

Methylation occurs when the family of DNA methyltransferases (DNMTs) adds a methyl group (-CH3) to the fifth carbon of a cytosine (Lyko F., 2017), creating the base 5-methylcytosine (5-meC) (Hotchkiss RD., 1948) (Figure 7). The 5-meC mark is recognized by proteins containing the methyl-CpG binding domain (MBD) (e.g. MeCP2) (Nan et al., 1993), which recruits repressor proteins through their transcription repressor domain. These repressor complexes interfere with the binding of the ribonucleic acid (RNA) polymerase II and transcription factors to the DNA, silencing gene expression (Nan et al., 1993). The maintenance of the methylation mark in the DNA is also regulated by the ten-eleven translocation (TET) family of proteins, which are responsible for the demethylation of the cytosines (Rasmussen and Helin, 2016) (Figure 7).

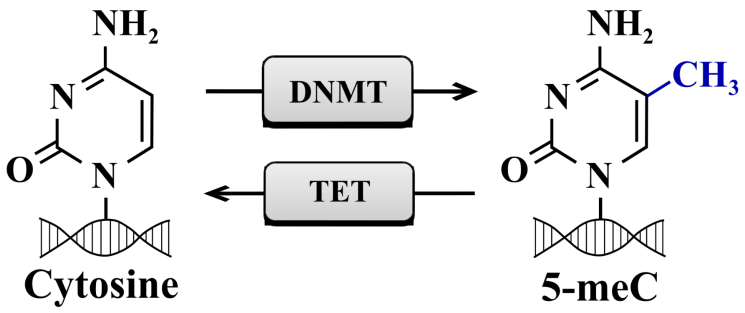

Figure 7. Methylation and demethylation of the cytosine nucleotide. Methylation of a naked cytosine mediated by DNMTs, creating the modified nucleotide 5-methylcytosine (5-meC). Demethylation is catalysed by the TET proteins. Figure modified from Celarain and Tomas-Roig, 2020. *DNMT: DNA methyltransferase; TET: ten-eleven-ten; 5-meC: 5-methylcytosine; CH3: methyl group.*

Methylation can also interact with histone modifications to regulate gene expression (Moore et al., 2012). Histones are proteins that, along with the DNA, form the nucleosome, the core structure where the DNA is packed in the nucleus of eukaryotes (Li et al., 2014). Histones can undergo covalent post-translational modifications like methylation in their N-terminal tail. These modifications change the way the DNA is compacted around the nucleosomes, facilitating or hindering the accessibility of the transcription machinery to it (Li et al., 2014). Tri-methylation of histone H3 lysine 4 (H3K4m3), for example, is considered a transcription activator mark (Li et al., 2014).

1.2.1.2. Distribution of DNA methylation throughout the genome

Methylation mainly occurs in cytosines that are followed by a guanine residue (CG dinucleotides) (Bird AP, 1986). CG dinucleotides are rare to find in the genome (BirdAP., 1986), except in small regions called CpG islands (CGIs) (Bird AP., 1986). CGIs are often located near promoter and regulatory regions (Deaton and Bird, 2011). In vertebrates, ~70-80% of the CG dinucleotides are methylated; while those located inside CGIs remain mainly unmethylated (Bird AP., 1986). Methylation can also occur in cytosines followed by thymine, adenine or another cytosine, but its exact mechanism is still not well understood (Jang et al., 2017). Intergenic regions, transposable elements and intragenic regions concentrate the majority of methylated cytosines distributed in the genome (Auclair and Weber, 2012).

When methylation occurs at the promoter, the first exon and the first intron, gene expression is downregulated (Anastasiadi et al., 2018; Ando et al., 2019; Brenet et al., 2011; Inoue and Oishi, 2005). However, methylation in the gene body has been associated with increased gene

expression in dividing cells (Aran et al., 2010; Yang et al., 2014). Although its exact function is still under study, some studies have reported that gene body methylation plays a role in splicing regulation (Gelfman et al., 2013; Maunakea et al., 2013; Neri et al., 2017). Additionally, methylation seems to act as a 'mark' to help distinguish between intron and exons, and between constitutive and alternative exons during splicing (Gelfman et al., 2013; Maunakea et al., 2013). Methylation recruits proteins like the CCCTC-binding factor (CTCF), which induce the blockage of RNA polymerase II and thus enable splicing (Shukla et al., 2011).

Enhancers are *cis*-regulatory regions outside the promoter region that stimulate gene expression by recruiting transcription factors and co-activator proteins in a cell type-specific manner (Ordoñez et al., 2019). Enhancers are usually located in the intergenic region (distal enhancers), sometimes several kilobases away from their target gene, and interact with the target promoter by chromatin looping (Whalen et al., 2016). Enhancers can also be located inside the gene region (intragenic enhancers), and they seem to function as alternative promoters (Kowalczyk et al., 2012). Methylation at enhancers has been associated with downregulation of their target genes (Aran et al., 2013), and aberrant methylation profiles have been found in diseases such as cancer (Heyn et al., 2016; Lin et al., 2020).

Transposable elements account for approximately 45% of the genome (Bannert and Kurth, 2004). They can be categorized as DNA transposons or retroelements (Bannert and Kurth, 2004). Retroelements are further divided in two categories: long terminal repeat (LTR) retrotransposons, which include endogenous retroviruses (ERVs); and non-long terminal repeat (non-LTR) retrotransposons, which include long-interspersed nuclear elements (LINEs), small-interspersed nuclear elements (SINEs) and the SINE-R-VNTR-Alu (SVAs) structural elements (Kojima KK., 2018; Ostertag et al., 2003). In somatic cells, methylation keeps the transposable elements repressed (Jansz N., 2019); however, their expression as a consequence of an aberrant methylation has been observed in diseases such as cancer (Kong et al., 2019) or autoimmune pathologies (Sukapan et al., 2014).

1.2.1.3. DNA methylation and miRNAs

Methylation regulates the transcription of DNA. Therefore, it can affect the expression of miRNAs (Glaich et al., 2019), which are small non-coding RNA molecules of approximately 20-24 nucleotides that block gene expression (Bartel DP., 2004). DNA sequence coding for

miRNAs is transcribed as a long primary miRNA transcript (pri-miRNA) in the nucleus (Figure 8). Pri-miRNAs comprise several kilobases with one or more hairpin structures of approximately 70 nucleotides. More than one mature miRNA can originate from a single pri-miRNA molecule (Bartel DP., 2004). The cleavage of the hairpin pri-miRNAs structures results in precursor miRNAs (pre-miRNAs) (Figure 8), which are transported from the nucleus to the cytoplasm through nuclear membrane pores (Lund et al., 2004), and then cleaved by Dicer (Bernstein et al., 2001) producing a double-stranded miRNA molecule of ~22 nucleotides (Figure 8). This double-stranded miRNA is incorporated into the RNA-induced silencing complex (RISC), which contains an Argonaute protein as a core component. The mature miRNA strand remains bound to the Argonaute protein, while the other strand is released and later degraded (Schwarz et al., 2003). Mature miRNA is guided by RISC to the 3' end of the target messenger RNA (mRNA) sequence, promoting its degradation (Bernstein et al., 2001) (Figure 8).

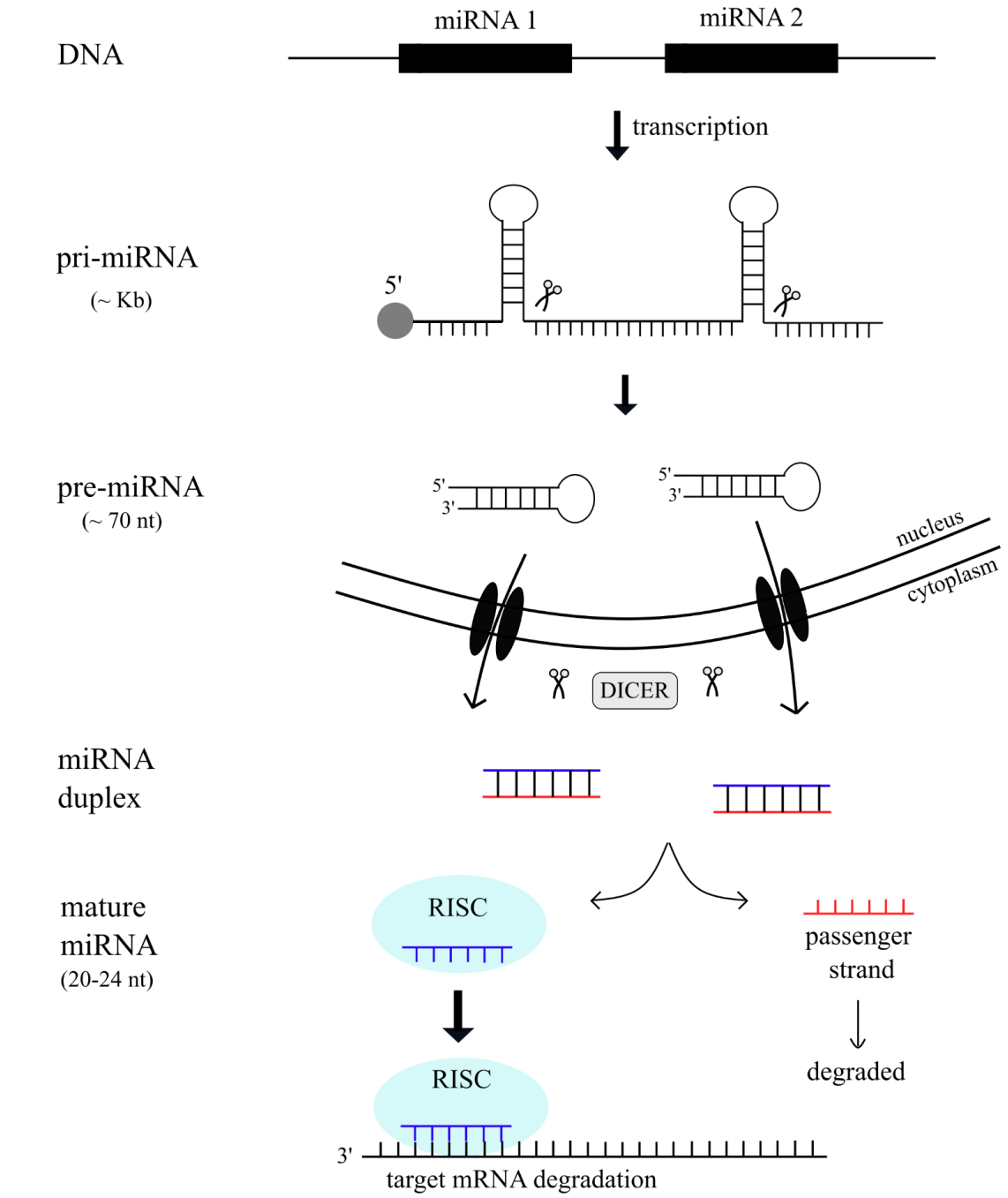

Figure 8. Biogenesis of miRNAs. Figure source: own elaboration. *DICER: dicer 1, ribonuclease III; kb: kilobase; miRNA: microRNA; mRNA: messenger RNA; nt: nucleotide; pre-miRNA: precursor miRNA; pri-miRNA: primary miRNA; RISC: RNA-induced silencing complex.*

miRNA genes can be categorized into two types: intergenic miRNAs and intragenic miRNAs. Intergenic miRNAs are located in the intergenic region of the genome far from other annotated genes, and have their own putative promoter. Their predicted transcription start site (TSS) is located in two regions: around -10 kilobases (kb) from the pre-miRNA

sequence and within the range -2 kb to +1 kb from the pre-miRNA sequence (Saini et al., 2007). Intragenic miRNAs, on the other hand, are embedded inside a host gene, and can be processed from either the exon or the intron of the host primary transcript (Lagos-Quintana M., 2003; Rodriguez A., 2004; Saini et al., 2007). Intragenic miRNAs usually share the promoter of their host gene, but they can also present their own putative promoter (Ozsolak et al., 2008). The majority of the predicted TSS for intronic miRNAs are located within the range of 4-6 kb upstream of the pre-miRNA sequence, in most cases coinciding with the annotated TSS of the host transcript (Saini et al., 2007).

miRNA genes can also be organized in clusters (Saini et al., 2007). Clustered miRNAs are co-transcribed together as a polycistronic primary transcript (Kabekkodu et al., 2018). Consequently, more than one pre-miRNA can be processed from the same transcript (Baskerville S., 2005). Adjacent miRNAs (<50 kb) are usually co-expressed (Baskerville S., 2005), and very few TSS locations have been predicted in the regions between the clustered miRNA (Saini et al., 2007), suggesting that they share the same promoter.

miRNA genes can also present different methylation patterns, ranging from high methylation levels upstream and downstream of the gene, to low levels or absence of methylation (Glaich et al., 2019). When a miRNA is embedded inside a CGI, its expression is silenced by methylation (Furuta et al., 2009); but when the miRNA is located outside a CGI, the outcome is unclear. In some cases, methylation contributes to gene silencing (Neves et al., 2010; Laddha et al., 2013); in other cases, methylation has been positively correlated with miRNA expression (Glaich et al., 2019; Nojima et al., 2016). Finally, methylation of enhancers related to miRNAs (Bell et al., 2016) can also modulate miRNA expression, showing the same inhibitory effect as methylation does at CGIs (Morales et al., 2017).

1.2.1.4. Contribution of DNA methylation to MS pathology

Methylation is essential for maintaining mammalian cell homeostasis (Weber and Schübeler, 2007). Alterations in the methylation status of certain genes have been reported to have a clear impact on human diseases (Jin and Liu, 2018). In MS, methylation changes have been described in normal appearing white matter (NAWM) (Huynh et al., 2014), demyelinated regions (Chomyk et al., 2017), cell-free plasma (Liggett et al., 2010), peripheral blood mononuclear cells (PBMCs) (Kulakova et al., 2016), and specific immune cells (Ewing et al.,

2019; Maltby et al., 2015). Table 1 shows the main studies on DNAme in MS published in the last two decades.

Table 1. Methylation studies in MS.

Author (year)	Groups of study	Tissue / cell	Method
Mastronardi et al., 2007	MS / Control	NAWM	Bisulphite / Sequencing
Ramagopalan et al., 2008	MS discordant twins	Whole blood	Bisulphite / sequencing
Baranzini et al., 2010	Twins (RRMS / Control)	CD4+ lymphocytes	Bisulphite / sequencing
Liggett et al., 2010	RRMS / Control	circulating cell-free DNA (plasma)	Restriction enzymes / array
Janson et al., 2010	RRMS / Control	CD4+ T (PBMCs / SFMCs)	Bisulphite / Sequencing
Kumagai et al., 2012	RRMS / SPMS / PPMS / Control	Buffy coat	Bisulphite / Sequencing
Graves et al., 2013	RRMS / Control	CD4+ T lymphocytes (CpG)	Bisulphite / array
Huynh et al., 2014	MS (CP/PP/SP) and non-neurological Control	Pathology-free brain regions (NAWM)	Bisulphite / Beadchip
Maltby et al., 2015	MS / Control	CD8+ lymphocytes	Bisulphite / array
Bos et al., 2015	RRMS / Control	Whole blood, CD4+T, CD8+T	Bisulphite / array
Kulakova et al., 2016	RRMS / PPMS / Control	PBMCs	Bisulphite / Beadchip
Lehman-Werman et al., 2016	RRMS / NMO / Control	Blood (ODG, cell-free DNA)	Bisulphite / Sequencing
Neven et al., 2016	MS / Control	Whole blood	Bisulphite / pirosequencing
Olsen et al., 2016	RRMS / Control	Brain, liver, spinal cord/Serum	Bisulphite / sequencing
Chomyk et al., 2017	MS // EAE	Myelinated / demyelinated hippocampus	Bisulphite / array
Marabita et al., 2017	MS smoker / non-smoker	PBMCs	Bisulphite / Beadchip
Wagner et al., 2017	RRMS / SPMS / Control	Peripheral blood	Bisulphite / melting profile
Dunaeva et al., 2017	RRMS / Control	cell-free DNA (serum)	Bisulphite / sequencing
Field et al., 2017	MS / Control	PBMCs / neural tissue	MALDI-TOF / Illumina Human Methylation 450 array
Ayuso et al., 2017	RRMS / Control	T cells	Bisulphite / sequencing
Sokratous et al., 2018	RRMS / Control	Whole Blood	MS-MLPA
Ruhrmann et al., 2018	RRMS / Control	CD4+ T cells	Infinium Human Methylation 450 array
Rhead et al., 2018	RRMS / Control	PBMCs	Bisulphite / Human Methylation 450 array

Maltby et al., 2018	RRMS / Control	CD19+ B cells	Bisulphite / Illumina Human Methylation 450 array
Souren et al., 2019	Discordant MS Twins	PBMCs / CD4+T cells	EPIC array / Bisulphite sequencing
Ewing et al., 2019	RRMS / SPMS / Control	CD4+ T cells / CD+ 8 T cells / CD19+ B cells / Monocytes	Infinium Human Methylation 450 array
Hosseini et al., 2020	RRMS / Control	CD4+ T cells	MS-qPCR
Buhelt et al., 2021	RRMS / Control	CD8+ T cells	Bisulphite / pirosequencing
Nourian et al., 2021	RRMS / Control	Whole blood	High Resolution Melting real-time PCR
Ma et al., 2021	MS / Control	CD4+ T cells / CD+ 8 T cells / CD19+ B cells/ Monocytes	Bisulphite/sequencing
Brorson et al., 2022	RRMS / Control	CD4+ and CD+ 8 T cells	Bisulphite / Human Methylation 450 array
Kiselev et al., 2022	RRMS / Control	CD4+ T cells / CD14+ monocytes	Infinium Human Methylation 450 array
Kular et al., 2022	MS / Control	NAWM	Infinium Methylation EPIC BeadChip

EAE: experimental autoimmune encephalomyelitis; MALDI-TOF: matrix-assisted laser desorption/ionization-time of flight; MS-MLPA: methylation-specific multiplex ligation-dependent probe amplification; MS-qPCR: methylation-specific quantitative polymerase chain reaction; NMO: neuromyelitis optica; ODG: oligodendroglia; PBMC: peripheral blood mononuclear cells; PPMS: primary-progressive multiple sclerosis; RRMS: relapsing-remitting multiple sclerosis; SFMC: synovial fluid mononuclear cells; SPMS: secondary-progressive multiple sclerosis.

As a result of these studies, aberrant methylation levels have been associated with the different pathophysiological phases of the disease: the BBB breakdown, exacerbated inflammatory response, demyelination of axons, remyelination failure and neurodegeneration (Celarain and Tomas-Roig, 2019; 2020). For example, hypermethylation of genes codifying for adhesion molecules could compromise BBB integrity (Dietrich JB., 2002; Huynh et al., 2014; Liggett et al., 2010; Ortiz et al., 2014); while aberrant methylation of genes involved in immune-mediated inflammatory processes may aggravate the course of the disease (Adhikari et al., 2017; Kumagai et al., 2012; Liggett et al., 2010; Sokratous et al., 2018; Yoshikawa et al., 2001). In a similar way, demethylation of genes implicated in the stability of the myelin sheath might enhance demyelination (Calabrese et al., 2011; Mastronardi et al., 2007), whereas hypermethylation of genes codifying for growth factors (Huynh et al., 2014) involved in the migration and recruitment of oligodendrocytes (Franklin RJM., 2002) would lead to remyelination failure. The role of methylation in neurodegenerative processes has been mainly studied in PPMS or SPMS patients, reporting aberrant expression in essential genes involved in the methylation/demethylation cycle (Du et al., 2015; Fagone et al., 2016; Kulakova et al., 2016; Wu et al., 2017).

2. Hypothesis and objectives

2.1. HYPOTHESIS

Under pathological conditions like MS, certain modifications in the DNAme pattern of both Bmem and Treg cells could be related to early onset and progression of the disease.

2.2. OBJECTIVES

2.2.1. General objective

To identify aberrant alterations in the methylome profile of Bmem and Treg cells derived from MS patients in two distinct scenarios: (a) at diagnosis and (b) at later stages of the disease.

2.2.2. Specific objectives

a. To characterize the whole-genome DNAme profile of our target immune cell subsets derived from controls, RRMS and SPMS patients using the methylated DNA immunoprecipitation followed by sequencing (MeDIP-seq) approach.

b. To validate the results obtained in the MeDIP-seq step at the RNA level by the use of gene expression microarrays.

c. To study the association between methylation levels and RNA levels in selected candidate genes.

d. To analyse the association between clinical, radiological and cognitive variables and the RNA expression of candidate genes in RRMS patients.

3. Patients and methods

3.1. PATIENTS

3.1.1. Design of the study

10 RRMS, 10 SPMS patients and 10 controls were recruited for the pilot study. RRMS patients and controls were age and gender matched, while RRMS and SPMS patients were gender matched. Fresh whole peripheral blood was collected from all participants, and later the Bmem and Treg cell populations were properly isolated.

3.1.2. Recruitment of the subjects of the study

Patients in the Neurology Unit of the Dr Josep Trueta Hospital (Girona, Spain) and the Neuroimmunology and Multiple Sclerosis Unit (UNIEM) of the Santa Caterina Hospital (Salt, Spain) were enrolled in this study. Controls were recruited among local volunteers.

3.1.2.1. Criteria of inclusion and exclusion

The inclusion criteria for both RRMS and SPMS patients was as follows: (i) age ≥ 18; (ii) Caucasian ethnicity; (iii) to be diagnosed as RRMS or SPMS according to the McDonald criteria for MS (2010); (iv) to have signed an informed consent. In contrast, the exclusion criteria for either RRMS, SPMS or controls required at least one of the following factors: (i) any sign of infection at the sampling time; (ii) the use of psychoactive substances; (iii) prior blood transfusion; (iv) a history of allergies or autoimmune diseases; (v) being a current smoker. An additional exclusion criterion for the RRMS and SPMS cohorts was not having received an immunomodulatory treatment for the last 5 years.

3.1.2.2. Ethical Statement

The study was approved by the Ethical Committee of Clinical Research (CEIC) of the Dr Josep Trueta Hospital (Royal Decree 223/2004, Local Decree 406/2006, Biomedical Research Law 14/2007) according to the Helsinki Statement and the Organic Law 15/1999 of 13 December on the Protection of Personal Data.

3.1.3. Variables of the study

The variables collected from the participants of the study included demographics, clinical, radiological and cognitive variables.

Demographic variables

Demographics variables obtained at the moment of sampling were age (years) and gender.

Clinical and radiological variables

The expanded disability status scale (EDSS) score (Kurtzke JF., 1983) was recorded for the MS patients by qualified clinicians at the moment of sampling. Radiological variables were obtained in the RRMS cohort at diagnosis by a neuroradiologist using a Philips 1.5 Tesla MRI scanner according to the 2021 MAGNIMS-CMSC-NAIMS consensus (Wattjes et al., 2021). The variables analysed were the number of gadolinium-enhanced (Gd+) lesions in T1, the number of lesions in T2 and the presence or absence of black holes.

Cognitive variables

RRMS patients and controls were subjected to a battery of neuropsychological tests including the Selective Reminding Test (SRT), the 10/36 Spatial Recall Test (SPART), the Symbol Digit Modalities Test (SDMT), the Paced Auditory Serial Addition Test (PASAT-3), and the Word List Generation test (WLG) (Oreja-Guevara et al., 2019) by qualified clinicians just after the sampling.

3.2. METHODS

3.2.1. Collection of fresh whole peripheral blood

The extraction of fresh whole peripheral blood was performed in EDTA tubes at UNIEM (Santa Caterina Hospital; Salt, Spain); while the flow cytometry and the cell sorting procedure were completed shortly after the blood extraction at the Germans Trias i Pujol Research Institute (IGTP) (Badalona, Spain).

Procedure

Between 80 and 110 mL of whole peripheral blood was collected from each of the volunteers and then kept at room temperature until processing. The isolation of target cell populations was performed using a modified protocol from Cossarizza et al., 2019. In brief, red blood cells were lysed with PharmLyse lysis buffer (BD Bioscience, San Diego, CA), and later removed by discarding the supernatant remaining after centrifugation. The cell pellet was washed once with flow cytometry staining buffer (FACS buffer) (Cossarizza et al., 2019) followed by centrifugation, and after removing the supernatant, the pellet was resuspended with phosphate buffered saline (PBS) with 1% foetal bovine serum (FBS). A portion of the sample was used to estimate the total number of cells. After quantification, a maximum of 450 million cells were processed in aliquots of 25 million each. In order to enable the separation of the target cell populations, an incubation with the following antibodies was performed under dark conditions: CD127 (ref.560822, BD Biosciences, USA), CD194 (ref. 561123, BD Biosciences, USA), CD3 (ref. 555339, BD Biosciences, USA), CD4 (ref.552838, BD Biosciences, USA), CD25 (ref.555432, BD Biosciences, USA), CD27 (ref.560222, BD Biosciences, USA) and HLA-DR (ref. 559866, BD Biosciences, USA). Samples were then washed once, centrifuged and resuspended in FACS buffer, centrifuged again and finally resuspended in PBS with 1% FBS. The detailed standard operating procedure (SOP) is described in Annex I.

3.2.2. Flow cytometry and cell sorting

Flow cytometry and cell sorting were performed on the FACSAria II cytometer (BD Biosciences, USA). Bmem cell and Treg cell populations were separated using double discrimination and frontal and lateral dispersion (Figure 9). The gating strategy used for each cell population was as follows: $CD3^-$ $CD14^-$ $HLA\text{-}DR^+$ $CD27^+$ for Bmem cells (Sanz et al., 2019; Wu et al., 2011), and $CD4^+$ $CD3^+$ $CD25^+$ $CD194^+$ $CD127^-$ for Treg cells (Soldevila et al., 2013).

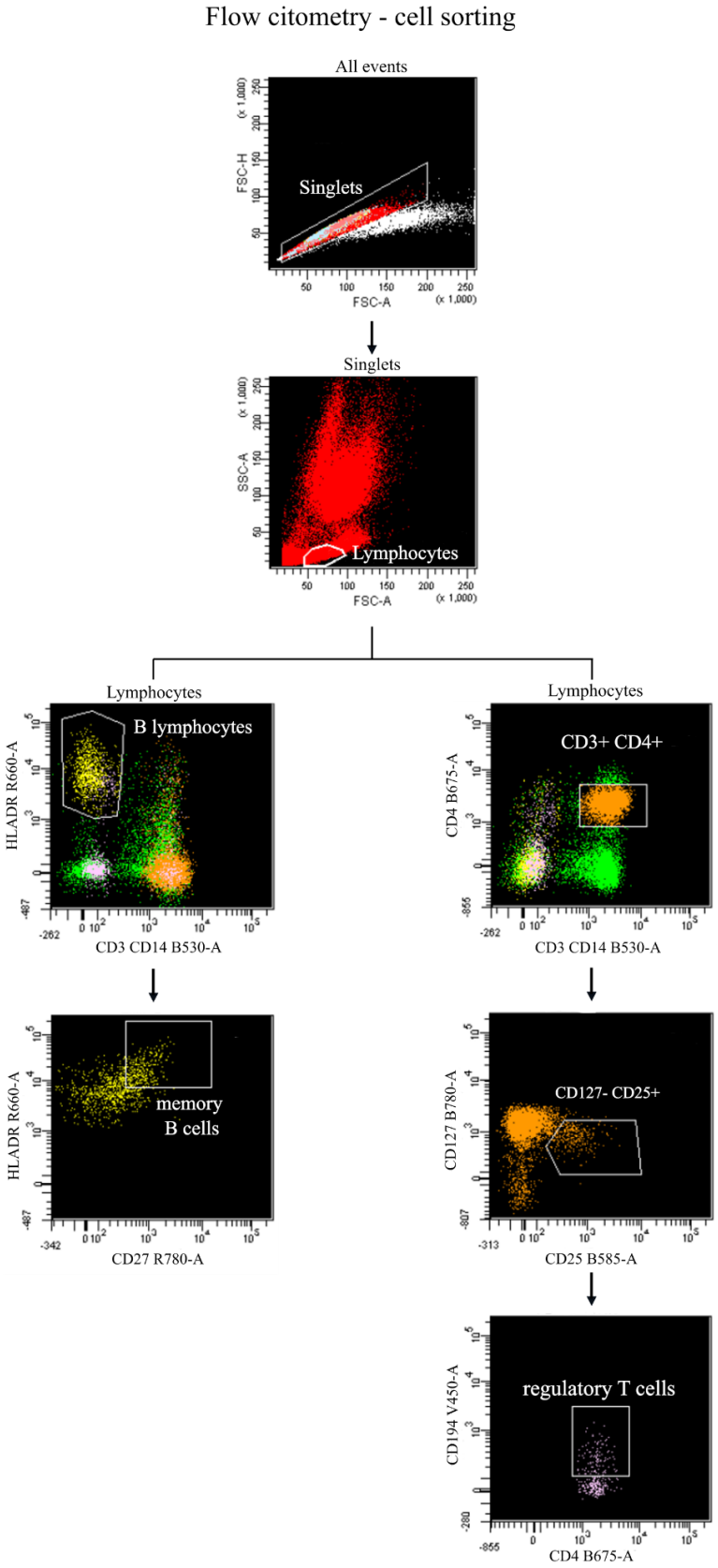

Figure 9. Gating strategy used for the isolation of memory B cells and regulatory T cells derived from the whole peripheral blood. The gating strategy for each cell population was the following: $CD3^{-}$ $CD14^{-}$ $HLA\text{-}DR^{+}$ $CD27^{+}$ for memory B cells and $CD4^{+}$ $CD3^{+}$ $CD25^{+}$ $CD194^{+}$ $CD127^{-}$ for regulatory T cells. Figure source: own elaboration.

3.2.3. DNA and RNA extraction

The All prep DNA/RNA/protein Mini Kit (Qiagen, Germany) was used to extract DNA and RNA from target immune cell subsets following the manufacturer instructions. In the last step, 100 µL of EB buffer was used to elute the DNA, and 30 µL of RNase free water was used to elute the RNA. The quality and the concentration of the DNA was measured using the NanoDrop 1000 (Thermo Scientific, USA). The quality and concentration of the RNA was measured using the Agilent 2100 Bioanalyzer (Agilent, USA). Until their use, DNA samples were kept at -20ºC. RNA samples were stored at -80ºC until their use.

3.2.4. Immunoprecipitation of methylated DNA (MeDIP)

The aim of the MeDIP procedure was to obtain the enriched fraction of the whole genome methylated DNA by immunoprecipitation, and subsequently to prepare DNA libraries required for next-generation sequencing (NGS) (Figure 10).

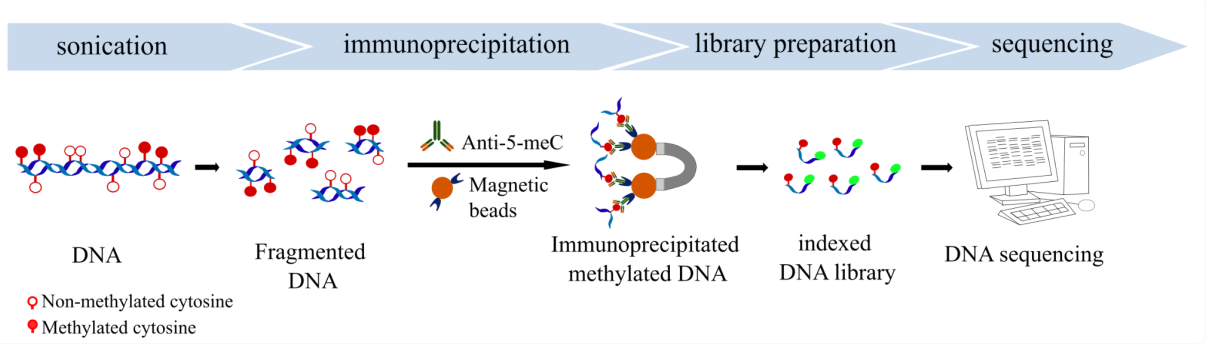

Figure 10. Summary of the MeDIP protocol. Genomic DNA was fragmented by sonication and incubated with an anti-human 5-methylcytosine antibody. Samples were incubated with magnetic beads for their immunoprecipitation. Methylated DNA fragments were captured using a magnetic rack and indexed during the library preparation. Finally, DNA libraries were sent for sequencing. Figure source: own elaboration. *5-meC: 5-methylcytosine; MeDIP: methylated DNA immunoprecipitation*.

Procedure

In brief, 600 to 1000 nanograms (ng) of genomic DNA were fragmented with Bioruptor Pico (Diagenode, Belgium), using ten cycles of 30 seconds of sonication followed by 30 seconds of inactivity. Samples were run on 1.5% agarose gel to validate the fragment size, which ranged from 100 to 300 base pair (bp) with a mean size of ~200 bp. Fragmented DNA was purified using the Monarch PCR & DNA Cleanup Kit (NEB, New England) prior to DNA library preparation. In the first part of the library preparation, the iDeal Library Kit (Diagenode, Belgium) was used to repair and stabilize the fragmented DNA with a poly-(A) tail and the addition of an adaptor. After purification with AMPure XP Beads (Beckman

Court, USA), DNA samples were subjected to immunoprecipitation (IP) using the MagMeDIP kit (Diagenode, Belgium). Briefly, DNA fragments were denatured at 95ºC and then incubated with an antibody against the 5-meC bound to magnetic beads. Using a magnetic rack, the methylated DNA fraction was immunoprecipitated (IP sample). A fraction (10%) of the initial fragmented DNA sample (input sample) was separated prior to the antibody incubation and immunoprecipitation to serve as control. IP and input samples were purified using the iPure Kit v2 (Diagenode, Belgium). In the second part of the library preparation, DNA fragments were indexed by a quantitative PCR (qPCR) procedure using the iDeal Library Kit (Diagenode, Belgium), and later purified using the AMPure XP Beads (Beckman Court, USA). DNA libraries were stored at -20ºC until sequencing. The detailed SOP is described in Annex II.

3.2.5. Next-generation sequencing and bioinformatics

DNA libraries were subjected to NGS at the National Center of Genomic Analysis (CNAG-CRG, Barcelona) using the Illumina HiSeq 2500 System (Illumina, San Diego). The following options were selected: single-read sequencing; between 20 to 25 million reads per sample; and a length of 50 nucleotides per read. Three input samples were used as reference samples for each cell type population.

A FASTQ file containing the nucleotide sequence of the millions of reads was generated for each DNA library. The quality of the raw reads was checked using FASTQC (Andrews S., 2010). Then, raw reads were aligned to the Genome Reference Consortium Human Build 38 (hg38) (Schneider et al., 2017) using GEM-mapper v3 (Marco-Sola et al., 2012). This alignment generated a sequence alignment/map (SAM) file that was converted to the binary alignment/map (BAM) format using SAMtools (Li et al., 2009). Afterwards, BAM files were sorted to organize the alignment data by its position in the reference genome (Li et al., 2009) and indexed to BAI files using SAMtools (Li et al., 2009). In order to see how well our reads aligned to the reference genome, the Mapping Quality (MapQ) score was used (Li et al., 2008). The MapQ score represents the confidence that a read has been correctly mapped to the genomic coordinates. MapQ score can range from 0 to 60. A MapQ value threshold of 20 was chosen, meaning that all reads with a MapQ score < 20 were removed from the analysis. The next step was to identify duplicate reads, as they can increase the risk of over-representing specific sequences amplified during the PCR step of the library

preparation. For this purpose, the "uniq" option from the MEDIPS package was used, and the default value of uniq=$1e^{-3}$ was chosen (Lienhard et al., 2013). Then, the difference between the length of the raw reads (50 bases) and the length of the DNA fragments after the library preparation (average of 300 bases) was corrected using the "extend" parameter from the MEDIPS package (Lienhard et al., 2013). This parameter extends the read sequence to a given length of nucleotides. As recommended by the MEDIPS package, an "extend" value of 300 nucleotides was chosen. Later, in order to analyse the large amount of data in a manageable way, the genome was divided into adjacent regions of a certain size called "windows". A window size of 100 nucleotides was selected, i.e., the genome was divided into adjacent regions of 100 bases.

Methylation differences among the groups of study were calculated using the bioconductor package edgeR (Robinson et al., 2009). This method uses the weighted trimmed mean of M-values (TMM) approximation to normalize the differential expression (Robinson and Oshlack, 2010). The output of this analysis was a browser extensible data (BED) file containing the whole list of differentially methylated regions (DMRs) among the groups of study. The normalized methylation values for each DMR were given as reads per kilobase per million (rpkm), which corrects for length sequences and sequencing depth. The methylation status of each DMRs was presented as the fold change in logarithmic base 2 ($\log_2$FC) value. A DMR with a $\log_2FC < 0$ value indicates a hypomethylated region in comparison to the group of reference, while a DMR with a $\log_2FC > 0$ value points out a hypermethylated region when compared to the group of reference. The statistical significance was set at $P < 0.05$.

The analysis of genomic distribution of each DMR was performed using the Hypergeometric Optimization of Motif EnRichment (HOMER) tool version 4.11 (Heinz et al., 2010). HOMER function 'annotatePeaks.pl' match each DMR with their genomic locations such as promoter-TSS (starting from -1 kb to +100 bp); transcription termination site (TTS; starting from -100 bp to +1 kb), exon (coding); 5'-untranslated region (UTR) exon; 3'-UTR exon; intronic region; non-coding region; or intergenic region. Additionally, HOMER provides information on DMRs containing repeats and transposable elements, or if the DMR falls into a CGI. Lastly, each DMRs was assigned to its corresponding gene (differentially methylated gene or DMG) using the information provided by the 'annotatePeaks.pl' function (Heinz et al., 2010). In the current study, a miRNA gene was considered differentially methylated if a

DMR was reported in the region up to ± 10 kb from the 5' end of the pre-miRNA sequence (Saini et al., 2007).

The flowchart depicted in Figure 11 reveals the main steps followed once raw sequencing data was obtained. The script used during the differential methylation analysis is described in Annex III.

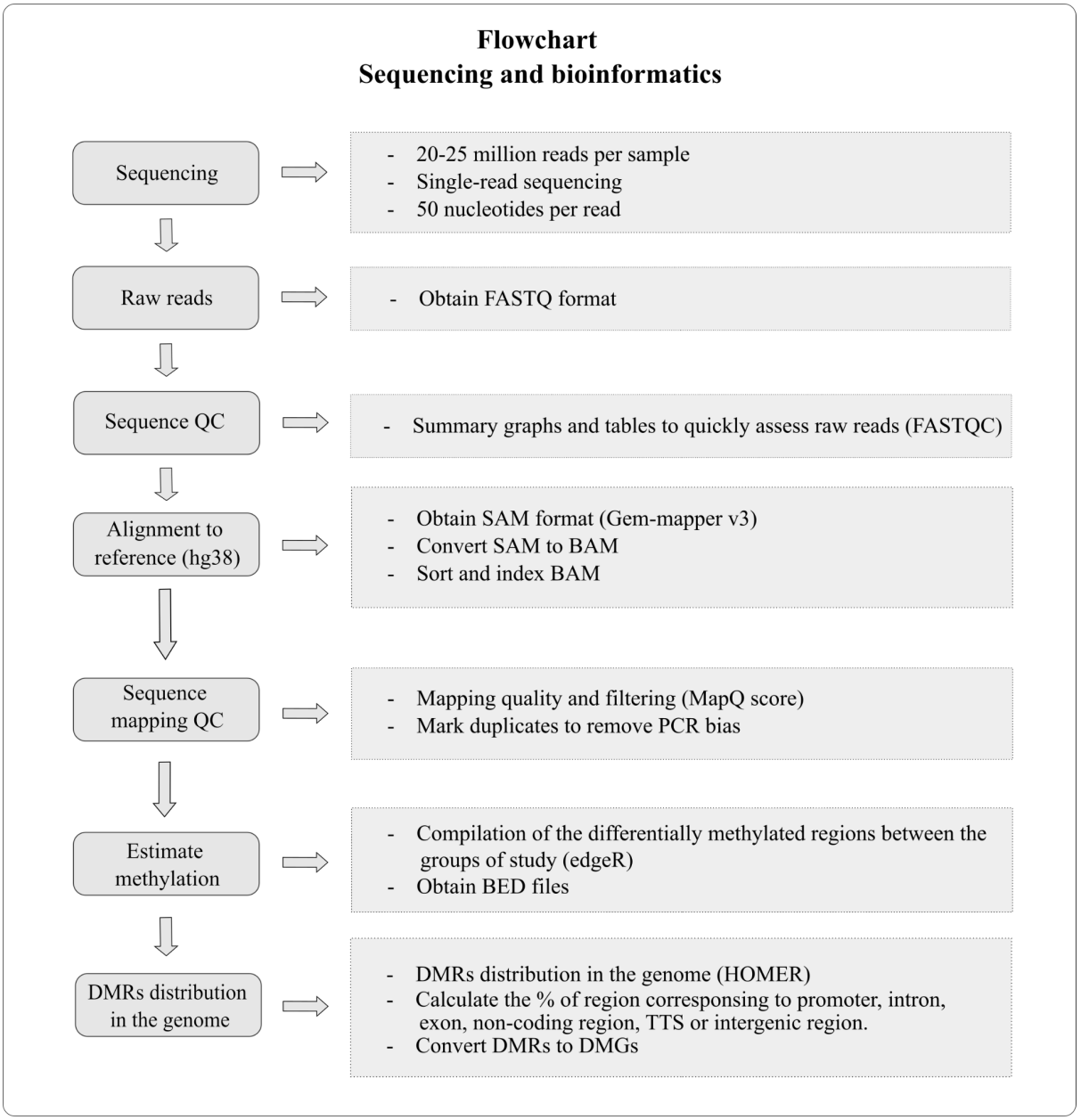

Figure 11. Flowchart of the sequencing and the bioinformatics analysis. Figure source: own elaboration. *BAM: binary alignment/map; BED: browser extensible data; DMG: differentially methylated gene; DMR: differentially methylated region; hg38: genome reference consortium human build 38; QC: quality control; SAM: sequence alignment/map.*

3.2.6. Gene ontology, KEGG pathway and miRNA targets

Gene ontology (GO) analysis was performed using PANTHER version 16.0 (Thomas et al., 2003; 2006), GOrilla (Eden et al., 2007; 2009), and Enrichr (Xie et al., 2021). The Kyoto encyclopaedia of genes and genomes (KEGG) pathway analysis was performed using miRPath version 3.0 (Vlachos et al., 2015). The miRDB (Chen and Wang, 2019) and TargetScan version 7.2 (Agarwal et al., 2015) databases were used to predict miRNA targets.

3.2.7. Transcriptome of candidate DMGs

The effects of methylation on the RNA expression of DMGs were assessed using transcriptome analysis based on microarray technology. Two types of candidate DMGs were selected: those coding for protein or pseudogenes (hereon, referred to as *candidate genes*); and those codifying for miRNAs (hereon, referred to as *candidate miRNA genes*). The transcriptome analysis of candidate genes was performed using NanoString nCounter® Elements™ XT technology (NanoString, USA). In contrast, the analysis of candidate miRNA genes was conducted using the TaqMan® Advanced miRNA Assay (Applied Biosystems, Germany) and the TaqMan® OpenArray™ Human Advanced microRNA panels (Applied Biosystems, Germany).

3.2.7.1. NanoString nCounter® Elements™ XT

The NanoString nCounter® Elements™ XT (NanoString, USA) is a highly sensitive technology that measures gene expression by detecting individual mRNA molecules attached to fluorescent barcodes (Figure 12). The number of counts for each candidate gene represents the number of times the fluorescent barcode attached to the target mRNA is detected (Figure 12). In this study, a total of 22 candidate genes involved in the immune response, cellular signalling, cell metabolism, protein processing, as well as cytokine and interleukin regulation were chosen for their analysis. Two housekeeping genes previously reported in MS were selected for normalization (Oturai et al., 2016).

3.2.7.1.a. Procedure

The probe pair (Probe A and Probe B) design and construction were performed according to NanoString (Seattle, USA) standard protocol, while the synthesis was performed by IDT (Coralville, USA). The nCounter® Elements™ TagSet (containing Reporter Tags and

universal Capture Tags) and the nCounter® Elements™ reagents were purchased from NanoString (Seattle, USA). From 40 to 120 ng of RNA was mixed with probe pairs, the nCounter® Elements™ TagSets and the hybridization buffer as shown in Annex IV. The hybridization reaction occurred at 67ºC for 24 hours using a thermal cycler. Samples were processed using the nCounter® Prep Station (NanoString, USA), and the mRNA was counted using the nCounter digital analyser (NanoString, USA). Raw counts were obtained as RLF files and then loaded into the nSolver Analysis software version 4.0. The detailed SOP is described in Annex IV.

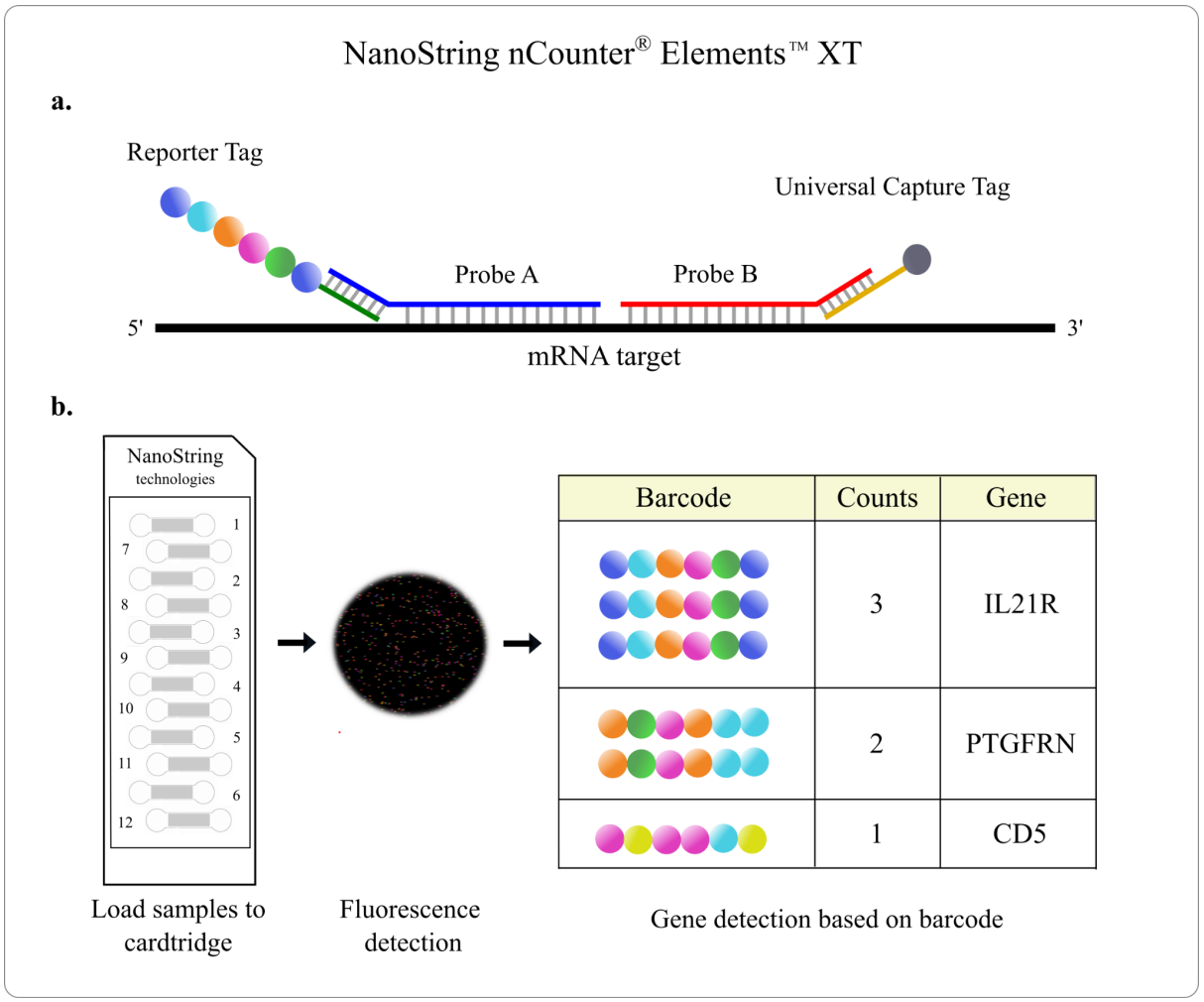

Figure 12. NanoString nCounter® Elements™ XT technology. **(a)** The mRNA of the candidate gene (target mRNA) was hybridized with a fluorescent barcode (Reporter Tag), a biotinylated universal Capture Tag, and target-specific oligonucleotide probe pairs (Probe A and Probe B) prior to its quantification. Probe A is an oligonucleotide with a complementary sequence to both target mRNA and Reporter Tag. Probe B is an oligonucleotide sequence with complementarity to both target RNA and universal Capture Tag. Each pair of Probe A + Probe B is specific to the target mRNA. **(b)** After loading samples, individual mRNA molecules were detected and quantified based on their fluorescent barcode. Figure source: own elaboration.

3.2.7.1.b. Expression analysis of candidate genes

Raw counts were normalized using ubiquitin-conjugating enzyme E2 D2 (*UBE2D2*) and hypoxanthine phosphoribosyltransferase 1 (*HPRT1*) and later subjected to probe-specific background correction using the nSolver Advanced Analysis Software version 4.0 (NanoString Technologies, USA). Genes showing less than 15 counts (Bmem cell cohort) or less than 10 counts (Treg cell cohort) in more than 25% of the samples were removed from the analysis. The differential mRNA expression among the groups of study was analysed using the Fast/Approximate option. The statistical significance level was set at $P < 0.05$. The differential mRNA expression among the groups of study was estimated based on $\log_2$ fold change ($\log_2$FC), with a 95% confidence interval. A $\log_2$FC < 0 indicates a downregulation, while a $\log_2$FC > 0 indicates an upregulation of the candidate gene in RRMS patients when compared to controls. In the result section, the normalized count values are depicted in the figures, while the $\log_2$FC values are described in the tables. Only the significant results are described in the results.

3.2.7.2. TaqMan® OpenArray™ Human Advanced microRNA panel

The TaqMan® OpenArray™ is a multiple real-time PCR plate composed of 48 subarrays with 64 through-holes each. The surface of the array has a hydrophobic coating, while the through-holes are hydrophilic which contributes to the retention of 33 nanolitres (nL) of volume by surface tension (Figure 13). In this thesis, the expression of 164 miRNAs in Bmem cells and 181 miRNAs in Treg cells was analysed using the custom-made TaqMan® OpenArray™ Human Advanced microRNA panel on a QuantStudio™ 12K Flex system (Thermo Fisher Scientific, USA).

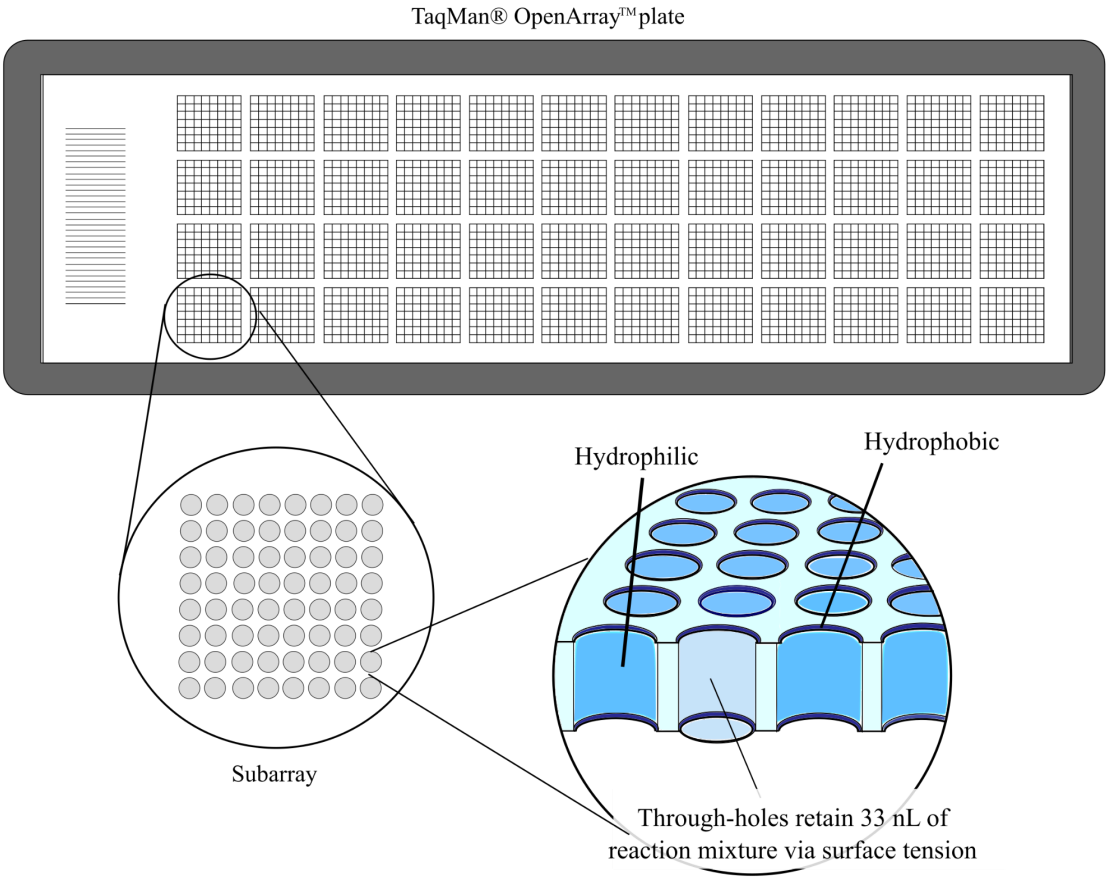

Figure 13. A TaqMan® OpenArray™ plate. Figure extracted from the QuantStudio™ 12K Flex System product bulletin (retrieved from: www.tools.thermofisher.com/content/sfs/brochures/cms_081550.pdf) and later modified. *nL: nanoliters.*

3.2.7.2.a. Procedure

Between 5 and 10 ng of RNA were first poly(A)-tailed and then ligated with an adaptor using the TaqMan® Advanced miRNA Assay (Applied Biosystems, Germany). Mature miRNAs were reverse transcribed to complementary DNAs (cDNA) using the TaqMan® Advanced miRNA Assay (Applied Biosystems, Germany) and later subjected to 18 cycles of pre-amplification. The quality control of retrotranscription was performed using the individual Taqman® advanced miRNA assays hsa-miR-24a-3p, hsa-miR-146a-5p and hsa-miR-150a-5p, according to the manufacturer's instructions (Applied Biosystems, Germany). After validation, pre-amplified cDNA was diluted 1:20 in 0.1X Tris-EDTA buffer pH 8.0 and mixed with the TaqMan® OpenArray™ Real-Time PCR Master Mix (Thermo Fisher, USA). Samples were loaded automatically from a 384-well plate onto the TaqMan® OpenArray™ Human Advanced microRNA panel using the OpenArray™ AccuFill system (Thermo Fisher, USA). Finally, the TaqMan® OpenArray™ Human Advanced microRNA plates were placed into the QuantStudio™ 12K Flex Real-Time PCR System (Applied

Biosystem, Germany) for its quantification, selecting a maximum of 40 cycles of amplification. Two replicates were used per sample. Amplification data were obtained in electronic data sheet (EDS) files. The detailed SOP is described in Annex V.

3.2.7.2.*b. Quality control and pre-processing of the amplification curves*

The EDS files containing amplification data were uploaded into the Cloud Dashboard application provided by the manufacturer (Thermo Fisher, USA). ROX and FAM signals were used to evaluate the quality of sample loading and the performance of PCR reactions. Wells that showed either a lack of or a deficient ROX or FAM signal were removed from the analysis. The quality of the amplification was determined based on the following parameters: the amplification score (Amp_Score); the quantification cycle (Cq) and the estimated confidence of the Cq value (Cq_conf). The association between the Cq_conf, the Amp_Score and the Cq values was analyzed using Spearman's rho test in order to define the optimal threshold for each parameter. We selected the samples with an Amp_Score ≥ 0.8, a Cq_conf ≥ 0.5 and a Cq value between 15 and 35.

Variability between technical replicates is common in this type of procedure. The reference analysis method in these cases is to include only replicates with a difference of ≤ 0.5 cycles between them. This approximation in our study would mean the loss of a large amount of data and therefore, a reduction in statistical power. In contrast, the statistical analysis for each replicate was performed separately. Furthermore, only those results showing significant differences in both replicates were included (Figure 14).

3.2.7.2.*c. Data normalization*

The global normalization (GN) method was applied. GN uses the mean expression value of all expressed miRNAs in a given sample as a normalization factor (Cq reference) (Mestdagh et al., 2009). The Cq reference is then applied to calculate the relative expression (RE) of each miRNA as depicted below:

$$RE = 2^{-\Delta Cq}$$

where:

$$\Delta Cq = (Cq\ miRNA - Cq\ reference)$$

and where:

Cq miRNA = the Cq value of the selected miRNA

Cq reference = the mean Cq value of all expressed miRNA in a given sample

3.2.7.2.*d. Expression analysis of candidate miRNAs*

After checking quality control, candidate miRNAs were subjected to statistical analysis. Only miRNAs showing statistically significant results in both replicates were considered for the analysis (Figure 14). The information about one of the replicates will be shown in the figures and tables in the result section. Data for the second replicate will be described in the corresponding annex.

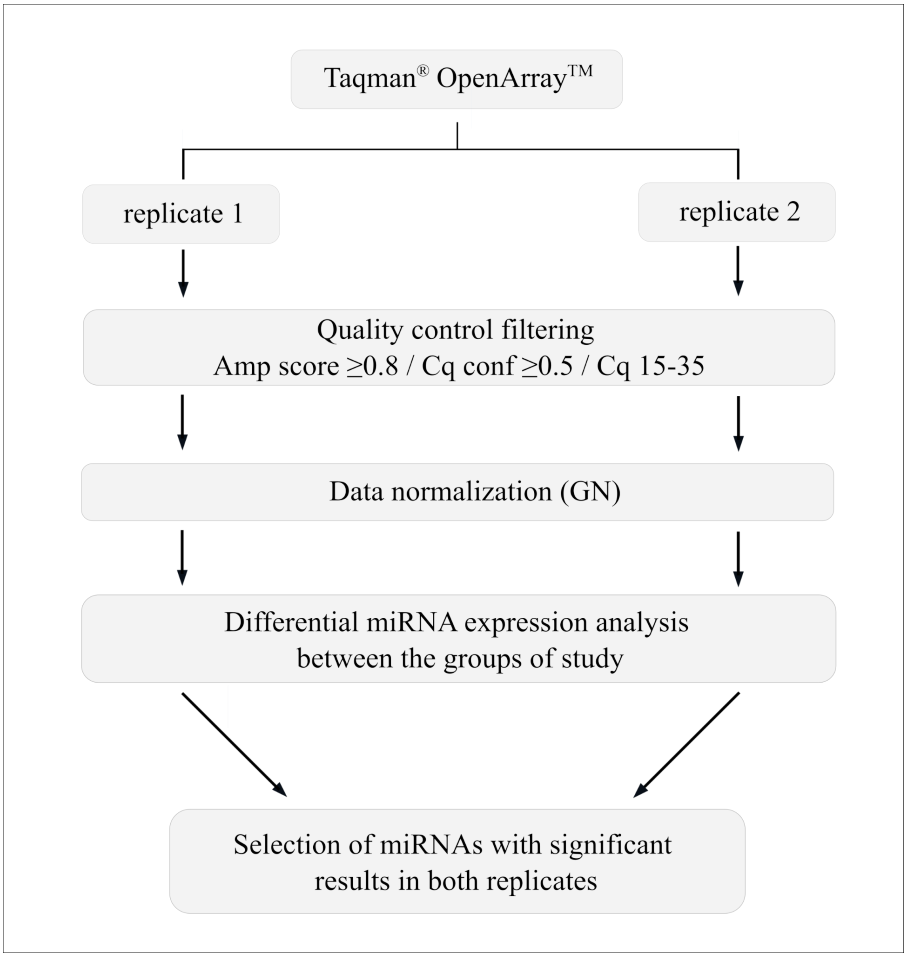

Figure 14. Flowchart followed during the differential expression analysis of miRNAs. Figure source: own elaboration. *Amp_Score: amplification score; Cq: quantification cycle; Cq_Conf: calculated confidence of the Cq value; GN: global normalization.*

3.3. STATISTICAL ANALYSIS

The statistical analysis comprised a variety of non-parametric tests due to the small sample size. The confidence interval (CI) for all statistical analysis was established at 95% and the significance level was set at $P < 0.05$.

3.3.1. Genome wide methylation differences among the groups of study

The exact test for negative binomial distribution of the edgeR bioconductor package (Robinson et al., 2009) was used to search for statistical differences in the normalized methylation values among the groups of study. EdgeR uses the weighted trimmed mean of M-values (TMM) approximation to normalize the differential expression (Robinson and Oshlack, 2010).

3.3.2. Expression analysis of candidate genes

The simplified negative binomial method and the linear regression method of the nSolver Advanced Analysis Software version 4.0 (NanoString, USA) was used to evaluate the statistical differences between the normalized expression of each candidate gene among RRMS and controls.

3.3.3. Expression analysis of candidate miRNAs

The two-tailed Mann-Whitney U test was performed using GraphPad Prism® version 6.01 for Windows (GraphPad Software, USA; retrieved from www.graphpad.com) to compare the normalized expression of miRNAs between the two biological groups.

3.3.4. Relation between methylation and expression of candidate genes

The relation between the normalized mRNA expression of candidate genes and the normalized methylation values (rpkm) for each DMR was estimated in RRMS and controls by Spearman's rho test using the IBM®SPSS®Statistics software version 21 (IBM Corp., USA). Values less than |0.25| would indicate no association, low association if |0.25-0.50|, moderate association if |0.50-0.70|, and strong association if |0.7-1.0| (Udovičić et al., 2007). The graphical representation of the correlation was depicted as a scatter plot using GraphPad Prism® version 6.01 for Windows (GraphPad Software, USA; retrieved from www.graphpad.com).

3.3.5. Relation between methylation and expression of candidate miRNAs

The relation between the normalized expression of candidate miRNAs and the normalized methylation values (rpkm) on each DMR was estimated in the groups of study by Spearman's rho test using the IBM®SPSS®Statistics software version 21 (IBM Corp, USA). Values less than |0.25| would indicate no association, between |0.25-0.50| low association, between |0.50-0.70| moderate association, and between |0.7-1.0| strong association (Udovičić et al., 2007). The correlation was pictured as a scatter plot using GraphPad Prism® version 6.01 for Windows (GraphPad Software, USA; retrieved from www.graphpad.com).

3.3.6. Relation between candidate gene expression and clinical, radiological and neuropsychological variables

The relation between clinical, radiological and neuropsychological variables and the normalized expression of candidate genes was analysed in the RRMS group using the IBM®SPSS®Statistics software version 21 (IBM Corp, USA). For the analysis between gene expression and dichotomous variables, the two-tailed Mann-Whitney U test was used. The relation between the candidate gene expression and numerical variables was studied using Spearman's rho test. Values less than |0.25| would indicate no association, low association if |0.25-0.50|, moderate association if |0.50-0.70|, and strong association if |0.7-1.0| (Udovičić et al., 2007).

3.3.7. Relation between candidate miRNA expression and clinical, radiological and neuropsychological variables

The relation between clinical, radiological and neuropsychological variables and the normalized expression of candidate miRNAs was analysed in the groups of study using the IBM®SPSS®Statistics software version 21 (IBM Corp, USA). The two-tailed Mann-Whitney U test was used for the comparison between miRNA expression and dichotomous variables. The Spearman coefficient (rho of Spearman) was used to explore the relation between miRNA expression and numerical variables. Values less than |0.25| would indicate no association, between |0.25-0.50| low association, between |0.50-0.70| moderate association, and between |0.7-1.0| strong association (Udovičić et al., 2007). The correlation was pictured as a scatter plot using GraphPad Prism® version 6.01 for Windows (GraphPad Software, USA; retrieved from www.graphpad.com).

4. Results

The aim of the study was to characterize the methylation pattern of two distinct immune cell types (Bmem cells and Treg cells) collected from whole peripheral blood of controls and MS patients, and subsequently, to underpin the findings at both mRNA and miRNA expression levels.

4.0. SUBJECTS OF STUDY

10 RRMS, 10 SPMS and 10 controls were recruited for this study. One individual of the RRMS group was removed from the study due to the patient developing a different neurological disorder. The summary of demographic and clinical data collected from MS patients and controls is depicted in Table 2. The detailed data for each participant of study is available in Annex VI.

Table 2. Summary of demographic, clinical and radiological data collected from controls, RRMS patients, and SPMS patients. *EDSS: expanded disability status scale; Gd+: gadolinium-enhanced; IQR: interquartile range; RRMS: relapsing-remitting multiple sclerosis; SPMS: secondary-progressive multiple sclerosis.*

	Control (n=10)	RRMS (n=9)	SPMS (n=10)
Gender (n, %)			
male	3 (30%)	3 (33%)	3 (30%)
female	7 (70%)	6 (67%)	7 (70%)
Age (median, range / IQR)	39.5 (25-53 / 37-48)	41 (24-53 / 34-48)	68 (59-74 / 65-71)
EDSS (median, range / IQR)	-	1.5 (1.5-2.0 / 1.5-2.0)	6.5 (4.0-8.0 / 6.0-7.0)
T2 lesions (median, range / IQR)	-	15 (9-43 / 13-19)	-
Gd+ lesions (n)			
0	-	3	-
1	-	3	-
2	-	1	-
3	-	1	-
4	-	1	-
Black holes			
yes	-	2	-
no	-	7	-

4.1. STUDY OF THE WHOLE GENOME METHYLOME PROFILE

4.1.1. Samples

In Bmem cells, samples from 9 RRMS patients, 10 SPMS patients and 10 controls were used for DNA sequencing. In contrast, a cohort of 7 RRMS patients, 5 SPMS patients and 7 controls were used for Treg DNA sequencing. The remaining Treg samples (2 RRMS, 5 SPMS and 3 controls) were discarded because this cell type did not reach the optimal amount of DNA required for sequencing. The samples used for DNA sequencing are depicted in Annex VI.

4.1.2. Genome-wide methylation differences among the groups of study

The methylome of Bmem and Treg cells derived from RRMS patients, SPMS patients, and controls was studied using MeDIP-seq approximation. Methylation differences related to disease onset were determined by comparing the methylation status of RRMS patients with their matched controls. Additionally, the methylation profile between SPMS and RRMS patients was compared in order to determine epigenetic changes related to the progressive stages of the disease.

4.1.2.1. Description of differentially methylated regions

A total of 453,110 significant DMRs were found between RRMS patients and controls, whereas 847,248 significant DMRs were detected in SPMS vs RRMS patients in the Bmem population (Figure 15a). In the Treg cell subset, 406,017 significant DMRs were reported in RRMS when compared to controls, while 2,291,588 significant DMRs were quantified when comparing SPMS to RRMS (Figure 15e). Overall, the majority of the DMRs were hypomethylated at the initial stages of the disease in both cell types (69% and 63% in Bmem cells and Treg cells, respectively) (Figure 15a). However, a global hypermethylation was determined in the advanced stage of the disease (70% in Bmem cells and 67% in Treg cells) (Figure 15e). When analysing the distribution of the DMRs across the genome, it was found that almost all the methylation differences (> 90%) were localized either within introns or in the intergenic region; while a residual percentage corresponded to exons (< 5%), TTS (< 1.5%), promoter-TSS (< 1.5%), and non-coding sequences (< 0.6%) (Figure 15b and 15f).

When further exploring the DMRs, it was observed that in both immune cell types, between 43% to 49% of DMRs were located in transposable elements (LINE, SINE, ERV, DNA transposons, SVA) (Figure 15c and 15g). In the Bmem cell subset, the methylation status across the

transposable elements differed during the course of the disease, showing a predominant hypomethylation pattern at diagnosis of the disease -with the exception of SVAs- that shifted to hypermethylation at later stages of the disease (Figure 15c). This pattern was also observed in Treg cells for LINEs, ERVs and DNA transposons, while SINEs and SVAs showed the opposite methylation pattern (Figure 15g).

In parallel, DMRs falling into CGIs were also analysed. We found 1336 and 865 differentially methylated CGIs in RRMS patients vs controls in Bmem and Treg cells, respectively (Figure 15d and 15h). A total of 8437 and 24,549 CGIs were differentially methylated in SPMS vs RRMS in Bmem and Treg cells, respectively (Figure 15d and 15h). Most DMRs located in CGIs (>83%) were hypermethylated in both cell types at diagnosis of the disease while more than 98% were hypomethylated at later stages of the disease progression (Figure 15d and 15h). GO enrichment analysis revealed that genes containing hypermethylated CGIs located within their sequence or nearby (up to ±50 kb) were involved in the regulation of the transcription (GO:0006355) and the Wnt pathway (GO:1904953).

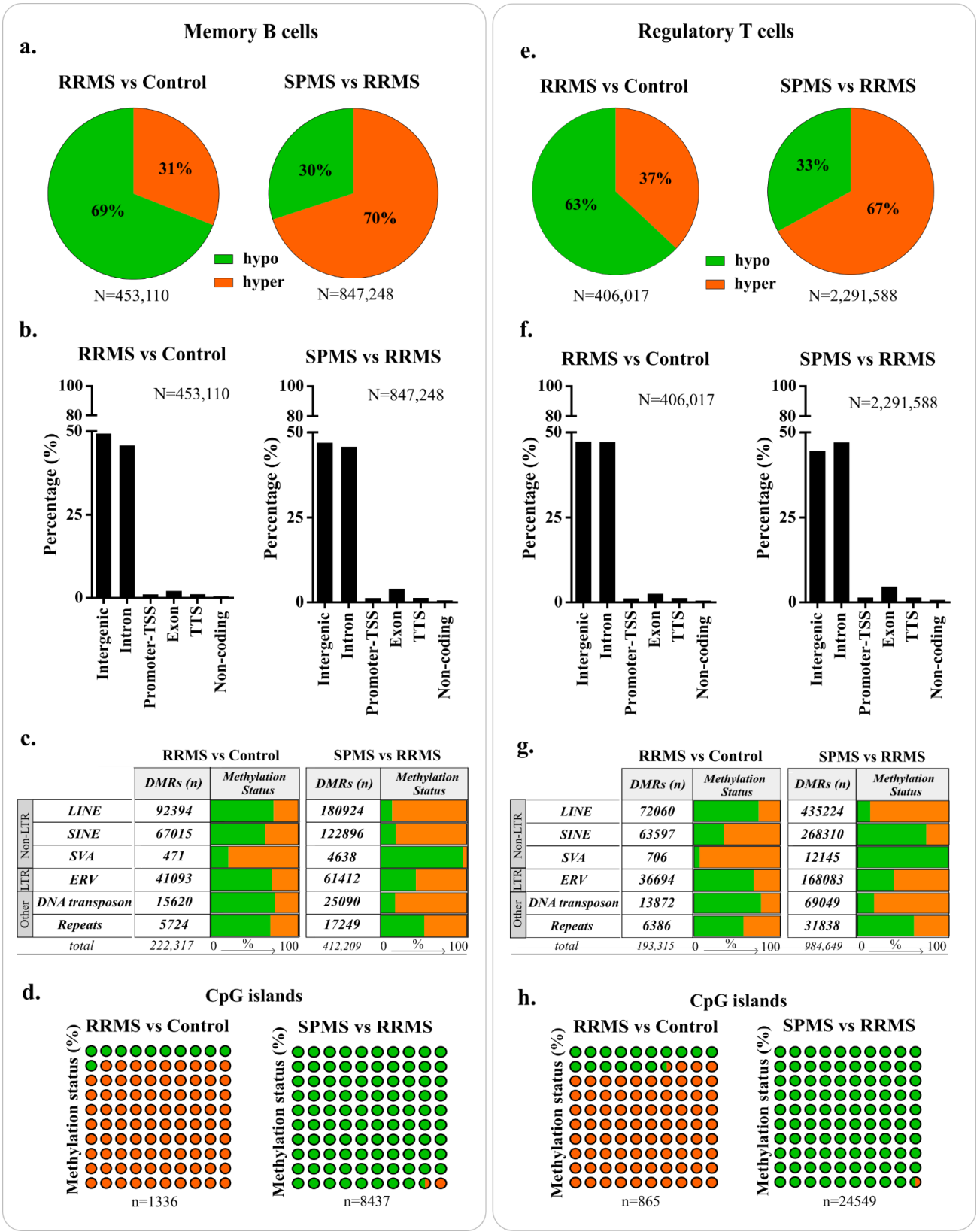

Figure 15. Description of the DMRs determined in MS patients at diagnosis (RRMS vs control) and at later stages of clinical course (SPMS vs RRMS) in memory B and regulatory T cells. (a, e) Methylation status of DMRs shown as a percentage. **(b, f)** Genomic distribution of DMRs. **(c, g)** Methylation status of DMRs containing either transposable element or repeat sequence. **(d, h)** Number of DMRs falling into a CpG island and their methylation status. Each circle represents 1%. In all the cases, hypomethylation and hypermethylation statuses are

shown as green and orange colours, respectively. *DMR: differentially methylated region; ERV: endogenous retrovirus; hyper: hypermethylated; hypo: hypomethylated; LINE: long interspersed nuclear element; LTR: long terminal repeats; RRMS: relapsing-remitting multiple sclerosis; SINE: short interspersed nuclear element; SPMS: secondary-progressive multiple sclerosis; SVA: SINE-VNTR-Alu; TSS: transcription start site; TTS: transcription termination site.*

4.1.2.2. Description of differentially methylated genes

HOMER was used to assign each DMR to its corresponding annotated gene resulting in DMGs (Heinz et al., 2010). In Bmem cells, 22,165 and 23,651 genes displayed differential methylation patterns at the diagnosis and the progressive stages of the disease, respectively (Figure 16). In contrast, Treg cells showed 21,122 and 25,539 genes differentially methylated under the same clinical conditions, respectively (Figure 16). Interestingly, most of the DMGs overlapped when different stages of the disease were compared in both cell types (Figure 16). GO analysis revealed that the pool of common genes between all conditions of study (n=18,175) corresponded to physiological mechanisms involved in cellular metabolism, signalling regulation, and communication (Figure 16c and 16d).

DMGs codifying for miRNAs were also examined. We reported globally 1449 and 1429 miRNA genes exhibiting differential methylation in Bmem cells at the diagnosis and later course of the disease, respectively (Figure 17). In Treg cells, 1214 and 1643 miRNA genes showed differential methylation at the diagnosis and advanced stages of the disease, respectively (Figure 17). More than 60% of miRNA genes (n=1015) were common in both cell subsets derived from SPMS, RRMS and controls (Figure 17c). GO databases revealed that these miRNA genes were associated with gene silencing, metabolism, cytokine production, migration and inflammatory responses (Figure 17c and 17d).

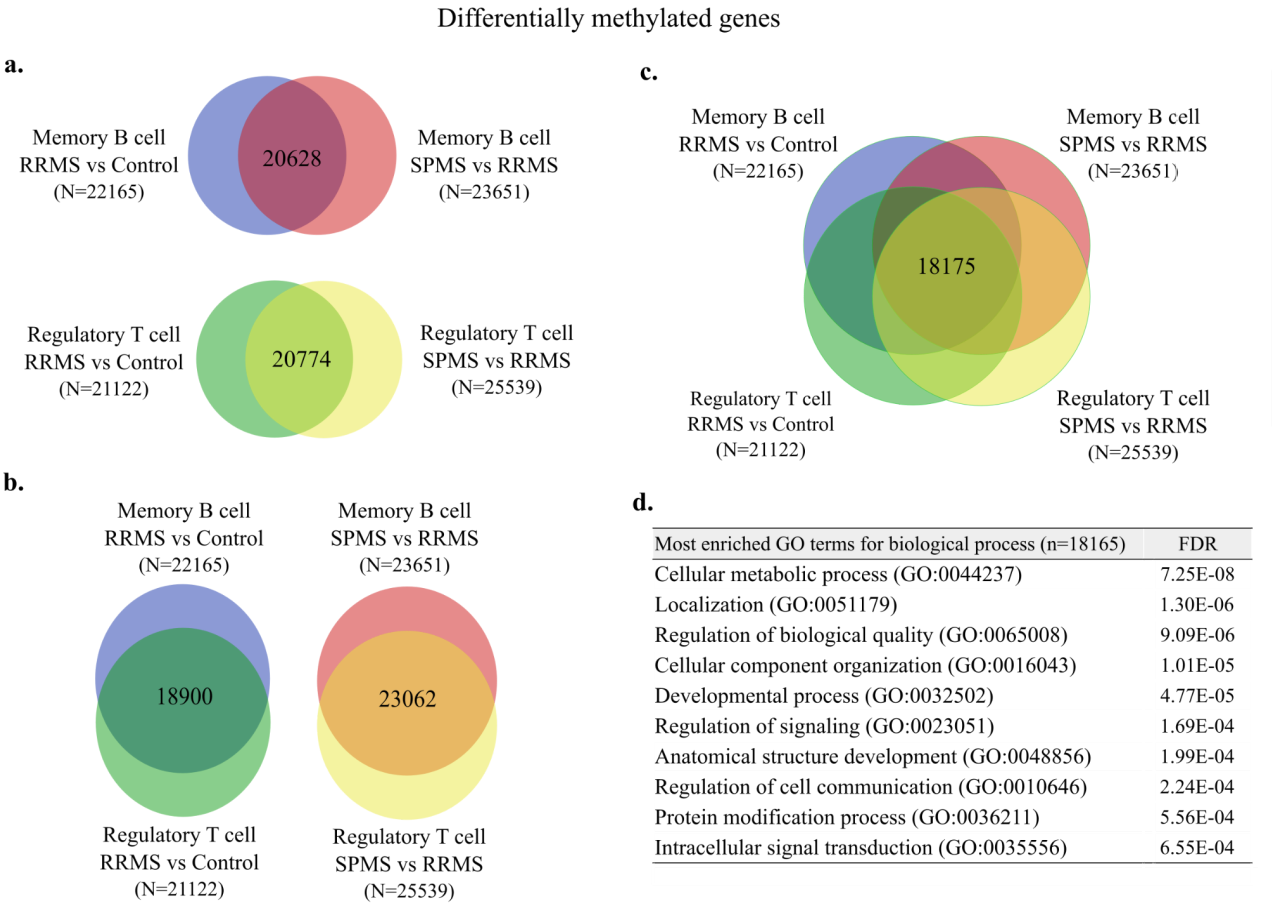

d.

Most enriched GO terms for biological process (n=18165)	FDR
Cellular metabolic process (GO:0044237)	7.25E-08
Localization (GO:0051179)	1.30E-06
Regulation of biological quality (GO:0065008)	9.09E-06
Cellular component organization (GO:0016043)	1.01E-05
Developmental process (GO:0032502)	4.77E-05
Regulation of signaling (GO:0023051)	1.69E-04
Anatomical structure development (GO:0048856)	1.99E-04
Regulation of cell communication (GO:0010646)	2.24E-04
Protein modification process (GO:0036211)	5.56E-04
Intracellular signal transduction (GO:0035556)	6.55E-04

Figure 16. Number of common DMGs in memory B and regulatory T cells resulting from the comparison between controls, RRMS and SPMS patients. (a) Venn diagram showing the common DMGs between the two conditions of the disease. **(b)** Venn diagram of the overlapped DMGs between the same conditions of the disease in both immune cell types. **(c)** Venn diagram showing the shared DMGs among all experimental conditions. **(d)** Description of the most enriched GO terms for biological processes for the common DMGs (n=18175). *DMG: differentially methylated gene; FDR: false discovery rate; RRMS: relapsing-remitting multiple sclerosis; SPMS: secondary-progressive multiple sclerosis.*

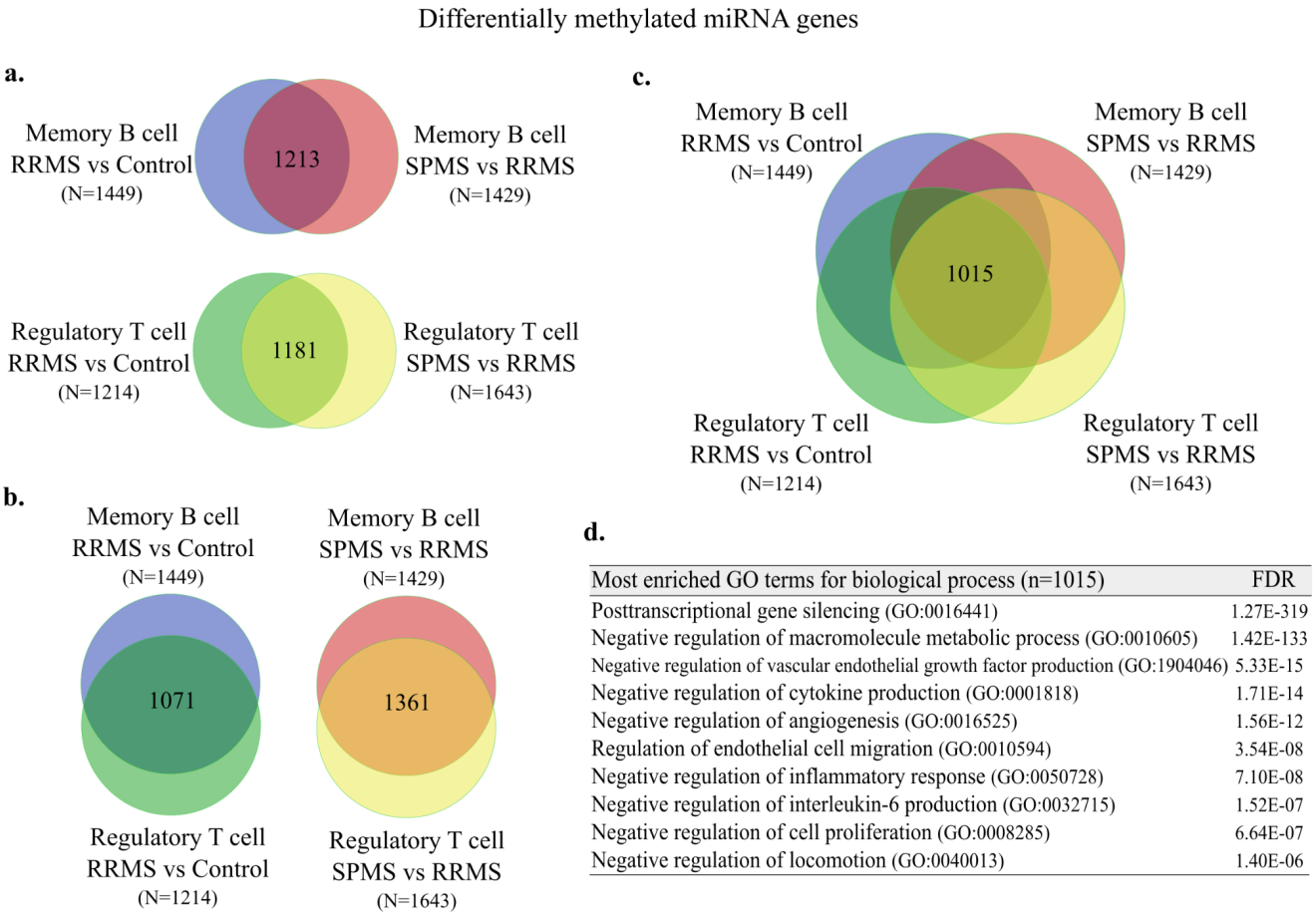

d.

Most enriched GO terms for biological process (n=1015)	FDR
Posttranscriptional gene silencing (GO:0016441)	1.27E-319
Negative regulation of macromolecule metabolic process (GO:0010605)	1.42E-133
Negative regulation of vascular endothelial growth factor production (GO:1904046)	5.33E-15
Negative regulation of cytokine production (GO:0001818)	1.71E-14
Negative regulation of angiogenesis (GO:0016525)	1.56E-12
Regulation of endothelial cell migration (GO:0010594)	3.54E-08
Negative regulation of inflammatory response (GO:0050728)	7.10E-08
Negative regulation of interleukin-6 production (GO:0032715)	1.52E-07
Negative regulation of cell proliferation (GO:0008285)	6.64E-07
Negative regulation of locomotion (GO:0040013)	1.40E-06

Figure 17. Number of common differentially methylated miRNA genes in memory B and regulatory T cells resulting from the comparison between controls, RRMS and SPMS patients. (a) Venn diagram showing the common miRNA genes between the two conditions of the disease. **(b)** Venn diagram of the overlapped miRNA genes between the same conditions of the disease in both immune cell types. **(c)** Venn diagram of the shared miRNA genes among all experimental conditions. **(d)** Description of the most enriched GO terms for biological processes for the common miRNA genes (n=1015). *FDR: false discovery rate; RRMS: relapsing-remitting multiple sclerosis; SPMS: secondary-progressive multiple sclerosis.*

4.1.3. Summary

Herein, we have described significant global methylation modifications in the Bmem and Treg cell subsets collected from MS patients. RRMS patients showed a remarkable hypomethylation in comparison to both controls and SPMS patients. Nearly half of the DMRs were associated with transposable elements. Genes presenting DMRs within their sequence were involved in cellular metabolism, signalling regulation, and cell communication. Furthermore, differentially methylated miRNA genes were related to inflammatory response, cytokine production and gene silencing.

4.2. VALIDATION STUDY AT RNA LEVEL: CANDIDATE GENES

An objective of the present study was to assess how DNA methylation could affect the expression of genes at the mRNA level in both immune cell subsets of RRMS patients and their matched controls.

4.2.1. List of studied candidate genes

A detailed description of the candidate genes is shown below (Table 3).

Table 3. List of candidate genes selected for the transcriptome analysis by NanoString nCounter® Elements™ XT.

Gene Symbol	Gene complete name	ENSEMBL ID
Candidate genes		
ABR	ABR Activator Of RhoGEF And GTPase	ENSG00000159842
ALOX5	Arachidonate 5-Lipoxygenase	ENSG00000012779
BRICD5	BRICHOS domain-containing protein 5	ENSG00000182685
CARD11	Caspase Recruitment Domain Family Member 11	ENSG00000198286
CD5	CD5 Molecule	ENSG00000110448
DDR1	Epithelial discoidin domain-containing receptor 1	ENSG00000204580
DTYMK	Thymidylate kinase	ENSG00000168393
ECEL1P2	Endothelin Converting Enzyme Like 1 Pseudogene 2	ENSG00000244280
ESRRG	Estrogen Related Receptor Gamma	ENSG00000196482
GCC1	GRIP and coiled-coil domain-containing protein 1	ENSG00000179562
IL21R	Interleukin 21 Receptor	ENSG00000103522
LILRA4	Leukocyte immunoglobulin-like receptor subfamily A member 4	ENSG00000239961
LTBR	Lymphotoxin Beta Receptor	ENSG00000111321
MDGA2	MAM Domain Containing Glycosylphosphatidylinositol Anchor 2	ENSG00000139915
NEU4	Neuraminidase 4	ENSG00000204099
NOS1	Nitric oxide synthase 1	ENSG00000089250
OSBP2	Oxysterol Binding Protein 2	ENSG00000184792
PDE4D	cAMP-specific 3' 5'-cyclic phosphodiesterase 4D	ENSG00000113448
PTGFRN	Prostaglandin F2 receptor negative regulator	ENSG00000134247
SEC31B	Protein transport protein Sec31B	ENSG00000075826
SHISAL1	Protein shisa-like-1	ENSG00000138944
ZNF469	Zinc Finger Protein 469	ENSG00000225614
Housekeeping genes		
UBE2D2	Ubiquitin Conjugating Enzyme E2 D2	ENSG00000131508
HPRT1	Hypoxanthine Phosphoribosyltransferase 1	ENSG00000165704

4.2.2. Methylation profile of the candidate genes

Candidate genes exhibited methylation differences between RRMS patients and controls in at least one of the following regions: promoter-TSS, first exon, first intron, gene body or the upstream intergenic region (up to -10 kb from the TSS). The location of the DMRs for each candidate gene is summarized in Table 4.

Table 4. Location of the DMRs within the candidate gene sequence in memory B and regulatory T cells when comparing RRMS patients with their controls. The (x) mark indicates the presence of at least one DMR in the selected genomic region. The 'intergenic' category comprises the region up to -10 kb upstream of the TSS of the candidate gene. *DMR: differentially methylated region ; kb: kilobase; TSS: transcription start site; RRMS: relapsing-remitting multiple sclerosis.*

	Memory B cell				
	Intergen	Promoter	Exon 1	Intron 1	Gene body
ABR		x		x	x
ALOX5		x	x	x	x
BRICD5					
CARD11				x	x
CD5		x		x	x
DDR1	x				
DTYMK					x
ECEL1P2	x				
ESRRG		x		x	x
GCC1		x			x
IL21R				x	x
LILRA4					x
LTBR		x			x
MDGA2		x		x	x
NEU4	x			x	x
NOS1				x	x
OSBP2				x	x
PDE4D		x	x	x	x
PTGFRN		x		x	x
SEC31B					x
SHISAL1				x	x
ZNF469	x				

	Regulatory T cell				
	Intergen	Promoter	Exon 1	Intron 1	Gene body
ABR		x		x	x
ALOX5		x	x		x
BRICD5	x	x			
CARD11				x	x
CD5				x	x
DDR1		x			
DTYMK		x			x
ECEL1P2		x			
ESRRG		x		x	x
GCC1	x				
IL21R					x
LILRA4					x
LTBR					x
MDGA2				x	x
NEU4		x		x	
NOS1		x		x	x
OSBP2		x	x		x
PDE4D		x		x	x
PTGFRN				x	x
SEC31B				x	x
SHISAL1					x
ZNF469	x				

4.2.3. Transcriptome of candidate genes

The expression of 22 genes was analysed using the microarray-based NanoString nCounter® Elements™ XT (Diagenode, Belgium).

4.2.3.1. Samples

In Bmem cells, 6 RRMS and 6 control samples were analysed. In contrast, 6 RRMS and 6 control samples were examined in Treg cells (Annex VI).

4.2.3.2. Performance of the NanoString nCounter® Elements™ XT

Among the candidate genes, 16 and 14 genes were detected in Bmem and Treg cells, respectively (Table 5). The rest of genes did not reach the minimum detection threshold across all samples and therefore they were excluded from the analysis (Table 5).

Table 5. List of detected and undetected candidate genes in memory B and regulatory T cells when mRNA was studied using the NanoString nCounter® Elements™ XT.

	Memory B cells	Regulatory T cells
Detected genes	ABR, ALOX5, BRICD5, CARD11, CD5, DDR1, DTYMK, GCC1, IL21R, LILRA4, LTBR, NOS1, OSBP2, PDE4D, PTGFRN, SEC31B	ABR, ALOX5, BRICD5, CARD11, CD5, DTYMK, ECEL1P2, GCC1, IL21R, NOS1, OSBP2, PDE4D, PTGFRN, SEC31B
Undetected genes	ECEL1P2, ESRRG, MDGA2, NEU4, SHISAL1, ZNF469	DDR1, ESRRG, LILRA4, LTBR, MDGA2, NEU4, SHISAL1, ZNF469

4.2.3.3. Differential mRNA expression between RRMS patients and controls

In Bmem cells, *IL21R*, *PTGFRN*, *NOS1* and *OSBP2* showed differential mRNA expression levels in RRMS patients when compared to control individuals: *IL21R* was downregulated in RRMS patients ($log_2FC=-0.70;\ P=0.011$); while *NOS1* ($log_2FC=1.05;\ P=0.026$), *PTGFRN* ($log_2FC=0.98;\ P=0.030$), and *OSBP2* ($log_2FC=0.90;\ P=0.038$) showed an upregulated pattern in the RRMS group (Figure 18a and Table 6a). In Treg cells, lower *ECEL1P2* expression was found in RRMS patients than in the control group ($log_2FC=-1.64;\ P=0.040$) (Figure 18b and Table 6b).

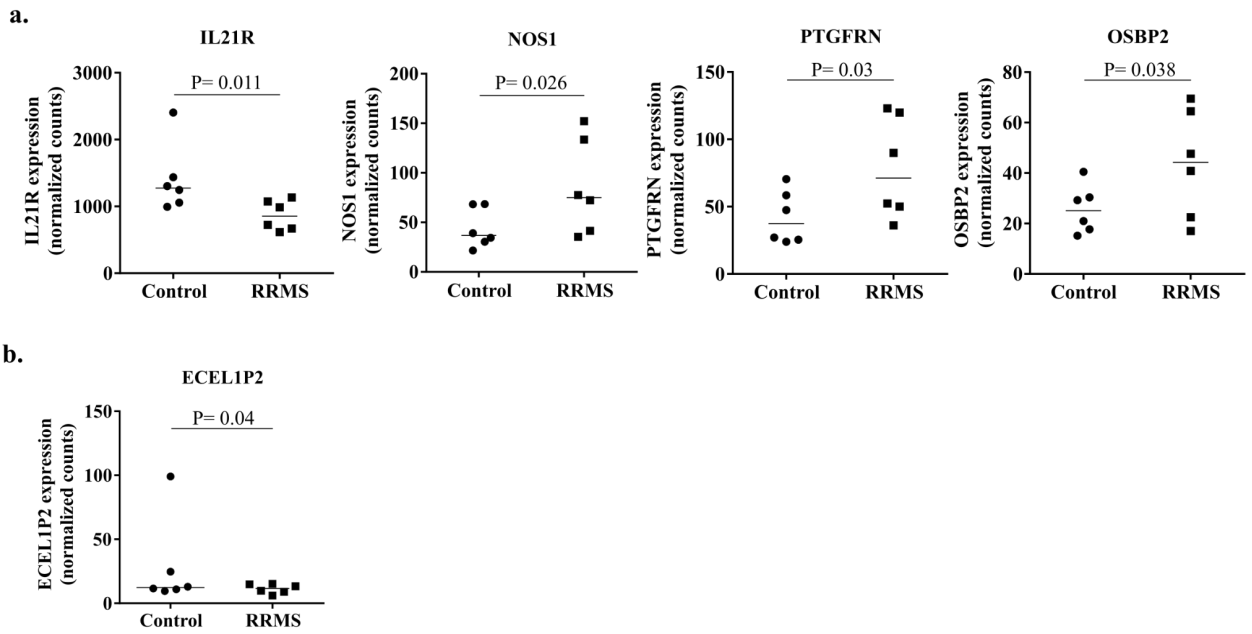

Figure 18. Candidate genes showing differential expression between RRMS patients and controls in memory B and regulatory T cells. (a) Relative expression of *IL21R*, *NOS1*, *PTGFRN*, *OSBP2* in memory B cells of RRMS patients and controls. **(b)** Relative expression of *ECEL1P2* in regulatory T cells of RRMS patients and controls. The line indicates the median. *ECEL1P2: endothelin converting enzyme like 1 pseudogene 2; IL21R: interleukin 21 receptor; NOS1: nitric oxide synthase 1; OSBP2: oxysterol binding protein 2; PTGFRN: prostaglandin F2 receptor inhibitor; RRMS: relapsing-remitting multiple sclerosis.*

Table 6. Differentially expressed candidate genes in memory B and regulatory T cells of RRMS vs. controls. Candidate genes showing a significant differential expression between RRMS patients and controls in **(a)** memory B and **(b)** regulatory T cells. Results are shown as log_2FC with STD error and the upper and lower confidence intervals. Linear FC with upper and lower confidence limits is also shown. *ECEL1P2: endothelin converting enzyme like 1 pseudogene 2; FC: fold change; IL21R: interleukin 21 receptor; NOS1: nitric oxide synthase 1; OSBP2: oxysterol binding protein 2; PTGFRN: prostaglandin F2 receptor inhibitor; RRMS: relapsing-remitting multiple sclerosis; STD: standard.*

a.

Gene	Log2 FC	STD error (log2)	Lower confidence limit (log2)	Upper confidence limit (log2)	Linear FC	Lower confidence limit (linear)	Upper confidence limit (linear)	*P-value*
IL21R	**-0.70**	0.23	-1.15	-0.26	0.61	0.45	0.84	**0.011**
NOS1	**1.05**	0.40	0.26	1.84	2.07	1.20	3.58	**0.026**
PTGFRN	**0.98**	0.39	0.22	1.74	1.97	1.16	3.35	**0.030**
OSBP2	**0.90**	0.38	0.16	1.64	1.86	1.12	3.11	**0.038**

b.

Gene	Log2 FC	STD error (log2)	Lower confidence limit (log2)	Upper confidence limit (log2)	Linear FC	Lower confidence limit (linear)	Upper confidence limit (linear)	*P-value*
ECEL1P2	**-1.64**	0.69	-3.00	-0.28	0.32	0.12	0.82	**0.040**

4.2.3.4. Biological role and gene ontology analysis

The underlying mechanisms of the genes dysregulated in immune cells of RRMS patients (*PTGFRN, IL21R, OSBP2, NOS1, ECEL1P2*) were under investigation. Due to the pseudogenic nature of *ECEL1P2*, its parental gene, *ECEL1*, was chosen for the analysis. The results are shown in Table 7.

Table 7. Biological mechanisms and pathways associated with *PTGFRN, IL21R, OSBP2, NOS1* and *ECEL1*. The references shown in brackets are GO for gene ontology, WP for wikipathways and P for PANTHER. *ECEL1: endothelin converting enzyme like 1; IL21R: interleukin 21 receptor; NOS1: nitric oxide synthase 1; OSBP2: oxysterol binding protein 2; PTGFRN: prostaglandin F2 receptor inhibitor.*

Gene	Associated biological processes and pathways
PTGFRN	Prostaglandin synthesis and regulation (WP98) Myoblast fusion (GO:0007520)
IL21R	Interleukin-21-mediated signaling pathway (GO:0038114) Immunoglobulin mediated immune response (GO:0016064) Natural killer cell activation (GO:0030101) Regulatory circuits of the STAT3 signaling pathway (WP4538)
OSBP2	Lipid transporter activity (GO:0005319) Cholesterol binding (GO:0015485)
NOS1	Nitric oxide biosynthetic process (GO:0006809) Nitric oxide mediated signal transduction (GO:0007263) Regulation of calcium ion transport (GO:0051924) Regulation of transcription by RNA polymerase II (GO:0006357) Second-messenger-mediated signaling (GO:0019932)
ECEL1	Endothelin signaling pathway (P00019) Proteolysis (GO:0006508) Protein processing (GO:0016485) Protein maturation (GO:0051604)

4.2.4. Relation between mRNA expression and clinical, radiological and neuropsychological variables in RRMS patients

The relation between the mRNA expression of the dysregulated candidate genes and the clinical, radiological and cognitive variables collected from RRMS patients was determined. In this preliminary study, no statistical differences were reported.

4.2.5. Study of the methylation profile and mRNA expression in candidate genes

The relation between methylation levels in significant DMRs and the mRNA expression of the dysregulated candidate genes (*PTGFRN, IL21R, OSBP2, NOS1, ECEL1P2*) was investigated in RRMS patients and controls.

4.2.5.1. *PTGFRN*

Prostaglandin F2 receptor inhibitor (*PTGFRN*) is an 80,443-base-long gene located in the *plus* strand of chr1p13.1 (Figure 19a). In our study, it was found that the promoter of *PTGFRN* was hypermethylated in Bmem cells collected from RRMS patients in comparison to controls ([chr1:116908901-116909000], *Methylation* $log_2FC=0.76$, *P=0.041;* [chr1:116909001-116909100], *Methylation* $log_2FC=0.75$, *P=0.049*) (Figure 19b). In this region, elevated levels of methylation were associated with higher mRNA expression ([chr1:116908901-116909000], *rho= 0.77, P=0.004;* [chr1:116909001-116909100], *rho= 0.74, P=0.007*) (Figure 19c). We also detected a methylation pattern at +13.5 kb downstream of the TSS displaying a positive correlation with mRNA levels ([chr1:116923401-116923500], *rho=0.60; P=0.041)* (Figure 19c); while in the DMR located at +30.4 kb upstream of the TSS, the correlation followed the opposite pattern ([chr1:116940301-11640400], *rho=-0.57, P=0.027*) (Figure 19c). This DMR corresponds to the intragenic enhancer GH01J116939 as revealed by GeneHancer (Fishilevich et al., 2017).

a.

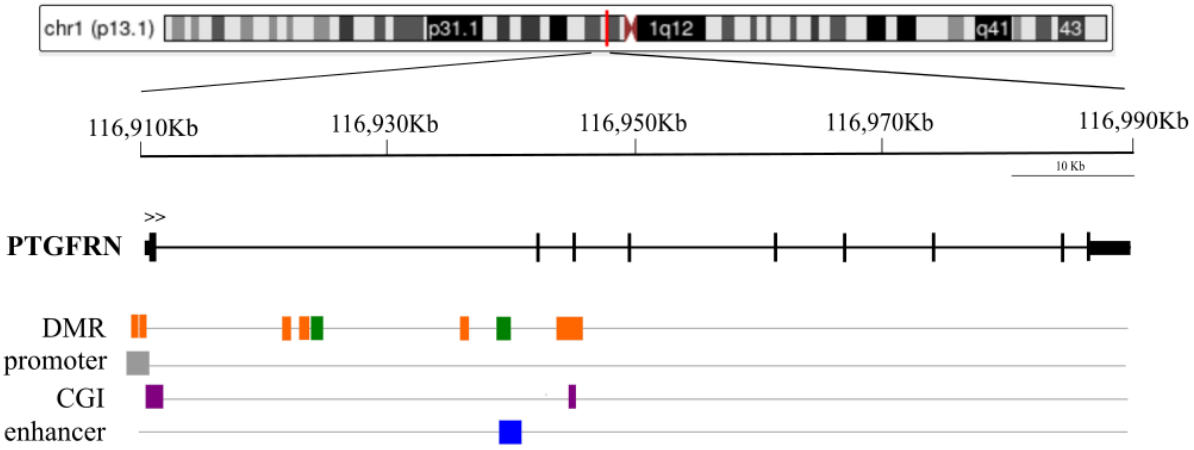

b.

Chr	Start	End	Annotation	Gene	Distance to TSS (bp)	Methylation Log_2FC	Methylation Status	Methylation P value
chr1	116908901	116909000	promoter-TSS	PTGFRN	-965	0.76	hyper	0.041
chr1	116909001	116909100	promoter-TSS	PTGFRN	-865	0.75	hyper	0.049
chr1	116920001	116920100	gene body	PTGFRN	10135	2.42	hyper	0.014
chr1	116923401	116923500	gene body	PTGFRN	13535	1.28	hyper	0.025
chr1	116924001	116924100	gene body	PTGFRN	14135	-0.82	hypo	0.018
chr1	116937201	116937300	gene body	PTGFRN	27335	1.66	hyper	0.024
chr1	116940101	116940200	gene body	PTGFRN	30235	-2.49	hypo	0.006
chr1	116940201	116940300	gene body	PTGFRN	30335	-2.76	hypo	0.001
chr1	116940301	116940400	gene body	PTGFRN	30435	-3.63	hypo	<0.001
chr1	116943901	116944000	gene body	PTGFRN	34035	1.65	hyper	0.036
chr1	116944001	116944100	gene body	PTGFRN	34135	1.36	hyper	0.036
chr1	116944101	116944200	gene body	PTGFRN	34235	1.89	hyper	0.021
chr1	116944201	116944300	gene body	PTGFRN	34335	1.70	hyper	0.012
chr1	116944401	116944500	gene body	PTGFRN	34535	1.02	hyper	0.022
chr1	116944501	116944600	gene body	PTGFRN	34635	1.00	hyper	0.034

c.

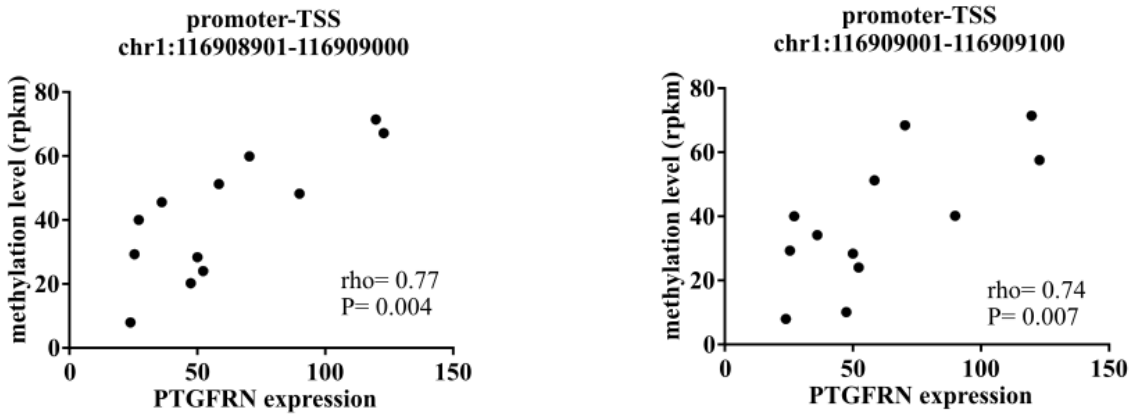

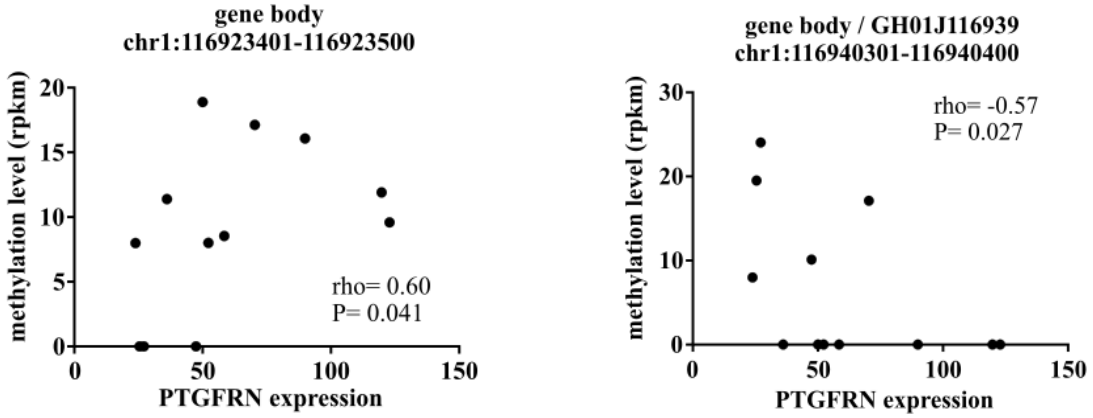

Figure 19. Description of the genomic location, methylation profile, and mRNA expression of *PTGFRN* in memory B cells of RRMS patients and controls. (a) Genomic mapping of *PTGFRN* in chr1p13.1. The two arrows indicate the direction of the transcription. The DMRs resulting from the comparison between RRMS and controls are displayed in green and orange if hypomethylated or hypermethylated, respectively. The promoter region (grey box) and the CGIs (purple box) are represented according to UCSC Genome Browser (Kent et al., 2002). The enhancer region (blue box) is depicted based on GeneHancer (Fishilevich et al., 2017). **(b)** List of DMRs between RRMS and controls in memory B cells located within the *PTGFRN* sequence. The coordinates for each DMR are given in the columns 'Start' and 'End'. **(c)** Scatter plot and correlation coefficient between the relative mRNA expression of *PTGFRN* and the normalized methylation values (rpkm) in memory B cells of RRMS patients and their matched controls in the given coordinates. *bp: base pair; CGI: CpG island; chr: chromosome; DMR: differentially methylated region; hyper: hypermethylated; hypo: hypomethylated; kb: kilobase; Methylation Log_2FC: fold change in logarithmic base 2 of the methylation value between RRMS patients and controls; PTGFRN: prostaglandin F2 receptor inhibitor; rho: Spearman's test rho value; rpkm: read per kilobase million; RRMS: relapsing-remitting multiple sclerosis; TSS: transcription start site.*

4.2.5.2. *IL21R*

Interleukin 21 receptor (*IL21R*) is a 49,882-base-long gene located in the *plus* strand of chr16p12.1. *IL21R* is composed of three transcript variants named 1, 2 and 3 (Figure 20a). In Bmem cells, five hypermethylated regions located between +777 bp and +1.3 kb downstream of the main TSS were observed in RRMS patients when compared to controls ([chr16:27402901-27403000], *Methylation $log_2FC=1.20$, $P=0.012$;* [chr16:27403101-27403200], *Methylation $log_2FC=0.81$, $P=0.045$;* [chr16:27403201-27403300], *Methylation $log_2FC=1.04$, $P=0.023$;* [chr16:27403401-27403500], *Methylation $log_2FC=1.14$, $P=0.040$;* [chr16:27403501-27403600], *Methylation $log_2FC=1.33$, $P=0.022$*) (Figure 20b). In all of these DMRs, methylation was inversely associated with mRNA expression, and in four of them, the correlation was statistically significant ([chr16:27402901-27403000], *rho= -0.62, P=0.028;* [chr16:27403101-27403200], *rho= -0.55, P=0.063;* [chr16:27403201-27403300], *rho= -0.60, P=0.041;* [chr16:27403401-27403500], *rho= -0.63, P=0.029;* [chr16:27403501-27403600], *rho= -0.74, P=0.006)* (Figure 20c). In a similar way, it was found that in the gene body region

[chr16:27439901-27440000], higher methylation levels were associated with lower mRNA expression of the gene (*rho= -0.65, P=0.022)* (Figure 20c).

a.

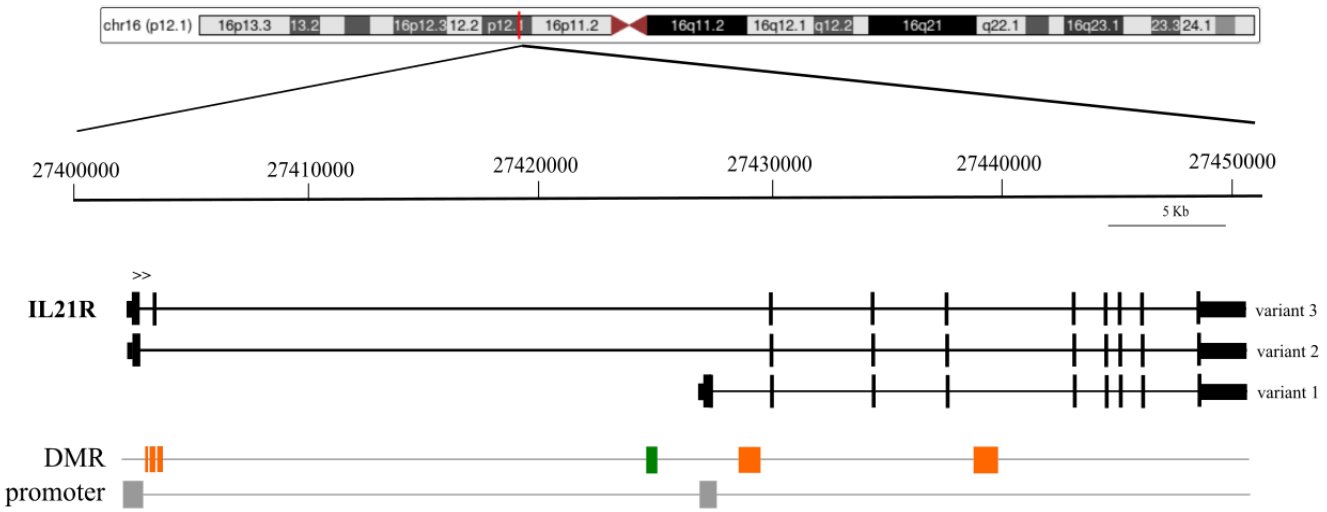

b.

Chr	Start	End	Annotation	Gene	Distance to main TSS (bp)	Methylation Log_2FC	Methylation status	Methylation P value
chr16	27402901	27403000	gene body	IL21R	777	1.20	hyper	0.012
chr16	27403101	27403200	gene body	IL21R	977	0.81	hyper	0.045
chr16	27403201	27403300	gene body	IL21R	1077	1.04	hyper	0.023
chr16	27403401	27403500	gene body	IL21R	1277	1.14	hyper	0.040
chr16	27403501	27403600	gene body	IL21R	1377	1.33	hyper	0.022
chr16	27424901	27425000	gene body	IL21R	22777	-1.20	hypo	0.043
chr16	27429001	27429100	gene body	IL21R	26877	1.00	hyper	0.014
chr16	27429101	27429200	gene body	IL21R	26977	1.01	hyper	0.016
chr16	27429201	27429300	gene body	IL21R	27077	0.91	hyper	0.019
chr16	27439801	27439900	gene body	IL21R	37677	0.71	hyper	0.049
chr16	27439901	27440000	gene body	IL21R	37777	0.91	hyper	0.043
chr16	27440001	27440100	gene body	IL21R	37877	1.14	hyper	0.004
chr16	27440101	27440200	gene body	IL21R	37977	1.54	hyper	0.018

c.

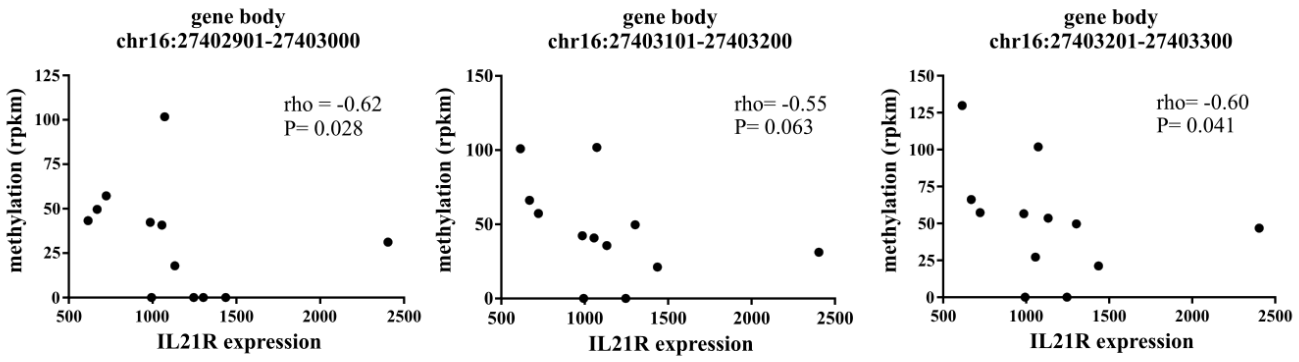

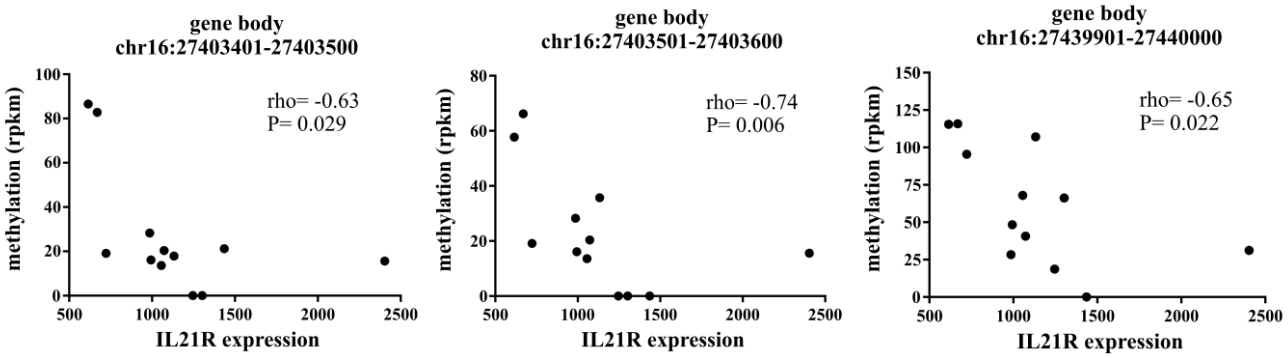

Figure 20. Description of the genomic location, methylation profile, and mRNA expression of *IL21R* in memory B cells of RRMS patients and controls. (a) Genomic mapping of the *IL21R* gene in chr16p12.1 and its transcript variants. The two arrows indicate the direction of the transcription. The DMRs resulting from the comparison between RRMS and controls are displayed in green and orange if hypomethylated or hypermethylated, respectively. The promoter region (grey box) is represented according to UCSC Genome Browser (Kent et al., 2002). **(b)** The DMRs within *IL21R* in memory B cells derived from RRMS patients in contrast to controls. The coordinates for each DMR are given in the columns 'Start' and 'End'. **(c)** Scatter plot and correlation coefficient between the relative mRNA expression of *IL21R* and the normalized methylation values (rpkm) in memory B cells of RRMS patients and controls in the given coordinates. *bp: base pair; chr: chromosome; DMR: differentially methylated region; hyper: hypermethylated; hypo: hypomethylated; IL21R: interleukin 21 receptor; Methylation log_2FC: fold change in logarithmic base 2 of the methylation value between RRMS patients and controls; rho: Spearman's test rho value; rpkm: read per kilobase million; RRMS: relapsing-remitting multiple sclerosis; TSS: transcription start site.*

4.2.5.3. *OSBP2*

Oxysterol binding protein 2 (*OSBP2*) is a 214,043-base-long gene located in the *plus* strand of chr22q12.2. *OSBP2* has six transcript variants named 1, 3, 4, 5, 6, and 7 (Figure 21a). In Bmem cells, RRMS patients presented 26 DMRs distributed across the gene in comparison to controls (Figure 21b). The region neighbouring the main promoter and its CGI was hypomethylated in RRMS patients, while the gene body was mainly hypermethylated (Figure 21a,b). In two of the DMRs located in the gene body, the level of methylation significantly correlated with *OSBP2* mRNA expression. The first DMR was located in the first intron of the transcript variant 5, at +104 kb from the main TSS, where higher methylation was associated with lower mRNA expression ([chr22:30797901-30798000], *rho=-0.65; P=0.023*) (Figure 21c). The second DMR was located close to the end of the gene, and showed a strong positive correlation between methylation and *OSBP2* expression ([chr22:30893201-30893300], *rho=0.79; P=0.002*) (Figure 21c). Interestingly, this region falls in the border between an exon and an intron region, suggesting that methylation in this region might be relevant during the splicing process of the gene.

a.

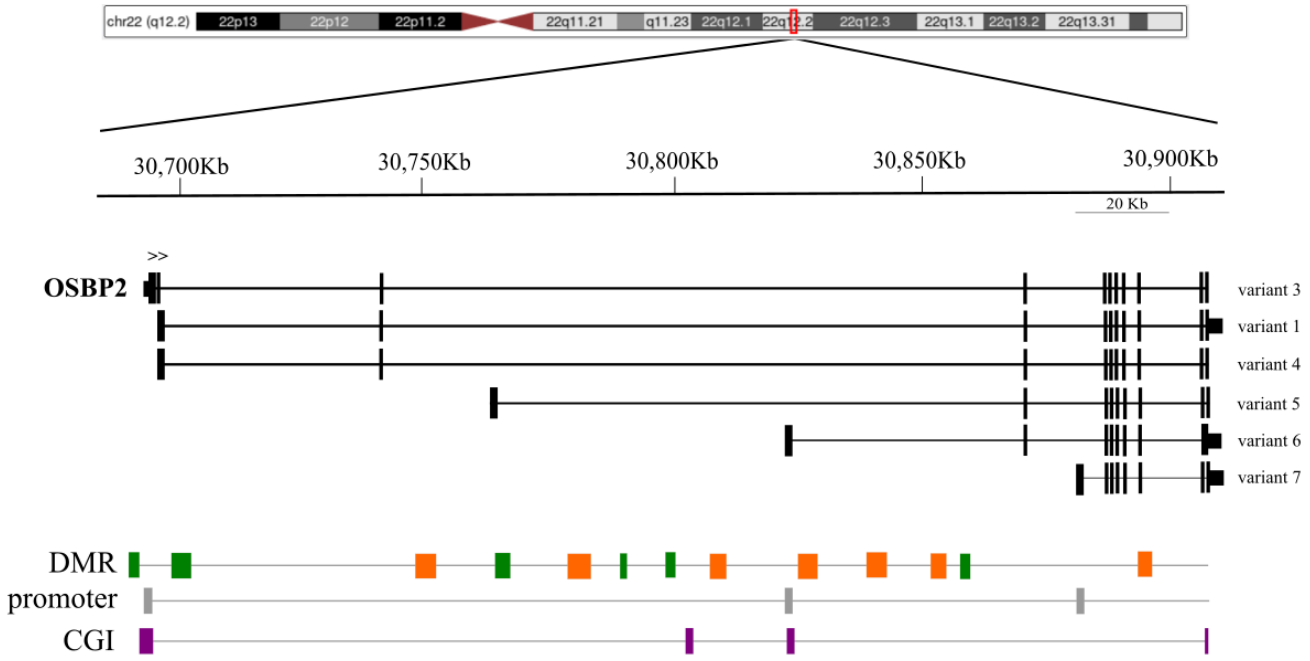

b.

Chr	Start	End	Annotation	Gene	Distance to main TSS (bp)	Methylation Log_2FC	Methylation Status	Methylayion P value
chr22	30690501	30690600	Intergen	OSBP2	-3231	-1.19	hypo	0.019
chr22	30690601	30690700	Intergen	OSBP2	-3131	-1.15	hypo	0.013
chr22	30690701	30690800	Intergen	OSBP2	-3031	-1.17	hypo	0.028
chr22	30699401	30699500	gene body	OSBP2	5619	-1.77	hypo	0.018
chr22	30699501	30699600	gene body	OSBP2	5719	-1.63	hypo	0.014
chr22	30699601	30699700	gene body	OSBP2	5819	-1.41	hypo	0.044
chr22	30748401	30748500	gene body	OSBP2	54619	2.14	hyper	0.010
chr22	30748501	30748600	gene body	OSBP2	54719	2.25	hyper	0.001
chr22	30748601	30748700	gene body	OSBP2	54819	1.43	hyper	0.029
chr22	30764401	30764500	gene body	OSBP2	70619	-1.96	hypo	0.038
chr22	30764501	30764600	gene body	OSBP2	70719	-3.35	hypo	0.001
chr22	30780101	30780200	gene body	OSBP2	86319	0.81	hyper	0.036
chr22	30780201	30780300	gene body	OSBP2	86419	0.87	hyper	0.014
chr22	30780301	30780400	gene body	OSBP2	86519	0.69	hyper	0.044
chr22	30780401	30780500	gene body	OSBP2	86619	0.72	hyper	0.029
chr22	30788801	30788900	gene body	OSBP2	95019	-1.08	hypo	0.038
chr22	30797901	30798000	gene body	OSBP2	104119	-1.90	hypo	0.013
chr22	30807601	30807700	gene body	OSBP2	113819	1.29	hyper	0.006
chr22	30824601	30824700	gene body	OSBP2	130819	0.91	hyper	0.019
chr22	30826301	30826400	gene body	OSBP2	132519	0.86	hyper	0.048
chr22	30838801	30838900	gene body	OSBP2	145019	1.27	hyper	0.039
chr22	30838901	30839000	gene body	OSBP2	145119	1.35	hyper	0.037
chr22	30839001	30839100	gene body	OSBP2	145219	1.46	hyper	0.036
chr22	30851701	30851800	gene body	OSBP2	157919	1.64	hyper	0.024
chr22	30856901	30857000	gene body	OSBP2	163119	-0.84	hypo	0.047
chr22	30893201	30893300	gene body	OSBP2	199419	1.67	hyper	0.030

c.

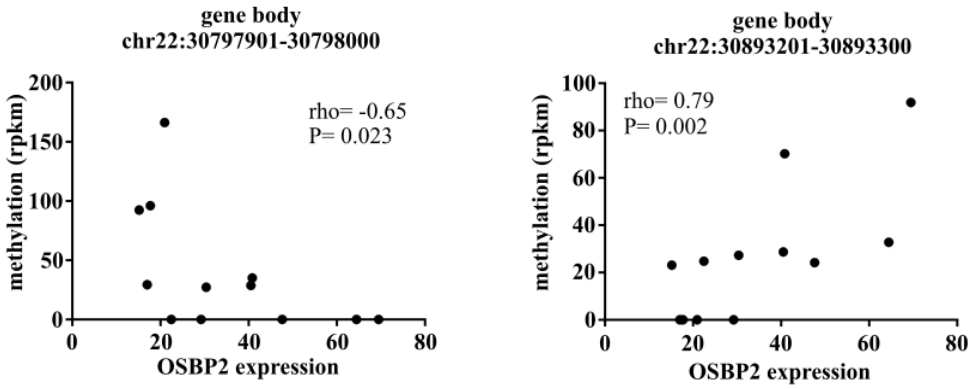

Figure 21. Description of the genomic location, methylation profile, and mRNA expression of *OSBP2* in memory B cells of RRMS patients and controls. (a) Genomic mapping of the *OSBP2* gene in chr22q12.2 and its transcript variants. The two arrows indicate the direction of the transcription. The DMRs resulting from the comparison between RRMS and controls are displayed in green and orange if hypomethylated or hypermethylated, respectively. The promoter region (grey box) and the CGIs (purple box) are represented based on the UCSC Genome Browser (Kent et al., 2002). **(b)** The list of DMRs related to *OSBP2* in memory B cells of RRMS patients in comparison to controls. The coordinates for each DMR are given in the columns 'Start' and 'End'. **(c)** Scatter plot and correlation coefficient between the relative mRNA expression of *OSBP2* and the normalized methylation values (rpkm) in memory B cells of RRMS patients and controls in the given coordinates. *bp: base pair; CGI: CpG island; chr: chromosome; DMR: differentially methylated region; hyper: hypermethylated; hypo: hypomethylated; kb: kilobase; Methylation log_2FC: fold change in logarithmic base 2 of the methylation value between RRMS patients and controls; OSBP2: oxysterol binding protein 2; rho: Spearman's test rho value; rpkm: read per kilobase million; RRMS: relapsing-remitting multiple sclerosis; TSS: transcription start site.*

4.2.5.4. *NOS1*

Nitric oxide synthase 1 (*NOS1*) is a 153,485-base-long gene located in the *minus* strand of chr12q24.22. *NOS1* has four transcript variants named 1, 2, 3 and 4 (Figure 22a). In our cohort of Bmem cells, RRMS patients presented an aberrant methylation pattern in 43 regions in comparison to controls; with 65% of them showing a hypomethylated status (Figure 22b). In eleven of the DMRs distributed across the gene body and the 3'-UTR, methylation levels were significantly correlated with *NOS1* mRNA expression (Figure 22c).

a.

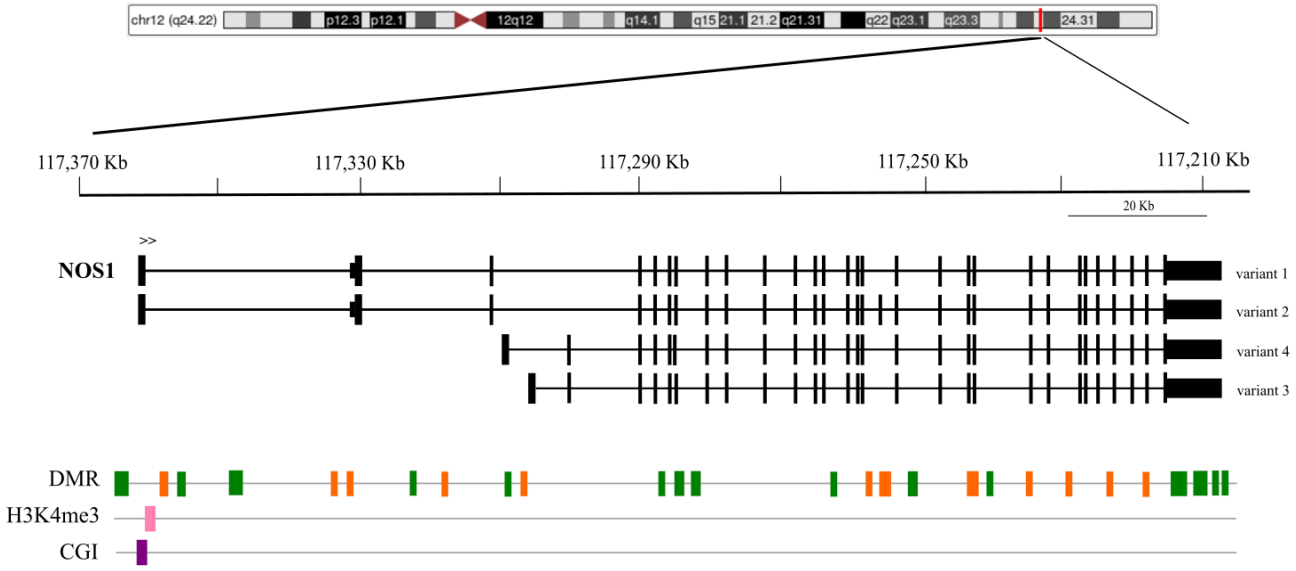

b.

Chr	Start	End	Annotation	Gene	Distance to main TSS (bp)	Methylation Log_2FC	Methylation Status	Methylation P value
chr12	117365201	117365300	intergen	NOS1	-3449	-1.45	hypo	0.038
chr12	117365101	117365200	intergen	NOS1	-3349	-1.58	hypo	0.045
chr12	117365001	117365100	intergen	NOS1	-3249	-1.94	hypo	0.013
chr12	117359201	117359300	gene body	NOS1	2551	2.09	hyper	0.021
chr12	117359101	117359200	gene body	NOS1	2651	1.75	hyper	0.014
chr12	117356701	117356800	gene body	NOS1	5051	-0.83	hypo	0.007
chr12	117356501	117356600	gene body	NOS1	5251	-0.62	hypo	0.028
chr12	117349401	117349500	gene body	NOS1	12351	-1.83	hypo	<0.001
chr12	117349301	117349400	gene body	NOS1	12451	-0.92	hypo	0.015
chr12	117349201	117349300	gene body	NOS1	12551	-0.83	hypo	0.034
chr12	117349101	117349200	gene body	NOS1	12651	-0.92	hypo	0.019
chr12	117335001	117335100	gene body	NOS1	26751	1.21	hyper	0.021
chr12	117332701	117332800	gene body	NOS1	29051	1.37	hyper	0.037
chr12	117323601	117323700	gene body	NOS1	38151	-1.00	hypo	0.049
chr12	117319301	117319400	gene body	NOS1	42451	1.26	hyper	0.008
chr12	117310901	117311000	gene body	NOS1	50851	-1.07	hypo	0.025
chr12	117308801	117308900	gene body	NOS1	52951	1.79	hyper	0.039
chr12	117289601	117289700	gene body	NOS1	72151	-1.28	hypo	0.029
chr12	117289501	117289600	gene body	NOS1	72251	-1.62	hypo	0.014
chr12	117286201	117286300	gene body	NOS1	75551	-1.52	hypo	0.029
chr12	117283901	117284000	gene body	NOS1	77851	-0.91	hypo	0.019
chr12	117283801	117283900	gene body	NOS1	77951	-1.02	hypo	0.045
chr12	117264701	117264800	gene body	NOS1	97051	-0.97	hypo	0.029
chr12	117259601	117259700	gene body	NOS1	102151	0.90	hyper	0.019
chr12	117257501	117257600	gene body	NOS1	104251	1.07	hyper	0.047
chr12	117257401	117257500	gene body	NOS1	104351	1.27	hyper	0.023

chr12	117253301	117253400	gene body	NOS1	108451	-1.78	hypo	0.014
chr12	117253201	117253300	gene body	NOS1	108551	-1.46	hypo	0.034
chr12	117245101	117245200	gene body	NOS1	116651	1.52	hyper	0.036
chr12	117245001	117245100	gene body	NOS1	116751	1.42	hyper	0.027
chr12	117242801	117242900	gene body	NOS1	118951	-1.28	hypo	0.048
chr12	117237001	117237100	gene body	NOS1	124751	1.35	hyper	0.027
chr12	117231101	117231200	gene body	NOS1	130651	0.81	hyper	0.042
chr12	117225401	117225500	gene body	NOS1	136351	1.07	hyper	0.047
chr12	117220501	117220600	gene body	NOS1	141251	0.83	hyper	0.023
chr12	117214801	117214900	3'-UTR	NOS1	146951	-0.88	hypo	0.015
chr12	117214701	117214800	3'-UTR	NOS1	147051	-1.30	hypo	0.001
chr12	117214601	117214700	3'-UTR	NOS1	147151	-2.00	hypo	<0.001
chr12	117213601	117213700	3'-UTR	NOS1	148151	-2.01	hypo	0.032
chr12	117211001	117211100	3'-UTR	NOS1	150751	-1.44	hypo	0.008
chr12	117210901	117211000	3'-UTR	NOS1	150851	-3.32	hypo	0.003
chr12	117209801	117209900	3'-UTR	NOS1	151951	-1.27	hypo	0.020
chr12	117207901	117208000	TTS	NOS1	153851	-1.01	hypo	0.009

c.

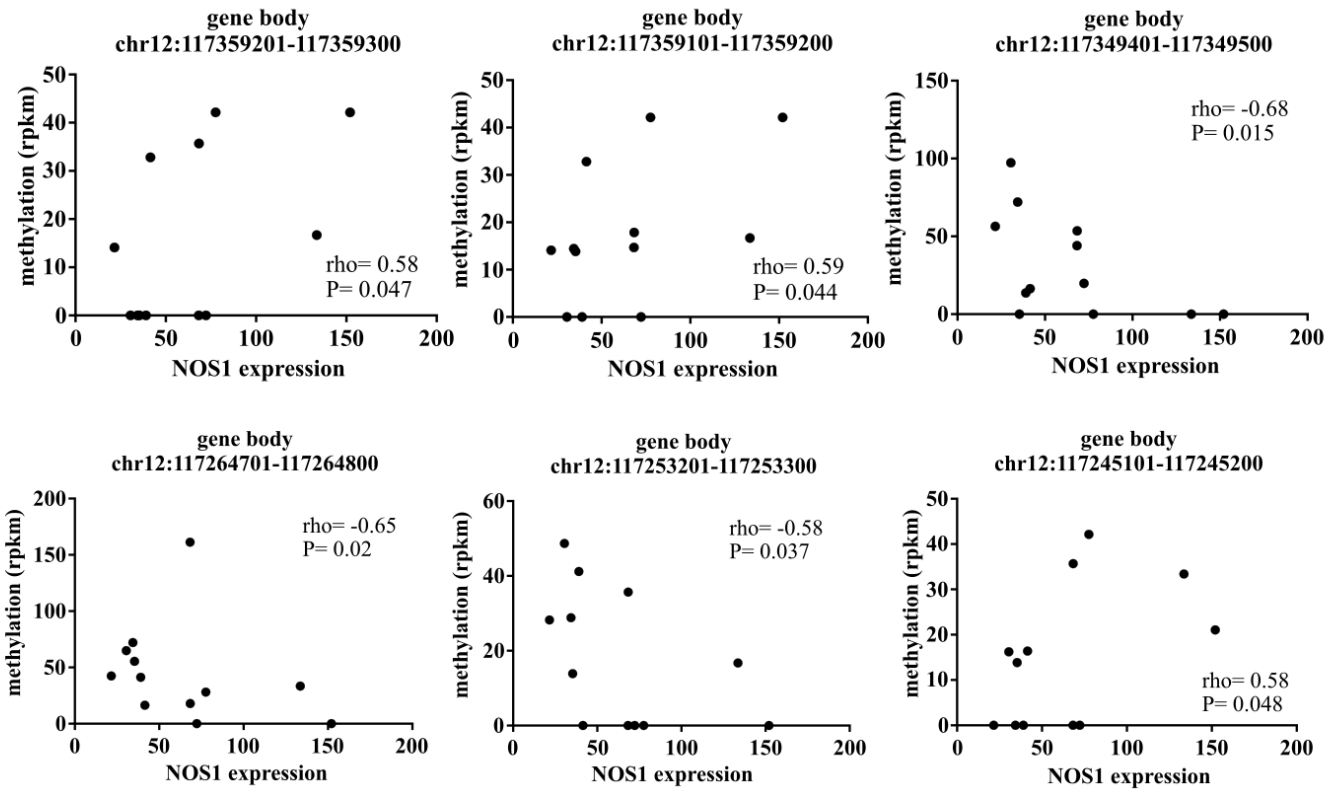

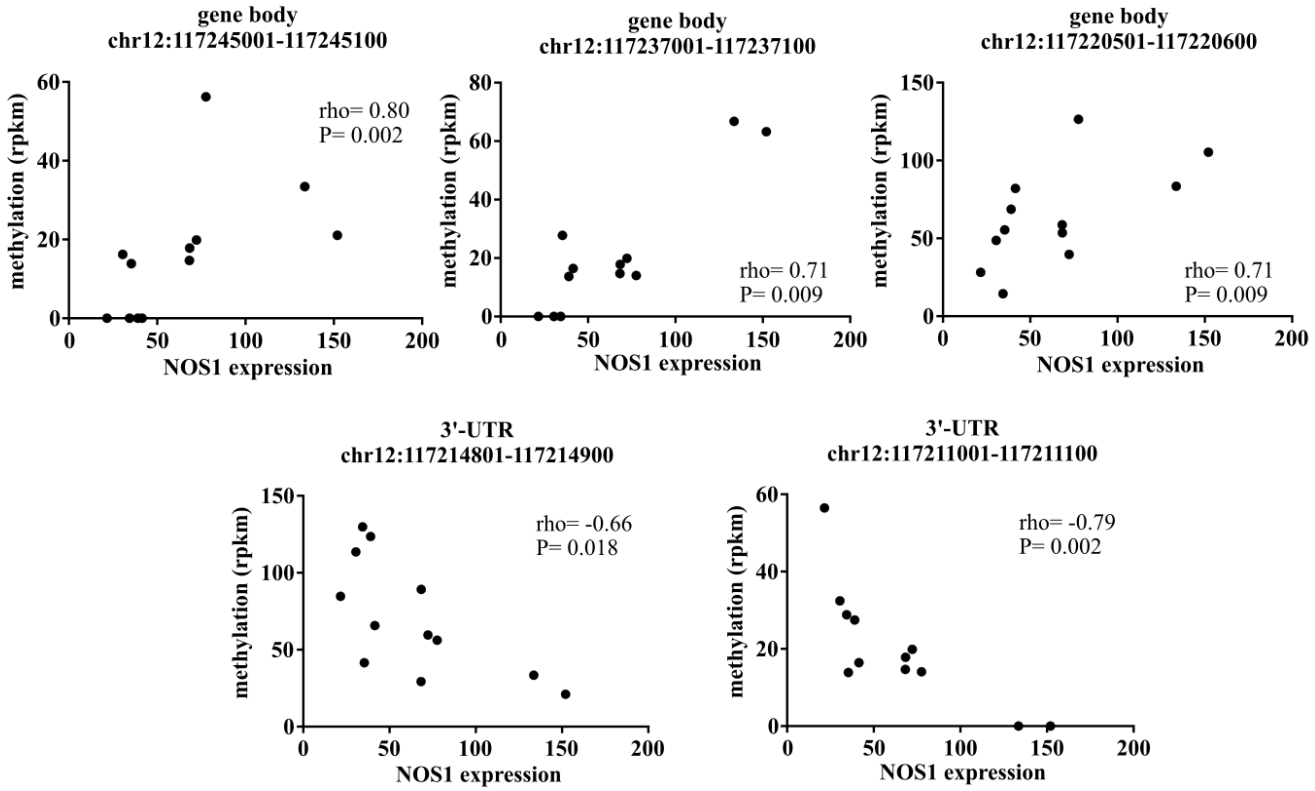

Figure 22. Description of the genomic location, methylation profile, and mRNA expression of *NOS1* in memory B cells of RRMS patients and controls. (a) Genomic mapping of the *NOS1* gene in chr12q24.22 and its transcript variants. The two arrows indicate the direction of the transcription. The DMRs resulting from the comparison between RRMS and controls are displayed in green and orange if hypomethylated or hypermethylated, respectively. The DNase-H3K4me3 mark (pink box) and the CGI (purple box) are represented based on the UCSC Genome Browser (Kent et al., 2002). **(b)** The list of DMRs related to *NOS1* in memory B cells of RRMS patients in comparison to controls. The coordinates for each DMR are given in the columns 'Start' and 'End'. **(c)** Scatter plot and correlation coefficient between the relative mRNA expression of *NOS1* and the normalized methylation values (rpkm) in memory B cells of RRMS patients and controls in the given coordinates. *bp: base pair; CGI: CpG island; chr: chromosome; DMR: differentially methylated region; hyper: hypermethylated; hypo: hypomethylated; kb: kilobase; Methylation log_2FC: fold change in logarithmic base 2 of the methylation value between RRMS patients and controls; NOS1: nitric oxide synthase 1; rho: Spearman's test rho value; rpkm: read per kilobase million; RRMS: relapsing-remitting multiple sclerosis; TSS: transcription start site.*

4.2.5.5. *ECEL1P2*

Endothelin converting enzyme like 1 pseudogene 2 (*ECEL1P2*) is a pseudogene located in the *minus* strand of chr2q37.1 (Figure 23a). In our study, it was found that RRMS patients had a 200-base-long hypermethylated region in the promoter of *ECEL1P2* in comparison to controls ([chr2:232387601-232387700], *Methylation $log_2FC=1.75$, $P=0.031$*; [chr2:232387701-232387800], *Methylation $log_2FC=1.53$, $P=0.030$*) (Figure 23a,b). This region is part of a CGI (Figure 23a). However, no significant association was found between ECEL1P2 mRNA expression and methylation in this region ([chr2:232387601-232387700], *rho=0.02; P=0.95;* [chr2:232387701-232387800], *rho=-0.15; P=0.68*) (Figure 23c).

a.

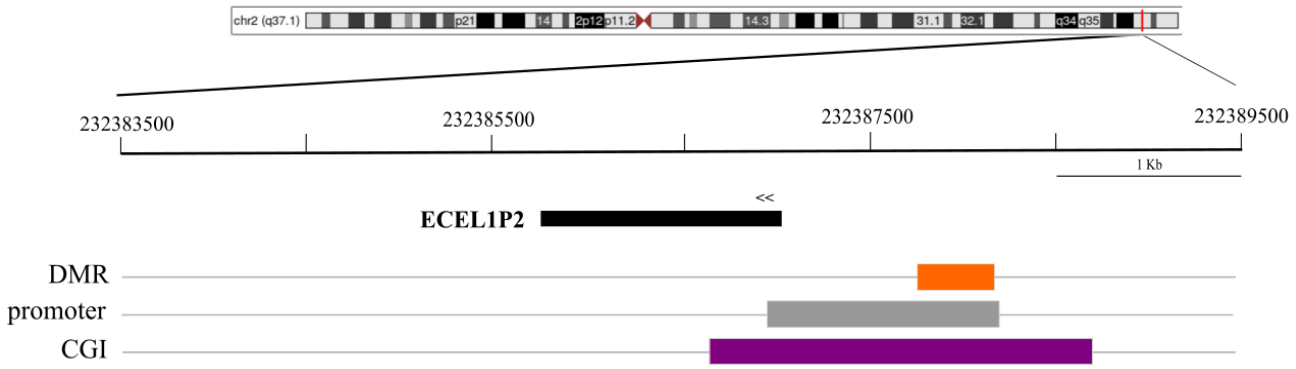

b.

Chr	Start	End	Annotation	Gene	Distance to TSS (bp)	Methylation Log_2FC	Methylation Status	Methylation P value
chr2	232387601	232387700	promoter-TSS	ECEL1P2	-607	1.75	hyper	0.031
chr2	232387701	232387800	promoter-TSS	ECEL1P2	-707	1.53	hyper	0.030

c.

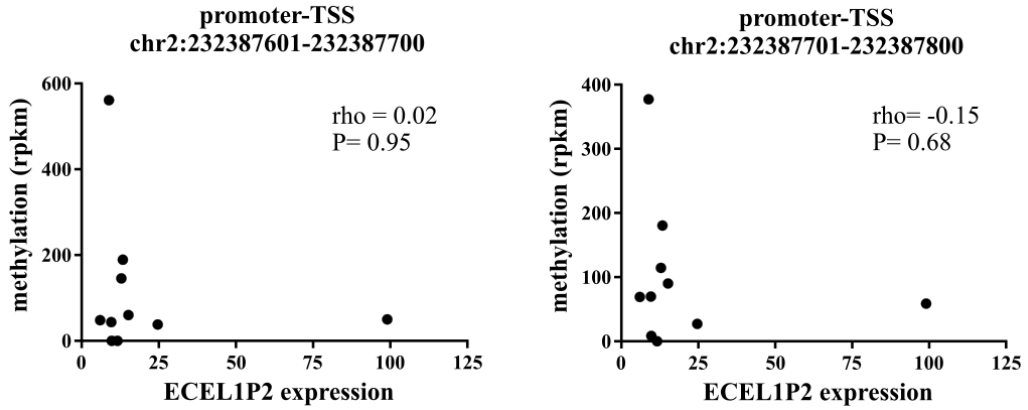

Figure 23. Description of the genomic location, methylation profile, and mRNA expression of *ECEL1P2* in regulatory T cells of RRMS patients and controls. (a) Genomic mapping of *ECEL1P2* in chr2q37.1. The two arrows indicate the direction of the transcription. The DMRs resulting from the comparison between RRMS and controls are displayed in orange indicating hypermethylation. The promoter region (grey box) and the CGIs (purple box) are represented according to UCSC Genome Browser (Kent et al., 2002). **(b)** The list of the DMRs related to *ECEL1P2* in regulatory T cells isolated from RRMS patients when compared to controls. The coordinates for each DMR are given in the columns 'Start' and 'End'. **(c)** Scatter plot and correlation coefficient between the relative mRNA expression of *ECEL1P2* and the normalized methylation values (rpkm) in regulatory T cells of RRMS patients and controls in the given coordinates. *bp: base pair; CGI: CpG island; chr: chromosome; DMR: differentially methylated region; ECEL1P2: endothelin converting enzyme like 1 pseudogene 2; hyper: hypermethylated; hypo: hypomethylated; Methylation log_2FC: fold change in logarithmic base 2 of the methylation value between RRMS patients and controls; rho: Spearman's test rho value; rpkm: read per kilobase million; RRMS: relapsing-remitting multiple sclerosis; TSS: transcription start site.*

4.2.6. Summary

We analysed the mRNA expression of 22 differentially methylated candidate genes in both cell subsets collected from RRMS patients and controls. In Bmem cells, *PTGFRN*, *NOS1* and *OSBP2* showed upregulation in RRMS patients while *IL21R* was downregulated in comparison to controls. All these genes exhibited a significant association between mRNA expression and the addition of methyl groups at different locations within their nucleotide sequence. In Treg cells, RRMS patients presented lower mRNA levels of *ECEL1P2* than the control group. No association was observed between methylation in *ECEL1P2* promoter and its transcription rate.

4.3. VALIDATION STUDY AT RNA LEVEL: CANDIDATE miRNA GENES

We explored how changes in the methylation pattern of miRNA genes in both immune cells could affect their expression at RNA level. For this purpose, the relative expression of 164 and 181 mature miRNAs was analysed in Bmem and Treg cells, respectively, using TaqMan® OpenArray™ Human Advanced microRNA panels (Applied Biosystems, Germany). In some cases, both strands of the mature miRNA (5p and 3p strands) were analysed (e.g., miR-450-3p and miR-450-5p were analysed for the *MIR450* gene).

4.3.1. List of studied candidate miRNAs

The complete list of studied mature miRNAs is described in Annex VII.

4.3.2. Methylation profile of the studied miRNA genes

The location of DMRs associated with candidate miRNA genes in both cell types is summarized in Table 8 and Table 9. The pre-miRNA sequence was used as a reference to assign the location of DMRs as follows: up to ± 2 kb from pre-miRNA sequence; between 2 kb to 10 kb from both sides of the pre-miRNA sequence; and more than ± 10 kb from the pre-miRNA sequence. This approximation was set according to Saini et al., 2007.

Table 8. Distribution of the DMRs related to candidate miRNA genes in memory B cells. The '0' indicates the position where the pre-miRNA sequence starts. The (X) refers to the comparison between RRMS and controls while (Q) is assigned when comparing SPMS vs RRMS. *DMR: differentially methylated region; kb: kilobase; RRMS: relapsing-remitting multiple sclerosis; SPMS: secondary-progressive multiple sclerosis.*

Memory B cells						
GENE NAME	**> -10 kb**	**-2 kb to -10 kb**	**-2 kb to 0**	**0 to +2 kb**	**+2 kb to +10 kb**	**> +10 kb**
MIR1-1	Q	Q	Q	Q	Q	
MIR100	XQ	XQ	XQ	XQ	XQ	XQ
MIR101-1			X			
MIR103A1		XQ				
MIR103A2	XQ	Q	Q			
MIR107	XQ		Q	X	XQ	XQ
MIR122	XQ	Q	Q			
MIR124-1	XQ	Q	Q			
MIR1249				Q	Q	
MIR125B	Q	Q	X	X	XQ	XQ
MIR126		Q		Q	Q	
MIR1260A	XQ	Q	Q			
MIR1264					Q	XQ
MIR128	XQ				X	XQ
MIR129-2		Q			XQ	XQ
MIR1298	X					X
MIR132				XQ		
MIR133A1	XQ	Q				XQ
MIR133B			XQ			
MIR135A	X	Q				
MIR137	XQ	Q			X	
MIR143	X	Q				
MIR145					X	XQ
MIR146A		Q			XQ	XQ
MIR146B		X			XQ	
MIR148A	XQ	Q	X		Q	XQ
MIR148B					Q	
MIR150			X	Q		
MIR151A	XQ	XQ	X			
MIR153-1		Q	Q	Q	Q	
MIR155	XQ	Q		Q	XQ	
MIR15A	Q	X				
MIR17	XQ	Q				
MIR181A	XQ	Q				XQ
MIR181B1					XQ	XQ
MIR181C		XQ	Q			
MIR183	XQ		XQ			
MIR185			Q	X	Q	Q
MIR186				Q	XQ	
MIR190A	XQ	X	Q		X	XQ
MIR1911	XQ			Q	X	XQ
MIR193A		X		Q		
MIR194-1	XQ	X				
MIR196A1	XQ	Q				
MIR199A1			Q		XQ	Q
MIR200C		X	Q	Q		
MIR203A	XQ	Q				
MIR204	XQ	XQ			X	XQ
MIR205					Q	XQ
MIR206	XQ					
MIR21	XQ	XQ			XQ	Q
MIR210			Q		X	
MIR211	XQ		Q		XQ	Q
MIR216A			XQ	Q		
MIR218	XQ	XQ	Q		XQ	XQ
MIR219A			XQ	XQ		
MIR22				Q		
MIR221				X		

MIR222	XQ	XQ				
MIR223	XQ				Q	
MIR23A			Q			
MIR23B		XQ	XQ			
MIR26A1	XQ	XQ			Q	X
MIR26B					XQ	
MIR28	XQ	XQ	X		X	XQ
MIR29A				XQ	XQ	XQ
MIR29C				Q	XQ	XQ
MIR30A		Q			Q	XQ
MIR30C-1					XQ	XQ
MIR30C-2	XQ	X			XQ	XQ
MIR30D	Q	Q		Q		
MIR30E		Q		X		
MIR31	X	X	X	Q	XQ	Q
MIR32	XQ			Q	XQ	XQ
MIR320A				Q	Q	
MIR320B1				XQ	X	Q
MIR325	XQ	Q	X	Q		XQ
MIR326					X	XQ
MIR328	Q	XQ	Q			
MIR335					X	XQ
MIR338		Q	Q			
MIR339			Q	XQ	Q	Q
MIR342				X	X	XQ
MIR34A	XQ	XQ		X	XQ	Q
MIR361	XQ	XQ			Q	Q
MIR363				Q	XQ	XQ
MIR373				X	XQ	Q
MIR374B	XQ	X	Q			
MIR375					X	
MIR376C			Q			
MIR378A					Q	XQ
MIR383	XQ	XQ		X	Q	XQ
MIR411				Q		
MIR424			Q			
MIR448	XQ	X			Q	XQ
MIR449A					Q	
MIR450B					XQ	XQ
MIR452		X	Q			
MIR454		Q		Q	XQ	Q
MIR455	XQ	XQ	Q	Q		X
MIR483				Q	XQ	XQ
MIR486-1			Q			
MIR487A				X		
MIR489	XQ		Q			
MIR490	Q	XQ		Q	Q	XQ
MIR497			Q			
MIR502					Q	
MIR505			Q		XQ	XQ
MIR513A1			XQ		X	
MIR515-1				XQ		
MIR518E			Q			
MIR520H			XQ			
MIR523				X		
MIR532	XQ	X				
MIR548D1	Q					
MIR548E	XQ	XQ	XQ		X	XQ
MIR548K			X		XQ	XQ
MIR548N	XQ	XQ		Q	XQ	XQ
MIR551A	XQ	Q	Q		Q	XQ
MIR570		Q	X	Q	XQ	X
MIR576	XQ	XQ	Q	Q	XQ	XQ
MIR583	XQ	XQ	XQ	X	XQ	XQ
MIR593	XQ	Q		Q		XQ
MIR615				XQ	Q	

MIR628		XQ	XQ		Q	XQ
MIR633	XQ	X			XQ	Q
MIR642A		Q				
MIR645	XQ		X		XQ	Q
MIR652	Q	XQ		X	Q	Q
MIR653					XQ	XQ
MIR660				Q		
MIR664A				XQ	Q	XQ
MIR770-1	X	X	X	X		
MIR876			X		XQ	XQ
MIR885	XQ	XQ	X			XQ
MIR9-1					XQ	XQ
MIR92A1						XQ
MIR92B					XQ	
MIR93			X			
MIR937			Q	Q	Q	Q
MIR939		Q	Q	Q	Q	
MIR99A	XQ	XQ	XQ	XQ	XQ	XQ
MIR99B			Q	Q		
MIRLET7A1	XQ					
MIRLET7B		XQ	Q	XQ	XQ	XQ
MIRLET7C			X		Q	Q
MIRLET7E			Q	Q		
MIRLET7F-2	XQ	Q	Q			
MIRLET7G		Q	Q	Q	XQ	
MIRLETI				XQ	Q	XQ

Table 9. Distribution of the DMRs related to candidate miRNA genes in regulatory T cells. The '0' indicates the position where the pre-miRNA sequence starts. The (X) refers to the comparison between RRMS and controls while (Q) is assigned when comparing SPMS vs RRMS. *DMR: differentially methylated region; kb: kilobase; RRMS: relapsing-remitting multiple sclerosis; SPMS: secondary-progressive multiple sclerosis.*

Regulatory T cells						
GENE NAME	**> -10 kb**	**-2 kb to -10 kb**	**-2 kb to 0**	**0 to +2 kb**	**+2 kb to +10 kb**	**> +10 kb**
MIR1-1	XQ	XQ	XQ	Q	Q	
MIR100	XQ	XQ	XQ	XQ	XQ	XQ
MIR101-1		Q				
MIR103A		Q	Q	Q		
MIR103A2		XQ	Q			
MIR106B		Q	Q			
MIR107	XQ	Q	Q		Q	Q
MIR10A				XQ		
MIR10B			X	Q		
MIR122	XQ	XQ	Q			
MIR124-1	XQ	XQ	X	Q		
MIR1249		Q	Q	Q	XQ	
MIR125A			Q			
MIR125B1				Q	Q	XQ
MIR126		Q	Q	XQ	Q	
MIR1260A	XQ	XQ	XQ	Q		
MIR1264				Q	Q	Q
MIR127			Q	Q		
MIR128-1	XQ	XQ		Q	XQ	XQ
MIR129-2		Q		Q	Q	XQ
MIR1298	XQ	Q		Q		Q
MIR130A	Q	XQ			Q	
MIR132					X	
MIR133A1	X			Q	Q	XQ
MIR133B				Q		
MIR135A1		XQ	Q	Q	Q	
MIR137	XQ	XQ	Q			
MIR143	XQ	Q				
MIR145					XQ	XQ
MIR146A					XQ	XQ
MIR146B			Q		Q	

MIR148A	XQ	XQ	Q	Q	XQ	XQ
MIR148B					XQ	
MIR150		Q		Q		
MIR151A	XQ	XQ			X	
MIR153-1		XQ	Q		Q	
MIR155	X	XQ	Q		XQ	
MIR15A	Q	XQ				
MIR15B			Q			
MIR17	XQ	Q				
MIR181A1	XQ	XQ	Q			
MIR181B1				Q	XQ	XQ
MIR181C		Q	Q			
MIR183	XQ	XQ	Q	Q		
MIR185			Q	Q	XQ	XQ
MIR186		XQ	Q	Q	XQ	
MIR190A	XQ	Q	Q		Q	Q
MIR1911	XQ	Q	Q	XQ	Q	XQ
MIR193A	Q	Q	Q	Q	XQ	
MIR194-1	XQ	Q	XQ			
MIR195				Q		
MIR196A1	XQ	Q	XQ	XQ	X	
MIR199A		Q	Q	Q	XQ	Q
MIR200C		X	Q			
MIR203A	XQ	XQ				
MIR204	XQ	Q			Q	XQ
MIR205				Q	Q	XQ
MIR206	XQ			X		
MIR21	XQ	X			XQ	XQ
MIR210		Q	X			
MIR211	Q	Q	Q	Q	Q	XQ
MIR216A		Q				
MIR218-1	XQ	Q	X	Q	XQ	XQ
MIR219A1			XQ			
MIR22				Q		
MIR221				Q	Q	
MIR222	XQ	Q	Q			
MIR223	XQ	XQ		Q	Q	
MIR23A			Q			
MIR23B		XQ	Q			
MIR24-1			Q	Q		
MIR25			Q			
MIR26A1	XQ	XQ	Q		XQ	
MIR26B			Q	Q	Q	
MIR27B			Q	Q		
MIR28	Q	Q			Q	Q
MIR29A			Q	Q	XQ	X
MIR29C	X				Q	XQ
MIR30A		Q		XQ	Q	XQ
MIR30C1				Q	XQ	XQ
MIR30C2	XQ	XQ	Q		Q	XQ
MIR30D	XQ	XQ	Q	Q		
MIR30E		XQ	XQ			
MIR31	Q	Q		XQ	Q	Q
MIR32	XQ	XQ		Q	XQ	Q
MIR320A					XQ	
MIR320B1					XQ	Q
MIR323A			X			
MIR325	X	XQ		Q	XQ	XQ
MIR326		Q	Q		XQ	XQ
MIR328		XQ	Q	Q		
MIR335			Q	Q	Q	XQ
MIR338		XQ	XQ			
MIR339		Q	Q	Q	XQ	Q
MIR342				Q	XQ	XQ
MIR34A	XQ	XQ		Q	XQ	
MIR361	XQ	XQ	X		Q	XQ
MIR363				XQ	XQ	XQ
MIR369		X	Q	Q	X	X

MIR373			X		XQ	XQ
MIR374B	Q	XQ				
MIR375				Q		
MIR378A			Q	Q	XQ	Q
MIR383	XQ	XQ			Q	XQ
MIR410				Q		
MIR411						
MIR412				Q		
MIR424			Q			
MIR448	XQ	Q				XQ
MIR450B				Q	Q	XQ
MIR452		Q	X			
MIR454			Q		XQ	Q
MIR455	XQ	XQ	Q	Q	Q	XQ
MIR483			Q	Q	XQ	XQ
MIR486-1			Q			
MIR487A			Q			
MIR489	Q	Q				
MIR490	Q	Q	Q		XQ	XQ
MIR497HG			Q	Q		
MIR502				Q	Q	Q
MIR505		Q	XQ	Q	Q	XQ
MIR513A1			Q		Q	
MIR516B1			Q			
MIR518D			Q			
MIR518E			X			
MIR520H					X	
MIR548D1	XQ	Q				
MIR548E	XQ	Q	Q	Q	Q	XQ
MIR548K		Q		Q	XQ	XQ
MIR548N	XQ	Q	XQ	X	Q	XQ
MIR551A	XQ	XQ	Q	Q	XQ	XQ
MIR570		Q	Q	XQ	XQ	
MIR576	Q	Q	Q	Q	XQ	XQ
MIR583	XQ	XQ		Q	X	XQ
MIR593	XQ	XQ	XQ	X	XQ	XQ
MIR615				X	X	
MIR628	XQ	XQ		Q	Q	XQ
MIR633	XQ	Q	XQ	Q	XQ	
MIR642A		X				
MIR645	XQ	XQ		Q	XQ	Q
MIR652	Q	Q	Q		Q	Q
MIR653				Q	Q	XQ
MIR656			Q			
MIR660			XQ			
MIR664A				XQ	XQ	XQ
MIR770	Q	Q		Q	XQ	
MIR876		XQ	Q	Q	Q	XQ
MIR885	XQ	XQ	Q	Q	Q	XQ
MIR9-1					Q	XQ
MIR92A1				X	Q	XQ
MIR92B					Q	
MIR93			Q	Q		
MIR937			Q	Q	Q	Q
MIR939		Q	Q	Q	Q	
MIR99A	X	X	X	XQ	X	X
MIR99B			Q	Q		
MIRLET7A1	XQ		Q			
MIRLET7B			XQ	Q	Q	Q
MIRLET7C			Q	Q		Q
MIRLET7E			Q	Q		
MIRLET7F				Q		
MIRLET7F2	XQ	X	XQ			
MIRLET7G					Q	
MIRLET7I				Q	XQ	XQ

4.3.3. Transcriptome of candidate miRNAs genes

The relative expression of 164 and 181 mature miRNAs was assessed in Bmem and Treg cells, respectively, using TaqMan® OpenArray™ Human Advanced microRNA panels (Applied Biosystems, Germany).

4.3.3.1. Samples

In Bmem cells, the expression of miRNAs derived from 10 controls, 9 RRMS and 10 SPMS patients was studied (Annex VI). In Treg cells, a total of 5 controls, 5 RRMS and 3 SPMS samples were analysed; some samples were discarded due to the low amount of RNA available (Annex VI).

4.3.3.2. Performance of the TaqMan® OpenArray™ Human Advanced microRNA panel

In Bmem cells, 86 out of 164 candidate miRNAs (52%) showed expression in at least one of the samples (Table 10). In the Treg cell subset, 85 out of 181 candidate miRNAs (47%) exhibited detectable expression in at least one of the samples (Table 11).

Table 10. Classification of candidate miRNAs based on their detectability among samples in memory B cells. List of candidate miRNAs in the memory B cell population based on their detectability across samples. The left column corresponds to the distinct levels of miRNA expression across samples depicted in percentages. The middle column points out the number of miRNAs for each level. The right column comprises the list of miRNAs matched to the expression levels.

Memory B cells		
Category	n (cumulative)	*miRNAs*
Expressed in 100% of the samples	15	*let-7b-5p, let-7g-5p, miR-150-5p, miR-155-5p, miR-181a-5p, miR-181b-5p, miR-181c-5p, miR-223-3p, miR-26b-5p, miR-29a-3p, miR-339-5p, miR-342-3p, miR-361-3p, miR-448, miR-93-5p*
Highly expressed (70-99% of the samples)	26 (41)	*miR-1249-3p, miR-1260a, miR-128-3p, miR-146a-5p, miR-148b-3p, miR-151a-3p, miR-151a-5p, miR-17-5p, miR-185-5p, miR-186-5p, miR-193a-5p, miR-21-5p, miR-210-3p, miR-221-3p, miR-222-3p, miR-23a-3p, miR-26a-5p, miR-29c-5p, miR-30d-5p, miR-326, miR-328-3p, miR-361-5p, miR-486-5p, miR-532-3p, miR-532-5p, miR-92b-3p*
Moderately expressed (30-69% of the samples)	18 (59)	*let-7i-5p, miR-101-3p, miR-107, miR-145-5p, miR-148a-3p, miR-194-5p, miR-199a-3p, miR-320a, miR-338-3p, miR-374b-5p, miR-378a-3p, miR-378a-5p, miR-452-3p, miR-505-3p, miR-653-3p, miR-660-5p, miR-664a-3p, miR-92a-3p*
Lowly expressed (1-29% of the samples)	27 (86)	*let-7a-5p, let-7b-3p, miR-103a-2-5p, miR-103a-3p, miR-125b-5p, miR-132-3p, miR-133a-3p, miR-153-3p, miR-200c-3p, miR-204-5p, miR-22-3p, miR-23b-3p, miR-28-5p, miR-30c-1-3p, miR-30e-3p, miR-320b, miR-31-5p, miR-32-5p, miR-325, miR-34a-3p, miR-452-5p, miR-455-3p, miR-548e-3p, miR-583, miR-615-3p, miR-652-3p, miR-99b-5p*
Not expressed /undetected	78 (164)	*let-7c-5p, let-7e-5p, let-7f-2-3p, miR-1-3p, miR-100-3p, miR-100-5p, miR-122-5p, miR-124-3p, miR-126-5p, miR-1264, miR-129-2-3p, miR-1298-5p, miR-130a-3p, miR-133b, miR-135a-5p, miR-137, miR-143-3p, miR-145-3p, miR-146b-5p, miR-15a-5p, miR-183-3p, miR-190a-5p, miR-1911-5p, miR-196a-5p, miR-199a-5p, miR-203a-3p, miR-205-5p,*

		miR-206, miR-211-5p, miR-216a-5p, miR-218-5p, miR-219a-5p, miR-30a-3p, miR-30c-2-3p, miR-335-5p, miR-34a-5p, miR-363-3p, miR-373-3p, miR-375, miR-376c-3p, miR-383-5p, miR-411-5p, miR-424-5p, miR-449a, miR-450b-3p, miR-450b-5p, miR-454-3p, miR-483-3p, miR-483-5p, miR-487a-3p, miR-489-3p, miR-490-3p, miR-497-5p, miR-502-3p, miR-513a-5p, miR-515-3p, miR-518e-3p, miR-520h, miR-523-3p, miR-548d-5p, miR-548k, miR-548n, miR-551a, miR-570-3p, miR-576-3p, miR-593-5p, miR-628-3p, miR-633, miR-642a-5p, miR-645, miR-770-5p, miR-876-3p, miR-885-5p, miR-9-3p, miR-9-5p, miR-937-3p, miR-939-5p, miR-99a-3p

Table 11. Classification of candidate miRNAs based on their detectability among samples in regulatory T cells. List of candidate miRNAs in the regulatory T cell population based on their detectability across samples. The left column corresponds to the distinct levels of miRNA expression across samples depicted in percentages. The middle column points out the number of miRNAs for each level. The right column comprises the list of miRNAs matched to the expression levels.

Regulatory T cells		
Category	n (cumulative)	*miRNAs*
Expressed in 100% of the samples	15	*let-7b-5p, let-7g-5p, miR-150-5p, miR-181a-5p, miR-181b-5p, miR-181c-5p, miR-185-5p, miR-222-3p, miR-23a-3p, miR-24-3p, miR-339-5p, miR-342-3p, miR-361-3p, miR-448, miR-452-3p*
Highly expressed (70-99% of the samples)	18 (33)	*miR-1260a, miR-128-3p, miR-146a-5p, miR-155-5p, miR-17-5p, miR-21-5p, miR-210-3p, miR-221-3p, miR-223-3p, miR-25-3p, miR-29a-3p, miR-30d-5p, miR-326, miR-328-3p, miR-361-5p, miR-374b-5p, miR-92b-3p, miR-93-5p*
Moderately expressed (30-69% of the samples)	20 (53)	*let-7a-5p, let-7i-5p, miR-106b-3p, miR-107, miR-1249-3p, miR-125b-5p, miR-132-3p, miR-145-5p, miR-15b-5p, miR-186-5p, miR-193a-5p, miR-26a-5p, miR-26b-5p, miR-29c-5p, miR-320a, miR-452-5p, miR-486-5p, miR-653-3p, miR-664a-3p, miR-92a-3p*
Lowly expressed (1-29% of the samples)	32 (85)	*let-7c-5p, let-7e-5p, let-7f-5p, miR-101-3p, miR-103a-2-5p, miR-103a-3p, miR-106b-5p, miR-124-3p, miR-125a-5p, miR-1298-5p, miR-148a-3p, miR-148b-3p, miR-194-5p, miR-199a-3p, miR-199a-5p, miR-204-5p, miR-22-3p, miR-27b-3p, miR-28-5p, miR-30e-3p, miR-31-5p, miR-320b, miR-338-3p, miR-378a-3p, miR-378a-5p, miR-505-3p, miR-505-3p, miR-583, miR-628-3p, miR-660-5p, miR-9-3p, miR-99b-5p*
Not expressed /undetected	96 (181)	*let-7b-3p, let-7f-2-3p, miR-1-3p, miR-100-3p, miR-100-5p, miR-10a-5p, miR-10b-5p, miR-122-5p, miR-125a-3p, miR-126-5p, miR-1264, miR-127-3p, miR-129-2-3p, miR-130a-3p, miR-133a-3p, miR-133b, miR-135a-5p, miR-137, miR-143-3p, miR-145-3p, miR-146b-5p, miR-151a-3p, miR-151a-5p, miR-153-3p, miR-15a-5p, miR-183-3p, miR-190a-5p, miR-1911-5p, miR-195-5p, miR-196a-5p, miR-200c-3p, miR-203a-3p, miR-205-5p, miR-206, miR-211-5p, miR-216a-5p, miR-218-5p, miR-219a-5p, miR-23b-3p, miR-27b-5p, miR-30a-3p, miR-30c-1-3p, miR-30c-2-3p, miR-32-5p, miR-323a-3p, miR-325, miR-335-5p, miR-34a-3p, miR-34a-5p, miR-363-3p, miR-369-3p, miR-369-5p, miR-373-3p, miR-375, miR-383-5p, miR-410-3p, miR-411-5p, miR-412-3p, miR-424-5p, miR-450b-3p, miR-450b-5p, miR-454-3p, miR-455-3p, miR-483-3p, miR-483-5p, miR-487a-3p, miR-489-3p, miR-490-3p, miR-497-5p, miR-502-3p, miR-513a-5p, miR-516b-5p, miR-518d-3p, miR-518e-3p, miR-520h, miR-548d-5p, miR-548e-3p, miR-548k, miR-548n, miR-551a, miR-570-3p, miR-576-3p, miR-593-5p, miR-615-3p, miR-633, miR-642a-5p, miR-645, miR-652-3p, miR-656-3p, miR-770-5p, miR-876-3p, miR-885-5p, miR-9-5p, miR-937-3p, miR-939-5p, miR-99a-3p*

4.3.3.3. Quality control and pre-processing of the amplification curves

A correlation study including the Cq_conf, the Amp_Score and the Cq values was performed to define the optimal threshold for each parameter. Results indicated that Cq_conf and Amp_Score were strongly associated in both Bmem and Treg cells (Annex VIII and IX). However, in several data point samples with high Cq_conf values presented very low Amp_Score values, and vice

versa (Annex VIII and IX). Subsequently, both Cq_conf and Amp_Score measures were taken into account. The samples that satisfied the following criteria were included in the analysis: first, an Amp_Score ≥ 0.8; second, a Cq_conf ≥ 0.5; and finally, a Cq value between 15 and 35.

In both immune cell types, miR-92a-3p did not fit the criteria in any of the samples and consequently it was excluded from the study.

Afterwards, a correlation analysis between the Cq values of both replicates was performed for all detectable miRNAs. The replicates showed a very strong correlation both in Bmem (*rho=0.92; P<0.001*) and Treg cells (*rho=0.92; P<0.001*) as depicted in Figure 24. These results underpinned the way we used to analyse the replicates in order to avoid the loss of data that would diminish the statistical strength of our comparisons.

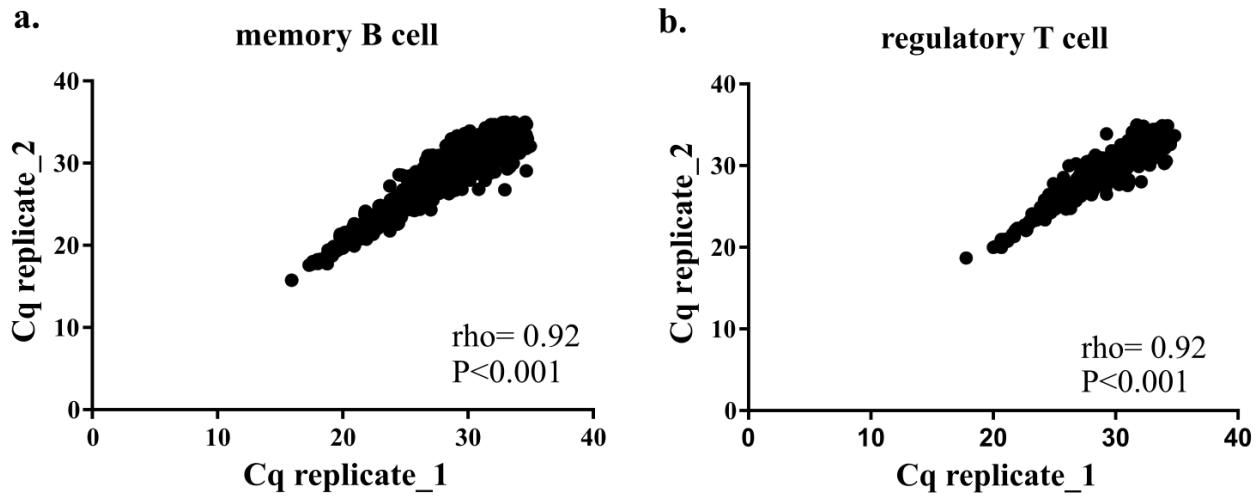

Figure 24. Scatter plot and correlation coefficient between the Cq values of the replicates for all detectable miRNAs in memory B and regulatory T cells. **(a)** Correlation between the Cq values of the replicates for the expressed miRNAs in memory B cells (n=86). **(b)** Correlation between the Cq values of the replicates for the expressed miRNAs in regulatory T cells (n=85). *Cq: quantification cycle; rho=Spearman's test rho value.*

4.3.3.4. Differential miRNA expression among the groups of study

Next, only miRNAs showing statistically significant results among the groups of study are further evaluated. In the Bmem population, it was found that miR-181c-5p was downregulated in RRMS patients in comparison to controls (*U=16.00; P=0.017*) (Figure 25 and Table 12a). On the other hand, SPMS patients presented lower expression of miR-150-5p (*U=15.00; P=0.013*); miR-193a-5p (*U=7.00; P=0.029*); miR-26a-5p (*U=13.00; P=0.027*); miR-29a-3p (*U=0.00; P<0.001*); miR-30d-5p (*U=2.00; P<0.001*); and miR-92b-3p (*U=6.00; P=0.001*) in comparison

to the RRMS group (Figure 25 and Table 12b). In contrast, no statistical differences were reported in the Treg cell population. Results for the second replicate are depicted in Annex X.

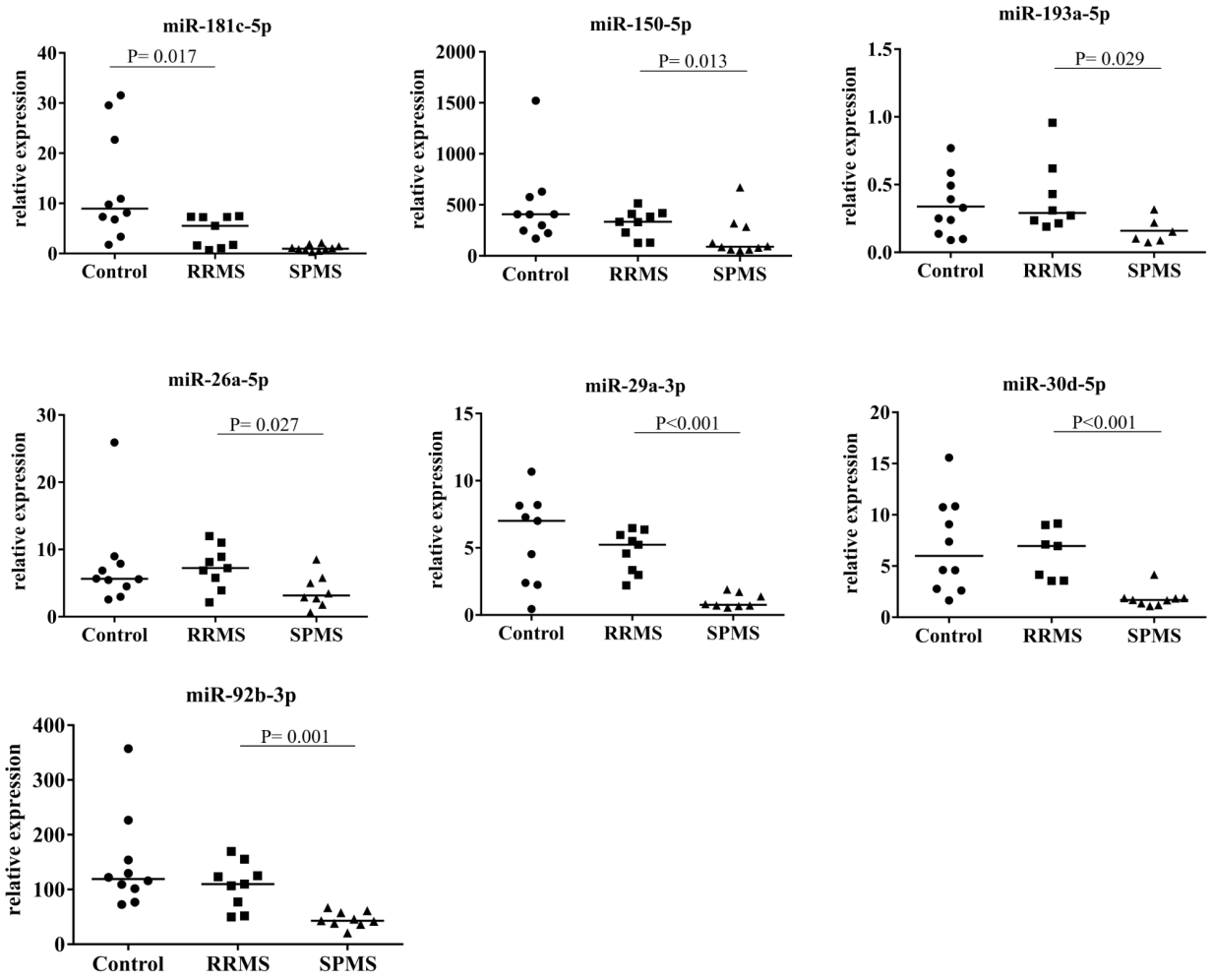

Figure 25. Candidate miRNAs showing differential expression among the groups of study in memory B cells. Relative expression of miR-181c-5p, miR-150-5p, miR-193a-5p, miR-26a-5p, miR-29a-3p, miR-30d-5p and miR-92b-3p in memory B cells isolated from controls, RRMS and SPMS patients. The line indicates the median. *RRMS: relapsing-remitting multiple sclerosis; SPMS: secondary-progressive multiple sclerosis.*

a.

	Control		RRMS		*p-value*
	Median RE	**IQR (Q1-Q3)**	**Median RE**	**IQR (Q1-Q3)**	
miR-181c-5p	8.96	6.78 – 22.69	5.53	1.60 – 7.27	*0.017*

b.

	RRMS		SPMS		*p-value*
	Median RE	**IQR (Q1-Q3)**	**Median RE**	**IQR (Q1-Q3)**	
miR-150-5p	334.59	229.20 – 411.16	89.88	62.77 – 284.19	*0.013*
miR-193a-3p	0.29	0.22 – 0.52	0.12	0.08 – 0.22	*0.029*
miR-26a-5p	7.23	5.78 – 8.91	3.17	2.26 – 5.38	*0.027*
miR-29a-3p	5.23	3.33 – 5.95	0.76	0.68 – 1.54	*<0.001*
miR-30d-5p	6.96	3.86 – 8.05	1.69	1.36 – 1.86	*<0.001*
miR-92b-3p	109.77	77.31 – 125.28	42.85	38.31 – 57.63	*0.001*

Table 12. Relative expression of candidate miRNAs showing significant differences among the groups of study in memory B cells. (a) Relative expression of miR-181c-5p in memory B cells derived from controls and RRMS patients. **(b)** Relative expression of miR-150-5p, miR-193a-5p, miR-26a-5p, miR-29a-3p, miR-30d-5p and miR-92b-3p in memory B cells of RRMS and SPMS patients. *IQR: interquartile range; Q1-Q3: first quartile-third quartile; RE: relative expression; RRMS: relapsing-remitting multiple sclerosis; SPMS: secondary-progressive multiple sclerosis.*

4.3.4. Relation between the relative expression of miRNAs and the clinical, radiological and neuropsychological variables in MS patients

The relation between the relative expression of dysregulated miRNAs (miR-150-5p, miR-181c-5p, miR-193a-5p, miR-26a-5p, miR-29a-3p, miR-30d-5p and miR-92b-3p) and the clinical, radiological and cognitive variables in MS patients was determined.

The findings reported here reveal a strong negative correlation between the expression of miR-181c-5p in Bmem cells collected from RRMS patients and the number of Gd+ lesions in the brain (*rho=-0.84, P=0.003*) (Figure 26). The analysis for the second replicate is described in Annex XI.

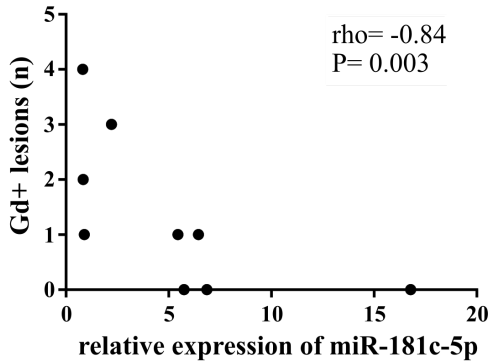

Figure 26. Scatter plot and correlation coefficient between the relative expression of miR-181c-5p in memory B cells and the number of Gd+ lesions in RRMS patients. *Gd+: gadolinium-enhanced; rho: Spearman's test rho value; RRMS: relapsing-remitting multiple sclerosis.*

4.3.5. Study of the methylation profile and relative expression of candidate miRNA genes

We investigated changes in methylation versus the expression of miR-181c-5p, miR-150-5p, miR-193a-5p, miR-26a-5p, miR-29a-3p, miR-30d-5p and miR-92b-3p in Bmem cells derived from the groups of study.

Results for the second replicate can be consulted in Annex XII.

4.3.5.1. *miR-181c-5p*

MIR181C is a 110-base-long gene located in the *plus* strand of chr19p13.12, within the intronic region of the Nanos C2HC-type zinc finger 3 (*NANOS3*) host gene (Pidiková and Herichová, 2021) (Figure 27a). In Bmem cells, it was found that the region upstream of *MIR181C* and the promoter of *NANOS3* was hypomethylated in RRMS patients when compared to controls ([chr19:13863201-13863300], *Methylation log_2FC=-1.08; P=0.022;* [chr19:13871101-13871200], *Methylation log_2FC=-1.50, P=0.036;* [chr19:13872001-13872100], *Methylation log_2FC=-0.98, P=0.044*). (Figure 27b). Furthermore, a positive trend was observed between the levels of the miR-181c-5p transcript and methylation in both the *NANOS3* promoter ([chr19:13863201-13863300]; *rho=0.42; P=0.076*) and the DMR located -2.6 kb upstream of the pre-miRNA sequence ([chr19:13872001-13872100]; *rho=0.39, P=0.09*) (Figure 27c).

a.

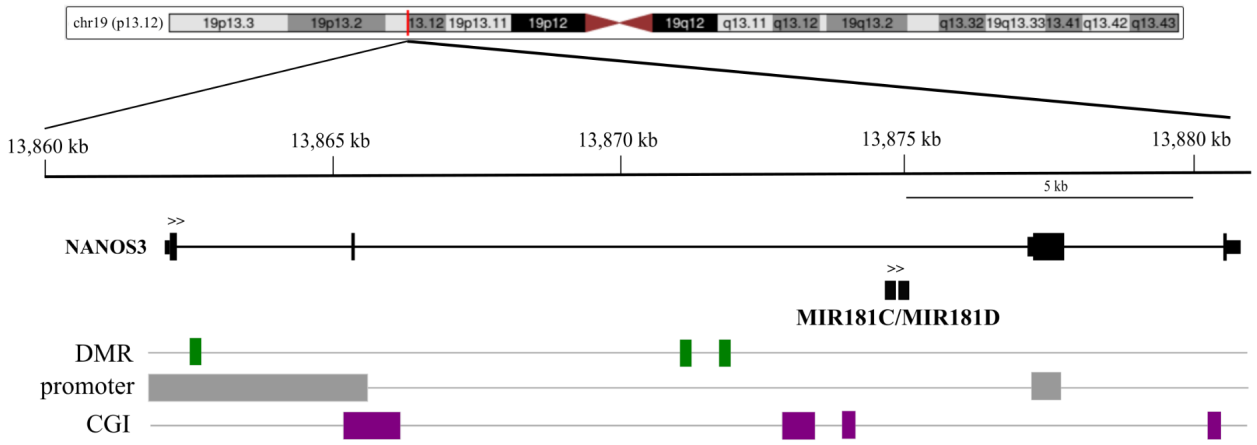

b.

Chr	Start	End	Gene	Distance to TSS (bp)	Methylation log_2FC	Methylation Status	Methylation P value
chr19	13863201	13863300	NANOS3	1215	-1.08	hypo	0.022

Chr	Start	End	Gene	Distance to pre-miRNA sequence (bp)	Methylation log_2FC	Methylation Status	Methylation P value
chr19	13871101	13871200	MIR181C	-3548	-1.50	hypo	0.035
chr19	13872001	13872100	MIR181C	-2648	-0.98	hypo	0.043

c.

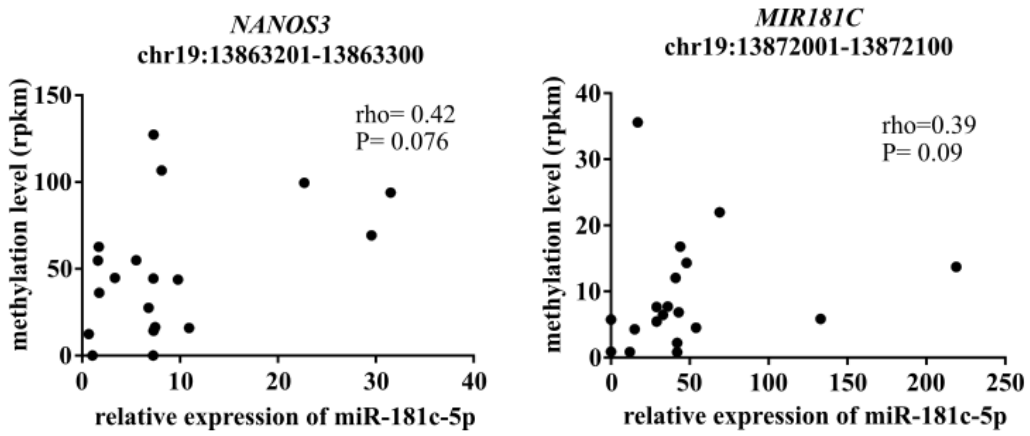

Figure 27. Description of the genomic location, methylation profile and relative expression of *MIR181C* in memory B cells of RRMS patients and controls. (a) Genomic mapping of *MIR181C* and its host gene *NANOS3* in chr19p13.12. The two arrows indicate the direction of transcription. The DMRs resulting from the comparison between RRMS patients and controls displayed in green indicate hypomethylation. The promoter regions (grey box) are represented according to Ensembl (Howe et al., 2020). The CGIs (purple box) are represented according to UCSC Genome Browser (Kent et al., 2002). **(b)** List of DMRs reported for *MIR181C* and *NANOS3* in memory B cells when comparing RRMS and controls. The coordinates for each DMR are given in the columns 'Start' and 'End'. **(c)** Scatter plot and correlation coefficient between the relative expression of miR-181c-5p and the normalized methylation values (rpkm) in memory B cells of RRMS patients and controls in the given coordinates. *bp: base pair; CGI: CpG island; chr: chromosome; DMR: differentially methylated region; hypo: hypomethylated; kb: kilobase; Methylation log_2FC: fold change in logarithmic base 2 of the methylation value between RRMS patients and controls; NANOS3: nanos C2HC-type zinc finger 3; rho: Spearman's test rho value; rpkm: reads per kilobase million; RRMS: relapsing-remitting multiple sclerosis; TSS: transcription start site.*

4.3.5.2. *miR-29a-3p*

MIR29A is a 64-base-long gene located in the *minus* strand of chr7q32.3. The precursor of miR-29a is co-expressed with the precursor of miR-29b1 (Chang et al., 2008; Mott et al., 2010) (Figure 28a). The miR-29b1/a cluster can be processed either from its putative promoter (Mott et al., 2010) or from the last intron of the primary transcript EU154353 (Chang et al., 2008; Eyholzer et al 2010) (Figure 28a). In Bmem cell subset, a hypermethylated pattern adjacent to the EU154353 promoter, at -2.1 kb upstream ([chr7:130915601-130915700], *Methylation* $log_2FC=1.53$, $P=0.023$) and at +2.8 kb downstream of the TSS ([chr7:130910401-130910500], *Methylation* $log_2FC=1.79$, $P=0.041$) was detected (Figure 28b). In the latter region, an inverse correlation between methylation and miR-29a-3p expression ([chr7:130910401-130910500]; $rho=-0.66$, $P=0.002$) was reported (Figure 28c). It was also found that elevated methylation levels at -2.7 kb upstream of the putative promoter of *MIR29B1/A* were correlated with lower expression of miR-29a-3p in MS patients ([chr7:130880201-130880300]; $rho=-0.62$, $P=0.006$) (Figure 28c). After using GeneHancer (GH) (Fishilevich et al., 2017), it was also observed that high levels of methylation in the distal enhancers GH07J130852, GH07J131001 and GH07J131042 were accompanied by lower miR-29a-3p expression: GH07J130852 ([chr7:130853301-130853400]; $rho=-0.69$, $P=0.003$), GH07J131001 ([chr7:131002201-131002300]; $rho=-0.56$, $P=0.021$), and GH07J131042 ([chr7:131043301-131301400]; $rho=-0.51$, $P=0.013$) (Figure 28c).

a.

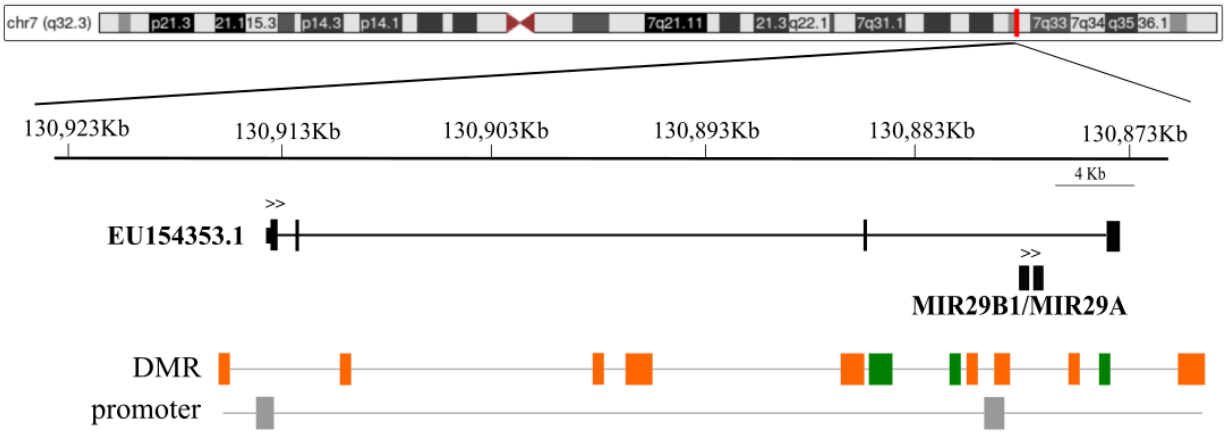

b.

Chr	Start	End	Primary Transcript	Distance to TSS (bp)	Methylation log_2FC	Methylation Status	Methylation P value
chr7	130915601	130915700	EU154353	-2187	1.53	hyper	0.023
chr7	130910401	130910500	EU154353	2859	1.79	hyper	0.041
chr7	130898601	130898700	EU154353	14659	0.71	hyper	0.043
chr7	130896301	130896400	EU154353	16959	0.84	hyper	0.013
chr7	130896201	130896300	EU154353	17059	0.68	hyper	0.033
chr7	130896101	130896200	EU154353	17159	0.73	hyper	0.020

Chr	Start	End	Gene	Distance to miRNA locus (bp)	Methylation log_2FC	Methylation Status	Methylation P value
chr7	130886601	130886700	MIR29B1/A	-9112	0.76	hyper	0.024
chr7	130886501	130886600	MIR29B1/A	-9012	0.72	hyper	0.035
chr7	130885201	130885300	MIR29B1/A	-7712	-1.22	hypo	0.021
chr7	130885101	130885200	MIR29B1/A	-7612	-1.04	hypo	0.014
chr7	130884901	130885000	MIR29B1/A	-7412	-0.68	hypo	0.022
chr7	130881101	130881200	MIR29B1/A	-3612	-1.04	hypo	0.034
chr7	130880201	130880300	MIR29B1/A	-2712	1.17	hyper	0.015
chr7	130878901	130879000	MIR29B1/A	-1412	1.32	hyper	0.020
chr7	130875701	130875800	MIR29B1/A	1758	1.27	hyper	0.030
chr7	130874101	130874200	MIR29B1/A	3358	-1.92	hypo	0.044

Chr	Start	End	Enhancer ID	Distance to *MIR29A* (Kb)	Methylation Log_2FC	Methylation Status	Methylation P value
chr7	131043301	131043400	GH07J131042	-166.5	1.99	hyper	0.020
chr7	131002401	131002500	GH07J131001	-125.6	1.45	hyper	0.049
chr7	131002301	131002400	GH07J131001	-125.5	1.41	hyper	0.019
chr7	131002201	131002300	GH07J131001	-125.4	1.47	hyper	0.012
chr7	130853301	130853400	GH07J130852	23.4	0.92	hyper	0.031

c.

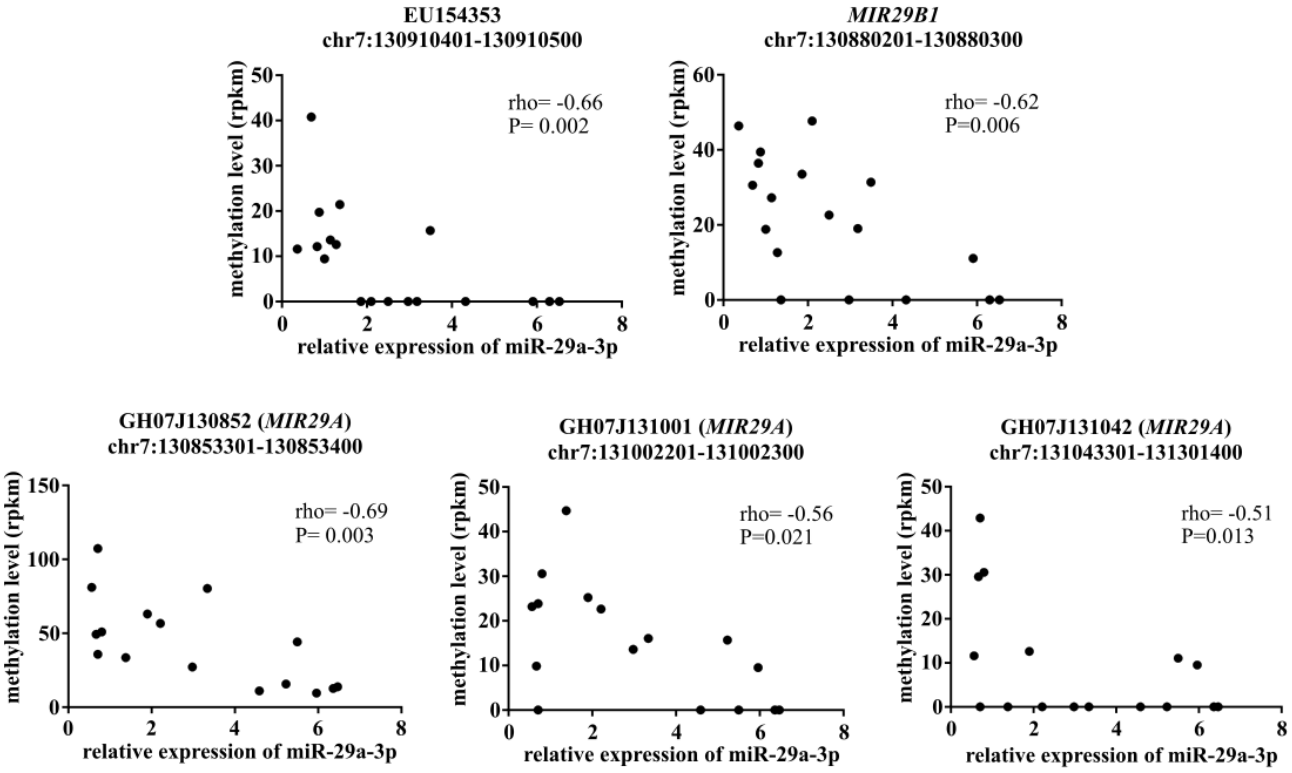

Figure 28. Description of the genomic location, methylation profile and relative expression of *MIR29A* in memory B cells of MS patients. (a) Genomic mapping of *MIR29A* within the primary transcript EU154353 in chr7q32.3. The two arrows indicate the direction of the transcription. The DMRs resulting from the comparison between SPMS and RRMS are displayed in green and orange if hypomethylated or hypermethylated, respectively. The promoter regions (grey box) are depicted according to UCSC Genome Browser (Kent et al., 2002) and the studies from Chang et al., 2008, Eyholzer et al., 2010 and Mott et al., 2010. **(b)** List of DMRs related to *MIR29B1, MIR29A*, EU154353, and distal enhancers for *MIR29A* in memory B cells when comparing SPMS and RRMS patients. The coordinates for each DMR are given in the columns 'Start' and 'End'. **(c)** Scatter plot and correlation coefficient between the relative expression of miR-29a-3p and the normalized methylation values (rpkm) in memory B cells of RRMS and SPMS patients in the given coordinates. *bp: base pair; chr: chromosome; DMR: differentially methylated region; hyper: hypermethylated; hypo: hypomethylated; kb: kilobase; Methylation log_2FC: fold change in logarithmic base 2 of the methylation value between SPMS and RRMS patients; rho: Spearman's test rho value; rpkm: read per kilobase million; RRMS: relapsing-remitting multiple sclerosis; SPMS: secondary-progressive multiple sclerosis; TSS: transcription start site.*

4.3.5.3. *miR-26a-5p*

MIR26A1 is a 77-base-long gene located in the *plus* strand of the host gene CTD small phosphatase like (*CTDSPL*), in chr3p22.2. (Figure 29a). In Bmem cells, SPMS patients showed 23 DMRs within the *MIR26A1/CTDSPL* locus when compared to RRMS patients (Figure 29b). The majority of the DMRs (91%) were hypermethylated in SPMS patients, with only two regions showing hypomethylation (Figure 29b). Particularly, in the DMR located in the gene body of *CTDSPL,* at +9.8 kb downstream of the pre-miR-26a1 sequence, high levels of methylation were

inversely correlated with miR-26a-5p expression ([chr3:37979201-37979300]; *rho=-0.58, P=0.012*) (Figure 29c).

a.

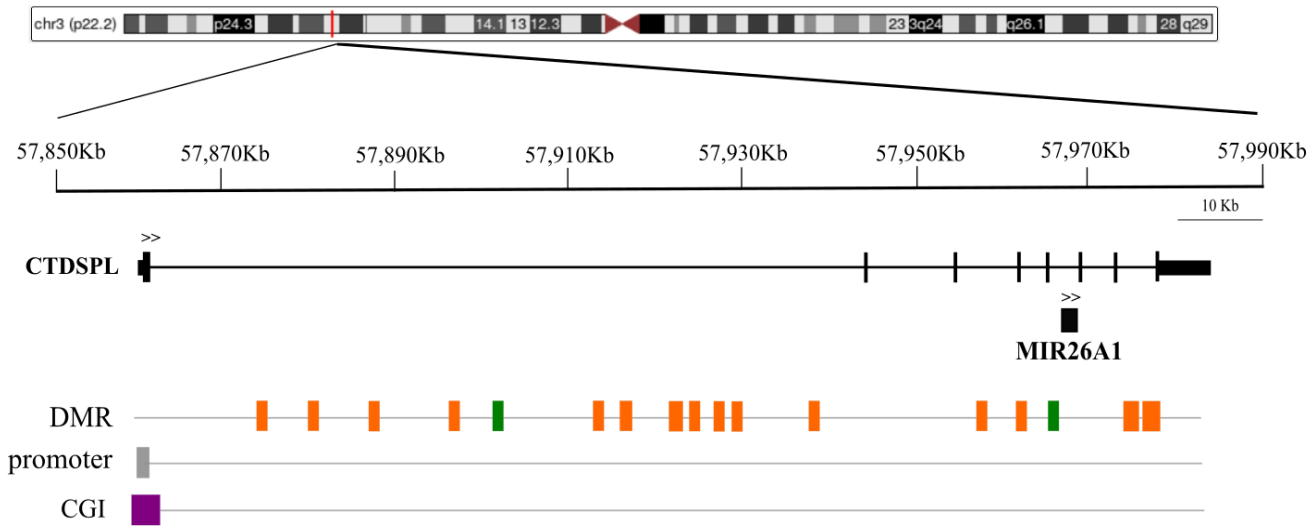

b.

Chr	Start	End	Gene	Distance to TSS (bp)	Methylation Log_2FC	Methylation Status	Methylation P value
chr3	37875601	37875700	CTDSPL	13771	2.00	hyper	0.013
chr3	37880901	37881000	CTDSPL	19071	1.45	hyper	0.034
chr3	37881401	37881500	CTDSPL	19571	1.27	hyper	0.029
chr3	37889101	37889200	CTDSPL	27271	1.59	hyper	0.036
chr3	37897901	37898000	CTDSPL	36071	2.26	hyper	0.018
chr3	37903101	37903200	CTDSPL	41271	-1.27	hypo	0.034
chr3	37914601	37914700	CTDSPL	52771	1.54	hyper	0.029
chr3	37918001	37918100	CTDSPL	56171	0.71	hyper	0.045
chr3	37918201	37918300	CTDSPL	56371	1.80	hyper	0.036
chr3	37923801	37923900	CTDSPL	61971	0.69	hyper	0.042
chr3	37925401	37925500	CTDSPL	63571	2.00	hyper	0.032
chr3	37926801	37926900	CTDSPL	64971	2.00	hyper	0.032
chr3	37928901	37929000	CTDSPL	67071	2.24	hyper	0.040
chr3	37931001	37931100	CTDSPL	69171	1.01	hyper	0.047
chr3	37940001	37940100	CTDSPL	78171	1.15	hyper	0.044

Chr	Start	End	Gene	Distance to pre-miRNA sequence (bp)	Methylation Log_2FC	Methylation Status	Methylation P value
chr3	37959501	37959600	MIR26A1	-9853	1.49	hyper	0.005
chr3	37964201	37964300	MIR26A1	-5153	1.15	hyper	0.019
chr3	37967101	37967200	MIR26A1	-2253	-1.92	hypo	0.043
chr3	37977701	37977800	MIR26A1	8347	1.35	hyper	0.032
chr3	37977801	37977900	MIR26A1	8447	1.20	hyper	0.044
chr3	37979101	37979200	MIR26A1	9747	1.88	hyper	0.008
chr3	37979201	37979300	MIR26A1	9847	2.00	hyper	0.002
chr3	37979301	37979400	MIR26A1	9947	1.63	hyper	0.005

c.

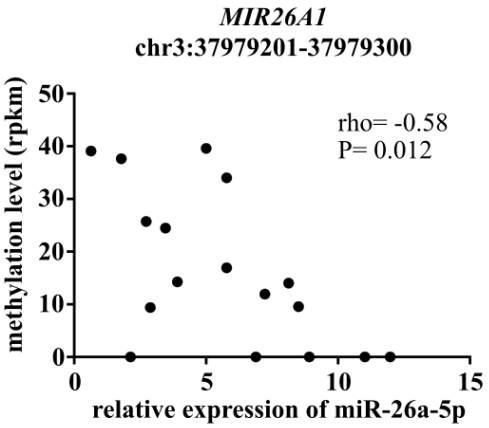

Figure 29. Description of the genomic location, methylation profile and relative expression of *MIR26A1* in memory B cells of MS patients. (a) Genomic mapping of *MIR26A1* and the host gene *CTDSPL* in chr3p22.2. The two arrows indicate the direction of the transcription. The DMRs resulting from the comparison between SPMS and RRMS are displayed in green and orange if hypomethylated or hypermethylated, respectively. The promoter region (grey box) and the CGI (purple box) are represented according to UCSC Genome Browser (Kent et al., 2002). **(b)** List of DMRs in memory B cells of SPMS patients in comparison to RRMS patients for *MIR26A1* and *CTDSPL*. The coordinates for each DMR are given in the columns 'Start' and 'End'. **(c)** Scatter plot and correlation coefficient between the relative expression of miR-26a-5p and the normalized methylation values (rpkm) in memory B cells of RRMS and SPMS patients in the given coordinates. *bp: base pair; CTDSPL: CTD Small Phosphatase Like; chr: chromosome; DMR: differentially methylated region; hyper: hypermethylated; hypo: hypomethylated; kb: kilobase; Methylation Log_2FC: fold change in logarithmic base 2 of the methylation value between SPMS and RRMS patients; rho: Spearman's test rho value*; *rpkm: reads per kilobase million; RRMS: relapsing-remitting multiple sclerosis; SPMS: secondary-progressive multiple sclerosis; TSS: transcription start site.*

4.3.5.4. *miR-150-5p*

The *MIR150* gene is an 84-nucleotide sequence located in the *minus* strand of chr19q13.33 (Figure 30a). In the Bmem cell subset, elevated methylation levels in the region located at +1017 bp downstream of the pre-miR-150 sequence were reported when comparing SPMS to RRMS patients ([chr19:49499801-49499900], *Methylation* $log_2FC=1.72$, $P=0.021$) (Figure 30b). Correlation analysis revealed a weak negative association between methylation in this region and miR-150-5p expression ([chr19:49499801-49499900]; *rho=-0.34, P=0.16*) (Figure 30c).

a.

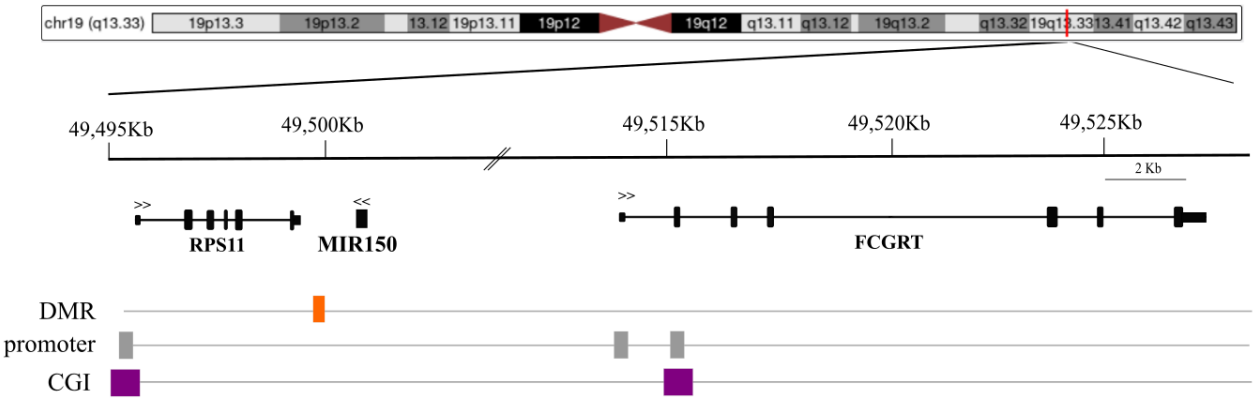

b.

Chr	Start	End	Gene	Distance to pre-miRNA sequence (bp)	Methylation Log_2FC	Methylation Status	Methylation P value
chr19	49499801	49499900	MIR150	1017	1.72	hyper	0.021

c.

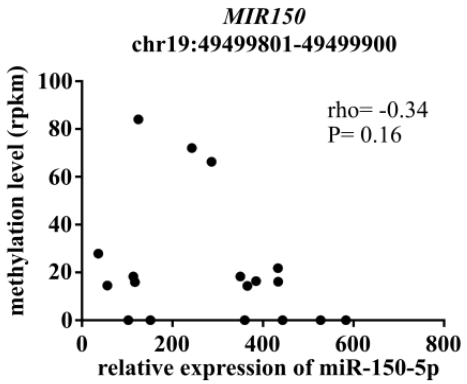

Figure 30. **Description of the genomic location, methylation profile and relative expression of *MIR150* in memory B cells of MS patients. (a)** Genomic mapping of *MIR150* in chr19q13.33. The two arrows indicate the direction of the transcription. The DMR resulting from the comparison between SPMS and RRMS displayed in orange indicates hypomethylation. The promoter regions (grey box) and the CGIs (purple box) are represented according to UCSC Genome Browser (Kent et al., 2002). **(b)** The DMR related to *MIR150* observed in memory B cells when comparing SPMS and RRMS patients. The coordinates for the DMR are given in the columns 'Start' and 'End'. **(c)** Scatter plot and correlation coefficient between the relative expression of miR-150-5p and the normalized methylation values (rpkm) in memory B cells of RRMS and SPMS patients in the given coordinates. *bp: base pair; CGI: CpG island; chr: chromosome; DMR: differentially methylated region; FCGRT: Fc gamma receptor and transporter; hyper: hypermethylated; kb: kilobase; Methylation Log_2FC: fold change in logarithmic base 2 of the methylation value between SPMS and RRMS patients; rho: Spearman's test rho value; rpkm: reads per kilobase million; RPS11: ribosomal protein s11; RRMS: relapsing-remitting multiple sclerosis; SPMS: secondary-progressive multiple sclerosis; TSS: transcription start site.*

4.3.5.5. *mir193a-5p*

MIR193A is a 100 bp size gene located within the *plus* strand of chr17p13.12 (Figure 31a). In the Bmem cell population, a hypomethylated region located +355 bp downstream of the pre-miR-193a sequence was determined in SPMS when compared to RRMS patients

([chr17:31560301-31560400], *Methylation log_2FC=-0.82, P=0.048*) (Figure 31b). However, no correlation was found between miR-193a-5p expression and methylation in this region ([chr17:31560301-31560400]; *rho=0.00; P=0.99*) (Figure 31c).

a.

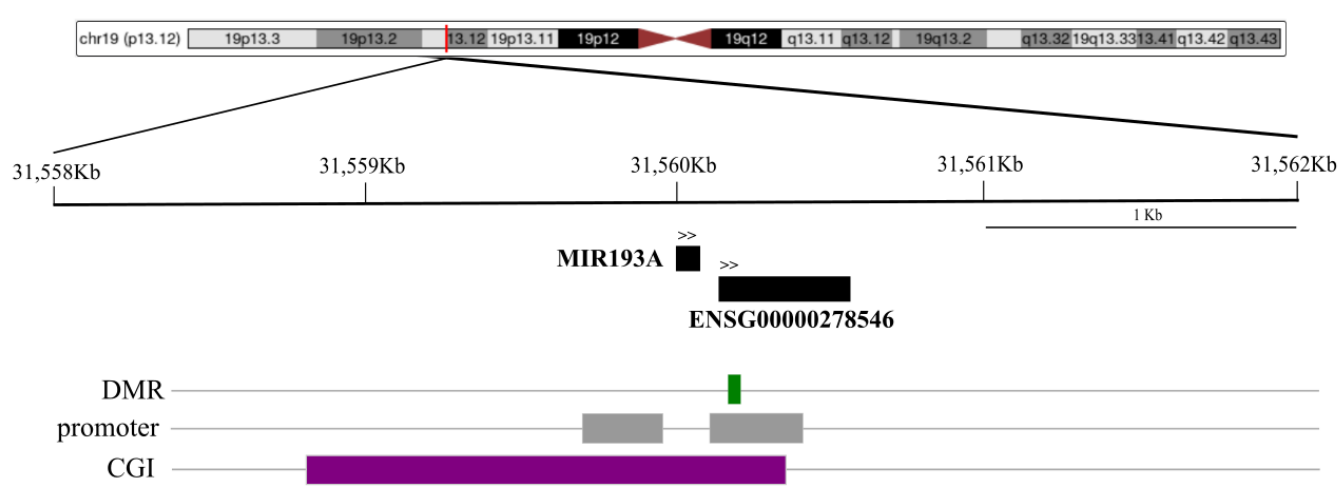

b.

Chr	Start	End	Gene	Distance to pre-miRNA sequence (bp)	Methylation Log_2FC	Methylation Status	Methylation P value
chr17	31560301	31560400	MIR193A	355	-0.82	hypo	0.047

c.

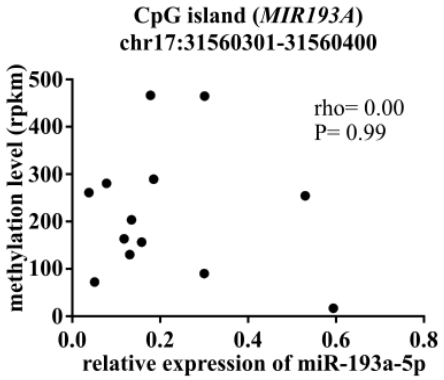

Figure 31. Description of the genomic location, methylation profile and relative expression of *MIR193A* in memory B cells of MS patients. **(a)** Genomic mapping of *MIR193A* in chr17p13.12. The two arrows indicate the direction of the transcription. The DMR resulting from the comparison between SPMS and RRMS displayed in green indicates hypomethylation. The promoter regions (grey box) and the CGI (purple box) are represented according to UCSC Genome Browser (Kent et al., 2002). **(b)** The DMR related to *MIR193A* observed in memory B cells when comparing SPMS to RRMS patients. The coordinates for the DMR are given in the columns 'Start' and 'End'. **(c)** Scatter plot and correlation coefficient between the relative expression of miR-193a-5p and the normalized methylation values (rpkm) in memory B cells of RRMS and SPMS patients in the given coordinates. *bp: base pair; CGI: CpG island; chr: chromosome; DMR: differentially methylated region; hypo: hypomethylated; kb: kilobase; Methylation Log_2FC: fold change in logarithmic base 2 of the methylation value between SPMS and RRMS patients; rho: Spearman's test rho value; rpkm: reads per kilobase million; RRMS: relapsing-remitting multiple sclerosis; SPMS: secondary-progressive multiple sclerosis; TSS: transcription start site.*

4.3.5.6. *miR-30d-3p*

The *MIR30D* gene is a 70-nucleotide sequence found in the *minus* strand of chr8q24.22 (Figure 32a). *MIR30D* is clustered with the *MIR30B* gene, which is located < 5 kb downstream of the miR-30d encoding gene. Due to their proximity, both miRNAs are probably co-transcribed (Saini et al., 2007). In the present investigation, six DMRs associated with the *MIR30D/B* cluster were found in Bmem cells collected from SPMS in contrast to RRMS patients ([chr8:134801201-134801300], *Methylation* $log_2FC=1.37$, *P=0.045*; [chr8:134801301-134801400], *Methylation* $log_2FC=0.72$, *P=0.043;* [chr8:134802201-134802300], *Methylation* $log_2FC=2.57$, *P=0.003;* [chr8:134804401-134804500], *Methylation* $log_2FC=-1.57$, *P=0.037;* [chr8:134809901-134810000], *Methylation* $log_2FC=-1.57$, *P=0.023;* [chr8:134812601-134812700], *Methylation* $log_2FC=2.00$, *P=0.032*) (Figure 32b). GeneHancer revealed that three of the DMRs were part of the proximal enhancer GH08J134799 (Fishilevich et al., 2017). Interestingly, it was found that elevated methylation levels in this enhancer strongly correlated with lower miR-30d-3p expression ([chr8:134802201-134802300]; *rho=-0.77; P<0.001*) (Figure 32c).

a.

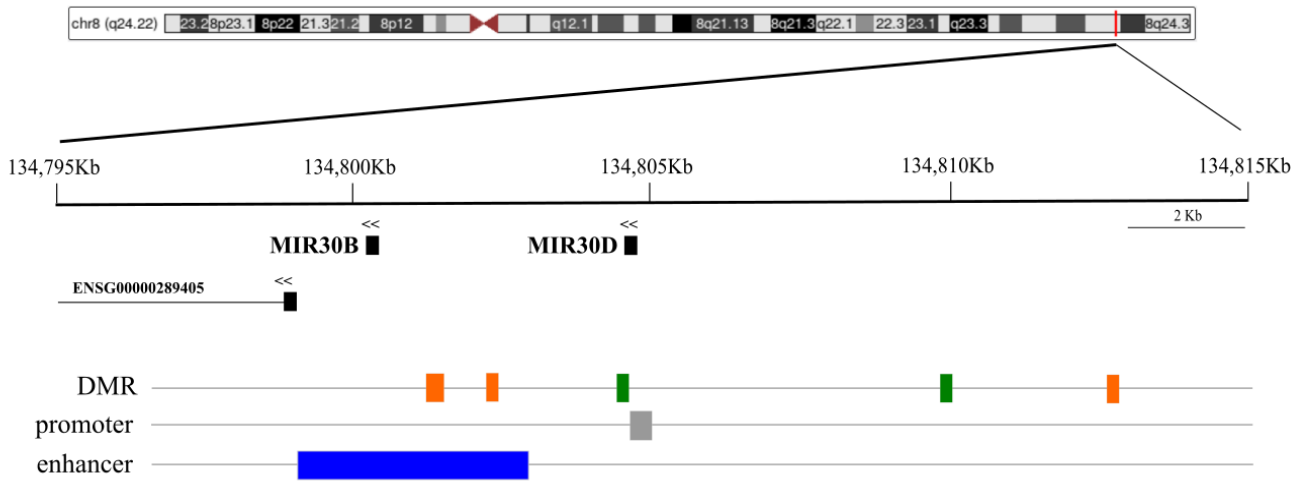

b.

Chr	Start	End	Gene	Distance to pre-miRNA sequence (bp)	Methylation Log_2FC	Methylation Status	Methylation P value
chr8	134801201	134801300	MIR30D	3744	1.37	hyper	0.045
chr8	134801301	134801400	MIR30D	3644	0.72	hyper	0.043
chr8	134802201	134802300	MIR30D	2744	2.57	hyper	0.003
chr8	134804401	134804500	MIR30D	494	-1.57	hypo	0.037
chr8	134809901	134810000	MIR30D	-5006	-1.57	hypo	0.023
chr8	134812601	134812700	MIR30D	-7706	2.00	hyper	0.032

c.

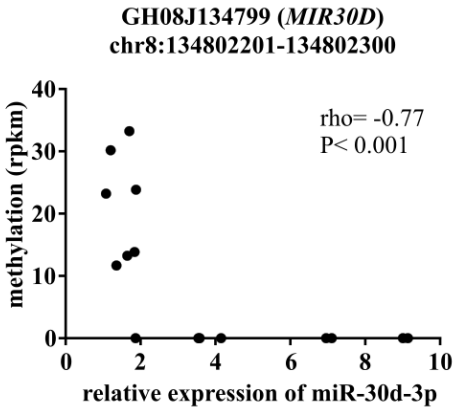

Figure 32. Description of the genomic location, methylation profile and relative expression of *MIR30D* in memory B cells of MS patients. **(a)** Genomic mapping of *MIR30D* in chr8q24.22. The two arrows indicate the direction of the transcription. The DMRs resulting from the comparison between SPMS and RRMS patients are displayed in green and orange if hypomethylated or hypermethylated, respectively. The promoter region (grey box) is represented according to UCSC Genome Browser (Kent et al., 2002). The enhancer region (blue box) is depicted based on GeneHancer (Fishilevich et al., 2017). **(b)** List of DMRs related to *MIR30D* observed in memory B cells when comparing SPMS to RRMS patients. The coordinates for the DMRs are given in the column 'Start' and 'End'. **(c)** Scatter plot and correlation coefficient between the relative expression of miR-30d-3p and the normalized methylation values in memory B cells of RRMS and SPMS patients in the given coordinates. *bp: base pair; chr: chromosome; DMR: differentially methylated region; hyper: hypermethylated; hypo: hypomethylated; kb: kilobase; Methylation Log_2FC: fold change in logarithmic base 2 of the methylation value between SPMS and RRMS patients; rho: Spearman's test rho value; rpkm: reads per kilobase million; RRMS: relapsing-remitting multiple sclerosis; SPMS: secondary-progressive multiple sclerosis; TSS: transcription start site.*

4.3.5.7. *miR-92b-3p*

MIR92B comprises a 96-base-long sequence located in the *plus* strand of chr1q22, embedded inside the THBS3 antisense RNA 1 (*THBS3-AS1*) gene (Figure 33a). In our study, a 400-base-long hypomethylated region upstream of the *MIR92B/THBS3-AS1* locus was determined in Bmem cells derived from SPMS patients when compared to RRMS patients ([chr1:155191701-155191800], *Methylation log_2FC=-1.76, P=0.031;* [chr1:155191801-155191900], *Methylation log_2FC=-1.89, P=0.015;* [chr1:155191901-155192000], *Methylation log_2FC=-1.78, P=0.025;* [chr1:155192001-155192100], *Methylation log_2FC=-1.79, P=0.016*), along with a single hypermethylated region at +2.6 kb downstream of the locus ([chr1:155197801-155197900], *Methylation log_2FC=0.89, P=0.009*) (Figure 33b). GeneHancer revealed that the hypermethylated region corresponds to the enhancer GH01J155191 (Fishilevich et al., 2017), where methylation showed a weak negative association with miR-92b-3p expression ([chr1:155197801-155197900]; *rho=-0.38; P=0.127)* (Figure 33c).

a.

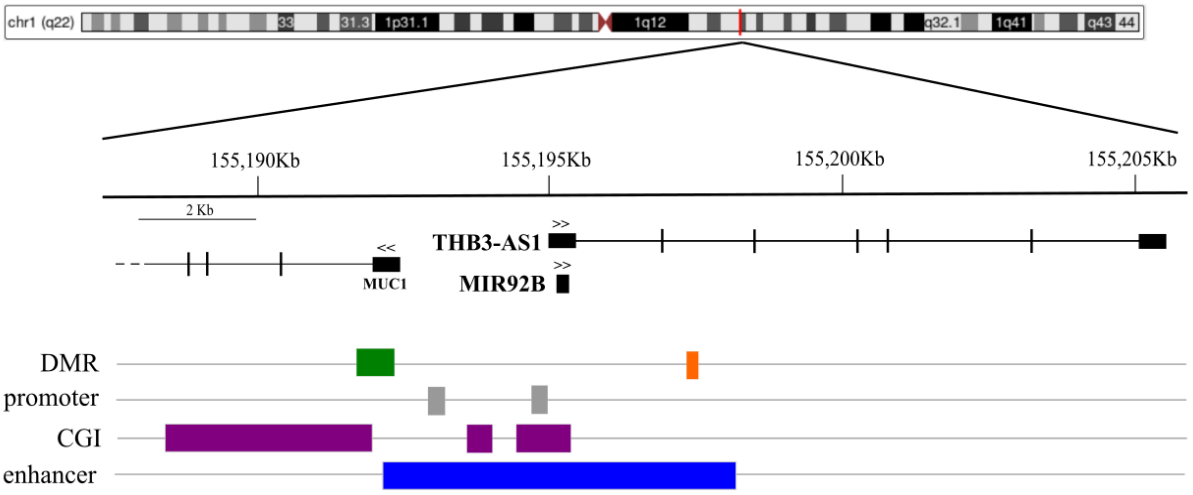

b.

Chr	Start	End	Gene	Distance to pre-miRNA sequence (bp)	Methylation log_2FC	Methylation Status	Methylation P value
chr1	155191701	155191800	MIR92B	-3476	-1.76	hypo	0.031
chr1	155191801	155191900	MIR92B	-3376	-1.89	hypo	0.015
chr1	155191901	155192000	MIR92B	-3276	-1.78	hypo	0.025
chr1	155192001	155192100	MIR92B	-3176	-1.79	hypo	0.016
chr1	155197801	155197900	MIR92B	2525	0.89	hyper	0.009

c.

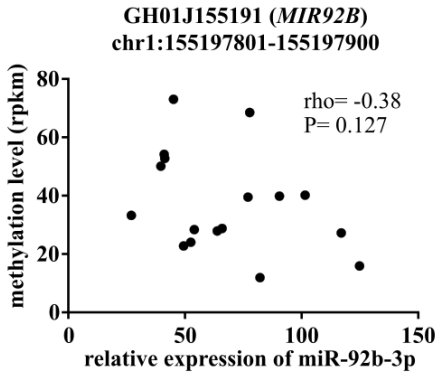

Figure 33. Description of the genomic location, methylation profile and relative expression of *MIR92B* in memory B cells of MS patients. **(a)** Genomic location of *MIR92B* and *THBS3-AS1* in chr1q22. The two arrows indicate the direction of the transcription. The DMRs resulting from the comparison between SPMS and RRMS patients are displayed in green and orange if hypomethylated or hypermethylated, respectively. The promoter regions (grey box) and the CGIs (purple box) are represented according to UCSC Genome Browser (Kent et al., 2002). The enhancer region (blue box) is depicted based on GeneHancer (Fishilevich et al., 2017). **(b)** The list of DMRs related to *MIR92B* observed in memory B cells of SPMS patients when compared to RRMS patients. The coordinates for the DMRs are given in the columns 'Start' and 'End'. **(c)** Scatter plot and correlation coefficient between the relative expression of miR-92b-3p and the normalized methylation values (rpkm) in memory B cells of RRMS and SPMS patients in the given coordinates. *bp: base pair; chr: chromosome; CGI: CpG island; DMR: differentially methylated region; hyper: hypermethylated; hypo: hypomethylated; kb: kilobase; Methylation Log_2FC: fold change in logarithmic base 2 of the methylation value between SPMS and RRMS patients; MUC1: mucin 1, cell surface associated; rho: Spearman's test rho value; rpkm: reads per kilobase million; RRMS: relapsing-remitting multiple sclerosis; SPMS: secondary-progressive multiple sclerosis; THBS3-AS1: THBS3 antisense RNA 1; TSS: transcription start site.*

4.3.6. miRNA targets and KEGG enrichment analysis

Two different databases were used to predict the biological impact of our finding: miRDB (Chen and Wang, 2019) and TargetScan (Agarwal et al., 2015). Targets with a prediction score greater than 80 were selected in the miRDB database. In the TargetScan database, in contrast, only those targets with conserved sites were taken into consideration. Table 13 shows the number of overlapping target genes predicted by miRDB and TargetScan, as well as the most enriched GO term for common targets. The complete list can be consulted in Annex XIII.

Table 13. Number of predicted targets for the dysregulated miRNAs based on miRDB and TargetScan databases. The 'common targets' column represents the number of predicted targets shared by both databases. The last column shows the most enriched GO terms for biological processes according to Enrichr associated with the common targets. *GO: gene ontology.*

miRNA	*miRDB*	*TargetScan*	Common Targets	Top associated GO terms for common targets
miR-150-5p	*184*	*351*	61	Negative regulation of nucleic acid-templated transcription (GO:1903507) Regulation of T-helper cell differentiation (GO:0045622) Negative regulation of cellular macromolecule biosynthetic process (GO:2000113)
miR-181c-5p	*613*	*164*	45	Positive regulation of synaptic transmission, GABAergic (GO:0032230) Pre-miRNA processing (GO:0031054)
miR-193a-5p	*44*	*214*	9	BMP signaling pathway involved in heart development (GO:0061312) Cardiac cell fate commitment (GO:0060911) Regulation of proton transport (GO:0010155)
miR-26a-5p	*497*	*1582*	82	Negative regulation of hippo signaling (GO:0035331) Positive regulation of nuclear-transcribed mRNA poly(A) tail shortening (GO:0060213) Negative regulation of gonadotropin secretion (GO:0032277)
miR-29a-3p	*447*	*978*	288	Positive regulation of oxidative stress-induced neuron death (GO:1903223) Regulation of focal adhesion disassembly (GO:0120182) Collagen fibril organization (GO:0030199)
miR-30d-3p	*21*	*808*	6	Positive regulation of hippo signaling (GO:0035332) Negative regulation of keratinocyte proliferation (GO:0010839) Cellular response to thyroid hormone stimulus (GO:0097067)
miR-92b-3p	*484*	*1*	0	-

It was also observed that miR-26a-5p and miR-29a-3p shared the target genes *LSM11*, *USP37* and *ZNF469* (Figure 34). On the other hand, miR-26a-5p and miR-30d-3p shared only the target gene *DLG5*; while miR-29a-3p and miR-30d-3p had the common target *KCTD5* (Figure 34). GO enrichment analysis using Enrichr (Xie et al., 2021) revealed that *LSM11* and *USP37* are mainly involved in the histone mRNA 3'-end processing and deubiquitination, *DLG5* in the hippo signalling pathway, and *KCTD5* in the proteasome-ubiquitination pathway.

The intrinsic nature of miRNAs as negative regulators (Bartel DP., 2004) points out that their downregulation should be accompanied, theoretically, by an increase of their target gene expression. We could not validate the association between miR26a-5p and miR-29a-3p with their

target gene *ZNF469*, due to the expression of ZNF469 being undetectable in both immune cells (Table 5).

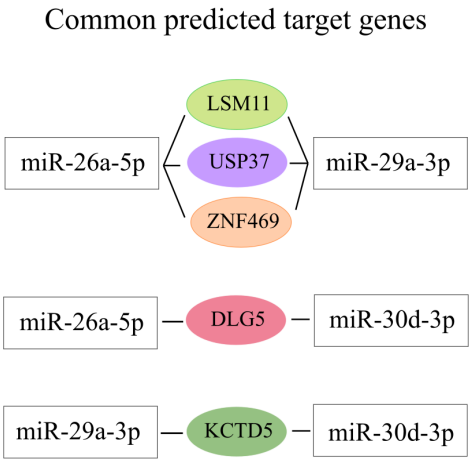

Figure 34. Common predicted targets for miR-26a-5p, miR-29a-3p and miR-30d-3p. *DLG5: discs large MAGUK scaffold protein 5; KCTD5: potassium channel tetramerization domain containing 5; LSM11: LSM11, u7 small nuclear RNA associated; USP37: ubiquitin specific peptidase 37; ZNF469: zinc finger protein 469.*

Afterwards, a KEGG enrichment analysis was performed using miRPath version 3.0 (Vlachos et al., 2015), selecting Fisher's exact test with $P < 0.001$ for the enrichment analysis. As shown in Figure 35, the most enriched KEGG pathways were related to the extracellular-matrix (ECM)-receptor interaction (*miR29a-3p, miR-30d-3p, miR-193a*) and the cell cycle (*miR30d-3p, miR-26a-5p*), followed by metabolism-related pathways such as steroid biosynthesis (*miR-26a-5p, miR-29a-3p, miR193a-5p, miR30d-3p*), lysine degradation (*miR-92b-3p, miR-26a-5p, miR-29a-3p*) and fatty acid biosynthesis (*miR-29a-3p*).

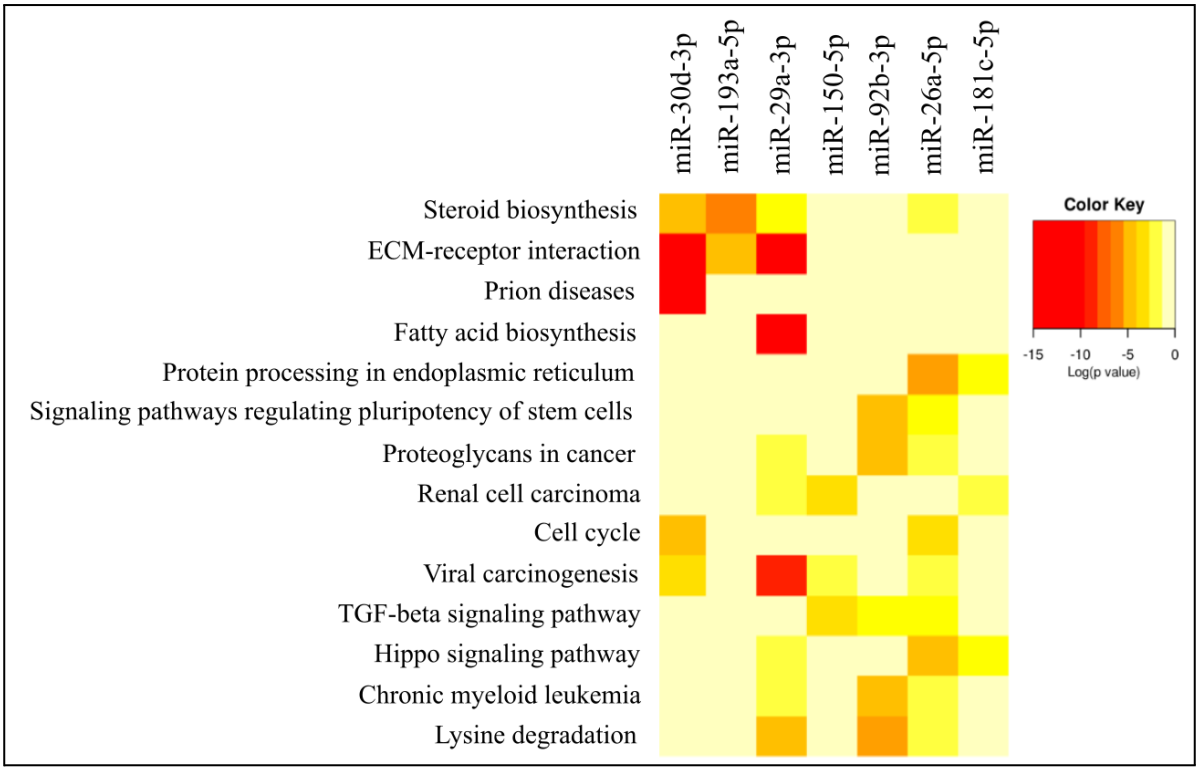

Figure 35. KEGG pathway analysis for the dysregulated miRNAs. *ECM: extracellular matrix; TGF: transforming growth factor.*

4.3.7. Summary

Herein, we have analysed the transcriptome of 161 differentially methylated miRNAs in Bmem cells and 184 differentially methylated miRNAs in Treg cells collected from controls, RRMS and SPMS patients. In Bmem cells, our results indicated that RRMS patients presented lower levels of miR-181c-5p than the control group as well as higher levels of miR-193a-5p, miR30d-3p, miR-92b-3p, miR-26a-5p, miR-29a-3p, and miR-150-5p than the SPMS group. These miRNAs were involved in metabolic regulation, protein processing and ECM-receptor interaction. Association analysis has revealed a moderate correlation between methylation levels and miRNA expression in nearby DMRs (± 10 kb) for *MIR29A* and *MIR26A1*, and in one DMR located in the *MIR30D* enhancer GH08J134799. In the Treg cohort, no significant differences were found among the groups of study.

5. Discussion

5.1. The importance of DNA methylation in MS

MS is a chronic autoimmune disease of the CNS characterized by the infiltration of autoreactive immune cells into the brain and spinal cord, causing inflammatory demyelination and ultimately, axonal damage and neuronal death (Coles et al., 1999; Lubetzki and Stankoff, 2014). The demyelination can be recovered to some extent by the remyelination carried out by oligodendrocytes; but eventually, this damage overwhelms the recovery capacity of the organism undergoing neurodegeneration.

The aetiology of MS remains unknown, but it is widely accepted to be the result of a complex interaction between genetics, environment and epigenetics. Epigenetics refers to heritable changes in the gene expression without changes in the DNA sequence (Allis and Jenuwein, 2016). Due to the reversible nature of these modifications, epigenetics favours the optimal adaptation of the organisms to the environment by stimulating or silencing genes. There are several epigenetic modifications, but one of the most studied mechanisms is the methylation of DNA. Aberrant DNAme could alter the genomic landscape, contributing to cellular homeostasis imbalance and many pathological processes (Jin and Liu, 2018). Changes in DNAme have been described in autoimmune diseases (Jin and Liu, 2018), including MS (Ayuso et al., 2017; Baranzini et al., 2010; Chomyk et al., 2017; Kumagai et al., 2012; Maltby et al., 2015, 2018; Ruhrmann et al., 2018). Aberrant DNAme might compromise some biological processes such as BBB integrity (Huynh et al., 2014; Liggett et al., 2010), inflammatory response (Kumagai et al., 2012), or myelin sheath compaction (Mastronardi et al., 2007) in MS.

Most of the methylation studies in MS have been focused on the study of DNAme using distinct tissues with remarkable cell heterogeneity like PBMCs, which comprise myeloid cells (macrophages and dendritic cells) as well as lymphoid cells (natural killer, B cells, T cells) (Betsou et al., 2019). The pattern of DNAme is different for each cell population (Lokk et al., 2014; Zhang et al., 2013); therefore, pooling different cell types could lead to inaccurate results and data misinterpretation (Baranzini et al., 2010; Chomyk et al., 2017; Field et al., 2017; Huynh et al., 2014; Kulakova et al., 2016; Kular et al., 2022; Kumagai et al., 2012; Lehman-Werman et al., 2016; Marabita et al., 2017; Mastronardi et al., 2007; Neven et al., 2016; Olsen et al., 2016; Ramagopalan et al., 2008; Rhead et al., 2018;

Sokratous et al., 2018; Souren et al., 2019; Wagner et al., 2017). To overcome this issue, we directed our efforts to isolate pure Bmem and Treg cells derived from whole peripheral blood.

5.2. Genome-wide methylome profile of MS patients

The effect of DNAme on two immune cell types (Bmem and Treg cells) collected from MS patients and their matched controls was examined. The aim of the study was to elucidate the contribution of DNAme to the physiopathology of the disease. Our findings revealed that both Bmem cells and Treg cells displayed aberrant methylation patterns in MS patients. At the onset of the disease, a global hypomethylation was reported, but this pattern shifted towards hypermethylation in later stages of the disease. Kulakova and colleagues (2016) studied changes in the DNAme of PMBCs derived from RRMS, PPMS and controls. They reported a hypomethylated pattern in RRMS patients, while the opposite was observed in PPMS patients and controls. Similarly, CD19+ B cells collected from RRMS patients exhibited global hypomethylation when compared to the control group (Ewing et al., 2019; Maltby et al., 2018), in agreement with our findings. No prior genome-wide studies covering the methylome of Bmem and Treg cells in MS have been published and therefore, this pilot study should be of great interest to the scientific community. Indeed, the current work contributes to elucidating the role of these cell types in the pathophysiology of the disease.

Our findings have revealed that nearly half of the global DMRs were located in regions containing either repeats or transposable elements. Transposable elements are highly mobile DNA sequences that can be classified into two categories: retrotransposons and DNA transposons (Bourque et al., 2018). Retrotransposons can be further divided into LTR and non-LTR (Bourque et al., 2018). The dysregulation of non-LTR such as LINE, SINE and SVA might compromise the genomic integrity, lastly contributing to the pathophysiology of Alzheimer's, cancer, amyotrophic lateral sclerosis or MS disease (Brudek et al., 2009; Konkel et al., 2010; Rodic et al., 2014; Saleh et al., 2019). Subsequently, cellular machinery represses the expression of these elements through the addition of methyl groups (Jansz N., 2019). Interestingly, in this study, a remarkable hypomethylation of the encoding regions for these transposable elements was identified in both cell types collected from RRMS patients, which could favour their expression. The hypomethylation of LINE-1 has been reported in autoimmune diseases (Nakkuntod et al., 2011; Sukapan et al., 2014), while transposable elements have been related with CNS inflammation and demyelination in MS (Mameli et al.,

2007). In later stages of MS progression (SPMS patients), it was observed that the hypomethylation status of these elements was reversed to a hypermethylated state.

CGIs are often found near promoters and regulatory regions of the DNA (Deaton et al., 2011). Under normal physiological conditions, CGIs are usually unmethylated in somatic tissues. Therefore, the addition of methyl groups to CGIs can block gene expression (Deaton et al., 2011). In this study, most of the DMR located within CGIs were hypermethylated in both Bmem and Treg cells derived from RRMS patients when compared to either controls or SPMS patients. The majority of the genes associated with hypermethylated CGIs were involved in the regulation of gene transcription, pointing out severe dysfunctions at the initial stages of the disease. In SPMS, in contrast, more than 98% of the differentially methylated CGIs were hypomethylated. The residual hypermethylated portion (2%) was related to DNA transcription and the Wnt pathway. Wnt signalling participates in immune cell proliferation, inflammatory response and maintenance of the BBB integrity (Lengfeld et al., 2017; Shi et al., 2016). Interestingly, the Wnt pathway can have both a proinflammatory (Pereira et al., 2008) and an anti-inflammatory effect (De Ferrari et al., 2003; Di Liddo et al., 2015), and becomes significantly relevant in the pathophysiology of autoimmune diseases (Beyer et al., 2012; Tveita and Rekvig, 2011; Wang et al., 2014), including MS (Xie et al., 2013; Yuan et al., 2012).

After matching each DMR to its corresponding gene (DMG), it was found that more than half of the DMGs among the groups of study were common in both immune cell types, suggesting that similar underlying biological mechanisms might be altered in both cell subsets during the pathophysiology of MS. In line with this, Ewing and colleagues (2019) studied the methylome of CD4+, CD8+, CD14+ and CD19+ cells from MS patients and their matched controls, and reported common underlying disrupted mechanisms. In MS, dysfunctions of immune homeostasis can trigger a range of alterations including disruption of metabolic pathways (Fitzgerald et al., 2021; La Rocca et al., 2017), mitochondrial damage (La Rocca et al., 2017), deregulation of cytokine production (Rieckmann et al.,1994), elevated levels of reactive oxygen species (ROS) (Gilgun-Sherki and Melamed, 2004) and severe inflammatory response (Amoruso et al., 2020). In our study, an aberrant DNA methylation pattern affecting cellular metabolism, inter- and intra-cellular signalling, and post-translational protein modifications was reported in both Bmem and Treg cells of MS patients. Similarly, genes encoding miRNAs exhibited differential methylation profiles compromising biological

mechanisms such as gene silencing, regulation of the inflammatory process, regulation of interleukin production and cell migration.

In summary, the findings presented here extend our knowledge about the methylation profile of Bmem and Treg cells at the onset and in later stages of MS. Global hypomethylation was reported at diagnosis, while the opposite pattern was achieved in the secondary progressive form of the disease. The main differences were related to cellular metabolism, intra-cellular signalling and inflammatory processes. Interestingly, a significant number of differentially methylated genes coding for miRNAs was reported in the physiopathology of the disease.

5.3. Relation between DNA methylation and mRNA expression in immune cells of MS patients and controls

The contribution of DNAme to gene transcription has been extensively studied in the last two decades (Anastasiadi et al., 2018; Ando et al., 2019; Brenet et al., 2011; Inoue and Oishi, 2005), but its exact mechanism is still not fully understood. It is known that when a cytosine is methylated, the genome accessibility of transcription factors to the DNA is compromised and therefore the gene transcription is repressed (Li et al., 2014; Moore et al., 2012). The scientific community agrees that the addition of methyl groups in the promoter region is negatively associated with gene expression (Fuso et al., 2011; Nagji et al., 2010; Xiang et al., 2008), but this assumption is not always applicable (Smith et al., 2020; Wang et al., 2014). On the other hand, methylation in the gene body is widely accepted to correlate with higher gene expression (Ball et al., 2009; Murrell et al., 2001), but in recent years it has been reported that methylation of either the first intron (Anastasiadi et al., 2018) or the first exon (Brenet et al., 2011) could be associated with lower gene expression.

DNAme is one of the epigenetic mechanisms that regulate the transcription machinery. DNAme together with histone modifications regulate the condensation of the chromatin and the accessibility of the transcription factors to the DNA (Cedar et al., 2009; Du et al., 2015; Moore et al., 2012; Zhang et al., 2020). Among the epigenetic modifications, miRNAs comprise a short sequence of nucleotides complementary to RNA; therefore, they control gene expression as well (Shivakumar et al., 2017; Wang et al., 2017). This complex interaction between different epigenetic mechanisms determines gene transcription and subsequently might explain why certain paradigms cannot be validated when only one of the

epigenetic mechanisms is studied. The methylation effect on gene expression has not been extensively studied in MS. Most of methylome studies targeting immune cells of MS patients reported no data at the RNA level (Bos et al., 2015; Brorson et al., 2022; Dunaeva et al., 2017; Ewing et al., 2019; Graves et al., 2013; Kiseley et al., 2022; Kulakova et al., 2016; Kumagai et al., 2012; Lehman-Werman et al., 2016; Liggett et al., 2010; Maltby et al., 2015; Neven et al., 2016; Nourian et al., 2021; Pinto-Medel et al., 2017; Ramagopalan et al., 2008; Sokratous et al., 2018), especially regarding miRNA genes. To the best of our knowledge, Ruhrmann and colleagues (2018) are the only ones to do such research. In their study, they found that hypermethylation of the *VMP1/MIR21* locus in CD4+ T cells of RRMS patients was associated with lower levels of miR-21, contributing to an upregulation of its target genes. In MS, miR-21 expression is altered (Muñoz San-Martin et al., 2019; Quintana et al., 2017; Ruhrmann et al., 2018), and is a potential biomarker for the disease (Muñoz San-Martin et al., 2019). Nevertheless, the methylation of miRNA genes warrants further investigations.

In this pilot study, an array-based transcriptome analysis of the candidate genes and specific miRNA genes showing methylation differences among the groups of study was performed in both cell types studied. The objective was to elucidate the complex interplay between methylation and gene expression in MS patients at the onset and at the progressive stage of the disease.

5.3.1. At the onset of disease

At the moment of diagnosis, we reported downregulation of *IL21R* and *MIR181C,* while *NOS1*, *PTGFRN* and *OSBP2* were upregulated in Bmem cells derived from RRMS patients compared to controls. In Treg cells, decreased transcription levels of ECEL1P2 were reported when comparing RRMS patients to controls. Association analysis between methylation and RNA expression revealed that methylation at certain regions of the *IL21R*, *NOS1*, *OSBP2*, and *PTGFRN* genes was moderately correlated with their transcriptional activity.

The interleukin 21 receptor (IL21R) is present on the cell surface of lymphoid cells (Mehta et al., 2004) including B cells and T cells (Tzartos et al., 2011). The ligand for this receptor, the interleukin 21 (IL21), can have both proinflammatory and protective functions (Mehta et al. 2004). Dysfunctions on the IL21/IL21R pathway are reported in the development of many

autoimmune diseases (Guan et al., 2015; Liu et al., 2012; McGuire et al., 2011) including MS (Benveniste et al., 2014; Liu et al., 2008; Piao et al., 2007; Tzartos et al., 2011). Indeed, this pathway is crucial for the proper function of Bmem cells (Rankin et al., 2010). The stimulation of the IL21R/IL21 axis activates the Jak/STAT pathway, which ultimately regulates the immune response (Benveniste et al., 2014). The activity of this pathway is exacerbated in MS (Benveniste et al., 2014). The use of inhibitors for the Jak/STAT pathway has a beneficial effect in preclinical models of MS, improving the clinical course and attenuating immune response (Benveniste et al., 2014). In the experimental autoimmune encephalomyelitis (EAE) preclinical model, the role of IL21R has been subjected to controversy. Lee and colleagues (2015) found that IL21R knockout mice exhibited neuroprotection, while others reported a worsening of symptoms (Liu et al., 2008; Piao et al., 2007). Here, it was found that the expression of IL21R was downregulated in Bmem cells from RRMS patients, and that IL21R transcript levels were negatively correlated with methylation in the first intron of the gene. The hypermethylation of *IL21R* has been previously described in patients with inflammatory autoimmune diseases (Wang et al., 2018), including RRMS (Ewing et al., 2019; Maltby et al., 2018). However, none of them were validated at the mRNA level. In Bmem, we suggest that the hypermethylation of *IL21R* accompanied by lower mRNA expression might contribute to the regulation of the immune response during the initial stages of MS. However, further studies warrant investigation.

Nitric oxide synthase 1 (NOS1) is a Ca++-dependent enzyme involved in the production of nitric oxide (NO) in the CNS and the peripheral nervous system (Ibiza et al., 2008; Lan et al., 2017). NO is a free radical involved in cell homeostasis, inflammation, immune responses and neurodegeneration (Bogdan C., 2015; Ibiza et al., 2008; Wang et al., 2015). NO can interact with other free radicals, forming peroxynitrite (Predonzani A., 2015). The production of peroxynitrite is associated with MS (Cross et al., 1998). NO is extremely toxic for the cells and subsequently, its expression is tightly regulated (Bogdan C., 2015). NO expression varies concomitantly in response to NOS production (Smith KJ., 2002). Here, elevated levels of NOS1 were reported in Bmem cells derived from RRMS patients. It could therefore be assumed that elevated levels of NO might be detected in RRMS patients. NOS1-derived NO promotes systemic inflammation (Duma et al., 2011; Srivastava and Baig, 2018). In MS, abnormal NO levels have been associated with mitochondrial dysfunction and, ultimately, oxidative stress (Lan et al., 2017). In our study, RRMS patients presented 43 DMR within the genomic region of the *NOS1* gene when compared to the control group. Ten of them fell into

the gene body and the 3'-UTR, and were accompanied by changes in NOS expression. Aberrant methylation of *NOS1* has been reported in autoimmune diseases (Nada et al., 2021), including EAE (Catanzaro et al., 2016) and MS (Ewing et al., 2019). Our results suggest that changes in *NOS1* methylation in Bmem cells might lead to an upregulation of NOS1/NO, impairing the immune cell homeostasis, which in turn aggravates the inflammatory response in the initial stages of MS.

Oxysterol binding protein 2 (OSBP2) belongs to a family of proteins that binds to oxysterols, the oxygenated derivatives of cholesterol (Spann and Glass, 2013). Specifically, OSBP2 binds to 7-ketocholesterol, a pro-oxidative, proinflammatory and cytotoxic product derived from the auto-oxidation of cholesterol by ROS production (Anderson et al., 2020). Reactive 7-ketocholesterol interacts with the phospholipids of the cell membrane inducing changes in the endoplasmic reticulum (ER) structure (Vejux et al., 2020), stimulates the overproduction of both ROS (Vejux and Lizard, 2009) and proinflammatory cytokines (Huang et al., 2014), and ultimately leads to mitochondrial dysfunction (Gramajo et al., 2010) and cell death (Vejux et al., 2020). In MS, 7-ketocholesterol has been measured in the CSF of patients during the relapse phase (Diestel et al., 2003) and while undergoing neuroaxonal injury (McComb et al., 2021). Dimethyl fumarate (DMF), one of the common treatments in MS, attenuates the production of ROS mediated by the overexpression of 7-ketocholesterol (Zarrouk et al., 2017). In our study, we found that one of the binding proteins for 7-ketocholesterol, OSBP2, was upregulated in Bmem cells collected from RRMS patients. In addition, OSBP2 mRNA levels were moderately correlated with the methylation status of the gene body region. The hypomethylation of *OSBP2* has been observed in cells exposed to arsenic (Rea et al., 2017), and arsenic exposure has been associated with aberrant ROS production (Jomova et al., 2011). Thus, elevated levels of OBSP2 might be a compensatory mechanism acting on oxidative stress in the initial stages of the disease (Adamczyk and Adamczyk-Sowa, 2016). Therefore, the upregulation of NOS1 reported in Bmem cells derived from RRMS patients could suggest that this cell type might be subjected to severe reduction-oxidation (redox) homeostasis imbalance when the first symptoms of inflammation appear.

Prostaglandin F2 receptor inhibitor (PTGFRN) is a glycosylated type I transmembrane immunoglobulin that suppresses the binding of the prostaglandin F2-alpha (PGF2-α) to the prostaglandin F2 receptor (PTGFR). In the cuprizone preclinical model of MS, the use of

inhibitors for the PGF2-α/PTGR pathway attenuated the demyelination of the corpus callosum and inhibited the release of proinflammatory cytokines (Iwasa et al., 2014). Quercetin, a flavonoid with anti-inflammatory properties, modulates the expression of PTGFRN (Radreau et al., 2009) and the JAK/STAT pathway activity, ameliorating the clinical signs of EAE (Muthian et al., 2004). In our study, the methylation of the *PTGFRN* promoter was positively correlated with the mRNA expression. This might be explained by the fact that the DMRs reported in the promoter region did not fall into the CGI and thus, methylation may have only a subtle or no effect on the chromatin condensation (Nagji et al., 2010; Smith et al., 2020; Wang et al., 2014). We also observed that the addition of methyl groups in the intragenic enhancer GH01J116939, located in the first intron of *PTGFRN*, was negatively associated with PTGFRN expression, which might be relevant for future investigations. Overall, these results suggest that an upregulation of PTGFRN in Bmem cells collected from RRMS patients might be a compensatory mechanism against an acute inflammatory reaction.

Endothelin converting enzyme like 1 pseudogene 2 (*ECEL1P2*) is one of the three pseudogenes derived from the parental gene *ECEL1* (endothelin converting enzyme like 1), located at a distance of ~100 kb from the *ECEL1P2* sequence. Pseudogenes are complete or partial copies derived from parental protein-coding genes (Pink et al., 2011). Some pseudogenes can be transcribed to non-coding RNA (Pink et al., 2011), regulating the expression of parental genes (An et al., 2016) and modulating both inflammation (Rapicavoli et al., 2013) and immune response (Tang and Zhuge, 2021). Indeed, we found detectable mRNA expression of ECEL1P2 in Treg cells. The sequence upstream of this pseudogene overlaps with a highly conserved ~2 kb CGI, which contains two promoter-like regions. In our study, the CGI showed higher methylation levels concomitantly with lower mRNA expression when comparing RRMS to controls. The hypermethylation of the *ECEL1P2* CGI region has been reported in Alzheimer's disease (Altuna et al., 2019; Zhang et al., 2020), and with tobacco use (Joehanes et al., 2016). The smoking-induced epigenetic signature did not revert even after 30 years of smoking cessation (Joehanes et al., 2016). Smoking is one of the main risk factors for developing MS (Wingerchuk DM., 2011) and therefore, dysregulation of *ECEL1P2* might contribute to the pathophysiology of the disease.

The miR-181 family comprises miR-181a, miR-181b and miR-181c (Safran et al., 2021). These miRNAs are involved in vascular inflammation, leukaemia and immune homeostasis

(Su et al., 2014; Sun et al., 2014). Concretely, miR-181c inhibits the Hippo signalling pathway (Chen et al., 2015), an intracellular pathway that regulates cell proliferation, apoptosis and the maintenance of the immune system homeostasis (Chen et al., 2020; Hong et al., 2018; Yamauchi et al., 2019). Additionally, miR-181c participates in oestrogen signalling (Benedetti et al., 2021; Fletcher et al., 2014), a pathway that controls the activation and survival of B cells (Grimaldi et al., 2002). Disruption of the miR-181 family has been previously reported in MS (Ghorbani et al., 2017; Zhang et al., 2018). In fact, upon CD4+ T cell activation by MOG exposure, a candidate autoantigen for MS, primary and secondary progressive MS patients displayed downregulation of both miR-181a and miR-181b in the white matter (Ghorbani et al., 2017). In EAE mice, the inhibition of miR-181c slows down the progression of the disease (Zhang et al., 2018). In this study, we found that RRMS patients exhibited lower levels of miR-181c in Bmem cells when compared to controls. This finding might point out that the Hippo and the oestrogen signalling are compromised in Bmem cells, aggravating the disease.

5.3.2. Later stages of the disease

In the later stages of the disease, a group of miRNA genes such as *MIR29A*, *MIR30D*, *MIR26A*, *MIR92B*, *MIR150* and *MIR193A* displayed lower expression in Bmem cells collected from SPMS patients compared to those recently diagnosed with MS. Among them, *MIR29A*, *MIR30D* and *MIR26A* presented DMRs associated with changes in miRNA expression.

MIR29A is an intragenic miRNA gene clustered with *MIR29B1,* and is highly expressed in adaptive immune cells (Chang et al., 2008; Liston et al., 2012). In Bmem cells of MS patients, we found that the methylation in the proximal upstream region of *MIR29B1/A* was negatively correlated with miR-29a-3p expression, in line with previous studies (Desjobert et al., 2011; Mazzoccoli et al., 2018). These findings suggest that methylation in the gene body of EU154353, the host primary transcript for the *MIR29B1/A* cluster (Chang et al., 2008) might negatively affect *MIR29A* transcription. miR-29a participates in multiple cellular processes including proliferation, migration, angiogenesis, metabolic homeostasis, ECM regulation and immunomodulation (Mohan et al., 2010; Shi et al., 2020; Wang et al., 2018). Interestingly, miR-29a expression was negatively associated with MS severity (Ingwersen et al., 2014). Indeed, the use of natalizumab increases the expression of miR-29a (Ingwersen et

al., 2014). Contrarily, lower levels of miR-29 are accompanied by elevated IgG (Shi et al., 2020) and IFN-gamma (IFN-γ) production (Smith et al., 2012), triggering both inflammatory and autoimmune responses (Cron et al., 2020; Dey et al., 2021). IFN-γ is a pleiotropic proinflammatory cytokine released by activated B cells (Harris et al., 2005) that contributes to oxidative stress, DNA damage (Hubackova et al., 2016) and ultimately, neurodegeneration (Kim et al., 2015). Elevated levels of IFN-γ exacerbate the immune response (Ishida et al., 2009), while knockdown animals displayed neuroprotective effects against neurodegeneration (Mangano et al., 2012). In a randomized clinical study, SPMS patients treated with specific antibodies for IFN-γ displayed slower clinical progression than the placebo group (Skurkovich et al., 2001). These findings point out that miR-29a might have a protective role in the physiopathology of MS. In Bmem cells of MS patients, we reported that the addition of methyl groups was accompanied by lower expression of miR-29a, which might favour clinical disease progression.

miR-30d ameliorates the inflammatory and oxidative damage response upon acute injury in the EAE model (Paintlia et al., 2013). Furthermore, miR-30d promotes the beta-oxidation of fatty acids (Veitch et al., 2022), and regulates the microbiome balance in MS (Liu et al., 2019). Interestingly, Liu and colleagues (2019) observed that oral administration of miR-30d extracted from faeces of EAE mice could ameliorate the disease by increasing the population of Treg cells mediated by the gut bacteria activity. This synergism has also been seen in SPMS patients (Kadowaki et al., 2019). Changes in miR-30d expression driven by methylation have recently been reported (Li et al., 2022). In our study, high levels of methylation in the *MIR30D* proximal enhancer (GH08J134799) were strongly associated with lower expression of miR-30d-3p in Bmem cells derived from MS patients, in agreement with Suzuki et al. (2017) and Tang et al. (2020). This enhancer has been previously validated in B cells (Howe et al., 2020), and possess different binding sites for Yin Yang 1 (YY1) (Safran et al., 2021), a structural transcription factor involved in the looping of the DNA that becomes essential for connecting promoters and distal enhancers (Weintraub et al., 2017). These findings point out the protective role of miR-30d, and its potential as a candidate target for (de)methylation therapy.

miR-26a is an intragenic miRNA gene located inside the host gene *CTDSPL*. In the Bmem cell population, *MIR26A1* exhibited an aberrant methylation pattern and changes in its expression in SPMS patients when compared to RRMS patients. Our results suggest that

methylation in the gene body of *CTDSPL* could negatively affect the expression of mature miR-26a-5p. The upregulation of miR-26a has been observed in PBMCs during relapse (Honardoost et al., 2014), and also after treatment with IFN-beta (De Felice et al., 2014). The downregulation of miR-26a in EAE has been correlated with a more severe clinical course of the disease (Zhang et al., 2014). Intracellularly, miR-26a confers protection against ER-induced stress (Xu et al., 2020). ER stress is a common hallmark of neurodegenerative disorders (Hetz and Saxena, 2017; Lindholm et al., 2006), including MS (Haile et al,, 2017). In immune cells, ER stress stimulates the secretion of proinflammatory cytokines, aggravating neuroinflammation (Fernandez et al., 2021). The unfolded protein response (UPR) is activated to counteract the protein homeostasis imbalance (Hetz and Saxena, 2017). When the UPR is overwhelmed, apoptosis is activated, contributing to MS lesions (Stone and Lin, 2015). In line with this, we found lower levels of miR-29a and miR-30d in Bmem cells collected from the SPMS group. Both miRNAs act on USP37, contributing to ER stress through the ubiquitin-proteasome system (Lu et al., 2021; Nolan et al., 2016; Qu et al., 2021; Su et al., 2012).

miR-92b protects against oxidative stress (Chen et al., 2021), has a neuroprotective effect (Huang et al., 2022) and suppresses inflammatory response (Liu et al., 2020) by blocking the release of proinflammatory cytokines (Sun et al., 2020) or by targeting the phosphatase and tensin homolog (PTEN) enzyme (Jiang et al., 2021). The PTEN pathway is commonly deregulated in B cells of MS patients (Sievers et al., 2012), and closely associated with the maintenance of immune anergy and autoreactivity in this cell type (Smith et al., 2019). Additionally, miR-92b controls cell migration (Song et al., 2016) and favours BBB damage when its expression is remarkably low (Shen et al., 2021). In this study, lower levels of miR-92b were reported in Bmem cells of SPMS patients, which might undermine the proper function of this immune cell subset during the disease progression.

miR-150 is expressed in mature lymphocytes (Wang et al., 2018; Xiao et al., 2007), and regulates proliferation, differentiation and response by targeting the transcription factor c-Myb in B cells (Xiao et al., 2007). miR-150 can also exert a protective role by reducing the production of inflammatory cytokines and, ultimately, controlling the immune response (Sang et al., 2016). Indeed, miR-150$^{-/-}$ mice exhibited elevated levels of Ig (Xiao et al., 2007), while the overexpression of this miRNA led to lower levels of proinflammatory cytokines and ER-stress (Zhu et al., 2022). In PBMCs of patients suffering from autoimmune diseases,

intracellular changes in miR-150 have been measured (Wang et al., 2018). In MS patients, elevated levels of circulating miR-150 have been detected in the CSF (Quintana et al., 2017). Patients subjected to natalizumab treatment displayed changes in miR-150 expression in distinct body fluids such as CSF and plasma, but also in B cells (Bergman et al., 2016; Dolati et al., 2018; Franzoi et al., 2021). These results support the protective role of miR-150 in the pathology of MS.

The miR-193 family comprises miR-193a and miR-193b, both of which are involved in cancer (Gao et al., 2021; Xun et al., 2020). Low levels of miR-193 have been seen in B-cell lymphoma (Gao et al., 2021). In a proinflammatory environment, the overexpression of miR-193a aggravates the production of proinflammatory cytokines, while its downregulation hinders the activation of the nuclear factor κB (NF-κB) pathway (Yin et al., 2021). NF-κB signalling is closely related to MS development (Yue et al., 2018), and it contributes to the immune response by favouring B and T cell maturation (Dejardin E., 2006; Yue et al., 2018). Indeed, mice lacking the NF-κB subunit 1 (NF-κB1) are resistant to EAE (Hilliard et al., 1999). In this study, lower levels of miR-193a-5p were measured in Bmem cells derived from SPMS in comparison to RRMS patients. There are currently no studies available of miR-193a-5p in immune cells collected from MS patients. However, GO-based analysis of the target genes for this miRNA pointed out a remarkable contribution of miR-193a to the transforming growth factor (TGF)-beta signalling pathway, which might influence specific immunological phenomena including lymphocyte activation, expression of MHC molecules and cytokines, production of cell adhesion molecules and lastly, apoptosis (Aoki et al., 2005).

5.4. Relation between miR-181c expression and Gd+ lesions in RRMS patients

The presence of demyelinating lesions in the CNS is one of the common hallmarks of MS (Compston and Coles, 2008). These lesions can be classified into active and inactive lesions. Active inflammatory lesions are detected by the injection of gadolinium (Trip and Miller, 2005). In normal conditions, gadolinium cannot cross the BBB, but upon inflammation, gadolinium can pass through it. Gadolinium-enhanced (Gd+) lesions provide information about the status of the lesion (Trip and Miller, 2005). In RRMS patients, we reported lower levels of miR-181c-5p in Bmem cells that were accompanied by higher numbers of Gd+ lesions. In line with our findings, other studies have reported lower levels of miR-181c in active white matter brain lesions in comparison to NAWM and PBMCs (Ma et al., 2014).

Changes in miR-181c expression contribute to the Hippo signalling pathway imbalance (Chen et al., 2015), lastly compromising cell proliferation, apoptosis and immune system homeostasis (Chen et al., 2020; Hong et al., 2018; Yamauchi et al., 2019). Many targets of miR-181c are related to inflammatory events (Yin et al., 2017; Zhang et al., 2015). The overexpression of miR-181c confers neuroprotection after a spinal cord injury (Zhang et al., 2021b). These data, along with our findings, suggest that elevated levels of miR-181c might protect against the pathophysiological underlying mechanisms in MS.

5.5. Future perspectives for (de)methylation therapies in MS

Aberrant methylation is a common hallmark of many pathological diseases (Jin and Liu, 2018), including MS (Celarain and Tomas-Roig, 2020). Due to the reversible nature of epigenetic mechanisms, methylation therapies have arisen as a promising therapeutic strategy to reverse epigenetic modifications. Different demethylation enzymes have been developed over the last decade, the most common being the DNMT inhibitors such as decitabine, azacitidine and its derivative 5-aza-2'-deoxycytidine (DAC) (Neja SA., 2020). These epigenetic drugs have been used in cancer, with promising therapeutic applications (Asano et al., 2019; Biktasova et al., 2017; Ren et al., 2018; Takeshima et al., 2020). Decitabine and azacitidine are epigenetic drugs approved by the U.S. Food and Drug Administration (FDA) for the treatment of myelodysplastic syndromes (Howell et al., 2010) and acute leukaemia (Momparler et al., 1984). In MS, epigenetic drugs have been tested both *in vivo* and *in vitro* (Mangano et al., 2014; Peedicayil J., 2016). The majority of studies are focused on histone deacetylases inhibitors, but recently demethylation agents are arousing more interest (Mangano et al., 2014). The use of DAC in the EAE model leads to lower lymphocyte infiltration into the spinal cord, higher release of anti-inflammatory cytokines and elevated levels of circulating Treg cells. Similarly, treatment with demethylating drugs increases the Treg population and reduces the inflammatory response in a distinct *in vivo* model of inflammatory disease (Landman et al., 2021). However, safety precautions should be taken into consideration before the use of epigenetic drugs for therapeutic purposes in humans, though. First, the tested drugs both *in vivo* and *in vitro* affect the whole genome (Neja SA., 2020). The indiscriminate removal of methyl groups could lead to side effects unsuitable for therapeutic interventions in humans. With no control over demethylation, deleterious genes and DNA elements could be accidentally activated, jeopardizing the integrity of the organism. Second, the cytotoxic effects of these epigenetic drugs should not be

underestimated. For example, decitabine is 10 times more toxic than azacitidine (Howell et al., 2010).

In order to address these issues, several site-specific (de)methylation mechanisms have been developed in the last decade (Neja SA., 2020), using mainly the clustered regularly interspaced short palindromic repeats (CRISPR) technology, the zinc finger proteins (ZNFs) and the transcription activator-like effector (TALEs) protein bound to either TET enzymes (for demethylation) or DNMT enzymes (for methylation) and to single guide RNA (Neja SA., 2020). The approach based on Cas9 targeting the demethylation of the breast cancer gene 1 (*BRCA1*) promoter has been implemented (Choudhury et al., 2016). An elegant study performed by Liu and colleagues (2016) managed to edit the methylome of the mammalian genome using the CRISPR/Cas9 system fused with either TETs or DNMTs. Briefly, they demethylated distal enhancers to increase their target gene expression, but also blocked the attachment of CTCF to the DNA by methylating its binding sites. Furthermore, they stimulated the expression of brain-derived neurotrophic factors (BDNFs) in mouse cortical neurons by demethylating one of its alternative promoters.

Epigenetic therapies could also help to alleviate the health, social and economic burden caused by complex and disabling diseases such as MS (Aubry et al., 2013). In MS, the annual cost per patient ranges from 4600 – 34,800 € in mild disease (EDSS 0-3), to 8300 – 131,500 € in severe disease (EDSS 7-9) (Berg et al., 2016). This situation, added to the reduced treatment options available for progressive MS, underpinned the importance of developing novel and personalized treatments. Implementation of epigenetic therapies for MS could alleviate the economic and social burden, especially in those countries where the national health care system does not fully cover the cost of the treatments (Gharibi et al., 2021).

In addition, epigenetic therapies could offer a personalized treatment, offering an alternative to unresponsive patients. In this line, new generation drugs based on inhibitors for the Bruton's tyrosine kinase (BTK) -a molecule implicated in B cell signalling-, are being developed for the progressive forms of MS with promising results (Garcia-Merino A., 2021). During the clinical trials, however, a subset of patients developed an acquired resistance to the treatment attributable to uncontrolled epigenetic mechanisms (Burke et al., 2021; Shaffer et al., 2021). Directed (de)methylation therapies in certain regions of the DNA could help to

revert this acquired resistance. These results point out the importance of cell-type specific studies based on DNA methylation, as we reported here.

The involvement of miRNAs in treatment-resistance has also been studied (Magee et al., 2015). The family of miR-181, miR-29 and miR-30, for example, are tightly linked to chemotherapy sensitivity (Lu et al., 2014; Okamoto et al., 2013; Wen et al., 2020), while miR-181d levels have been related to drug response in autoimmune diseases (Cavalcante et al., 2019). The expression of some of these miRNAs could be guided by the addition or removal of methylation marks at certain genomic regions of their locus. Treatments in MS such as Natalizumab and IFN-beta alter both DNA methylation pattern (Souren et al., 2019) and miRNA expression (Franzoi et al., 2021). Novel therapies directed toward specific DMR could potentially improve the treatment response and ultimately, the quality of life of the patients.

In conclusion, the results reported here underpin the contribution of DNAme in neurological disorders and its potential therapeutic applications. Herein, a methylation-dependent effect on the expression of seven genes (*PTGFRN, IL21R, OSBP2, NOS1, MIR29A, MIR26A, MIR30D*) has been observed in Bmem cells derived from MS patients. Among these genes, *MIR29A,* and to a lesser extent *MIR30D* and *MIR26A*, could be key therapeutic candidates for site-targeted DNAme modifications due to their protective effect in MS (De Felice et al., 2014; Ingwersen et al., 2014; Liu et al., 2019; Zhang et al., 2014), and the scarce treatment options available for SPMS patients (Oh et al., 2019). Restoration of the basal methylation status of these miRNA genes could increase their expression and therefore, revert neurodegeneration alleviating the clinical symptoms observed in SPMS patients. Nonetheless, side effects of site-targeted methylation therapies are still under study (Kuscu et al., 2014; Lei et al., 2018), and the precise effect of epigenetics drugs on MS warrants further investigation.

5.6. Limitation of the study

This is a pilot study based on the methylome differences reported in distinct immune cells derived from MS patients. These results were validated at the RNA level, contributing to understanding the underlying mechanisms of the disease.

The most relevant limitations of this study are:

a. **Sample size**

   The sample size was limited to not more than 10 individuals per group, meaning that our cohort might not be an accurate representation of the general population.

b. **Geographic distribution of the participants of the study**

   The recruitment of MS patients and controls was limited to the province of Girona. Therefore, the influence of region-specific environmental and genetic factors on our results cannot be discarded.

c. **Age of volunteers**

   The age difference between RRMS and SPMS patients was remarkably significant. The methylation status of the DNA follows an age-dependent manner. Thus, the influence of age-related methylation changes in SPMS patients cannot be discarded.

d. **Low amount of starting material in Treg cells**

   The limited amount of DNA obtained from Treg cells led to the disposal of 11 samples (3 controls, 3 RRMS and 5 SPMS) prior to sequencing. Similarly, only 13 samples (5 controls, 5 RRMS and 3 SPMS) were available for the study of miRNA expression.

e. **Lack of previous knowledge on the topic**

   To the best of our knowledge, no prior research on the methylome of Treg cells in MS has been performed. This knowledge gap limited the discussion and comparison of the results with other peer-reviewed studies.

These limitations could be addressed by increasing the sample size and by establishing national and international collaborations to obtain a more heterogeneous sample. The age difference between the RRMS and SPMS groups could be solved by recruiting age-matched controls. Finally, functional studies at the protein level should be carried out to validate the biological effect of the methylation-driven changes on gene expression.

6. Conclusions

1. RRMS and SPMS patients displayed aberrant genome-wide methylation profiles in Bmem cell and Treg cell populations. RRMS patients showed global hypomethylation in comparison to either controls or SPMS patients.

2. Intergenic and intronic regions comprised more than 90% of the DMRs detected among the groups of study. Nearly half of the DMRs were located within repeats and transposable elements of the DNA, suggesting that they might not be properly regulated by methylation, lastly contributing to the pathology of the disease.

3. At the moment of diagnosis, the transcriptome analysis of candidate DMGs and miRNAs showed lower levels of IL21R and MIR181C concomitantly with higher levels of NOS1, PTGFRN and OSBP2 in Bmem cells derived from RRMS patients compared to controls. In Treg cells, decreased transcription levels of ECEL1P2 were reported when comparing RRMS to controls. Association analysis between methylation levels and RNA expression revealed that methylation at certain regions of *IL21R*, *NOS1*, *OSBP2* and *PTGFRN* was moderately correlated with their transcriptional activity. These genes are involved in inflammation, signal transduction, redox homeostasis and immune response.

4. At the progressive stage of the disease, the transcriptome analysis of differentially methylated candidate miRNA genes revealed lower levels of miR-193a-5p, miR30d-3p, miR-92b-3p, miR-26a-5p, miR-29a-3p and miR-150-5p in SPMS patients than in RRMS patients. Association analysis between methylation and RNA expression revealed that methylation at the proximal region of *MIR29A* and *MIR26A1*, as well as in the enhancers for *MIR29A* and *MIR30D*, negatively correlated with miRNA levels. These miRNAs are related to the immune response, inflammation, oxidative stress and cell metabolism.

5. The expression of miR-181c-5p in Bmem cells derived from RRMS patients showed a strong negative association with the number of Gd+ lesions in the brain. miR-181c qualifies as a promising candidate to counteract the clinical damage seen in MS.

7. References

Abbas AK, Lichtman AH, Pillai S, Amsterdam E. Basic immunology: functions and disorders of the immune system. 6th edition. Philadelphia: Elsevier; 2020.
Adamczyk B, Adamczyk-Sowa M. New Insights into the Role of Oxidative Stress Mechanisms in the Pathophysiology and Treatment of Multiple Sclerosis. Oxidative Medicine and Cellular Longevity. 2016;2016:1–18.
Adhikari A, Martel C, Marette A, Olivier M. Hepatocyte SHP-1 is a Critical Modulator of Inflammation During Endotoxemia. Scientific Reports. 2017 May 22;7(1).
Agarwal V, Bell GW, Nam J-W, Bartel DP. Predicting effective microRNA target sites in mammalian mRNAs. eLife. 2015 Aug 12;4.
Al-Hajri Z, Del Bigio MR. Brain damage in a large cohort of solvent abusers. Acta Neuropathologica. 2010 Feb 21;119(4):435–45.
Alberts B, Johnson A, Lewis J, Raff M, Roberts K, Walter P. Helper T Cells and Lymphocyte Activation. Nih.gov. Garland Science; 2015.
Allen NJ, Lyons DA. Glia as architects of central nervous system formation and function. Science. 2018 Oct 12;362(6411):181–5.
Allis CD, Jenuwein T. The molecular hallmarks of epigenetic control. Nature Reviews Genetics. 2016 Jun 27;17(8):487–500.
Altuna M, Urdánoz-Casado A, Sánchez-Ruiz de Gordoa J, Zelaya MV, Labarga A, Lepesant JMJ, et al. DNA methylation signature of human hippocampus in Alzheimer's disease is linked to neurogenesis. Clinical Epigenetics. 2019 Jun 19;11(1).
Amoruso A, Blonda M, Gironi M, Grasso R, Di Francescantonio V, Scaroni F, et al. Immune and central nervous system-related miRNAs expression profiling in monocytes of multiple sclerosis patients. Scientific Reports. 2020 Apr 9;10(1).
An Y, Furber KL, Ji S. Pseudogenes regulate parental gene expressionviaceRNA network. Journal of Cellular and Molecular Medicine. 2016 Aug 25;21(1):185–92.
Anastasiadi D, Esteve-Codina A, Piferrer F. Consistent inverse correlation between DNA methylation of the first intron and gene expression across tissues and species. Epigenetics & Chromatin. 2018 Jun 29;11(1).
Andersen MH, Schrama D, thor Straten P, Becker JC. Cytotoxic T Cells. Journal of Investigative Dermatology. 2006 Jan;126(1):32–41.
Anderson A, Campo A, Fulton E, Corwin A, Jerome WG, O'Connor MS. 7-Ketocholesterol in disease and aging. Redox Biology. 2020 Jan;29:101380.
Ando M, Saito Y, Xu G, Bui NQ, Medetgul-Ernar K, Pu M, et al. Chromatin dysregulation and DNA methylation at transcription start sites associated with transcriptional repression in cancers. Nature Communications. 2019 May 16;10(1).
Andrews S. (2010). FastQC: A Quality Control Tool for High Throughput Sequence Data. Available online at: http://www.bioinformatics.babraham.ac.uk/projects/fastqc/
Aoki CA, Borchers AT, Li M, Flavell RA, Bowlus CL, Ansari AA, et al. Transforming growth factor β (TGF-β) and autoimmunity. Autoimmunity Reviews. 2005 Sep;4(7):450–9.
Aran D, Sabato S, Hellman A. DNA methylation of distal regulatory sites characterizes dysregulation of cancer genes. Genome Biology. 2013;14(3):R21.
Aran D, Toperoff G, Rosenberg M, Hellman A. Replication timing-related and gene body-specific methylation of active human genes. Human Molecular Genetics. 2010 Nov 26;20(4):670–80.
Asano N, Takeshima H, Yamashita S, Takamatsu H, Hattori N, Kubo T, et al. Epigenetic reprogramming underlies efficacy of DNA demethylation therapy in osteosarcomas. Scientific Reports. 2019 Dec;9(1).

Ascherio A, Munger KL. Environmental risk factors for multiple sclerosis. Part II: Noninfectious factors. Annals of Neurology. 2007 May 10;61(6):504–13.
Aubry W, Lieberthal R, Willis A, Bagley G, Willis SM, Layton A. Budget impact model: epigenetic assay can help avoid unnecessary repeated prostate biopsies and reduce healthcare spending. American health & drug benefits. 2013;6(1):15–24.
Auclair G, Weber M. Mechanisms of DNA methylation and demethylation in mammals. Biochimie. 2012 Nov;94(11):2202–11.
Ayuso T, Aznar P, Soriano L, Olaskoaga A, Roldán M, Otano M, et al. Vitamin D receptor gene is epigenetically altered and transcriptionally up-regulated in multiple sclerosis. Campbell M, editor. PLOS ONE 2017 Mar 29;12(3):e0174726.
Baker D, Marta M, Pryce G, Giovannoni G, Schmierer K. Memory B Cells are Major Targets for Effective Immunotherapy in Relapsing Multiple Sclerosis. EBioMedicine. 2017 Feb;16:41–50.
Ball MP, Li JB, Gao Y, Lee J-H, LeProust EM, Park I-H, et al. Targeted and genome-scale strategies reveal gene-body methylation signatures in human cells. Nature Biotechnology. 2009 Mar 29;27(4):361–8.
Bannert N, Kurth R. Retroelements and the human genome: New perspectives on an old relation. Proceedings of the National Academy of Sciences. 2004 Oct 5;101(suppl_2):14572–9.
Baranzini SE, Mudge J, van Velkinburgh JC, Khankhanian P, Khrebtukova I, Miller NA, et al. Genome, epigenome and RNA sequences of monozygotic twins discordant for multiple sclerosis. Nature. 2010 Apr;464(7293):1351–6.
Barroso M, Tucker H, Drake L, Nichol K, Drake JR. Antigen-B Cell Receptor Complexes Associate with Intracellular major histocompatibility complex (MHC) Class II Molecules. Journal of Biological Chemistry. 2015 Nov;290(45):27101–12.
Bartel DP. MicroRNAs:Genomics, Biogenesis, Mechanism, and Function. Cell. 2004 Jan;116(2):281–97.
Baskerville S. Microarray profiling of microRNAs reveals frequent coexpression with neighboring miRNAs and host genes. RNA. 2005 Jan 20;11(3):241–7.
Baumann N, Pham-Dinh D. Biology of Oligodendrocyte and Myelin in the Mammalian Central Nervous System. Physiological Reviews. 2001 Apr 1;81(2):871–927.
Bell L, Lenhart A, Rosenwald A, Monoranu CM, Berberich-Siebelt F. Lymphoid Aggregates in the CNS of Progressive Multiple Sclerosis Patients Lack Regulatory T Cells. Frontiers in Immunology. 2020 Jan 15;10.
Bell RE, Golan T, Sheinboim D, Malcov H, Amar D, Salamon A, et al. Enhancer methylation dynamics contribute to cancer plasticity and patient mortality. Genome Research. 2016 Feb 23;26(5):601–11.
Benedetti R, Papulino C, Sgueglia G, Chianese U, De Marchi T, Iovino F, et al. Regulatory Interplay between miR-181a-5p and Estrogen Receptor Signaling Cascade in Breast Cancer. Cancers. 2021 Feb 1;13(3):543.
Benveniste EN, Liu Y, McFarland BC, Qin H. Involvement of the Janus Kinase/Signal Transducer and Activator of Transcription Signaling Pathway in Multiple Sclerosis and the Animal Model of Experimental Autoimmune Encephalomyelitis. Journal of Interferon & Cytokine Research. 2014 Aug;34(8):577–88.
Berg J, Gannedahl M, Capsa D, Eriksson J, Thompson A, Kobelt G. The Cost Of Multiple Sclerosis In 16 European Countries: Functional Status, Symptoms And Mental Factors Drive Costs. Value in Health. 2016 Nov;19(7):A352.
Bergman P, Piket E, Khademi M, James T, Brundin L, Olsson T, et al. Circulating miR-150 in CSF is a novel candidate biomarker for multiple sclerosis. Neurology - Neuroimmunology

Neuroinflammation. 2016 Apr 20;3(3):e219.
Bernstein E, Caudy AA, Hammond SM, Hannon GJ. Role for a bidentate ribonuclease in the initiation step of RNA interference. Nature. 2001 Jan;409(6818):363–6.
Betsou F, Gaignaux A, Ammerlaan W, Norris PJ, Stone M. Biospecimen Science of Blood for Peripheral Blood Mononuclear Cell (PBMC) Functional Applications. Current Pathobiology Reports. 2019 May 11;7(2):17–27.
Beyer C, Schramm A, Akhmetshina A, Dees C, Kireva T, Gelse K, et al. β-catenin is a central mediator of pro-fibrotic Wnt signaling in systemic sclerosis. Annals of the Rheumatic Diseases. 2012 Feb 10;71(5):761–7.
Biktasova A, Hajek M, Sewell A, Gary C, Bellinger G, Deshpande HA, et al. Demethylation Therapy as a Targeted Treatment for Human Papillomavirus–Associated Head and Neck Cancer. Clinical Cancer Research . 2017 Sep 15;23(23):7276–87.
Bird AP. CpG-rich islands and the function of DNA methylation. Nature. 1986 May;321 (6067):209–13.
Bogdan C. Nitric oxide synthase in innate and adaptive immunity: an update. Trends in Immunology. 2015 Mar;36(3):161–78.
Bos SD, Page CM, Andreassen BK, Elboudwarej E, Gustavsen MW, Briggs F, et al. Genome-Wide DNA Methylation Profiles Indicate CD8+ T Cell Hypermethylation in Multiple Sclerosis. Ting AH, editor. PLOS ONE. 2015 Mar 3;10(3):e0117403.
Bourque G, Burns KH, Gehring M, Gorbunova V, Seluanov A, Hammell M, et al. Ten things you should know about transposable elements. Genome Biology. 2018 Nov 19;19(1).
Brenet F, Moh M, Funk P, Feierstein E, Viale AJ, Socci ND, et al. DNA Methylation of the First Exon Is Tightly Linked to Transcriptional Silencing. Papavasiliou N, editor. PLoS ONE. 2011 Jan 18;6(1):e14524.
Brorson IS, Eriksson AM, Høgestøl E, Leikfoss IS, Harbo HF, Berge T, et al. Global DNA methylation changes in treated and untreated MS patients measured over time. Journal of Neuroimmunology. 2022 Mar;364:577808.
Brudek T, Christensen T, Aagaard L, Petersen T, Hansen HJ, Møller-Larsen A. B cells and monocytes from patients with active multiple sclerosis exhibit increased surface expression of both HERV-H Env and HERV-W Env, accompanied by increased seroreactivity. Retrovirology. 2009 Nov 16;6(1).
Buhelt S, Laigaard H-M, von Essen MR, Ullum H, Oturai A, Sellebjerg F, et al. IL2RA Methylation and Gene Expression in Relation to the Multiple Sclerosis-Associated Gene Variant rs2104286 and Soluble IL-2Rα in CD8+ T Cells. Frontiers in Immunology. 2021 Jul 27;12.
Burke K, Nuttall B, Karl DL, Callahan M, Mendler K, Criscione S, et al. Novel Mechanisms of Acalabrutinib Resistance in Patients with Chronic Lymphocytic Leukemia By Whole Genome Methylome Sequencing. Blood. 2021 Nov 5;138(Supplement 1):4361–1.
Calabrese R, Zampieri M, Mechelli R, Annibali V, Guastafierro T, Ciccarone F, et al. Methylation-dependent PAD2 upregulation in multiple sclerosis peripheral blood. Multiple Sclerosis Journal 2011 Aug 30;18(3):299–304.
Catanzaro G, Pucci M, Viscomi MT, Lanuti M, Feole M, Angeletti S, et al. Epigenetic modifications of Dexras 1 along the nNOS pathway in an animal model of multiple sclerosis. Journal of Neuroimmunology. 2016 May;294:32–40.
Cavalcante P, Mizrachi T, Barzago C, Scandiffio L, Bortone F, Bonanno S, et al. MicroRNA signature associated with treatment response in myasthenia gravis: A further step towards precision medicine. Pharmacological Research. 2019 Oct;148:104388.
Cedar H, Bergman Y. Linking DNA methylation and histone modification: patterns and

paradigms. Nature Reviews Genetics. 2009 May;10(5):295–304.
Celarain N, Tomas-Roig J. Aberrant DNA methylation profile exacerbates inflammation and neurodegeneration in multiple sclerosis patients. Journal of Neuroinflammation. 2020 Jan 14;17(1).
Celarain N, Tomas-Roig J. Changes in Deoxyribonucleic Acid Methylation Contribute to the Pathophysiology of Multiple Sclerosis. Frontiers in Genetics. 2019 Nov 12;10.
Cepok S;Zhou D;Srivastava R;Nessler S;Stei S;Büssow K;Sommer N;Hemmer B. Identification of Epstein-Barr virus proteins as putative targets of the immune response in multiple sclerosis. The Journal of clinical investigation. 2005;115(5).
Chang T-C, Yu D, Lee Y-S, Wentzel EA, Arking DE, West KM, et al. Widespread microRNA repression by Myc contributes to tumorigenesis. Nature Genetics. 2008 Jan ;40(1):43–50.
Chaplin DD. Overview of the immune response. Journal of Allergy and Clinical Immunology . 2010 Feb;125(2):S3–23.
Chen L, Chi H, Kinashi T. Editorial: Hippo Signaling in the Immune System. Frontiers in Immunology. 2020 Oct 14;11.
Chen M, Wang M, Xu S, Guo X, Jiang J. Upregulation of miR-181c contributes to chemoresistance in pancreatic cancer by inactivating the Hippo signaling pathway. Oncotarget. 2015 Oct 26;6(42):44466–79.
Chen YC, Hsu PY, Su MC, Chen TW, Hsiao CC, Chin C-H, et al. MicroRNA Sequencing Analysis in Obstructive Sleep Apnea and Depression: Anti-Oxidant and MAOA-Inhibiting Effects of miR-15b-5p and miR-92b-3p through Targeting PTGS1-NF-κB-SP1 Signaling. Antioxidants. 2021 Nov 22;10(11):1854.
Chen Y, Wang X. miRDB: an online database for prediction of functional microRNA targets. Nucleic Acids Research. 2019 Aug 31;48(D1):D127–31.
Chomyk AM, Volsko C, Tripathi A, Deckard SA, Trapp BD, Fox RJ, et al. DNA methylation in demyelinated multiple sclerosis hippocampus. Scientific Reports 2017 Aug 18 ;7(1).
Choudhury SR, Cui Y, Lubecka K, Stefanska B, Irudayaraj J. CRISPR-dCas9 mediated TET1 targeting for selective DNA demethylation at BRCA1 promoter. Oncotarget. 2016 Jun 23;7(29):46545–56.
Claudio L, Raine CS, Brosnan CF. Evidence of persistent blood-brain barrier abnormalities in chronic-progressive multiple sclerosis. Acta Neuropathologica. 1995 Sep;90(3):228–38.
Coles AJ, Wing MG, Molyneux P, Paolillo A, Davie CM, Hale G, et al. Monoclonal antibody treatment exposes three mechanisms underlying the clinical course of multiple sclerosis. Annals of neurology. 1999;46(3):296-304.
Compston A, Coles A. Multiple sclerosis. The Lancet. 2008 Oct;372(9648):1502–17.
Compston A, Confavreux C. The distribution of multiple sclerosis. McAlpine's Multiple Sclerosis. 2006;71–111.
Cossarizza A, Chang H, Radbruch A, Acs A, Adam D, Adam‐Klages S, et al. Guidelines for the use of flow cytometry and cell sorting in immunological studies (second edition). European Journal of Immunology. 2019 Oct;49(10):1457–973.
Costantino CM, Baecher-Allan C, Hafler DA. Multiple Sclerosis and Regulatory T Cells. Journal of Clinical Immunology . 2008 Sep 2;28(6):697–706.
Cron MA, Payet CA, Fayet O-M, Maillard S, Truffault F, Fadel E, et al. Decreased expression of miR-29 family associated with autoimmune myasthenia gravis. Journal of Neuroinflammation. 2020 Oct 8;17(1).
Cross AH, Manning PT, Keeling RM, Schmidt RE, Misko TP. Peroxynitrite formation within the central nervous system in active multiple sclerosis. Journal of Neuroimmunology. 1998 Aug;88(1-2):45–56.

Cyster JG, Allen CDC. B Cell Responses: Cell Interaction Dynamics and Decisions. Cell . 2019 Apr;177(3):524–40.
Danikowski KM, Jayaraman S, Prabhakar BS. Regulatory T cells in multiple sclerosis and myasthenia gravis. Journal of Neuroinflammation. 2017 Jun 9;14(1).
De Felice B, Mondola P, Sasso A, Orefice G, Bresciamorra V, Vacca G, et al. Small non-coding RNA signature in multiple sclerosis patients after treatment with interferon-β. BMC Medical Genomics. 2014 May 17;7(1).
De Ferrari GV, Chacón MA, Barría MI, Garrido JL, Godoy JA, Olivares G, et al. Activation of Wnt signaling rescues neurodegeneration and behavioral impairments induced by β-amyloid fibrils. Molecular Psychiatry. 2003 Feb;8(2):195–208.
Deaton AM, Bird A. CpG islands and the regulation of transcription. Genes & Development. 2011 May 15;25(10):1010–22.
Dejardin E. The alternative NF-κB pathway from biochemistry to biology: Pitfalls and promises for future drug development. Biochemical Pharmacology. 2006 Oct;72(9):1161–79.
Desjobert C, Renalier M-H, Bergalet J, Dejean E, Joseph N, Kruczynski A, et al. MiR-29a down-regulation in ALK-positive anaplastic large cell lymphomas contributes to apoptosis blockade through MCL-1 overexpression. Blood. 2011 Jun 16;117(24):6627–37.
Dey S, Udari LM, Rivera Hernandez P, Kwon JJ, Willis B, Easler JJ, et al. Loss of miR-29a/b1 promotes inflammation and fibrosis in acute pancreatitis. JCI Insight. 2021 Oct 8;6(19).
Di Liddo R, Bertalot T, Schuster A, Schrenk S, Tasso A, Zanusso I, et al. Anti-inflammatory activity of Wnt signaling in enteric nervous system: in vitro preliminary evidence in rat primary cultures. Journal of Neuroinflammation. 2015;12(1):23.
Diestel A, Aktas O, Hackel D, HäkeI, Meier S, Raine CS, et al. Activation of Microglial Poly(ADP-Ribose)-Polymerase-1 by Cholesterol Breakdown Products during Neuroinflammation. Journal of Experimental Medicine. 2003 Dec 1;198(11):1729–40.
Dietrich JB. The adhesion molecule ICAM-1 and its regulation in relation with the blood–brain barrier. Journal of Neuroimmunology. 2002 Jul;128(1-2):58–68.
Dobson R, Ramagopalan S, Davis A, Giovannoni G. Cerebrospinal fluid oligoclonal bands in multiple sclerosis and clinically isolated syndromes: a meta-analysis of prevalence, prognosis and effect of latitude. Journal of Neurology, Neurosurgery & Psychiatry. 2013 Feb 21;84(8):909–14.
Dolati S, Marofi F, Babaloo Z, Aghebati-Maleki L, Roshangar L, Ahmadi M, et al. Dysregulated Network of miRNAs Involved in the Pathogenesis of Multiple Sclerosis. Biomedicine & Pharmacotherapy. 2018 Aug;104:280–90.
Du Q, Luu P-L, Stirzaker C, Clark SJ. Methyl-CpG-binding domain proteins: readers of the epigenome. Epigenomics. 2015 Sep;7(6):1051–73.
Duma D, Fernandes D, Bonini MG, Stadler K, Mason RP, Assreuy J. NOS-1-derived NO is an essential triggering signal for the development of systemic inflammatory responses. European Journal of Pharmacology. 2011 Oct;668(1-2):285–92.
Dunaeva M, Derksen M, Pruijn GJM. LINE-1 Hypermethylation in Serum Cell-Free DNA of Relapsing Remitting Multiple Sclerosis Patients. Molecular Neurobiology. 2017 Jul 13;55(6):4681–8.
Eden E, Lipson D, Yogev S, Yakhini Z. Discovering Motifs in Ranked Lists of DNA Sequences. Fraenkel E, editor. PLoS Computational Biology. 2007;3(3):e39.
Eden E, Navon R, Steinfeld I, Lipson D, Yakhini Z. GOrilla: a tool for discovery and visualization of enriched GO terms in ranked gene lists. BMC Bioinformatics. 2009;10(1).
El-Zayat SR, Sibaii H, Mannaa FA. Toll-like receptors activation, signaling, and targeting: an overview. Bulletin of the National Research Centre. 2019 Dec;43(1).

Elhamamsy AR. Role of DNA methylation in imprinting disorders: an updated review. Journal of Assisted Reproduction and Genetics. 2017 Mar 9;34(5):549–62.
EMSP - Barometer [Internet]. Msbarometer.eu. 2020. Available from: https://msbarometer.eu/2020.
Ewing E, Kular L, Fernandes SJ, Karathanasis N, Lagani V, Ruhrmann S, et al. Combining evidence from four immune cell types identifies DNA methylation patterns that implicate functionally distinct pathways during Multiple Sclerosis progression. EBioMedicine 2019 May;43:411–23.
Eyholzer M, Schmid S, Wilkens L, Mueller BU, Pabst T. The tumour-suppressive miR-29a/b1 cluster is regulated by CEBPA and blocked in human AML. British Journal of Cancer. 2010 Jul;103(2):275–84.
Fagone P, Mangano K, Di Marco R, Touil-Boukoffa C, Chikovan T, Signorelli S, et al. Expression of DNA methylation genes in secondary progressive multiple sclerosis. Journal of Neuroimmunology. 2016 Jan;290:66–9.
Fernández D, Geisse A, Bernales JI, Lira A, Osorio F. The Unfolded Protein Response in Immune Cells as an Emerging Regulator of Neuroinflammation. Frontiers in Aging Neuroscience. 2021 Jun 11;13.
Fetahu IS, Höbaus J, Kállay E. Vitamin D and the epigenome. Frontiers in Physiology. 2014 Apr 29;5:164.
Field J, Fox A, Jordan MA, Baxter AG, Spelman T, Gresle M, et al. Interleukin-2 receptor-α proximal promoter hypomethylation is associated with multiple sclerosis. Genes & Immunity. 2017 Jan 12;18(2):59–66.
Filippi M. Evidence for widespread axonal damage at the earliest clinical stage of multiple sclerosis. Brain. 2003 Feb 1;126(2):433–7.
Fishilevich S, Nudel R, Rappaport N, Hadar R, Plaschkes I, Iny Stein T, et al. GeneHancer: genome-wide integration of enhancers and target genes in GeneCards. Database. 2017 Jan 1;2017.
Fitzgerald KC, Smith MD, Kim S, Sotirchos ES, Kornberg MD, Douglas M, et al. Multi-omic evaluation of metabolic alterations in multiple sclerosis identifies shifts in aromatic amino acid metabolism. Cell Reports Medicine. 2021 Oct;2(10):100424.
Fletcher CE, Dart DA, Bevan CL. Interplay between steroid signalling and microRNAs: implications for hormone-dependent cancers. Endocrine Related Cancer. 2014 Jul 25;21(5):R409–29.
Franklin RJM. Why does remyelination fail in multiple sclerosis? Nature Reviews Neuroscience. 2002 Sep;3(9):705–14.
Franzoi AE de A, de Moraes Machado FS, de Medeiros Junior WLG, Bandeira IP, Brandão WN, Gonçalves MVM. Altered expression of microRNAs and B lymphocytes during Natalizumab therapy in multiple sclerosis. Heliyon. 2021 Jun;7(6):e07263.
Furuta M, Kozaki K, Tanaka S, Arii S, Imoto I, Inazawa J. miR-124 and miR-203 are epigenetically silenced tumor-suppressive microRNAs in hepatocellular carcinoma. Carcinogenesis. 2009 Oct 20;31(5):766–76.
Fuso A, Nicolia V, Pasqualato A, Fiorenza MT, Cavallaro RA, Scarpa S. Changes in Presenilin 1 gene methylation pattern in diet-induced B vitamin deficiency. Neurobiology of Aging. 2011 Feb;32(2):187–99.
Gao H-X, Li S-J, Wang M-B, Yan S-F, Cui W-L, Ma Z-P, et al. Screening and identification of differentially expressed microRNAs in diffuse large B-cell lymphoma based on microRNA microarray. Oncology Letters. 2021 Aug 27;22(5).

García-Merino A. Bruton's Tyrosine Kinase Inhibitors: A New Generation of Promising Agents for Multiple Sclerosis Therapy. Cells. 2021 Sep 27;10(10):2560.
Gelfman S, Cohen N, Yearim A, Ast G. DNA-methylation effect on cotranscriptional splicing is dependent on GC architecture of the exon–intron structure. Genome Research. 2013 Mar 1;23(5):789–99.
Gharibi F, Imani A, Dalal K. The catastrophic out-of-pocket health expenditure of multiple sclerosis patients in Iran. BMC Health Services Research. 2021 Mar 20;21(1).
Ghorbani S, Talebi F, Chan WF, Masoumi F, Vojgani M, Power C, et al. MicroRNA-181 Variants Regulate T Cell Phenotype in the Context of Autoimmune Neuroinflammation. Frontiers in Immunology. 2017 Jul 19;8.
Gilgun-Sherki Y, Melamed E. The role of oxidative stress in the pathogenesis of multiple sclerosis: The need for effective antioxidant therapy. Journal of Neurology. 2004 Mar 1;251(3):261–8.
Glaich O, Parikh S, Bell RE, Mekahel K, Donyo M, Leader Y, et al. DNA methylation directs microRNA biogenesis in mammalian cells. Nature Communications. 2019 Dec;10(1).
Godderis L, De Raedt K, Tabish AM, Poels K, Maertens N, De Ruyck K, et al. Epigenetic changes in lymphocytes of solvent-exposed individuals. Epigenomics. 2012 Jun;4(3):269–77.
Goldenberg MM. Multiple sclerosis review. P & T : a peer-reviewed journal for formulary management. 2012;37(3):175–84.
Gramajo AL, Zacharias LC, Neekhra A, Luthra S, Atilano SR, Chwa M, et al. Mitochondrial DNA Damage Induced by 7-Ketocholesterol in Human Retinal Pigment Epithelial Cells In Vitro. Investigative Opthalmology & Visual Science. 2010 Feb 1 ;51(2):1164.
Graves M, Benton M, Lea R, Boyle M, Tajouri L, Macartney-Coxson D, et al. Methylation differences at the HLA-DRB1 locus in CD4+ T-Cells are associated with multiple sclerosis. Multiple Sclerosis Journal. 2013 Dec 12;20(8):1033–41.
Grimaldi CM, Cleary J, Dagtas AS, Moussai D, Diamond B. Estrogen alters thresholds for B cell apoptosis and activation. The Journal of clinical investigation. 2002;109(12):1625–33.
Guan L, Wang X, Meng S, Shi L, Jiang W, Xiao L, et al. Increased IL-21/IL-21R expression and its proinflammatory effects in autoimmune thyroid disease. Cytokine. 2015 Apr;72(2):160–5.
Haile Y, Deng X, Ortiz-Sandoval C, Tahbaz N, Janowicz A, Lu J-Q, et al. Rab32 connects ER stress to mitochondrial defects in multiple sclerosis. Journal of Neuroinflammation. 2017 Jan 23;14(1).
Han YJ, Zhang J, Lee J-H, Mason JM, Karginova O, Yoshimatsu TF, et al. The BRCA1 Pseudogene Negatively Regulates Antitumor Responses through Inhibition of Innate Immune Defense Mechanisms. Cancer Research. 2021 Jan 20;81(6):1540–51.
Harbo HF, Gold R, Tintoré M. Sex and gender issues in multiple sclerosis. Therapeutic Advances in Neurological Disorders. 2013 May 13;6(4):237–48.
Harris DP, Goodrich S, Gerth AJ, Peng SL, Lund FE. Regulation of IFN-γ Production by B Effector 1 Cells: Essential Roles for T-bet and the IFN-γ Receptor. The Journal of Immunology. 2005 May 19;174(11):6781–90.
Hauser SL, Oksenberg JR. The Neurobiology of Multiple Sclerosis: Genes, Inflammation, and Neurodegeneration. Neuron. 2006 Oct;52(1):61–76.
Heinz S, Benner C, Spann N, Bertolino E, Lin YC, Laslo P, et al. Simple Combinations of Lineage-Determining Transcription Factors Prime cis-Regulatory Elements Required for Macrophage and B Cell Identities. Molecular Cell. 2010;38(4):576–89.
Hetz C, Saxena S. ER stress and the unfolded protein response in neurodegeneration. Nature Reviews Neurology. 2017 Jul 21;13(8):477–91.
Heyn H, Vidal E, Ferreira HJ, Vizoso M, Sayols S, Gomez A, et al. Epigenomic analysis detects

aberrant super-enhancer DNA methylation in human cancer. Genome Biology . 2016 Jan 26;17(1).
Hilliard B, Samoilova EB, Liu TS, Rostami A, Chen Y. Experimental autoimmune encephalomyelitis in NF-kappa B-deficient mice: roles of NF-kappa B in the activation and differentiation of autoreactive T cells. Journal of immunology. 1999 Sep 1;163(5):2937-43.
Honardoost MA, Kiani-Esfahani A, Ghaedi K, Etemadifar M, Salehi M. miR-326 and miR-26a, two potential markers for diagnosis of relapse and remission phases in patient with relapsing–remitting multiple sclerosis. Gene. 2014 Jul;544(2):128–33.
Hong L, Li X, Zhou D, Geng J, Chen L. Role of Hippo signaling in regulating immunity. Cellular & Molecular Immunology. 2018 Mar 22;15(12):1003–9.
Hosseini A, Babaloo Z, Gharibi T, Shomali N, Marofi F, Hashemi V, et al. Epigenetic mechanisms shape the underlining expression regulatory mechanisms of the STAT3 in multiple sclerosis disease. BMC Research Notes. 2020 Dec;13(1).
Hotchkiss RD. The quantitative separation of purines, pyrimidines, and nucleosides by paper chromatography. Journal of Biological Chemistry . 1948 Aug;175(1):315–32.
Howe KL, Achuthan P, Allen J, Allen J, Alvarez-Jarreta J, Amode MR, et al. Ensembl 2021. Nucleic Acids Research. 2020 Nov 2;49(D1):D884–91.
Howell PM, Liu Z, Khong HT. Demethylating Agents in the Treatment of Cancer. Pharmaceuticals. 2010 Jul 2;3(7):2022–44.
Huang J-D, Amaral J, Lee JW, Rodriguez IR. 7-Ketocholesterol-Induced Inflammation Signals Mostly through the TLR4 Receptor Both In Vitro and In Vivo. Khoury JE, editor. PLoS ONE. 2014 Jul 18;9(7):e100985.
Huang Y, Tang J, Li X, Long X, Huang Y, Zhang X. miR-92b-3p Exerts Neuroprotective Effects on Ischemia/Reperfusion-Induced Cerebral Injury via Targeting NOX4 in a Rat Model. Ali Sheikh MS, editor. Oxidative Medicine and Cellular Longevity. 2022 Mar 30;2022:1–16.
Hubackova S, Kucerova A, Michlits G, Kyjacova L, Reinis M, Korolov O, et al. IFNγ induces oxidative stress, DNA damage and tumor cell senescence via TGFβ/SMAD signaling-dependent induction of Nox4 and suppression of ANT2. Oncogene. 2016 Mar 10 ;35(10):1236–49.
Huynh JL, Garg P, Thin TH, Yoo S, Dutta R, Trapp BD, et al. Epigenome-wide differences in pathology-free regions of multiple sclerosis–affected brains. Nature Neuroscience. 2014 Jan; 17(1): 121–130.
Ibiza S, Serrador JM. The role of nitric oxide in the regulation of adaptive immune responses. Inmunología. 2008 Jul;27(3):103–17.
Inestrosa NC, Varela-Nallar L. Wnt signaling in neuronal differentiation and development. Cell and Tissue Research. 2014 Sep 19;359(1):215–23.
Ingwersen J, Menge T, Wingerath B, Kaya D, Graf J, Prozorovski T, et al. Natalizumab restores aberrant mi RNA expression profile in multiple sclerosis and reveals a critical role for miR‐20b. Annals of Clinical and Translational Neurology. 2014 Dec 5;2(1):43–55.
Inoue S, Oishi M. Effects of methylation of non-CpG sequence in the promoter region on the expression of human synaptotagmin XI (syt11). Gene. 2005 Mar;348:123–34.
Ishida W, Tsuru E, Tominaga A, Miyazaki J-i, Higuchi T, Sakamoto S, et al. Systemic overexpression of IFN-γ and IL-5 exacerbates early phase reaction and conjunctival eosinophilia, respectively, in experimental allergic conjunctivitis. British Journal of Ophthalmology. 2009 Aug 18;93(12):1680–5.
Iwasa K, Yamamoto S, Takahashi M, Suzuki S, Yagishita S, Awaji T, et al. Prostaglandin F2α FP receptor inhibitor reduces demyelination and motor dysfunction in a cuprizone-induced multiple sclerosis mouse model. Prostaglandins, Leukotrienes and Essential Fatty Acids. 2014

Nov;91(5):175–82.
Iwasaki A, Medzhitov R. Control of adaptive immunity by the innate immune system. Nature Immunology. 2015 Mar 19;16(4):343–53.
Jang H, Shin W, Lee J, Do J. CpG and Non-CpG Methylation in Epigenetic Gene Regulation and Brain Function. Genes. 2017 May 23;8(6):148.
Janson PCJ, Linton LB, Ahlén Bergman E, Marits P, Eberhardson M, Piehl F, et al. Profiling of CD4+ T Cells with Epigenetic Immune Lineage Analysis. The Journal of Immunology. 2010 Dec 3;186(1):92–102.
Jansz N. DNA methylation dynamics at transposable elements in mammals. Blewitt M, editor. Essays in Biochemistry. 2019 Oct 11;63(6):677–89.
Jiang K, Yang J, Song C, He F, Yang L, Li X. Enforced expression of miR-92b blunts E. coli lipopolysaccharide-mediated inflammatory injury by activating the PI3K/AKT/β-catenin pathway via targeting PTEN. International Journal of Biological Sciences. 2021;17(5):1289–301.
Jin Z, Liu Y. DNA methylation in human diseases. Genes & Diseases. 2018 Mar:5(1):1–8.
Joehanes R, Just AC, Marioni RE, Pilling LC, Reynolds LM, Mandaviya PR, et al. Epigenetic Signatures of Cigarette Smoking. Circulation: Cardiovascular Genetics. 2016 Oct;9(5):436–47.
Jomova K, Jenisova Z, Feszterova M, Baros S, Liska J, Hudecova D, et al. Arsenic: toxicity, oxidative stress and human disease. Journal of Applied Toxicology. 2011 Feb;31(2):95-107.
Jongen PJ, Ter Horst AT, Brands AM. Cognitive impairment in multiple sclerosis. Minerva medica. 2012;103(2).
Kabekkodu SP, Shukla V, Varghese VK, D' Souza J, Chakrabarty S, Satyamoorthy K. Clustered miRNAs and their role in biological functions and diseases. Biological Reviews. 2018 May 24;93(4):1955–86.
Kadowaki A, Saga R, Lin Y, Sato W, Yamamura T. Gut microbiota-dependent CCR9+CD4+ T cells are altered in secondary progressive multiple sclerosis. Brain. 2019 Feb 15;142(4):916–31.
Kent WJ, Sugnet CW, Furey TS, Roskin KM, Pringle TH, Zahler AM, et al. The Human Genome Browser at UCSC. Genome Research . 2002 May 16;12(6):996–1006.
Kim GH, Kim JE, Rhie SJ, Yoon S. The Role of Oxidative Stress in Neurodegenerative Diseases. Experimental Neurobiology. 2015 Dec 30;24(4):325–40.
Kirk J, Plumb J, Mirakhur M, McQuaid S. Tight junctional abnormality in multiple sclerosis white matter affects all calibres of vessel and is associated with blood-brain barrier leakage and active demyelination. The Journal of Pathology. 2003;201(2):319–27.
Kister I, Chamot E, Salter AR, Cutter GR, Bacon TE, Herbert J. Disability in multiple sclerosis: A reference for patients and clinicians. Neurology. 2013 Feb 20;80(11):1018–24.
Kitamura M, Kasai A. Cigarette smoke as a trigger for the dioxin receptor-mediated signaling pathway. Cancer Letters. 2007 Jul;252(2):184–94.
Kojima KK. Human transposable elements in Repbase: genomic footprints from fish to humans. Mobile DNA. 2018 Jan 4;9(1).
Kong Y, Rose CM, Cass AA, Williams AG, Darwish M, Lianoglou S, et al. Transposable element expression in tumors is associated with immune infiltration and increased antigenicity. Nature Communications. 2019 Nov 19;10(1).
Konkel MK, Batzer MA. A mobile threat to genome stability: The impact of non-LTR retrotransposons upon the human genome. Seminars in Cancer Biology. 2010 Aug ;20(4):211–21.
Kowalczyk Monika S, Hughes Jim R, Garrick D, Lynch Magnus D, Sharpe Jacqueline A,

Sloane-Stanley Jacqueline A, et al. Intragenic Enhancers Act as Alternative Promoters. Molecular Cell. 2012 Feb;45(4):447–58.
Kulakova OG; Kabilov MR; Danilova LV; Popova EV; Baturina OA; Tsareva EY; Baulina NM; Kiselev IS; Boyko AN; Favorov AV, Favorova OO, Vlassov VV. Whole-Genome DNA Methylation Analysis of Peripheral Blood Mononuclear Cells in Multiple Sclerosis Patients with Different Disease Courses. Acta naturae. 2016;8(3).
Kular L, Ewing E, Needhamsen M, Pahlevan Kakhki M, Covacu R, Gomez-Cabrero D, et al. DNA methylation changes in glial cells of the normal-appearing white matter in Multiple Sclerosis patients. Epigenetics. 2022 Jan 30;17(11):1311–30.
Kumagai C, Kalman B, Middleton FA, Vyshkina T, Massa PT. Increased promoter methylation of the immune regulatory gene SHP-1 in leukocytes of multiple sclerosis subjects. Journal of Neuroimmunology. 2012 May;246(1-2):51–7.
Kumar BV, Connors TJ, Farber DL. Human T Cell Development, Localization, and Function throughout Life. Immunity. 2018 Feb;48(2):202–13.
Kurosaki T, Kometani K, Ise W. Memory B cells. Nature Reviews Immunology. 2015 Feb 13;15(3):149–59.
Kurtzke JF. Rating neurologic impairment in multiple sclerosis: An expanded disability status scale (EDSS). Neurology. 1983 Nov 1;33(11):1444–4.
Kuscu C, Arslan S, Singh R, Thorpe J, Adli M. Genome-wide analysis reveals characteristics of off-target sites bound by the Cas9 endonuclease. Nature Biotechnology 2014 May 18;32(7):677–83.
Kutzelnigg A, Lucchinetti CF, Stadelmann C, Brück W, Rauschka H, Bergmann M, et al. Cortical demyelination and diffuse white matter injury in multiple sclerosis. Brain. 2005 Oct 17;128(11):2705–12.
La Rocca C, Carbone F, De Rosa V, Colamatteo A, Galgani M, Perna F, et al. Immunometabolic profiling of T cells from patients with relapsing-remitting multiple sclerosis reveals an impairment in glycolysis and mitochondrial respiration. Metabolism. 2017 Dec;77:39–46.
Laddha SV, Nayak S, Paul D, Reddy R, Sharma C, Jha P, et al. Genome-wide analysis reveals downregulation of miR-379/miR-656 cluster in human cancers. Biology Direct. 2013 Apr 24;8(1).
Lagos-Quintana M. New microRNAs from mouse and human. RNA. 2003 Feb 1;9(2):175–9.
Lan M, Tang X, Zhang J, Yao Z. Insights in pathogenesis of multiple sclerosis: nitric oxide may induce mitochondrial dysfunction of oligodendrocytes. Reviews in the Neurosciences . 2017 Dec 20;29(1):39–53.
Landman S, van der Horst C, van Erp PEJ, Joosten I, de Vries R, Koenen HJPM. Immune responses to azacytidine in animal models of inflammatory disorders: a systematic review. Journal of Translational Medicine. 2021 Jan 6;19(1).
Law PP, Holland ML. DNA methylation at the crossroads of gene and environment interactions. Blewitt M, editor. Essays in Biochemistry. 2019 Nov 29;63(6):717–26.
Lee Y, Mitsdoerffer M, Xiao S, Gu G, Sobel RA, Kuchroo VK. IL-21R signaling is critical for induction of spontaneous experimental autoimmune encephalomyelitis. Journal of Clinical Investigation. 2015 Sep 28;125(11):4011–20.
Lehmann-Werman R, Neiman D, Zemmour H, Moss J, Magenheim J, Vaknin-Dembinsky A, et al. Identification of tissue-specific cell death using methylation patterns of circulating DNA. Proceedings of the National Academy of Sciences. 2016 Mar 14;113(13).
Lei Y, Huang Y-H, Goodell MA. DNA methylation and de-methylation using hybrid site-targeting proteins. Genome Biology. 2018 Nov 6;19(1).
Lengfeld JE, Lutz SE, Smith JR, Diaconu C, Scott C, Kofman SB, et al. Endothelial Wnt/β-

catenin signaling reduces immune cell infiltration in multiple sclerosis. Proceedings of the National Academy of Sciences. 2017 Jan 30;114(7):E1168–77.
Levin MC. Multiple Sclerosis (MS) [Internet]. MSD Manual Professional Edition. MSD Manuals; 2021. Available from: https://www.msdmanuals.com/professional/neurologic-disorders/demyelinating-disorders/multiple-sclerosis-ms
Li H, Handsaker B, Wysoker A, Fennell T, Ruan J, Homer N, et al. The Sequence Alignment/Map format and SAMtools. Bioinformatics. 2009;25(16):2078–9.
Li H, Ruan J, Durbin R. Mapping short DNA sequencing reads and calling variants using mapping quality scores. Genome Research. 2008;18(11):1851–8.
Li J, Ding Y, Zheng L. Histone-Mediated Transgenerational Epigenetics. Transgenerational Epigenetics. 2014;87–103.
Li J, Sha Z, Zhu X, Xu W, Yuan W, Yang T, et al. Targeting miR-30d reverses pathological cardiac hypertrophy. eBioMedicine. 2022 Jul;81:104108.
Lienhard M, Grimm C, Morkel M, Herwig R, Chavez L. MEDIPS: genome-wide differential coverage analysis of sequencing data derived from DNA enrichment experiments. Bioinformatics. 2013;30(2):284–6.
Liggett T, Melnikov A, Tilwalli S, Yi Q, Chen H, Replogle C, et al. Methylation patterns of cell-free plasma DNA in relapsing–remitting multiple sclerosis. Journal of the Neurological Sciences. 2010 Mar;290(1-2):16–21.
Lin X, Li L, Liu X, Tian J, Zheng W, Li J, et al. Genome-wide analysis of aberrant methylation of enhancer DNA in human osteoarthritis. BMC Medical Genomics. 2020 Jan 3 ;13(1).
Lindholm D, Wootz H, Korhonen L. ER stress and neurodegenerative diseases. Cell Death & Differentiation. 2006 Jan 6;13(3):385–92.
Liston A, Papadopoulou AS, Danso-Abeam D, Dooley J. MicroRNA-29 in the adaptive immune system: setting the threshold. Cellular and Molecular Life Sciences. 2012 Sep 13;69(21):3533–41.
Liu E, Sun H, Wu J, Kuang Y. MiR‐92b‐3p regulates oxygen and glucose deprivation–reperfusion‐mediated apoptosis and inflammation by targeting TRAF3 in PC12 cells. Experimental Physiology. 2020 Sep 4;105(10):1792–801.
Liu R, Bai Y, Vollmer TL, Bai X-F, Jee Y, Tang Y, et al. IL-21 receptor expression determines the temporal phases of experimental autoimmune encephalomyelitis. Experimental Neurology. 2008 May;211(1):14–24.
Liu R, Wu Q, Su D, Che N, Chen H, Geng L, et al. A regulatory effect of IL-21 on T follicular helper-like cell and B cell in rheumatoid arthritis. Arthritis Research & Therapy. 2012;14(6):R255.
Liu S, Rezende RM, Moreira TG, Tankou SK, Cox LM, Wu M, et al. Oral Administration of miR-30d from Feces of MS Patients Suppresses MS-like Symptoms in Mice by Expanding Akkermansia muciniphila. Cell Host & Microbe. 2019 Dec;26(6):779-794.e8.
Liu XS, Wu H, Ji X, Stelzer Y, Wu X, Czauderna S, et al. Editing DNA Methylation in the Mammalian Genome. Cell. 2016 Sep;167(1):233-247.e17.
Lokk K, Modhukur V, Rajashekar B, Märtens K, Mägi R, Kolde R, et al. DNA methylome profiling of human tissues identifies global and tissue-specific methylation patterns. Genome Biology. 2014 Apr;15(4).
Love S. Demyelinating diseases. Journal of Clinical Pathology. 2006 May 5;59(11):1151–9.
Lu F, Zhang J, Ji M, Li P, Du Y, Wang H, et al. miR-181b increases drug sensitivity in acute myeloid leukemia via targeting HMGB1 and Mcl-1. International Journal of Oncology. 2014 Apr 16;45(1):383–92.
Lu L, Zhao H, Liu J, Zhang Y, Wang X. miRNA-mRNA Regulatory Network Reveals miRNAs

in HCT116 in Response to Folic Acid Deficiency via Regulating Vital Genes of Endoplasmic Reticulum Stress Pathway. Tsai F-M, editor. BioMed Research International. 2021 Apr 26;2021:1–14.
Lubetzki C, Stankoff B. Demyelination in multiple sclerosis. Handbook of Clinical Neurology . 2014;89–99.
Lublin FD, Reingold SC, Cohen JA, Cutter GR, Sorensen PS, Thompson AJ, et al. Defining the clinical course of multiple sclerosis: The 2013 revisions. Neurology. 2014 May 28 ;83(3):278–86.
Lund E, Güttinger S, Calado A, Dahlberg JE, Kutay U. Nuclear Export of MicroRNA Precursors. Science. 2004 Jan 2;303(5654):95–8.
Lyko F. The DNA methyltransferase family: a versatile toolkit for epigenetic regulation. Nature Reviews Genetics. 2017 Oct 16;19(2):81–92.
Ma Q, Caillier SJ, Muzic S, Wilson MR, Henry RG, Cree BAC, et al. Specific hypomethylation programs underpin B cell activation in early multiple sclerosis. Proceedings of the National Academy of Sciences. 2021 Dec 15;118(51).
Ma X, Zhou J, Zhong Y, Jiang L, Mu P, Li Y, et al. Expression, Regulation and Function of MicroRNAs in Multiple Sclerosis. International Journal of Medical Sciences. 2014;11(8):810–8.
Magee P, Shi L, Garofalo M. Role of microRNAs in chemoresistance. Annals of translational medicine. 2015;3(21):332.
Maltby VE, Graves MC, Lea RA, Benton MC, Sanders KA, Tajouri L, et al. Genome-wide DNA methylation profiling of CD8+ T cells shows a distinct epigenetic signature to CD4+ T cells in multiple sclerosis patients. Clinical Epigenetics. 2015 Nov 5;7(1).
Maltby VE, Lea RA, Graves MC, Sanders KA, Benton MC, Tajouri L, et al. Genome-wide DNA methylation changes in CD19+ B cells from relapsing-remitting multiple sclerosis patients. Scientific Reports. 2018 Nov 27;8(1).
Mameli G, Astone V, Arru G, Marconi S, Lovato L, Serra C, et al. Brains and peripheral blood mononuclear cells of multiple sclerosis (MS) patients hyperexpress MS-associated retrovirus/ HERV-W endogenous retrovirus, but not Human herpesvirus 6. Journal of General Virology. 2007 Jan 1;88(1):264–74.
Mangano EN, Litteljohn D, So R, Nelson E, Peters S, Bethune C, et al. Interferon-γ plays a role in paraquat-induced neurodegeneration involving oxidative and proinflammatory pathways. Neurobiology of Aging. 2012 Jul;33(7):1411–26.
Mangano K, Fagone P, Bendtzen K, Meroni PL, Quattrocchi C, Mammana S, et al. Hypomethylating Agent 5-Aza-2′-deoxycytidine (DAC) Ameliorates Multiple Sclerosis in Mouse Models. Journal of Cellular Physiology. 2014 Aug 27;229(12):1918–25.
Marabita F, Almgren M, Sjöholm LK, Kular L, Liu Y, James T, et al. Smoking induces DNA methylation changes in Multiple Sclerosis patients with exposure-response relationship. Scientific Reports. 2017 Nov 6;7(1).
Marck CH, Neate SL, Taylor KL, Weiland TJ, Jelinek GA. Prevalence of Comorbidities, Overweight and Obesity in an International Sample of People with Multiple Sclerosis and Associations with Modifiable Lifestyle Factors. Ramagopalan SV, editor. PLOS ONE. 2016 Feb 5;11(2):e0148573.
Marco-Sola S, Sammeth M, Guigó R, Ribeca P. The GEM mapper: fast, accurate and versatile alignment by filtration. Nature Methods. 2012;9(12):1185–8.
Marrie RA, Elliott L, Marriott J, Cossoy M, Blanchard J, Leung S, et al. Effect of comorbidity on mortality in multiple sclerosis. Neurology. 2015 May 27;85(3):240–7.
Marrie RA. Comorbidity in multiple sclerosis: implications for patient care. Nature Reviews

Neurology. 2017 Mar 17;13(6):375–82.
Mastronardi FG, Noor A, Wood DD, Paton T, Moscarello MA. Peptidyl arginine deiminase 2 CpG island in multiple sclerosis white matter is hypomethylated. Journal of Neuroscience Research. 2007 Jul;85(9):2006–16.
Maunakea AK, Chepelev I, Cui K, Zhao K. Intragenic DNA methylation modulates alternative splicing by recruiting MeCP2 to promote exon recognition. Cell Research . 2013 Aug 13;23(11):1256–69.
Mauri C, Bosma A. Immune Regulatory Function of B Cells. Annual Review of Immunology. 2012 Apr 23;30(1):221–41.
Mazzoccoli L, Robaina MC, Apa AG, Bonamino M, Pinto LW, Queiroga E, et al. MiR-29 silencing modulates the expression of target genes related to proliferation, apoptosis and methylation in Burkitt lymphoma cells. Journal of Cancer Research and Clinical Oncology. 2018 Jan 9;144(3):483–97.
McComb M, Browne RW, Bhattacharya S, Bodziak ML, Jakimovski D, Weinstock-Guttman B, et al. The cholesterol autoxidation products, 7-ketocholesterol and 7β-hydroxycholesterol are associated with serum neurofilaments in multiple sclerosis. Multiple Sclerosis and Related Disorders. 2021 May;50:102864.
McGuire HM, Walters S, Vogelzang A, Lee CMY, Webster KE, Sprent J, et al. Interleukin-21 Is Critically Required in Autoimmune and Allogeneic Responses to Islet Tissue in Murine Models. Diabetes. 2011 Feb 25;60(3):867–75.
Mehta DS, Wurster AL, Grusby MJ. Biology of IL-21 and the IL-21 receptor. Immunological Reviews. 2004 Dec;202(1):84–95.
Mestdagh P, Van Vlierberghe P, De Weer A, Muth D, Westermann F, Speleman F, et al. A novel and universal method for microRNA RT-qPCR data normalization. Genome Biology. 2009;10(6):R64.
Millar JH, Allison RS. Familial Incidence of Disseminated Sclerosis. The Ulster medical journal. 1954 Mar;23(Suppl 2):29.
Mirshafiey A;Kianiaslani M. Autoantigens and autoantibodies in multiple sclerosis. Iranian journal of allergy, asthma, and immunology. 2013;12(4).
Mohan H, Krumbholz M, Sharma R, Eisele S, Junker A, Sixt M, et al. Extracellular Matrix in Multiple Sclerosis Lesions: Fibrillar Collagens, Biglycan and Decorin are Upregulated and Associated with Infiltrating Immune Cells. Brain Pathology. 2010 Mar 25; 20(5): 966–975
Momparler RL, Bouchard J, Onetto N, Rivard GE. 5-AZA-2′-deoxycytidine therapy in patients with acute leukemia inhibits DNA methylation. Leukemia Research. 1984 Jan;8(2):181–5.
Moore LD, Le T, Fan G. DNA Methylation and Its Basic Function. Neuropsychopharmacology. 2012 Jul 11;38(1):23–38.
Morales S, Monzo M, Navarro A. Epigenetic regulation mechanisms of microRNA expression. Biomolecular Concepts. 2017 Dec 20;8(5-6):203–12.
Mott JL, Kurita S, Cazanave SC, Bronk SF, Werneburg NW, Fernandez-Zapico ME. Transcriptional suppression of mir-29b-1/mir-29a promoter by c-Myc, hedgehog, and NF-kappaB. Journal of Cellular Biochemistry. 2010 May 19;110(5):1155–64.
Multiple Sclerosis Foundation of Catalonia [Internet]. Available from: https://www.fem.es/es/
Multiple Sclerosis International Federation – Atlas of MS – 3rd Edition [Internet]. Atlasofms.org. 2020.
Muñoz-San Martín M, Reverter G, Robles-Cedeño R, Buxò M, Ortega FJ, Gómez I, et al. Analysis of miRNA signatures in CSF identifies upregulation of miR-21 and miR-146a/b in patients with multiple sclerosis and active lesions. Journal of Neuroinflammation. 2019 Nov 14;16(1).

Murrell A, Heeson S, Bowden L, Constância M, Dean W, Kelsey G, et al. An intragenic methylated region in the imprintedIgf2gene augments transcription. EMBO reports. 2001 Dec;2(12):1101–6.
Muthian G, Bright JJ. Quercetin, a Flavonoid Phytoestrogen, Ameliorates Experimental Allergic Encephalomyelitis by Blocking IL-12 Signaling Through JAK-STAT Pathway in T Lymphocyte. Journal of Clinical Immunology. 2004 Sep;24(5):542–52.
Nada S, Kahaleh B, Altorok N. Genome-wide DNA methylation pattern in systemic sclerosis microvascular endothelial cells: Identification of epigenetically affected key genes and pathways. Journal of Scleroderma and Related Disorders. 2021 Jul 28;239719832110337.
Nagji AS, Liu Y, Stelow EB, Stukenborg GJ, Jones DR. BRMS1 transcriptional repression correlates with CpG island methylation and advanced pathological stage in non-small cell lung cancer. The Journal of Pathology. 2010 Mar 10;221(2):229–37.
Nakkuntod J, Avihingsanon Y, Mutirangura A, Hirankarn N. Hypomethylation of LINE-1 but not Alu in lymphocyte subsets of systemic lupus erythematosus patients. Clinica Chimica Acta. 2011 Jul;412(15-16):1457–61.
Nan X, Meehan RR, Bird A. Dissection of the methyl-CpG binding domain from the chromosomal protein MeCP2. Nucleic Acids Research. 1993;21(21):4886–92.
National Multiple Sclerosis Society. Types of MS. 2013. Available from: https://www.nationalmssociety.org/What-is-MS/Types-of-MS
Neja SA. Site-Specific DNA Demethylation as a Potential Target for Cancer Epigenetic Therapy. Epigenetics Insights. 2020 Jan;13:251686572096480.
Neri F, Rapelli S, Krepelova A, Incarnato D, Parlato C, Basile G, et al. Intragenic DNA methylation prevents spurious transcription initiation. Nature. 2017 Feb 22;543(7643):72–7.
Netea MG, Schlitzer A, Placek K, Joosten LAB, Schultze JL. Innate and Adaptive Immune Memory: an Evolutionary Continuum in the Host's Response to Pathogens. Cell Host & Microbe. 2019 Jan;25(1):13–26.
Neven KY, Piola M, Angelici L, Cortini F, Fenoglio C, Galimberti D, et al. Repetitive element hypermethylation in multiple sclerosis patients. BMC Genetics. 2016 Jun 18;17(1).
Neves R, Scheel C, Weinhold S, Honisch E, Iwaniuk KM, Trompeter H-I, et al. Role of DNA methylation in miR-200c/141 cluster silencing in invasive breast cancer cells. BMC Research Notes. 2010 Aug 3;3(1).
Nojima M, Matsui T, Tamori A, Kubo S, Shirabe K, Kimura K, et al. Global, cancer-specific microRNA cluster hypomethylation was functionally associated with the development of non-B non-C hepatocellular carcinoma. Molecular Cancer. 2016 Apr 30;15(1).
Nolan K, Walter F, Tuffy LP, Poeschel S, Gallagher R, Haunsberger S, et al. Endoplasmic reticulum stress-mediated upregulation of miR-29a enhances sensitivity to neuronal apoptosis. Mallucci G, editor. European Journal of Neuroscience. 2016 Feb 9;43(5):640–52.
Nourian HY, Beh-Pajooh A, Aliomrani M, Amini M, Sahraian MA, Hosseini R, et al. Changes in DNA methylation in APOE and ACKR3 genes in multiple sclerosis patients and the relationship with their heavy metal blood levels. NeuroToxicology. 2021 Dec;87:182–7.
Nutt SL, Hodgkin PD, Tarlinton DM, Corcoran LM. The generation of antibody-secreting plasma cells. Nature Reviews Immunology. 2015 Feb 20;15(3):160–71.
Oh J, Alikhani K, Bruno T, Devonshire V, Giacomini PS, Giuliani F, et al. Diagnosis and management of secondary-progressive multiple sclerosis: time for change. Neurodegenerative Disease Management. 2019 Dec;9(6):301–17.
Okamoto K, Miyoshi K, Murawaki Y. miR-29b, miR-205 and miR-221 Enhance Chemosensitivity to Gemcitabine in HuH28 Human Cholangiocarcinoma Cells. Sarkar D, editor. PLoS ONE. 2013 Oct 17;8(10):e77623.

Oksenberg JR, Baranzini SE, Sawcer S, Hauser SL. The genetics of multiple sclerosis: SNPs to pathways to pathogenesis. Nature Reviews Genetics. 2008 Jun 10;9(7):516–26.
Olsen JA, Kenna LA, Tipon RC, Spelios MG, Stecker MM, Akirav EM. A Minimally-invasive Blood-derived Biomarker of Oligodendrocyte Cell-loss in Multiple Sclerosis. eBioMedicine. 2016 Aug;10:227–35.
Olsson T, Barcellos LF, Alfredsson L. Interactions between genetic, lifestyle and environmental risk factors for multiple sclerosis. Nature Reviews Neurology. 2016 Dec 9;13(1):25–36.
Ordoñez, Martínez-Calle, Agirre, Prosper. DNA Methylation of Enhancer Elements in Myeloid Neoplasms: Think Outside the Promoters? Cancers. 2019 Sep 24;11(10):1424.
Oreja-Guevara C, Ayuso Blanco T, Brieva Ruiz L, Hernández Pérez MÁ, Meca-Lallana Ramió-Torrentà L. Cognitive Dysfunctions and Assessments in Multiple Sclerosis. Frontiers in Neurology. 2019 Jun 4;10.
Ortiz GG, Pacheco-Moisés FP, Macías-Islas MÁ, Flores-Alvarado LJ, Mireles-Ramírez MA, González-Renovato ED, et al. Role of the Blood–Brain Barrier in Multiple Sclerosis. Archives of Medical Research. 2014 Nov;45(8):687–97.
Ostertag EM, Goodier JL, Zhang Y, Kazazian HH. SVA Elements Are Nonautonomous Retrotransposons that Cause Disease in Humans. The American Journal of Human Genetics. 2003 Dec;73(6):1444–51.
Oturai DB, Søndergaard HB, Börnsen L, Sellebjerg F, Romme Christensen J. Identification of Suitable Reference Genes for Peripheral Blood Mononuclear Cell Subset Studies in Multiple Sclerosis. Scandinavian Journal of Immunology. 2016 Jan;83(1):72–80.
Ozsolak F, Poling LL, Wang Z, Liu H, Liu XS, Roeder RG, et al. Chromatin structure analyses identify miRNA promoters. Genes & Development. 2008 Nov 15;22(22):3172–83.
Paintlia AS, Paintlia MK, Mohan S, Singh AK, Singh I. AMP-Activated Protein Kinase Signaling Protects Oligodendrocytes that Restore Central Nervous System Functions in an Experimental Autoimmune Encephalomyelitis Model. The American Journal of Pathology . 2013 Aug;183(2):526–41.
Peedicayil J. Epigenetic Drugs for Multiple Sclerosis. Current Neuropharmacology. 2016 Jan 22;14(1):3–9.
Pereira C, Schaer DJ, Bachli EB, Kurrer MO, Schoedon G. Wnt5A/CaMKII Signaling Contributes to the Inflammatory Response of Macrophages and Is a Target for the Antiinflammatory Action of Activated Protein C and Interleukin-10. Arteriosclerosis, Thrombosis, and Vascular Biology. 2008 Mar;28(3):504–10.
Pérez Carmona N, Fernández Jover E, Pérez Sempere Á. Epidemiología de la esclerosis múltiple en España. Revista de Neurología. 2019;69(01):32.
Piao W-H ., Jee YH, Liu RL, Coons SW, Kala M, Collins M, et al. IL-21 Modulates CD4+ CD25+ Regulatory T-Cell Homeostasis in Experimental Autoimmune Encephalomyelitis. Scandinavian Journal of Immunology. 2007 Dec 4;67(1):37–46.
Pidíková P, Herichová I. miRNA Clusters with Up-Regulated Expression in Colorectal Cancer. Cancers. 2021 Jun 14;13(12):2979.
Pink RC, Wicks K, Caley DP, Punch EK, Jacobs L, Francisco Carter DR. Pseudogenes: Pseudo-functional or key regulators in health and disease? RNA. 2011 Mar 11 ;17(5):792–8.
Pirko I, Noseworthy JH. Demyelinating Disorders of the Central Nervous System. Textbook of Clinical Neurology. 2007;1103–33.
Poser CM, Paty DW, Scheinberg L, McDonald WI, Davis FA, Ebers GC, et al. New diagnostic criteria for multiple sclerosis: Guidelines for research protocols. Annals of Neurology . 1983 Mar;13(3):227–31.
Predonzani A. Spotlights on immunological effects of reactive nitrogen species: When

inflammation says nitric oxide. World Journal of Experimental Medicine. 2015;5(2):64.
Qu J, Zou T, Lin Z. The Roles of the Ubiquitin–Proteasome System in the Endoplasmic Reticulum Stress Pathway. International Journal of Molecular Sciences. 2021 Feb 3;22(4):1526.
Quintana E, Ortega FJ, Robles-Cedeño R, Villar ML, Buxó M, Mercader JM, et al. miRNAs in cerebrospinal fluid identify patients with MS and specifically those with lipid-specific oligoclonal IgM bands. Multiple Sclerosis Journal. 2017 Jan 9;23(13):1716–26.
Quintana FJ. Regulation of central nervous system autoimmunity by the aryl hydrocarbon receptor. Seminars in Immunopathology. 2013 Sep 3;35(6):627–35.
Radreau P, Rhodes JD, Mithen RF, Kroon PA, Sanderson J. Hypoxia-inducible factor-1 (HIF-1) pathway activation by quercetin in human lens epithelial cells. Experimental Eye Research. 2009 Dec;89(6):995–1002.
Ramagopalan SV, Dyment DA, Morrison KM, Herrera BM, DeLuca GC, Lincoln MR, et al. Methylation of class II transactivator gene promoter IV is not associated with susceptibility to Multiple Sclerosis. BMC Medical Genetics. 2008 Jul 7;9(1).
Ramagopalan SV, Knight JC, Ebers GC. Multiple sclerosis and the major histocompatibility complex. Current Opinion in Neurology. 2009 Jun;22(3):219–25.
Rankin AL, MacLeod H, Keegan S, Andreyeva T, Lowe L, Bloom L, et al. IL-21 Receptor Is Critical for the Development of Memory B Cell Responses. The Journal of Immunology. 2010 Dec 17;186(2):667–74.
Rapicavoli NA, Qu K, Zhang J, Mikhail M, Laberge R-M, Chang HY. A mammalian pseudogene lncRNA at the interface of inflammation and anti-inflammatory therapeutics. eLife. 2013 Jul 23;2.
Rasmussen KD, Helin K. Role of TET enzymes in DNA methylation, development, and cancer. Genes & Development. 2016 Apr 1;30(7):733–50.
Rawson JB, Sun Z, Dicks E, Daftary D, Parfrey PS, Green RC, et al. Vitamin D Intake Is Negatively Associated with Promoter Methylation of the Wnt Antagonist Gene DKK1 in a Large Group of Colorectal Cancer Patients. Nutrition and Cancer. 2012 Sep 11 ;64(7):919–28.
Razin A, Cedar H. DNA methylation and gene expression. Microbiological Reviews. 1991 Sep;55(3):451–8.
Rea M, Eckstein M, Eleazer R, Smith C, Fondufe-Mittendorf YN. Genome-wide DNA methylation reprogramming in response to inorganic arsenic links inhibition of CTCF binding, DNMT expression and cellular transformation. Scientific Reports. 2017 Feb;7(1).
Ren X, Li H, Song X, Wu Y, Liu Y. 5-Azacytidine treatment induces demethylation of DAPK1 and MGMT genes and inhibits growth in canine mammary gland tumor cells. OncoTargets and Therapy. 2018 May;Volume 11:2805–13.
Rhead B, Brorson IS, Berge T, Adams C, Quach H, Moen SM, et al. Increased DNA methylation of SLFN12 in CD4+ and CD8+ T cells from multiple sclerosis patients. Fang D, editor. PLOS ONE. 2018 Oct 31;13(10):e0206511.
Rieckmann P, Albrecht M, Kitze B, Weber T, Tumani H, Broocks A, et al. Cytokine mRNA levels in mononuclear blood cells from patients with multiple sclerosis. Neurology. 1994 Aug;44(8):1523–3.
Riedhammer C, Weissert R. Antigen Presentation, Autoantigens, and Immune Regulation in Multiple Sclerosis and Other Autoimmune Diseases. Frontiers in Immunology. 2015 Jun 17;6.
Robertson KD, Hayward SD, Ling PD, Samid D, Ambinder RF. Transcriptional activation of the Epstein-Barr virus latency C promoter after 5-azacytidine treatment: evidence that demethylation at a single CpG site is crucial. Molecular and Cellular Biology. 1995 Nov;15(11):6150–9.

Robinson MD, McCarthy DJ, Smyth GK. edgeR: a Bioconductor package for differential expression analysis of digital gene expression data. Bioinformatics. 2009 Nov 11;26(1):139–40.
Robinson MD, Oshlack A. A scaling normalization method for differential expression analysis of RNA-seq data. Genome Biology . 2010 ;11(3):R25.
Rodić N, Sharma R, Sharma R, Zampella J, Dai L, Taylor MS, et al. Long Interspersed Element-1 Protein Expression Is a Hallmark of Many Human Cancers. The American Journal of Pathology. 2014 May;184(5):1280–6.
Rodriguez A. Identification of Mammalian microRNA Host Genes and Transcription Units. Genome Research. 2004 Sep 13;14(10a):1902–10.
Ruhrmann S, Ewing E, Piket E, Kular L, Cetrulo Lorenzi JC, Fernandes SJ, et al. Hypermethylation of MIR21 in CD4+ T cells from patients with relapsing-remitting multiple sclerosis associates with lower miRNA-21 levels and concomitant up-regulation of its target genes. Multiple Sclerosis Journal.2018 Sep;24(10):1288-1300.
Safran M, Rosen N, Twik M, BarShir R, Stein TI, Dahary D, et al. The GeneCards Suite. Practical Guide to Life Science Databases . 2021 ;27–56.
Saini HK, Griffiths-Jones S, Enright AJ. Genomic analysis of human microRNA transcripts. Proceedings of the National Academy of Sciences. 2007 Oct 26;104(45):17719–24.
Sakaguchi S, Yamaguchi T, Nomura T, Ono M. Regulatory T Cells and Immune Tolerance. Cell. 2008 May;133(5):775–87.
Saleh A, Macia A, Muotri AR. Transposable Elements, Inflammation, and Neurological Disease. Frontiers in Neurology. 2019 Aug 20;10.
Sang W, Wang Y, Zhang C, Zhang D, Sun C, Niu M, et al. MiR-150 impairs inflammatory cytokine production by targeting ARRB-2 after blocking CD28/B7 costimulatory pathway. Immunology Letters. 2016 Apr;172:1–10.
Sanz I, Wei C, Jenks SA, Cashman KS, Tipton C, Woodruff MC, et al. Challenges and Opportunities for Consistent Classification of Human B Cell and Plasma Cell Populations. Frontiers in Immunology. 2019 Oct 18;10.
Schildknecht A, Brauer S, Brenner C, Lahl K, Schild H, Sparwasser T, et al. FoxP3+ regulatory T cells essentially contribute to peripheral CD8+ T-cell tolerance induced by steady-state dendritic cells. Proceedings of the National Academy of Sciences. 2009 Dec 15;107(1):199–203.
Schneider VA, Graves-Lindsay T, Howe K, Bouk N, Chen H-C, Kitts PA, et al. Evaluation of GRCh38 and de novo haploid genome assemblies demonstrates the enduring quality of the reference assembly. Genome Research. 2017 Apr 10;27(5):849–64.
Schwarz DS, Hutvágner G, Du T, Xu Z, Aronin N, Zamore PD. Asymmetry in the Assembly of the RNAi Enzyme Complex. Cell. 2003 Oct;115(2):199–208.
Serafini B, Rosicarelli B, Magliozzi R, Stigliano E, Aloisi F. Detection of Ectopic B-cell Follicles with Germinal Centers in the Meninges of Patients with Secondary Progressive Multiple Sclerosis. Brain Pathology. 2004 Apr;14(2):164–74.
Shaffer AL, Phelan JD, Wang JQ, Huang D, Wright GW, Kasbekar M, et al. Overcoming Acquired Epigenetic Resistance to BTK Inhibitors. Blood Cancer Discovery. 2021 Sep 14;2(6):630–47.
Shastry BS. SNP alleles in human disease and evolution. Journal of Human Genetics. 2002 Nov;47(11):0561–6.
Shen J, Li G, Zhu Y, Xu Q, Zhou H, Xu K, et al. Foxo1‐induced miR‐92b down‐regulation promotes blood‐brain barrier damage after ischaemic stroke by targeting NOX4. Journal of Cellular and Molecular Medicine. 2021 May 6;25(11):5269–82.
Shi J, Chi S, Xue J, Yang J, Li F, Liu X. Emerging Role and Therapeutic Implication of Wnt

Signaling Pathways in Autoimmune Diseases. Journal of Immunology Research. 2016;2016:1–18.
Shi X, Ye L, Xu S, Guo G, Zuo Z, Ye M, et al. Downregulated miR-29a promotes B cell overactivation by upregulating Crk-like protein in systemic lupus erythematosus. Molecular Medicine Reports. 2020 May 21;22(2):841–9.
Shivakumar M, Lee Y, Bang L, Garg T, Sohn K-A, Kim D. Identification of epigenetic interactions between miRNA and DNA methylation associated with gene expression as potential prognostic markers in bladder cancer. BMC Medical Genomics. 2017 May;10(S1).
Shukla S, Kavak E, Gregory M, Imashimizu M, Shutinoski B, Kashlev M, et al. CTCF-promoted RNA polymerase II pausing links DNA methylation to splicing. Nature . 2011 Nov;479(7371):74–9.
Sievers C, Meira M, Hoffmann F, Fontoura P, Kappos L, Lindberg RLP. Altered microRNA expression in B lymphocytes in multiple sclerosis. Clinical Immunology. 2012 Jul;144(1):70–9.
Simmonds M, Gough S. The HLA Region and Autoimmune Disease: Associations and Mechanisms of Action. Current Genomics. 2007 Nov 1;8(7):453–65.
Simpson S, Wang W, Otahal P, Blizzard L, van der Mei IAF, Taylor BV. Latitude continues to be significantly associated with the prevalence of multiple sclerosis: an updated meta-analysis. Journal of Neurology, Neurosurgery & Psychiatry. 2019 Jun 19 ;90(11):1193–200.
Skurkovich S, Boiko A, Beliaeva I, Buglak A, Alekseeva T, Smirnova N, et al. Randomized study of antibodies to IFN-g and TNF-a in secondary progressive multiple sclerosis. Multiple Sclerosis Journal. 2001 Oct;7(5):277–84.
Smith J, Sen S, Weeks RJ, Eccles MR, Chatterjee A. Promoter DNA Hypermethylation and Paradoxical Gene Activation. Trends in Cancer. 2020 May;6(5):392–406.
Smith KJ, Lassmann H. The role of nitric oxide in multiple sclerosis. The Lancet Neurology. 2002 Aug;1(4):232–41.
Smith KM, Guerau-de-Arellano M, Costinean S, Williams JL, Bottoni A, Mavrikis Cox G, et al. miR-29ab1 Deficiency Identifies a Negative Feedback Loop Controlling Th1 Bias That Is Dysregulated in Multiple Sclerosis. The Journal of Immunology. 2012 Jul 6;189(4):1567–76.
Smith MJ, Ford BR, Rihanek M, Coleman BM, Getahun A, Sarapura VD, et al. Elevated PTEN expression maintains anergy in human B cells and reveals unexpectedly high repertoire autoreactivity. JCI Insight. 2019 Feb 7;4(3).
Sokratous M, Dardiotis E, Bellou E, Tsouris Z, Michalopoulou A, Dardioti M, et al. CpG Island Methylation Patterns in Relapsing-Remitting Multiple Sclerosis. Journal of Molecular Neuroscience. 2018 Mar;64(3):478–84.
Soldevila B, Alonso N, Martínez-Arconada MJ, Granada ML, Boada A, Vallejos V, et al. Regulatory T cells and other lymphocyte subpopulations in patients with melanoma developing interferon-induced thyroiditis during high-dose interferon-α2b treatment. Clinical Endocrinology. 2013 Mar 12;78(4):621–8.
Song H, Zhang Y, Liu N, Wan C, Zhang D, Zhao S, et al. miR-92b regulates glioma cells proliferation, migration, invasion, and apoptosis via PTEN/Akt signaling pathway. Journal of Physiology and Biochemistry. 2016 Feb 18;72(2):201–11.
Sospedra M, Martin R. Immunology of multiple sclerosis. Annual Review of Immunology. 2005 Apr 1;23(1):683–747.
Souren NY, Gerdes LA, Lutsik P, Gasparoni G, Beltrán E, Salhab A, et al. DNA methylation signatures of monozygotic twins clinically discordant for multiple sclerosis. Nature Communications. 2019 May 7;10(1).
Spann NJ, Glass CK. Sterols and oxysterols in immune cell function. Nature Immunology. 2013

Aug 20;14(9):893–900.
Srivastava M, Baig MS. NOS1 mediates AP1 nuclear translocation and inflammatory response. Biomedicine & Pharmacotherapy. 2018 Jun;102:839–47.
Sternberg Z, Chadha K, Lieberman A, Hojnacki D, Drake A, Zamboni P, et al. Quercetin and interferon-β modulate immune response(s) in peripheral blood mononuclear cells isolated from multiple sclerosis patients. Journal of Neuroimmunology. 2008 Dec;205(1-2):142–7.
Stone S, Lin W. The unfolded protein response in multiple sclerosis. Frontiers in Neuroscience. 2015 Jul 29;9.
Strickland FM, Hewagama A, Wu A, Sawalha AH, Delaney C, Hoeltzel MF, et al. Diet Influences Expression of Autoimmune-Associated Genes and Disease Severity by Epigenetic Mechanisms in a Transgenic Mouse Model of Lupus. Arthritis & Rheumatism. 2013 Jul;65(7):1872–81.
Su R, Lin HS, Zhang XH, Yin XL, Ning HM, Liu B, et al. MiR-181 family: regulators of myeloid differentiation and acute myeloid leukemia as well as potential therapeutic targets. Oncogene. 2014 Sep 1;34(25):3226–39.
Su SF, Chang YW, Andreu-Vieyra C, Fang JY, Yang Z, Han B, et al. miR-30d, miR-181a and miR-199a-5p cooperatively suppress the endoplasmic reticulum chaperone and signaling regulator GRP78 in cancer. Oncogene. 2012 Oct 22;32(39):4694–701.
Sukapan P, Promnarate P, Avihingsanon Y, Mutirangura A, Hirankarn N. Types of DNA methylation status of the interspersed repetitive sequences for LINE-1, Alu, HERV-E and HERV-K in the neutrophils from systemic lupus erythematosus patients and healthy controls. Journal of Human Genetics. 2014 Jan 16;59(4):178–88.
Sun H, Tian J, Li J. MiR-92b-3p ameliorates inflammation and autophagy by targeting TRAF3 and suppressing MKK3-p38 pathway in caerulein-induced AR42J cells. International Immunopharmacology. 2020 Nov;88:106691.
Sun X, Sit A, Feinberg MW. Role of miR-181 family in regulating vascular inflammation and immunity. Trends in Cardiovascular Medicine. 2014 Apr;24(3):105–12.
Sundberg EJ, Deng L, Mariuzza RA. TCR recognition of peptide/MHC class II complexes and superantigens. Seminars in Immunology . 2007 Aug;19(4):262–71.
Suzuki HI, Young RA, Sharp PA. Super-Enhancer-Mediated RNA Processing Revealed by Integrative MicroRNA Network Analysis. Cell. 2017 Mar;168(6):1000-1014.e15.
Takeshima H, Yoda Y, Wakabayashi M, Hattori N, Yamashita S, Ushijima T. Low-dose DNA demethylating therapy induces reprogramming of diverse cancer-related pathways at the single-cell level. Clinical Epigenetics. 2020 Sep 21;12(1).
Tang F, Zhang Y, Huang QQ, Qian MM, Li ZX, Li YJ, et al. Genome-Wide Identification and Analysis of Enhancer-Regulated microRNAs Across 31 Human Cancers. Frontiers in Genetics. 2020 Jun 30;11.
Tang S, Zhuge Y. An immune-related pseudogene signature to improve prognosis prediction of endometrial carcinoma patients. BioMedical Engineering OnLine. 2021 Jun 30;20(1).
Thomas PD, Campbell MJ, Kejariwal A, Mi H, Karlak B, Daverman R, et al. PANTHER: A Library of Protein Families and Subfamilies Indexed by Function. Genome Research . 2003;13(9):2129–41.
Thomas PD, Kejariwal A, Guo N, Mi H, Campbell MJ, Muruganujan A, et al. Applications for protein sequence-function evolution data: mRNA/protein expression analysis and coding SNP scoring tools. Nucleic Acids Research. 2006;34:W645–50.
Thompson AJ, Banwell BL, Barkhof F, Carroll WM, Coetzee T, Comi G, et al. Diagnosis of multiple sclerosis: 2017 revisions of the McDonald criteria. The Lancet Neurology. 2018 Feb;17(2):162–73.

Trip SA, Miller DH. Imaging in multiple sclerosis. Journal of Neurology, Neurosurgery & Psychiatry 2005;76:iii11-iii18.
Turvey SE, Broide DH. Innate immunity. Journal of Allergy and Clinical Immunology. 2010 Feb ;125(2):S24–32.
Tveita AA, Rekvig OP. Alterations in Wnt pathway activity in mouse serum and kidneys during lupus development. Arthritis & Rheumatism. 2011 Jan 28;63(2):513–22.
Tzartos JS, Craner MJ, Friese MA, Jakobsen KB, Newcombe J, Esiri MM, et al. IL-21 and IL-21 Receptor Expression in Lymphocytes and Neurons in Multiple Sclerosis Brain. The American Journal of Pathology. 2011 Feb;178(2):794–802.
Udovicic M, Bazdaric K, Bilic-Zulle L, Petrovecki M. What we need to know when calculating the coefficient of correlation? Biochemia Medica. 2007;10–5.
van Langelaar J, Rijvers L, Smolders J, van Luijn MM. B and T Cells Driving Multiple Sclerosis: Identity, Mechanisms and Potential Triggers. Frontiers in Immunology. 2020 May 8;11.
Veitch S, Njock M-S, Chandy M, Siraj MA, Chi L, Mak H, et al. MiR-30 promotes fatty acid beta-oxidation and endothelial cell dysfunction and is a circulating biomarker of coronary microvascular dysfunction in pre-clinical models of diabetes. Cardiovascular Diabetology. 2022 Feb 24;21(1).
Vejux A, Abed-Vieillard D, Hajji K, Zarrouk A, Mackrill JJ, Ghosh S, et al. 7-Ketocholesterol and 7β-hydroxycholesterol: In vitro and animal models used to characterize their activities and to identify molecules preventing their toxicity. Biochemical Pharmacology. 2020 Mar;173:113648.
Vejux A, Lizard G. Cytotoxic effects of oxysterols associated with human diseases: Induction of cell death (apoptosis and/or oncosis), oxidative and inflammatory activities, and phospholipidosis. Molecular Aspects of Medicine. 2009 Jun;30(3):153–70.
Vignali DAA, Collison LW, Workman CJ. How regulatory T cells work. Nature Reviews Immunology. 2008 Jul;8(7):523–32.
Villar LM, Sádaba MC, Roldán E, Masjuan J, González-Porqué P, Villarrubia N, et al. Intrathecal synthesis of oligoclonal IgM against myelin lipids predicts an aggressive disease course in MS. Journal of Clinical Investigation. 2005 Jan 3;115(1):187–94.
Vlachos IS, Zagganas K, Paraskevopoulou MD, Georgakilas G, Karagkouni D, Vergoulis T, et al. DIANA-miRPath v3.0: deciphering microRNA function with experimental support. Nucleic Acids Research. 2015 May 14;43(W1):W460–6.
von Büdingen H-C, Kuo TC, Sirota M, van Belle CJ, Apeltsin L, Glanville J, et al. B cell exchange across the blood-brain barrier in multiple sclerosis. Journal of Clinical Investigation. 2012 Nov 19;122(12):4533–43.
Wagner M, Sobczyński M, Bilińska M, Pokryszko-Dragan A, Cyrul M, Kuśnierczyk P, et al. Preliminary Study on the Role of TMEM39A Gene in Multiple Sclerosis. Journal of Molecular Neuroscience. 2017 Apr 25;62(2):181–7.
Wallin MT, Culpepper WJ, Nichols E, Bhutta ZA, Gebrehiwot TT, Hay SI, et al. Global, regional, and national burden of multiple sclerosis 1990–2016: a systematic analysis for the Global Burden of Disease Study 2016. The Lancet Neurology. 2019 Mar;18(3):269–85.
Wang D, Li C, Zhang X. The Promoter Methylation Status and mRNA Expression Levels of CTCF and SIRT6 in Sporadic Breast Cancer. DNA and Cell Biology. 2014 Sep;33(9):581–90.
Wang G, Gu Y, Xu N, Zhang M, Yang T. Decreased expression of miR-150, miR146a and miR424 in type 1 diabetic patients: Association with ongoing islet autoimmunity. Biochemical and Biophysical Research Communications. 2018 Apr;498(3):382–7.
Wang J, Zhang Q, Wang D, Yan W, Sha H, Zhao J, et al. MiR-29a: a potential therapeutic target

and promising biomarker in tumors. Bioscience Reports. 2018 Feb 8;38(1).
Wang L, Hagemann TL, Kalwa H, Michel T, Messing A, Feany MB. Nitric oxide mediates glial-induced neurodegeneration in Alexander disease. Nature Communications. 2015 Nov 26;6(1).
Wang S, Wu W, Claret FX. Mutual regulation of microRNAs and DNA methylation in human cancers. Epigenetics. 2017 Feb 6;12(3):187–97.
Wang X, Huang X, Yan Q, Bao C. Aberrant Activation of the WNT/β-Catenin Signaling Pathway in Lupus Nephritis. Samant R, editor. PLoS ONE. 2014 Jan 21;9(1):e84852.
Wang X, Lei D, Ding J, Liu S, Tao L, Zhang F, et al. A DNA-Methylated Sight on Autoimmune Inflammation Network across RA, pSS, and SLE. Journal of Immunology Research. 2018 Aug 12;2018:1–13.
Wang Z, Moult J. SNPs, protein structure, and disease. Human Mutation. 2001;17(4):263–70.
Wattjes MP, Ciccarelli O, Reich DS, Banwell B, de Stefano N, Enzinger C, et al. 2021 MAGNIMS–CMSC–NAIMS consensus recommendations on the use of MRI in patients with multiple sclerosis. The Lancet Neurology. 2021 Aug;20(8):653–70.
Waxman SG. Axonal conduction and injury in multiple sclerosis: the role of sodium channels. Nature Reviews Neuroscience. 2006 Dec 1 ;7(12):932–41.
Weber M, Schübeler D. Genomic patterns of DNA methylation: targets and function of an epigenetic mark. Current Opinion in Cell Biology . 2007 Jun;19(3):273–80.
Weintraub AS, Li CH, Zamudio AV, Sigova AA, Hannett NM, Day DS, et al. YY1 Is a Structural Regulator of Enhancer-Promoter Loops. Cell. 2017 Dec;171(7):1573-1588.e28.
Wen N, Lv Q, Du Z. MicroRNAs involved in drug resistance of breast cancer by regulating autophagy. Journal of Zhejiang University-SCIENCE B. 2020 Sep;21(9):690–702.
Whalen S, Truty RM, Pollard KS. Enhancer–promoter interactions are encoded by complex genomic signatures on looping chromatin. Nature Genetics. 2016 Apr 4;48(5):488–96.
Wingerchuk DM. Smoking: effects on multiple sclerosis susceptibility and disease progression. Therapeutic Advances in Neurological Disorders. 2011 Oct 18;5(1):13–22.
Wu GF, Alvarez E. The Immunopathophysiology of Multiple Sclerosis. Neurologic Clinics . 2011 May;29(2):257–78.
Wu X, Zhang Y. TET-mediated active DNA demethylation: mechanism, function and beyond. Nature Reviews Genetics. 2017 May 30;18(9):517–34.
Wu Y-CB, Kipling D, Dunn-Walters DK. The Relationship between CD27 Negative and Positive B Cell Populations in Human Peripheral Blood. Frontiers in Immunology. 2011;2.
Xiang N, Zhao R, Song G, Zhong W. Selenite reactivates silenced genes by modifying DNA methylation and histones in prostate cancer cells. Carcinogenesis. 2008 Aug 1;29(11):2175–81.
Xiao C, Calado DP, Galler G, Thai T-H, Patterson HC, Wang J, et al. MiR-150 Controls B Cell Differentiation by Targeting the Transcription Factor c-Myb. Cell. 2007 Oct ;131(1):146–59.
Xie C, Li Z, Zhang G-X, Guan Y. Wnt Signaling in Remyelination in Multiple Sclerosis: Friend or Foe? Molecular Neurobiology. 2013 Nov 16;49(3):1117–25.
Xie Z, Bailey A, Kuleshov MV, Clarke DJB, Evangelista JE, Jenkins SL, et al. Gene Set Knowledge Discovery with Enrichr. Current Protocols. 2021 Mar;1(3).
Xu H, Tian Y, Tang D, Zou S, Liu G, Song J, et al. An Endoplasmic Reticulum Stress–Micro RNA‐26a Feedback Circuit in NAFLD. Hepatology. 2020 Nov 6;73(4):1327–45.
Xun G, Ma M, Li B, Zhao S. miR‐138 and miR‐193 target long non‐coding RNA UCA1 to inhibit cell proliferation, migration, and invasion of lung cancer. Thoracic Cancer. 2020 Aug 6;11(9):2681–9.
Yam-Puc JC, Zhang L, Zhang Y, Toellner K-M. Role of B-cell receptors for B-cell development and antigen-induced differentiation. F1000Research. 2018 Apr 6;7:429.

Yamauchi T, Moroishi T. Hippo Pathway in Mammalian Adaptive Immune System. Cells. 2019 Apr 30;8(5):398.
Yang J, Reth M. Receptor Dissociation and B-Cell Activation. Current Topics in Microbiology and Immunology. 2015;27–43.
Yang X, Han H, De Carvalho Daniel D, Lay Fides D, Jones Peter A, Liang G. Gene Body Methylation Can Alter Gene Expression and Is a Therapeutic Target in Cancer. Cancer Cell . 2014 Oct;26(4):577–90.
Yao Q, Chen Y, Zhou X. The roles of microRNAs in epigenetic regulation. Current Opinion in Chemical Biology. 2019 Aug ;51:11–7.
Yin B, Umar T, Ma X, Chen Y, Chen N, Wu Z, et al. MiR-193a-3p targets LGR4 to promote the inflammatory response in endometritis. International Immunopharmacology. 2021 Sep;98:107718.
Yin M, Chen Z, Ouyang Y, Zhang H, Wan Z, Wang H, et al. Thrombin-induced, TNFR-dependent miR-181c downregulation promotes MLL1 and NF-κB target gene expression in human microglia. Journal of Neuroinflammation. 2017 Jun 29;14(1).
Yoshikawa H, Matsubara K, Qian G-S, Jackson P, Groopman JD, Manning JE, et al. SOCS-1, a negative regulator of the JAK/STAT pathway, is silenced by methylation in human hepatocellular carcinoma and shows growth-suppression activity. Nature Genetics. 2001 May;28(1):29–35.
Yu X, Graner M, Kennedy PGE, Liu Y. The Role of antibodies in the pathogenesis of Multiple Sclerosis. Frontiers in Neurology. 2020 Oct 20;11.
Yuan S, Shi Y, Tang S-J. Wnt Signaling in the Pathogenesis of Multiple Sclerosis-Associated Chronic Pain. Journal of Neuroimmune Pharmacology. 2012 May 2;7(4):904–13.
Yue Y, Stone S, Lin W. Role of nuclear factor κB in multiple sclerosis and experimental autoimmune encephalomyelitis. Neural Regeneration Research. 2018;13(9):1507.
Zaidi SK, Perez AW, White ES, Lian JB, Stein JL, Stein GS. An AML1-ETO/miR-29b-1 regulatory circuit modulates phenotypic properties of acute myeloid leukemia cells. Oncotarget. 2017 May 24;8(25):39994–40005.
Zarrouk A, Nury T, Karym E-M, Vejux A, Sghaier R, Gondcaille C, et al. Attenuation of 7-ketocholesterol-induced overproduction of reactive oxygen species, apoptosis, and autophagy by dimethyl fumarate on 158 N murine oligodendrocytes. The Journal of Steroid Biochemistry and Molecular Biology. 2017 May;169:29–38.
Zeilinger S, Kühnel B, Klopp N, Baurecht H, Kleinschmidt A, Gieger C, et al. Tobacco Smoking Leads to Extensive Genome-Wide Changes in DNA Methylation. Chen A, editor. PLoS ONE. 2013 May 17;8(5):e63812.
Zhang B, Gu X, Han X, Gao Q, Liu J, Guo T, et al. Crosstalk between DNA methylation and histone acetylation triggers GDNF high transcription in glioblastoma cells. Clinical Epigenetics. 2020 Mar 17;12(1).
Zhang B, Zhou Y, Lin N, Lowdon RF, Hong C, Nagarajan RP, et al. Functional DNA methylation differences between tissues, cell types, and across individuals discovered using the M&M algorithm. Genome Research. 2013 Jun 26 ;23(9):1522–40.
Zhang L, Li Y-J, Wu X-Y, Hong Z, Wei W-S. MicroRNA-181c negatively regulates the inflammatory response in oxygen-glucose-deprived microglia by targeting Toll-like receptor 4. Journal of Neurochemistry. 2015 Feb 12;132(6):713–23.
Zhang L, Silva TC, Young JI, Gomez L, Schmidt MA, Hamilton-Nelson KL, et al. Epigenome-wide meta-analysis of DNA methylation differences in prefrontal cortex implicates the immune processes in Alzheimer's disease. Nature Communications. 2020 Nov 30;11(1).
Zhang M, Wang L, Huang S, He X. Exosomes with high levels of miR-181c from bone marrow-

derived mesenchymal stem cells inhibit inflammation and apoptosis to alleviate spinal cord injury. Journal of Molecular Histology. 2021 Feb 6;52(2):301–11.
Zhang R, Tian A, Wang J, Shen X, Qi G, Tang Y. miR26a Modulates Th17/Treg Balance in the EAE Model of Multiple Sclerosis by Targeting IL6. NeuroMolecular Medicine. 2014 Nov 2;17(1):24–34.
Zhang Z, Xue Z, Liu Y, Liu H, Guo X, Li Y, et al. MicroRNA-181c promotes Th17 cell differentiation and mediates experimental autoimmune encephalomyelitis. Brain, Behavior, and Immunity. 2018 May;70:305–14.
Zhu M, Ye L, Zhu G, Zeng Y, Yang C, Cai H, et al. ROS-Responsive miR-150-5p Downregulation Contributes to Cigarette Smoke-Induced COPD via Targeting IRE1α. Virág L, editor. Oxidative Medicine and Cellular Longevity. 2022 May 5;2022:1–23.
Zozulya AL, Wiendl H. The role of regulatory T cells in multiple sclerosis. Nature Clinical Practice Neurology. 2008 Jun 24 ;4(7):384–98.

8. ANNEX I

PROTOCOL - Isolation of PBMCs from whole peripheral blood

The objective of this protocol is to remove erythrocytes and isolate total mononuclear blood cells from fresh peripheral blood collected from MS patients and controls, and to isolate Bmem cells and Treg cells from PBMCs using flow citometry followed by sorting.

PROCEDURE

0. Collect between 80-110 mL of peripheral blood from donors.

1. Aliquot sample by adding 5 mL of fresh blood to the necessary amount of 50 mL conical tubes. *Example: for a initial 100 mL blood volume, 20 conical tubes would be needed.*

2. Add 45 mL of PharmLyse™ Lysis Buffer 1X (LB) (BD Bioscience, CA) for a total volume of 50 mL per aliquot.

3. Incubate at room temperature (RT) for 10 minutes. Vortex every 3-5 minutes.

4. Centrifuge for 5 minutes at 300 g. Discard the supernatant.

5. Add 20 mL of FACS-flow buffer to the cell pellet. Vortex to resuspend the pellet.

6. Centrifuge for 5 minutes at 300 g. Discard supernatant by pipetting, and keep the celullar pellet.

7. Add 2.5 mL of PBS-1% FBS to the pellet, and resuspend either by pipetting or vortexing.

8. Pool all volumes into a single 50 mL conical tube. Annotate the total volume for step 10.

9. In order to estimate the amount of cells present in our sample, separate 25 µL of the sample (sub-sample), and mix it up with 25 µL of PerfectCounts beads (Cytognos, Spain) and 100 µL of FACS-flow solution.

10. Load the sub-sample into the FACSAria II instrument (BD Biosciences, CA). The formula used to calculate the number of cells present in the sample is the following:

$$Total\ number\ of\ cells\ (millions) = \frac{number\ of\ cells\ in\ 25\ \mu l\ sample}{number\ of\ events}\ x\ 1036\ x\ Vt\ (\mu l)$$

where:

Number of events = it was set to 3000
1036 = a constant factor in cytometry counting
Vt = the total volume of the sample

10. Once the amount of cells in our sample have been estimated, divide the sample from step 8 into aliquots of 25 millions of cells each in FACS tubes. *Example: for 200 millions of cells, make 8 alicuots.*

11. Centrifuge FACS tubes for 5 minutes at 300 g. Discard the supernatant.

12. Resuspend cell pellets in 300 µL of FACS-flow buffer.

13. Incubate samples with the following antibody mixture for 15 minutes in darkness.

Antibodies	**Volume per tube (µL)**
CD127 PECy7	7.5
CD194 V450	15
CD3 FITC	30
CD4 PerCpCy5.5	30
CD25 PE	40
CD27 APCH7	7.5
HLA-DR APC	30
Total	***160***

14. Centrifuge samples for 5 minutes at 300 g. Decant to remove supernatant.

15. Wash pellet once by adding 20 mL of FACS-flow buffer, centrifuge for 5 minutes at 300 g, and decant the supernatant.

16. Resuspend cell pellet in 1 mL of PBS-1%FBS.

17. Load samples into the FACSAria II instrument (BD Biosciences) for the sorting of the memory B cells (CD3– CD14– HLA-DR+ CD27+) and regulatory T cells (CD4+ CD3+ CD25+ CD194+ CD127–).

9. ANNEX II

PROTOCOL - MeDIP

The MeDIP procedure was performed to extract the methylated DNA fraction from our sample before the sequencing. The MeDIP protocol consisted of six major steps:

STEP 1. DNA shearing [Bioruptor® Pico (Diagenode)]
STEP 2. DNA purification & concentration [Monarch® Cleanup PCR (NEB)]
STEP 3. Library preparation I (end repair + adaptor ligation) [iDeal Library Preparation kit (Diagenode)]
STEP 4. Methylated DNA immunoprecipitation [MagMeDIP kit (Diagenode)]
STEP 5. DNA elution [iPure kit v2 (Diagenode)]
STEP 6. Library preparation II (PCR amplification) [iDeal Library Preparation kit (Diagenode)]

[STEP 1] DNA shearing Bioruptor® Pico (Diagenode)

The Bioruptor® Pico (Diagenode, Belgium) was used to sonicate DNA into ~200 bp fragments (range 100-300 bp).

PROCEDURE

1. Turn on the water cooler of the Bioruptor® Pico (Diagenode). Cool the water until it reaches 4ºC (it takes 30-45 minutes).

2. Meanwhile, prepare DNA samples on 1.5mL Bioruptor® Pico microtubes with caps (Diagenode, Belgium) taking into account the following:
   a. The amount of starting DNA can range between 400-1000 ng (recommended 1000 ng)
   b. The DNA concentration should be in the range between 1-20 ng/µL (recommended 10ng/µL)
   c. The recommended volume per tube is 100 µL
   d. DNA should be resuspended in Tris-EDTA 1X pH 8.0

3. Once DNA samples are prepared, vortex for 5-10 seconds and spin the samples. Store on ice 15 minutes before shearing to improve the sonication efficiency.

4. Put the microtubes inside the tube holder and place it inside the sonication bath. DO NOT leave any empty space in the tube holder; fill them with microtubes containing the same volume of water.

5. Turn on the Bioruptor® Pico and select the following program:

	Time	Cycle number
ON	30 seconds	10
OFF	30 seconds	

6. Once the sonication has finished, prepare a 1.5 % agarose gel and run DNA samples at 100V for 40 minutes.

7. DNA fragments should have a size between the range of 100-300bp, with a mean size of ~200bp as shown in Figure 36.

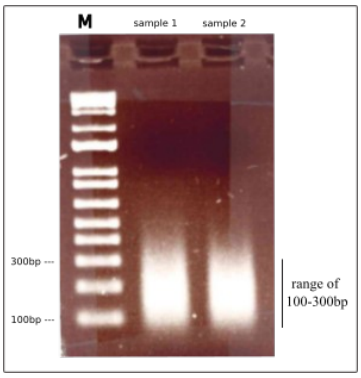

Figure 36. Electrophoresis in an agarose gel (1.5%) of the sonicated DNA after 10 cycles of sonication in the Bioruptor® Pico (Diagenode, Belgium). The 'M' corresponded to the DNA ladder; the second and the third column corresponded to sonicated DNA samples.

8. Store DNA samples at -20ºC until its usage.

[STEP 2] DNA purification & concentration Monarch® Cleanup PCR (NEB)

The Monarch® Cleanup PCR (NEB, New England) was used to purify and concentrate high-quality, double-stranded DNA prior to library preparation.

PROCEDURE

1. Dilute sonicated DNA samples with the DNA Cleanup Binding Buffer in a 1:5 ratio. Do not vortex, mix by pipetting.

2. Insert column into collection tube and load sample onto column by pipetting. Spin for 1 minute at full speed (≥ 16000g), then discard flow-through.

3. Re-insert column into collection tube. Add 200 µL of DNA Wash Buffer and spin for 1 minute at full speed (≥ 16000g). Discard the flow-through.

4. Repeat wash (step 3).

5. Transfer column to a clean 1.5 mL microtube. Use care to ensure that the tip of the column does not come into contact with the flow-though. If in doubt, re-spin for 1 minute at full speed (≥ 16000g) to ensure traces of salt and ethanol are not carried to next step.

6. Add 55 µL of DNA Elution Buffer to the center of the matrix. Wait for 5 minutes, then spin for a 1 minute at full speed (≥ 16000g) to elute the purified DNA.

[STEP 3] Library preparation I iDeal Library Preparation kit (Diagenode)

The iDeal Library Kit (Diagenode, Belgium) was used to prepare the first part of the DNA library. In this step, fragmented DNA was repaired with a poly-(A) tail and stabilized with the addition of

an adaptor. DNA fragments were afterwards purified using the AMPure XP Beads (Beckman Court, USA).

PROCEDURE

1. Thaw reagents on ice. In a sterile 200 µL nuclease-free tube, prepare the End Repair reaction by mixing the following components.

Reagents	**1 Rxn**
iDeal LibraryEnd Repair/dA-Tailing Enzyme Mix	3 µL
iDeal Library End Repair/dA-Tailing Buffer	6.5 µL
Fragmented DNA	55.5 µL
Total End Repair reaction volume	***65 µL***

2. Mix by pipetting followed by a quick spin.

3. Place tubes in a thermocycler, with the heated lid on, and run the following program:

Temp	Time
20°C	30 minutes
65 ºC	30 minutes
4 ºC	∞

4. Prepare the Ligation reaction mixture by adding the following components to the End Repair reaction tube.

Reagents	**1 Rxn**
iDeal Library Ligation Master Mix	15 µL
iDeal Library Adaptor for Illumina	2.5 µL
iDeal Library Ligation Enhancer	1 µL
End Repair reaction	65 µL
Total Ligation reaction volume	***83.5 µL***

5. Incubate at 20ºC for 15 minutes using a thermal cycler.

6. Add 3 µL of iDeal Library Uracil Excesion Reagent to the ligation mixture (final volume = 86.5 µL).

7. Mix well and incubate at 37ºC for 15 minutes using a thermal cycler.

8. Purify DNA fragments using AMPure XP Beads (Beckman Court, USA). For that purpose, resuspend 86.5 µL of AMPure XP beads by vortexing and add it directly to the Ligation reaction mixture as follows.

Reagents	1 Rxn
AMPure XP beads	86.5 µL
Ligation reaction	86.5 µL
Total volume	***173 µL***

8. Mix well by pipetting up and down at least 10 times.

9. Incubate for 5 minutes at room temperature (RT).

10. Quickly spin the tube and place the tube on magnetic rack to separate the beads from the supernatant (about 5 minutes).

11. Discard the supernatant. Keep the beads on the magnetic rack.
**Caution: DO NOT discard the beads.

12. Quickly add 190 µL of 80% freshly prepared ethanol to the tube placed in the magnetic rack. Incubate at RT for 30 seconds, and then carefully remove and discard the supernatant.

13. Repeat Step 12 twice (three washes in total).

14. Air dry the beads for 10 minutes while the tube is on the magnetic rack with the lid open.

15. Elute the DNA target from the beads using 23 µL of 10mM Tris-Hcl or 0.1X Tris-EDTA, pH 8.0.

16. Mix well by vortexing or by pipetting up and down.

17. Quickly spin the tube and place it on a magnetic rack for about 5 minutes.

18. Transfer 23 µL of the supernatant to a new microtube for the immunoprecipitation step.

Note. Be sure not to transfer any beads. Trace amounts of bead carry over may affect the optimal performance of the polymerase used in the iDeal Library PCR Master Mix in the subsequent PCR step.

[STEP 4] Methylated DNA immunoprecipitation MagMeDIP kit (Diagenode)

The immunoprecipitation of the methylated DNA is performed using the MagMeDIP kit (Diagenode, Belgium). During this step, two types of samples are obtained: IP samples and Input samples. The IP sample corresponds to the fraction of the reaction subjected to incubation with the anti-5-methylcytosine antibody followed by immunoprecipitation with magnetic beads. Thus, IP samples contained the methylated DNA fraction. The Input sample, on the other hand, corresponds to the fraction of the reaction undergoing all the MeDIP procedure but without the incubation with the antibody and magnetic beads. Thus, the Input sample contains both methylated and non-methylated DNA fragments. Input samples are used as reference samples during sequencing.

PROCEDURE

1. Prepare the IP incubation mix as described below.

Reagents	**1 IP + Input**
MagBuffer A	24 µL
MagBuffer B	6 µL
positive meDNA control	1.5 µL
negative unDNA control	1.5 µL
Adaptor-ligated DNA	23 µL
Water	34 µL
Total IP incubation mix volume	***90 µL****

*The total volume of 90 µL corresponds to the IP fraction (75 µL), Input fraction (7.5 µL), and excess (7.5 µL).

2. Add 67 µL of IP incubation mix to each adaptor-ligated DNA sample. Mix it by pipetting up and down, and give it a spin.

3. Incubate the tube at 95ºC for 3 minutes using a thermal cycler.

4. Quickly chill sample on ice (it is best to use ice-water) for 2 minutes.

5. Perform a spin to consolidate your sample.

6. Take out 7.5 µL and transfer it to a new labeled tube. It will be our Input sample. Keep at 4ºC until the "[STEP5] DNA elution" step.

7. Transfer from what is left 75 µL into a new 0.2 mL microtube. It will be our IP sample. Keep it at 4ºC. *Note: the remaining volume (~7.5µL) corresponds to excess.*

8. In a new microtube, dilute the anti-5-methylcytosine antibody 1:2 with water.

9. Prepare the Diluted Antibody mix by adding to the freshly diluted antibody reaction the following components in the same order as they are listed below.

Reagents	**1 IP**
Antibody anti-5-methylcytosine (1:2)	0.30 µL
MagBuffer A	0.60 µL
Water	2.10 µL
MagBuffer C	2 µL
Total Diluted Antibody mix volume	***5 µL***

10. Add 5 µL of Diluted Antibody mix to each IP sample from step 7 (final volume: 80 µL).

11. Mix and add 20 µL of washed beads to each IP sample tube (final volume: 100 µL).

12. Place them on a rotating wheel (40 rpm) at 4ºC overnight.

[Day 2]

13. Place MagWash buffer-1, MagWash buffer-2 and the magnetic rack on ice.

14. Spin down and place the IP sample tubes in the ice-cold magnetic rack for 1 minute. Discard the supernatant.

15. Wash IP Samples three times with ice-cold MagWash Buffer-1 as follows:
a. Add 100 µL of ice-cold MagWash Buffer-1 and invert the tube to resuspend the beads.
b. Incubate the IP sample for 4 minutes at 4ºC on a rotating wheel (40rpm).
c. Spin and place the tube in the magnetic rack for 1 minute. Discard the supernatant. Keep the captured beads.

20. Wash IP Samples once with ice-cold MagWash buffer-2 as follows:
a. Add per tube 100 µL of ice-cold MagWash Buffer-2 and invert it to resuspend the beads.
b. Incubate 'IP sample' for 4 minutes at 4ºC on a rotating wheel (40rpm).
c. Spin and place the tube in the magnetic rack for 1 minute. Discard the supernatant. Keep the captured beads.

21. After washing, discard the last traces of wash buffer by pipetting. Keep the bead pellets on ice and proceed immediately to the next step to purify and elute the DNA.

[STEP 5] DNA elution iPure kit v2 (Diagenode)

The purification and elution of the immunoprecipitated DNA is completed using the iPure Kit v2 (Diagenode, Belgium). In this step, the Input sample is reincorporated into the protocol.

PROCEDURE

0. Place Buffer A at 25ºC during 30 minutes before its use.

1. Prepare the Elution buffer by mixing Buffer A and B as follows:

Reagents	**1 Rxn**
Buffer A	115.4 µL
Buffer B	4.6 µL
Total Elution Buffer volume	***120 µL****

*100 µL of Elution buffer is needed per Ipure reaction; the remaning 20 µL is excess.

2. Add 50 µL of Elution Buffer to the bead pellet containing the IP sample (from step 21 of the [STEP 4] Methylated DNA immunoprecipitation section) for the first DNA elution.

3. Take out the Input sample from 4ºC (from step 6 of the [STEP 4] Methylated DNA immunoprecipitation section), and perform a pulse spin. Add 92.5 µL of Elution buffer for a final volume of 100 µL.

4. Incubate both IP and Input samples for 15 minutes at RT on a rotating wheel (40 rpm).

5. Spin the tubes and place them on the magnetic rack. After 1 minute, transfer the supernatant to a new labeled tube. **Note. The beads pellet from the IP sample that remains in the magnetic rack will be used again for a second DNA elution.*

6. Add 50 µL of Elution Buffer (second elution) to the beads pellet of IP sample. Incubate for 15 minutes at RT on a rotating wheel (40 rpm).

7. Spin the tube and place it on the magnetic rack. Wait for 1 minute and transfer the supernatant (50 µL) to the new labeled tube prepared in step 5 for a total volume of 100 µL.
**Note*. *Elutions for the IP sample (2 elutions of 50µL) and Iput sample (1 elution of 100µL) are now completed for a total volume of 100µL. Beads pellet are discarded*.

8. Add 2 µL of carrier to IP and Input samples. Vortex briefly and perform a short spin.

9. Add 100 µL of 100% isopropanol to IP and Input samples. Vortex briefly and perform a short spin.

10. Resuspend the Magnetic beads provided by the kit, and transfer 15 µL to each IP and input sample. The final volume is now 217 µL.

11. Incubate IP and Input samples for 10 minutes at RT on a rotating wheel (40 rpm).

12. Spin the tubes and place them on the magnetic rack. Wait for 1 minute and discard the supernatant. Keep the captured beads.

13. Wash beads by adding 100 µL of Wash buffer 1 to each sample. Close tubes and invert to resuspend the beads. Incubate for 5 minutes at RT on a rotating wheel (40 rpm).

15. Wait for 1 minute and discard the supernatatnt. Keep the captured beads.

16. Add 100 µL Wash buffer 2 to beads for a second wash. Close the tubes and invert to resuspend the beads. Incubate for 5 minutes at RT on a rotating wheel (40 rpm).
17. Briefly spin the tubes and place them on the magnetic rack. Wait for 1 minute and discard the buffer. Keep the captured beads.

19. Add 25 µL of Buffer C to each sample for the elution step. Close the tubes, invert to resuspend the beads, and incubate them for 15 minutes at RT on a rotating wheel (40 rpm).

20. Spin the tubes and place them on the magnetic rack. Wait for 1 minute and transfer the supernatants into a new labeled tube.

21. Place the eluted DNA on ice or store it at -20ºC until its usage.

[STEP 6] Library preparation II iDeal Library Preparation kit (Diagenode)

The second part of the library preparation was performed using the iDeal Library Kit (Diagenode, Belgium). In this step, index primers were added using a PCR procedure. Index sequences are used to label each sample in an unique way, allowing the pooling of many samples during sequencing.

PROCEDURE

1. Prepare the PCR Reaction mix by mixing the following components in sterile 0.2 mL PCR microtubes.

Reagents	1 Rxn
Eluted DNA	23 µL
iDeal Library PCR Master Mix	25 µL
iDeal Library Index Primer	1 µL
iDeal Library PCR primer	1 µL
Total PCR Reaction mix volume	***50 µL***

2. Place samples on a thermal cycler and incubated as follows:

Cycle step	Temp	Time	Cycles
Initial denaturation	98 ºC	30 seconds	1
Denaturation	98 ºC	10 seconds	8
Annealing	65 ºC	30 seconds	
Extension	72 ºC	30 seconds	
Final extension	72 ºC	5 minutes	1
Hold	4 ºC	∞	

3. In order to purify the amplified DNA, add 50 µL of resuspended AMPure XP beads to each PCR reaction tube. Mix well by pipetting up and down at least 10 times.

4. Incubate tubes for 5 minutes at RT.

5. Spin the tubes and place them on the magnetic rack for 5 minutes to separate beads from supernatant.

6. Carefully remove and discard the supernatant. Be careful not to disturb the beads containing DNA targets. (CAUTION: DO NOT discard beads).

7. Wash beads by adding 200 µL of 80% ethanol while they are in the magnetic rack. Incubate at RT for 30 seconds, and then carefully remove and discard the supernatant.
8. Repeat Step 7 once.

9. Air dry the beads for 10 minutes while the tubes are on the magnetic rack with the lid open.

10. Add 33 µL of either 10 mM Tris-Hcl pH 8.0 or 0.1X Tris-EDTA, pH 8.0 to elute the DNA. Mix well by pipetting up and down at least 10 times.

11. Spin the tube and place them on the magnetic rack for about 5 minutes to separate beads from supernatant.
12. Carefully transfer the supernatant containing eluted DNA to a new labeled tube. Store DNA libraries at -20ºC until its use.

10. ANNEX III

Script in R – Differential methylation analysis (MEDIPS)

```
#!/usr/bin/env Rscript

library(MEDIPS)
library(BSgenome.Hsapiens.UCSC.hg38)

chroms <- c("chr1","chr2","chr3","chr4","chr5","chr6","chr7","chr8",
"chr9","chr10","chr11","chr12","chr13","chr14","chr15","chr16",
"chr17","chr18","chr19","chr20","chr21","chr22","chrX")

# ENABLE command line arguments
args <- commandArgs(TRUE)

# Check index argumment is given
if(length(args) < 2) {
  print("Requires analysis index and chromosome parameters")
  quit()
}

# Read in data file descriptions
datafiles <- read.delim("datafiles.txt")
# Read in analysis descriptions
analyses <- read.delim("analyses.txt")

idx <- as.integer(args[1])
if(idx < 1 | idx > nrow(analyses)) {
  print("Index out of range")
  quit()
}

chr <- as.integer(args[2])
if(chr < 1 | chr > length(chroms)) {
  print("chrom out of range")
  quit()
}

res_idx <- (idx - 1) * length(chroms) + chr

analysis <- analyses[idx,]
print("Analysis chosen:")
print(analysis)

chrom <- chroms[[chr]]
chrlist <- c(chrom)
print(paste("Chromosome:", chrom))

if(analysis$Sex == "Both") {
  samples <- datafiles[datafiles$CellType == analysis$CellType,]
} else {
```

```
  samples <- datafiles[datafiles$CellType == analysis$CellType & datafiles$Sex == analysis$Sex,]
}
grp1 <- samples[samples$Status == analysis$Group1,]
grp2 <- samples[samples$Status == analysis$Group2,]

print("Group 1 samples")
grp1
print("Group 2 samples")
grp2

grp1_ip_samples <- grp1[grp1$DataType == "IP",]$Sample
grp1_input_samples <- grp1[grp1$DataType == "INPUT",]$Sample
grp2_ip_samples <- grp2[grp2$DataType == "IP",]$Sample
grp2_input_samples <- grp2[grp2$DataType == "INPUT",]$Sample

print(grp1_ip_samples)
print(grp1_input_samples)
print(grp2_ip_samples)
print(grp2_input_samples)


BSgenome="BSgenome.Hsapiens.UCSC.hg38"
uniq=0.001
extend=300
shift=0
ws=analysis$WindowSize

grp1_ip <- vector("list", length(grp1_ip_samples))
type <- paste(analysis$Group1, analysis$CellType, "IP", sep = "_")
i <- 1
for(sample in grp1_ip_samples) {
  grp1_ip[[i]]<-
MEDIPS.createSet(file=paste("align/",type,"_",sample,".bam",sep=""),BSgenome=BSgenome,exte
nd=extend, shift=shift, uniq=uniq,window_size=ws,chr.select=chrlist)
  i <- i + 1
}
grp1_input <- vector("list", length(grp1_input_samples))
type <- paste(analysis$Group1, analysis$CellType, "Input", sep = "_")
i <- 1
for(sample in grp1_input_samples) {
  grp1_input[[i]]<-
MEDIPS.createSet(file=paste("align/",type,"_",sample,".bam",sep=""),BSgenome=BSgenome,exte
nd=extend, shift=shift, uniq=uniq,window_size=ws,chr.select=chrlist)
  i <- i + 1
}

grp2_ip <- vector("list", length(grp2_ip_samples))
type <- paste(analysis$Group2, analysis$CellType, "IP", sep = "_")
i <- 1
for(sample in grp2_ip_samples) {
```

```
  grp2_ip[[i]]<-
MEDIPS.createSet(file=paste("align/",type,"_",sample,".bam",sep=""),BSgenome=BSgenome,exte
nd=extend, shift=shift, uniq=uniq,window_size=ws,chr.select=chrlist)
  i <- i + 1
}
grp2_input <- vector("list", length(grp2_input_samples))
type <- paste(analysis$Group2, analysis$CellType, "Input", sep = "_")
i <- 1
for(sample in grp2_input_samples) {
  grp2_input[[i]]<-
MEDIPS.createSet(file=paste("align/",type,"_",sample,".bam",sep=""),BSgenome=BSgenome,exte
nd=extend, shift=shift, uniq=uniq,window_size=ws,chr.select=chrlist)
  i <- i + 1
}

# Generate coupling set for CpG density normalization
CS = MEDIPS.couplingVector(pattern = "CG", refObj = grp2_ip[[1]])

# Perform differential methylation analysis

grp1_grp2_edgeR <- MEDIPS.meth(MSet1 = grp1_ip, MSet2 = grp2_ip, CSet = CS, ISet1 =
grp1_input, ISet2 = grp2_input, p.adj = "fdr",  diff.method = "edgeR", MeDIP = F, CNV = F,
minRowSum = 10)

file = paste("tmp_results_", res_idx, ".tsv", sep="")
write.table(grp1_grp2_edgeR, file ,sep="\t",quote=F,row.names=F,col.names=T)

# Output significant windows
dm=grp1_grp2_edgeR$edgeR.p.value<=0.05

# Add annotation - can't do this here as compute nodes don't have access to internet
anno.mart.gene <- read.delim(file="annotation.tsv")
reg.ann <- MEDIPS.setAnnotation(regions = grp1_grp2_edgeR[which(dm),], annotation =
anno.mart.gene)

# Output results

if(analysis$Sex == "Both") {
  file <- paste(analysis$Group1, "vs", analysis$Group2,analysis$CellType, ws, chrom,
"dmr_ann.tsv", sep = "_")
} else {
  file <- paste(analysis$Group1, "vs", analysis$Group2, analysis$CellType, analysis$Sex, ws,
chrom, "dmr_ann.tsv", sep = "_")
}
write.table(reg.ann, file ,sep="\t",quote=F,row.names=F,col.names=T)
```

11. ANNEX IV.

PROTOCOL - NanoString nCounter® Elements™ XT

In this procedure, the mRNA of 24 genes was hybridized with a fluorescent barcode (Reporter Tag), a biotinylated universal Capture Tag, and target-specific oligonucleotide probe pairs (Probe A and Probe B) prior to its quantification in the NanoString nCounter® Elements™ XT Analysis System. The kit used for the hybridization reaction was the nCounter® Elements™ TagSets (NanoString, USA).

The complete procedure is comprised of 3 steps:
STEP 1. Preparation of Master Stocks for Probe A and Probe B
STEP 2. Preparation of Working Pools for Probe A and Probe B
STEP 3. Hybridization reaction

[STEP 1] Preparation of Master Stocks for Probe A and Probe B

PROCEDURE

1. Prepare the Probe A Master Stock
    a. In a 1.5 mL microfuge tube, add 5 µL of each Probe A (starting concentration 1 µM) for a total volume of 120 µL.
    b. Add 880 µL of 0.1X Tris-EDTA (pH 8.0) for a final combined volume of 1 mL.
    c. The final concentration of each Probe A in the Probe A Master Stock will be 5 nM.

2. Prepare the Probe B Master Stock
    a. In a 1.5 mL microfuge tube, add 5 µL of each Probe B (starting concentration 5 µM) for a total volume of 120 µL.
    b. Add 880 µL of 0.1X Tris-EDTA (pH 8.0) to a final combined volume of 1 mL.
c. The final concentration of each Probe B in the Probe B Master Stock will be 25 nM.

[STEP 2] Preparation of Working Pools for Probe A and Probe B

PROCEDURE

1. Probe A Working Pool
    a. In a 1.5 mL microcentrifuge tube, add 4 µL of the Master Stock A to 29 µL of 0.1X Tris-EDTA (pH 8.0).
    b. Mix well and spin down the contents to the bottom of the tube.
    c. The final concentration of each Probe A in the Working Pool A will be 0.6 nM.

2. Probe B Working Pool
    a. In a 1.5 mL microcentrifuge tube, add 4 µL of the Master Stock A to 29 µL of 0.1X Tris-EDTA (pH 8.0).
    b. Mix well and spin down the contents to the bottom of the tube.
c. The final concentration of each Probe A in the Working Pool A will be 3 nM.

[STEP 3] Hibridization reaction

In this step, the RNA sample will be hybridized with Probe A, Probe B, and TagSet (Reporter Tag + Universal Capture Tag) to be ready for its quantification.

PROCEDURE

1. Thaw the Hybridization Buffer and the TagSet aliquot at room temperature. Mix by inversion, and briefly spin down.

2. Prepare a partial Master Mix by adding 70 µL of Hybridization Buffer and 7 µL of the Probe A Working Pool directly to the tube containing the TagSet aliquot. Mix by inversion, and spin down the reagents.

3. Add 7 µL of the Probe B Working Pool to the partial master mix to create the complete Master Mix. Mix by inversion, and spin down briefly.

4. Prepare the Hybridization Reaction by adding the following components to a new 1.5 mL tube:

Hybridization reaction	**1 Rxn**
Master Mix	8 µL
RNA sample	7 µL
Total Hybridization Reaction volume	***15 µL***

5. Mix by inversion, and briefly spin the tubes. Procede immediately to the next step.

6. Incubate samples at 67ºC for 24 hours to complete the hybridization.

7. The following day, load samples into the NanoString nCounter® Elements™ XT Analysis System (NanoString, WA) for its quantification.

12. ANNEX V.

PROTOCOL - TaqMan® Advanced miRNA Assay and Taqman® Open Array™ Human Advanced microRNA panel

The complete procedure is comprised of 6 steps:
STEP 1. Poly (A) tailing reaction
STEP 2. Adaptor ligation reaction
STEP 3. Reverse transcription of the mature miRNAs into cDNA
STEP 4. Pre-amplification of the cDNA-converted-miRNA
STEP 5. Quality control of the reverse transcription by real-time PCR
(TaqMan® Advanced miRNA assay)
STEP 6. Loading samples into the TaqMan® Advanced Human miRNA OpenArray™ Panels

[STEP 1] Poly (A) tailing reaction

The TaqMan® Advanced miRNA Assay (Applied Biosystems, Germany) was used to extend the 3' end of mature miRNAs by the addition of a poly(A) tail. Between 5 to 10 ng of total RNA was used as starting material.

PROCEDURE

1. Thaw RNA samples, gently vortex, and centrifuge briefly to spin down the contents and eliminate air bubbles. Meanwhile, in a 1.5 mL microcentrifuge tube prepare the Poly(A) Reaction Mix according to the following table.

Reagents	**1 Rxn**
10X Poly(A) Buffer	0.5 µL
ATP	0.5 µL
Poly(A) Enzyme	0.3 µL
RNase Inhibitor Protein	0.25 µL
RNase-free water	1.45 µL
Total Poly(A) Reaction Mix volume	***3 µL***

2. Vortex the Poly(A) Reaction Mix to thoroughly mix the contents. Centrifuge briefly to spin down the contents and eliminate air bubbles.

3. Add 2 µL of total RNA into a reaction plate, and add 3 µL of the freshly prepared Poly(A) Reaction Mix for a total volume of 5 µL per well.

4. Mix in each well of the reaction plate by pipetting.

5. Seal the reaction plate, vortex briefly to thoroughly mix the contents, and centrifuge to spin down the contents and eliminate air bubbles.

6. Place the reaction plate into a thermal cycler and incubate using the following settings.

Cycle step	Temp	Time	Cycles
Polyadenylation	37°C	45 minutes	1
Stop reaction	65 ºC	10 minutes	1
Hold	4 ºC	∞	1

[STEP 2] Adaptor ligation

The 5' end of mature miRNAs was extended by the ligation of an adaptor using TaqMan® Advanced miRNA Assay (Applied Biosystems, Germany).

PROCEDURE

1. In a 1.5 mL microcentrifuge tube prepare the Ligation Reaction Mix according to the following table.

Reagents	1 Rxn
5X DNA Ligase Buffer	3 µL
50% PEG 8000	4.5 µL
25X Ligation Adaptor	0.6 µL
RNA Ligase	1.5 µL
RNase-free water	0.4 µL
Total Ligation Reaction Mix volume	***10 µL***

2. Vortex the Ligation Reaction Mix to thoroughly mix the contents, then centrifuge briefly to spin down the contents and eliminate air bubbles.

3. Transfer 10 µL of the Ligation Reaction Mix to each well of the reaction plate containing the poly(A) tailing reaction product for a total volume of 15 µL per well.

4. Seal the reaction plate, vortex briefly to thoroughly mix the contents, and centrifuge to spin down the contents and eliminate air bubbles.

5. Place the reaction plate into a thermal cycler and incubate using the following settings.

Cycle step	Temp	Time	Cycles
Ligation	16°C	60 minutes	1
Hold	4 ºC	∞	-

[STEP 3] Reverse transcription of the mature miRNAs into cDNA

PROCEDURE

1. In a 1.5 mL microcentrifuge tube, prepare the RT Reaction Mix according to the following table.

Reagents	1 Rxn
5X RT Buffer	6 µL
dNTP Mix (25 mM each)	1.2 µL
20X Universal RT Primer	1.5 µL
10X RT Enzyme Mix	3 µL
RNase-free water	3.3 µL
Total RT reaction mix volume	***15 µL***

2. Vortex the RT Reaction Mix to thoroughly mix the contents, then centrifuge briefly to spin down the contents and eliminate air bubbles.

3. Transfer 15 µL of the RT Reaction Mix to each well of the reaction plate for a total volume of 30 µL per well.

4. Seal the reaction plate, then vortex briefly to thoroughly mix the contents, and centrifuge to spin down the contents and eliminate air bubbles.

5. Place the reaction plate into a thermal cycler and incubate using the following settings.

Cycle step	Temp	Time	Cycles
Reverse transcription	42 ºC	15 minutes	1
Stop reaction	85 ºC	5 minutes	1
Hold	4 ºC	∞	-

[STEP 4] Pre-amplification of the cDNA-converted-miRNA

PROCEDURE

1. In a 1.5 mL microcentrifuge tube, prepare the miR-Amp Reaction Mix according to the following table.

Reagents	1 Rxn
2X miR-Amp Master Mix	25 µL
20X miR-Amp Primer Mix	2.5 µL
RNase-free water	17.5 µL
Total miR-Amp Reaction Mix volume	***45 µL***

2. Vortex the miR-Amp Reaction Mix to thoroughly mix the contents, then centrifuge briefly to spin down the contents and eliminate air bubbles.

3. Tranfer 45 µL of the miR-Amp Reaction Mix to a new reaction plate.
4. Add 5 µL of the RT reaction product (from STEP3) for a total volume of 50 µL per well.

5. Seal the reaction plate, then vortex briefly to thoroughly mix the contents, and centrifuge to spin down the contents and eliminate air bubbles.

6. Place the new reaction plate into a thermal cycler, and incubate using the following settings.

Cycle step	Temp	Time	Cycles
Enzyme activation	95 ºC	5 minutes	1
Denature	95 ºC	3 seconds	18
Anneal/Extend	60 ºC	30 seconds	
Stop reaction	99 ºC	10 minutes	1
Hold	4 ºC	∞	1

7. Store samples at -80ºC until its usage.

[STEP 5] Quality control of the reverse transcription by real-time PCR

Before loading the pre-amplified cDNA-converted-miRNA samples into the TaqMan Advanced Human miRNA Open Array™ panel, a real-time PCR was performed to verify if the universal retrotranscription was successful in all samples. For that purpose, the miR-24, miR-146a and miR-150 assays (Applied Biosystem, Germany) were used in a PCR procedure.

PROCEDURE

1. Thaw samples on ice, vortex gently, and centrifuge briefly to spin down the contents and eliminate air bubbles.

2. Prepare a 1:10 dilution of the preamplified cDNA templates from STEP 4 with nuclease-free water.

3. In a 1.5-mL microcentrifuge tube, prepare the PCR Reaction Mix according to the following table.

Reagents	**1 Rxn**
Taqman Fast Advanced Master Mix (2X)	5 µL
Taqman Advanced miRNA assay (20X) *(miR-24, miR-146a or miR-150)*	0.5 µL
RNase-free water	2 µL
Total PCR Reaction Mix volume	***7.5 µL***
Diluted cDNA (1:10)	*2.5 µL*
Total	***10 µL***

4. Transfer 7.5 µL of the PCR Reaction Mix to each well of the PCR reaction plate, and add 2.5 µL of the diluted cDNA template (1:10) to each reaction well of the plate for a total volume of 10 µL.

5. Seal the PCR reaction plate, vortex briefly to thoroughly mix the contents, and centrifuge to spin down the contents and eliminate air bubbles.

6. Place the PCR reaction plate into the QuantStudio™ 7 instrument (Applied biosystem, Germany), with the following settings for the real-time PCR reaction.

Cycle step	Temp	Time	Cycles
Enzyme activation	95°C	20 seconds	1
Denature	95°C	1 second	40
Anneal / Extend	60°C	20 seconds	

[STEP 6] Loading samples into the TaqMan® Advanced Human miRNA OpenArray™ plates

Once the cDNA-converted-miRNA templates successfully pass the quality control in the real-time PCR step (STEP 5), samples were prepared to be loaded into the TaqMan® Human miRNA Open Array™ plates.

PROCEDURE

1. Remove the Taqman® OpenArray™ plates from the freezer to come to room temperature (~15 minutes).

2. Meanwhile, prepare a 1:20 dilution of the cDNA template from STEP 4 in 0.1X TE buffer (pH 8.0).

3. In a 96-well plate, mix the diluted cDNA template with the TaqMan® OpenArray™ RealTime PCR Master Mix as follows.

Reagents	1 Rxn
Taqman® Open Array™ Real-Time PCR Master Mix	2.5 µL
Diluted cDNA template	2.5 µL
Total Reaction Mix volume	***5 µL***

4. Add 5 µL of the Reaction Mix to each well of the OpenArray™ 384-well Sample Plate.

5. Seal the OpenArray™ 384-well Sample Plate with an aluminum foil seal, and then centrifuge at 1000 rpm for 1 minute.

6. Load the OpenArray™ 384-well Sample Plate into the OpenArray® AccuFill™ System (Thermo Fisher, USA). This system allows an automatized and reproducible way of transferring small volumes of sample from the OpenArray™ 384-well Sample Plate into the TaqMan® OpenArray™ Human Advanced microRNA plates.

7. Once all samples are loaded, fill the TaqMan® OpenArray™ Human Advanced microRNA plates with immersion fluid with a syringe and seal within 90 seconds to prevent evaporation.

8. Load the TaqMan® OpenArray™ Human Advanced microRNA plates into the QuantStudio™ 12K Flex Real-Time PCR System (Applied Biosystem, Germany), selecting a maximum of 40 cycles of amplification.

13. ANNEX VI

Detailed demographic, clinical, radiological, and experimental data for each participant of the study

The following table describes in detailed demographic, clinical, and radiological data for each participant of the study. The columns MeDIP-seq, NanoString, and Taqman® OpenArray™ indicates whether the DNA/RNA isolated from Bmem cells (B) or Treg cells (T) from the corresponding participant was used in the experiment. The (-) mark indicates 'not available/not applicable'. *Bmem: memory B; EDSS: expanded disability status scale; Gd+: gadolinium-enhanced; RRMS: relapsing-remitting multiple sclerosis; SPMS: secondary-progressive multiple sclerosis; T: regulatory T.*

n	Group	Gender	Age (years)	EDSS	T2 lesions (n)	Gd+ lesions (n)	Black holes (yes/no)	MeDIP-seq (DNA)	NanoString (RNA)	Taqman® OpenArray™ (RNA)
1	RRMS	Female	38	1.5	15	0	no	B	B	B, T
2	RRMS	Female	50	1.5	43	2	no	B, T	-	B, T
3	RRMS	Female	33	2	14	3	yes	B	T	B, T
4	RRMS	Female	35	1.5	15	1	yes	B, T	B, T	B, T
5	RRMS	Female	41	2	12	0	no	B, T	B, T	B
6	RRMS	Female	43	1.5	20	0	no	B, T	T	B
7	RRMS	Male	46	2	9	4	no	B, T	B	B, T
8	RRMS	Male	53	1.5	13	1	no	B, T	B, T	B
9	RRMS	Male	24	1.5	18	1	no	B, T	B, T	B
10	SPMS	Male	70	6	-	-	-	B, T	-	B, T
11	SPMS	Female	69	6.5	-	-	-	B, T	-	B, T
12	SPMS	Male	67	6	-	-	-	B	-	B
13	SPMS	Male	70	6.5	-	-	-	B	-	B
14	SPMS	Female	67	8	-	-	-	B	-	B
15	SPMS	Female	74	6	-	-	-	B, T	-	B, T
16	SPMS	Female	65	4	-	-	-	B, T	-	B
17	SPMS	Female	73	7	-	-	-	B	-	B
18	SPMS	Female	59	7	-	-	-	B	-	B
19	SPMS	Female	65	6.5	-	-	-	B, T	-	B
20	Control	Female	35	-	-	-	-	B, T	T	B
21	Control	Female	38	-	-	-	-	B, T	T	B
22	Control	Female	37	-	-	-	-	B	B	B, T
23	Control	Female	37	-	-	-	-	B, T	B	B, T
24	Control	Female	46	-	-	-	-	B, T	T	B, T
25	Control	Female	53	-	-	-	-	B	B	B, T
26	Control	Female	41	-	-	-	-	B	T	B
27	Control	Male	47	-	-	-	-	B, T	B	B, T
28	Control	Male	50	-	-	-	-	B, T	B, T	B
29	Control	Male	25	-	-	-	-	B, T	B, T	B

14. ANNEX VII

List of studied mature miRNAs using the Taqman® OpenArray™ Human advanced microRNA panels

Memory B cells

let-7a-5p, let-7b-3p, let-7b-5p, let-7c-5p, let-7e-5p, let-7f-2-3p, let-7g-5p, let-7i-5p, miR-1-3p, miR-100-3p, miR-100-5p, miR-101-3p, miR-103a-2-5p, miR-103a-3p, miR-107, miR-122-5p, miR-124-3p, miR-1249-3p, miR-125b-5p, miR-126-5p, miR-1260a, miR-1264, miR-128-3p, miR-129-2-3p, miR-1298-5p, miR-130a-3p, miR-132-3p, miR-133a-3p, miR-133b, miR-135a-5p, miR-137, miR-143-3p, miR-145-3p, miR-145-5p, miR-146a-5p, miR-146b-5p, miR-148a-3p, miR-148b-3p, miR-150-5p, miR-151a-3p, miR-151a-5p, miR-153-3p, miR-155-5p, miR-15a-5p, miR-17-5p, miR-181a-5p, miR-181b-5p, miR-181c-5p, miR-183-3p, miR-185-5p, miR-186-5p, miR-190a-5p, miR-1911-5p, miR-193a-5p, miR-194-5p, miR-196a-5p, miR-199a-3p ,miR-199a-5p, miR-200c-3p, miR-203a-3p, miR-204-5p, miR-205-5p, miR-206, miR-21-5p, miR-210-3p, miR-211-5p, miR-216a-5p, miR-218-5p, miR-219a-5p, miR-22-3p, miR-221-3p, miR-222-3p, miR-223-3p, miR-23a-3p, miR-23b-3p, miR-26a-5p, miR-26b-5p, miR-28-5p, miR-29a-3p, miR-29c-5p, miR-30a-3p, miR-30c-1-3p, miR-30c-2-3p, miR-30d-5p, miR-30e-3p, miR-31-5p, miR-32-5p, miR-320a, miR-320b, miR-325, miR-326, miR-328-3p, miR-335-5p, miR-338-3p, miR-339-5p, miR-342-3p, miR-34a-3p, miR-34a-5p, miR-361-3p, miR-361-5p, miR-363-3p, miR-373-3p, miR-374b-5p, miR-375, miR-376c-3p, miR-378a-3p, miR-378a-5p, miR-383-5p, miR-411-5p, miR-424-5p, miR-448, miR-449a, miR-450b-3p, miR-450b-5p, miR-452-3p, miR-452-5p, miR-454-3p, miR-455-3p, miR-483-3p, miR-483-5p, miR-486-5p, miR-487a-3p, miR-489-3p, miR-490-3p, miR-497-5p, miR-502-3p, miR-505-3p, miR-513a-5p, miR-515-3p, miR-516b-5p, miR-518e-3p, miR-520h, miR-523-3p, miR-532-3p, miR-532-5p, miR-548d-5p, miR-548e-3p, miR-548k, miR-548n, miR-551a, miR-570-3p, miR-576-3p, miR-583, miR-593-5p, miR-615-3p, miR-628-3p, miR-633, miR-642a-5p, miR-645, miR-652-3p, miR-653-3p, miR-660-5p, miR-664a-3p, miR-770-5p, miR-876-3p, miR-885-5p, miR-9-3p, miR-9-5p, miR-92a-3p, miR-92b-3p, miR-93-5p, miR-937-3p, miR-939-5p, miR-99a-3p, miR-99b-5p.

Regulatory T cells

let-7a-5p, let-7b-3p, let-7b-5p, let-7c-5p, let-7e-5p, let-7f-2-3p, let-7f-5p, let-7g-5p, let-7i-5p, miR-1-3p, miR-100-3p, miR-100-5p, miR-101-3p, miR-103a-2-5p, miR-103a-3p, miR-106b-3p, miR-106b-5p, miR-107, miR-10a-5p, miR-10b-5p, miR-122-5p, miR-124-3p, miR-1249-3p, miR-125a-3p, miR-125a-5p, miR-125b-5p, miR-126-5p, miR-1260a, miR-1264, miR-127-3p, miR-128-3p, miR-129-2-3p, miR-1298-5p, miR-130a-3p, miR-132-3p, miR-133a-3p, miR-133b, miR-135a-5p, miR-137, miR-143-3p, miR-145-3p, miR-145-5p, miR-146a-5p, miR-146b-5p, miR-148a-3p, miR-148b-3p, miR-150-5p, miR-151a-3p, miR-151a-5p, miR-153-3p, miR-155-5p, miR-15a-5p, miR-15b-5p, miR-17-5p, miR-181a-5p, miR-181b-5p, miR-181c-5p, miR-183-3p, miR-185-5p, miR-186-5p, miR-190a-5p, miR-1911-5p, miR-193a-5p, miR-194-5p, miR-195-5p, miR-196a-5p, miR-199a-3p, miR-199a-5p, miR-200c-3p, miR-203a-3p, miR-204-5p, miR-205-5p, miR-206, miR-21-5p, miR-210-3p, miR-211-5p, miR-216a-5p, miR-218-5p, miR-219a-5p, miR-22-3p, miR-221-3p, miR-222-3p, miR-223-3p, miR-23a-3p, miR-23b-3p, miR-25-3p, miR-26a-5p, miR-26b-5p, miR-27b-3p, miR-27b-5p, miR-28-5p, miR-29a-3p, miR-29c-5p, miR-30a-3p, miR-30c-1-3p, miR-30c-2-3p, miR-30d-5p, miR-30e-3p, miR-31-5p, miR-32-5p, miR-320a, miR-320b, miR-323a-3p, miR-325, miR-326, miR-328-3p, miR-335-5p, miR-338-3p, miR-339-5p, miR-342-3p, miR-34a-3p, miR-34a-5p, miR-361-3p, miR-361-5p, miR-363-3p, miR-369-3p, miR-369-5p, miR-373-3p, miR-374b-5p, miR-375, miR-378a-3p, miR-378a-5p, miR-383-5p, miR-410-3p, miR-411-5p, miR-412-3p, miR-424-5p, miR-448, miR-450b-3p, miR-450b-5p, miR-452-3p, miR-452-5p, miR-454-3p, miR-455-3p, miR-483-3p, miR-483-5p, miR-486-5p, miR-487a-3p, miR-489-3p, miR-490-3p, miR-497-5p, miR-502-3p, miR-505-3p, miR-505-3p, miR-513a-5p, miR-515-3p, miR-516b-5p, miR-518d-3p, miR-518e-3p, miR-520h, miR-548d-5p, miR-548e-3p, miR-548k, miR-548n, miR-551a, miR-570-3p, miR-576-3p, miR-583, miR-593-5p, miR-615-3p, miR-628-3p, miR-633, miR-642a-5p, miR-645, miR-652-3p, miR-653-3p, miR-656-3p, miR-660-5p, miR-664a-3p, miR-770-5p, miR-876-3p, miR-885-5p, miR-9-3p, miR-9-5p, miR-92a-3p, miR-92b-3p, miR-93-5p, miR-937-3p, miR-939-5p, miR-99a-3p, miR-99b-5p.

15. ANNEX VIII.

Association analysis between Cq_conf, Amp_Score and Cq values in memory B cells.

Scatter plot and correlation coefficient between Cq_conf, Amp_Score and Cq values in memory B cells for all detectable miRNAs (n=86). (**a).** Raw data before adjustment. (**b).** Data points adjusted for Amp_Score ≥ 0.8; Cq_conf ≥ 0.5 and Cq value between 15-35. *Amp_Score: amplification score; Bmem: memory B; Cq_conf: Cq confidence; Cq: quantification cycle; rho=Spearman's test rho value.*

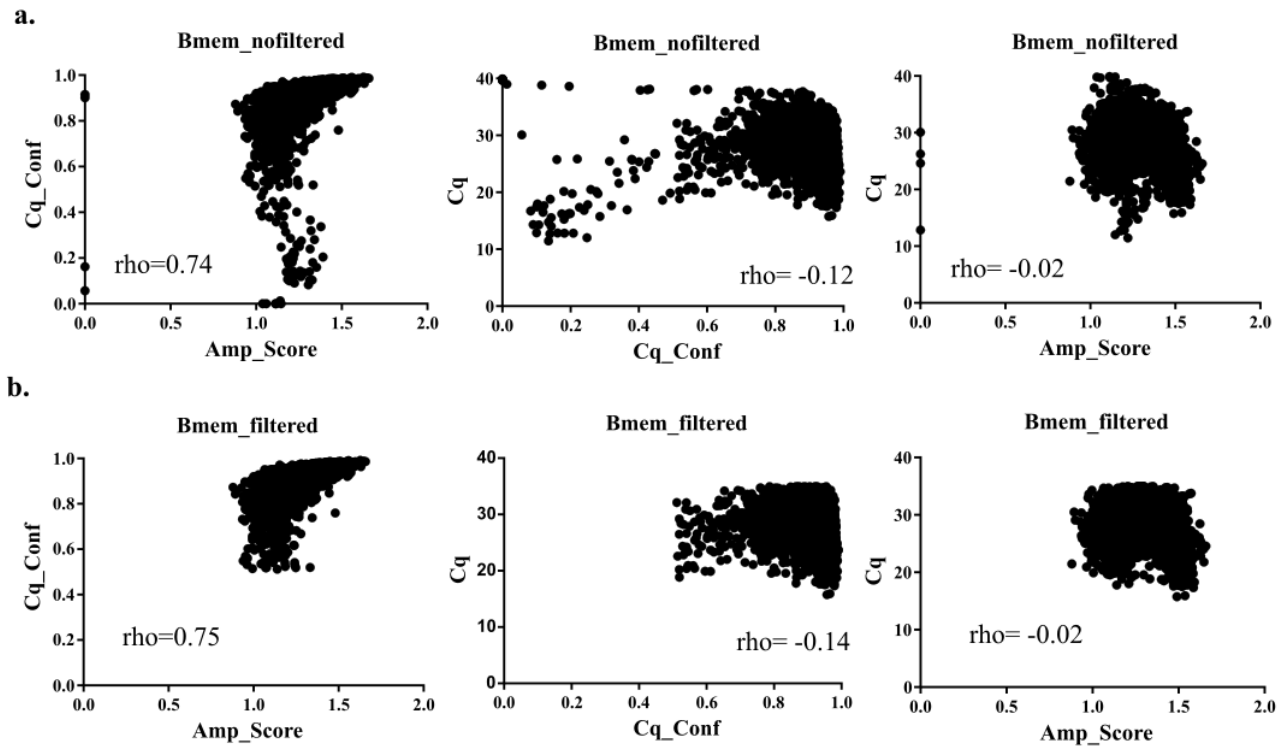

16. ANNEX IX

Association analysis between Cq_conf, Amp_Score and Cq values in regulatory T cells.

Scatter plot and correlation coefficient between Cq_conf, Amp_Score and Cq values in regulatory T cells for all detectable miRNAs (n=85). (a). Raw data before adjustment. (**b).** Data points adjusted for Amp_Score ≥ 0.8; Cq_conf ≥ 0.5 and Cq value between 15-35. *Amp_Score: amplification score; Cq_conf: Cq confidence; Cq: quantification cycle; rho=Spearman's test rho value; Treg: regulatory T.*

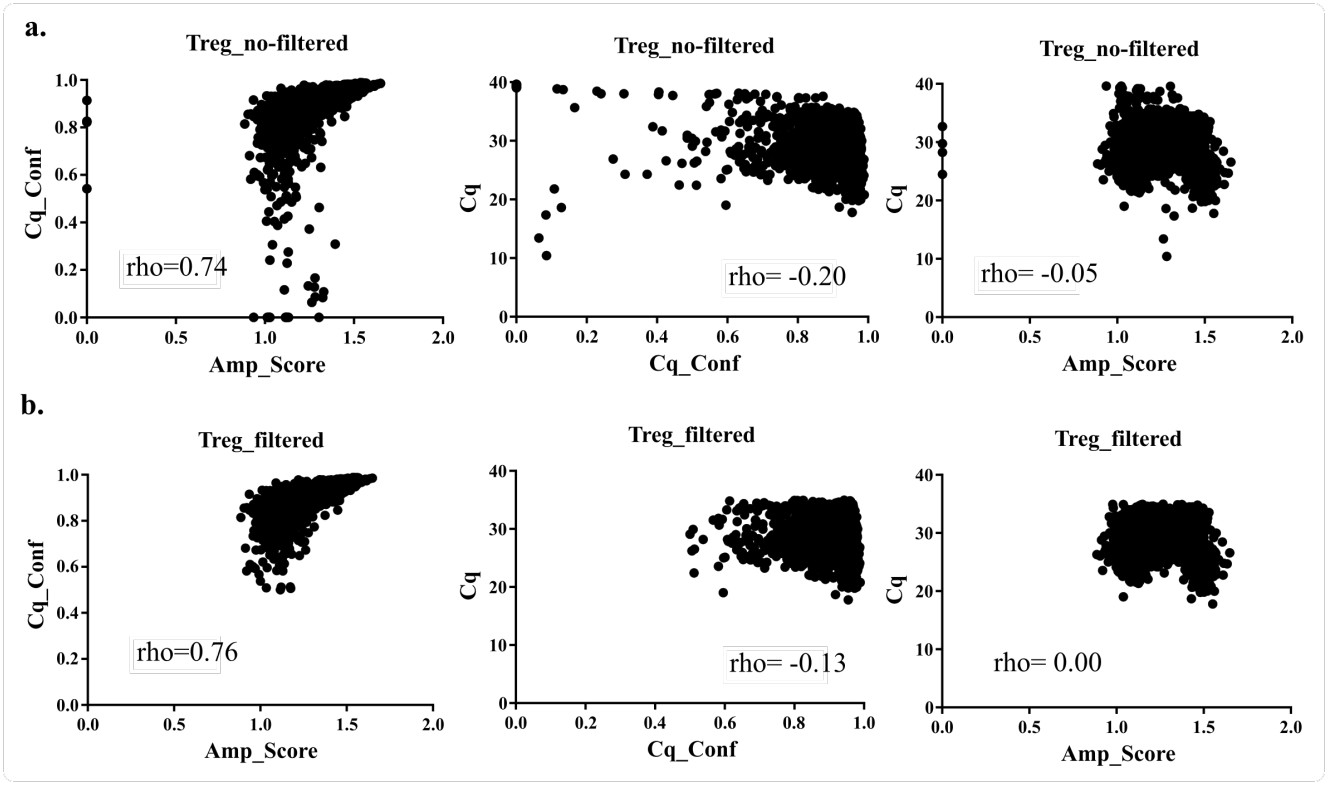

17. ANNEX X

Candidate miRNAs showing differential expression between the groups of study in memory B cells_second replicate.

Figure. Relative expression of the second replicate for miR-181c-5p, miR-150-5p, miR-193a-5p, miR-26a-5p, miR-29a-3p, miR-30d-5p and miR-92b-3p in memory B cells isolated from controls, RRMS and SPMS patients. The line indicates the median. *RRMS: relapsing-remitting Multiple Sclerosis; SPMS: secondary-progressive Multiple Sclerosis.*

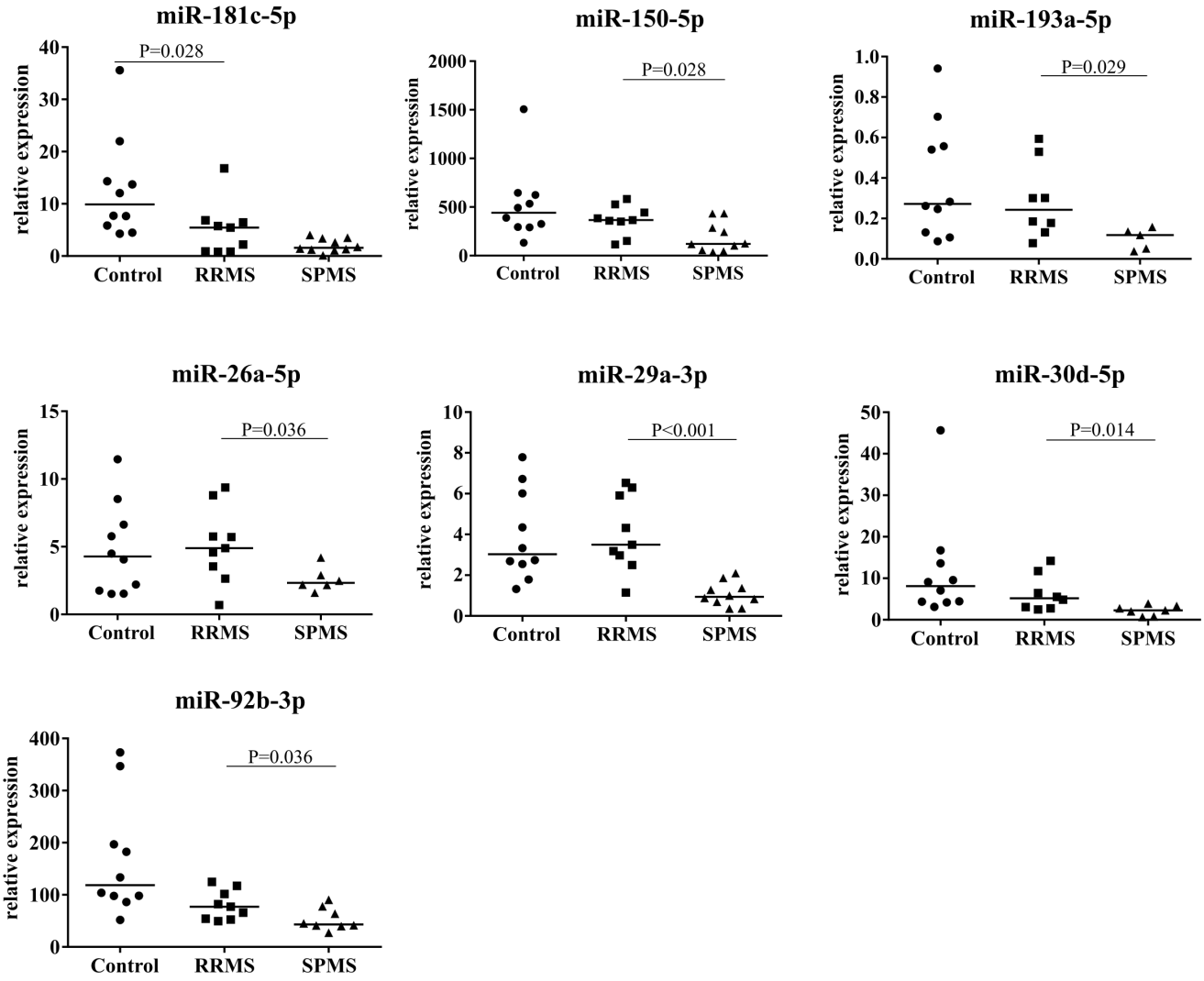

Table. Relative expression of candidate miRNAs showing differences between the groups of study in memory B cells. **(a).** Relative expression of miR-181c-5p in memory B cells derived from controls and RRMS patients. **(b).** Relative expression of miR-150-5p, miR-193a-5p, miR-26a-5p, miR-29a-3p, miR-30d-5p and miR-92b-3p in memory B cells of RRMS and SPMS patients. *IQR: interquartile range; Q1-Q3: first quartile-third quartile; RE: relative expression; RRMS: relapsing-remitting Multiple Sclerosis; SPMS: secondary-progressive Multiple Sclerosis.*

	Control		**RRMS**		***p-value***
	Median RE	**IQR (Q1-Q3)**	**Median RE**	**IQR (Q1-Q3)**	
miR-181c-5p	9.89	5.85 – 14.32	5.45	0.89 – 6.44	*0.028*

	RRMS		**SPMS**		***p-value***
	Median RE	**IQR (Q1-Q3)**	**Median RE**	**IQR (Q1-Q3)**	
miR-150-5p	365.38	350.12 – 443. 34	121.09	56.19 – 286.28	*0.028*
miR-193a-3p	0.24	0.154 – 0.41	0.12	0.05 – 0.13	*0.029*
miR-26a-5p	4.89	3.54 – 5.76	2.33	2.17 – 2.89	*0.036*
miR-29a-3p	3.5	2.96 – 5.91	0.93	0.69 – 1.36	*<0.001*
miR-30d-5p	5.17	2.92 – 9.08	2.26	1.41 – 3.04	*0.014*
miR-92b-3p	77.04	54.02 – 101.51	43.24	40.43 – 70.85	*0.036*

18. ANNEX XI

Correlation between the relative expression of miR-181c-5p in memory B cells and the number of Gd+ lesions in RRMS patients_second replicate.

Scatter plot and correlation coefficient between the relative expression of miR-181c-5p in memory B cells and the number of Gd+ lesions in RRMS patients for the second miRNA replicate. *Gd+: gadolinium-enhanced; rho: Spearman's test rho value; RRMS: relapsing-remitting multiple sclerosis.*

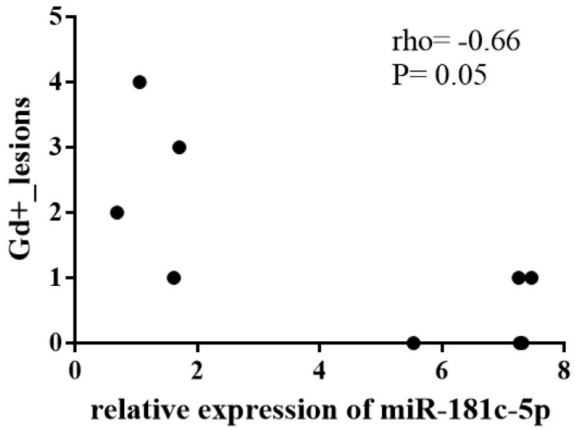

19. ANNEX XII

Association analysis between relative expression el miRNAs and the normalized methylation values in DMRs_second replicate. Scatter plot and correlation coefficient between the relative expression of miRNAs and the normalized methylation values (rpkm) for the second miRNA replicate. *rho: Spearman's test rho value; rpkm: reads per kilobase million.*

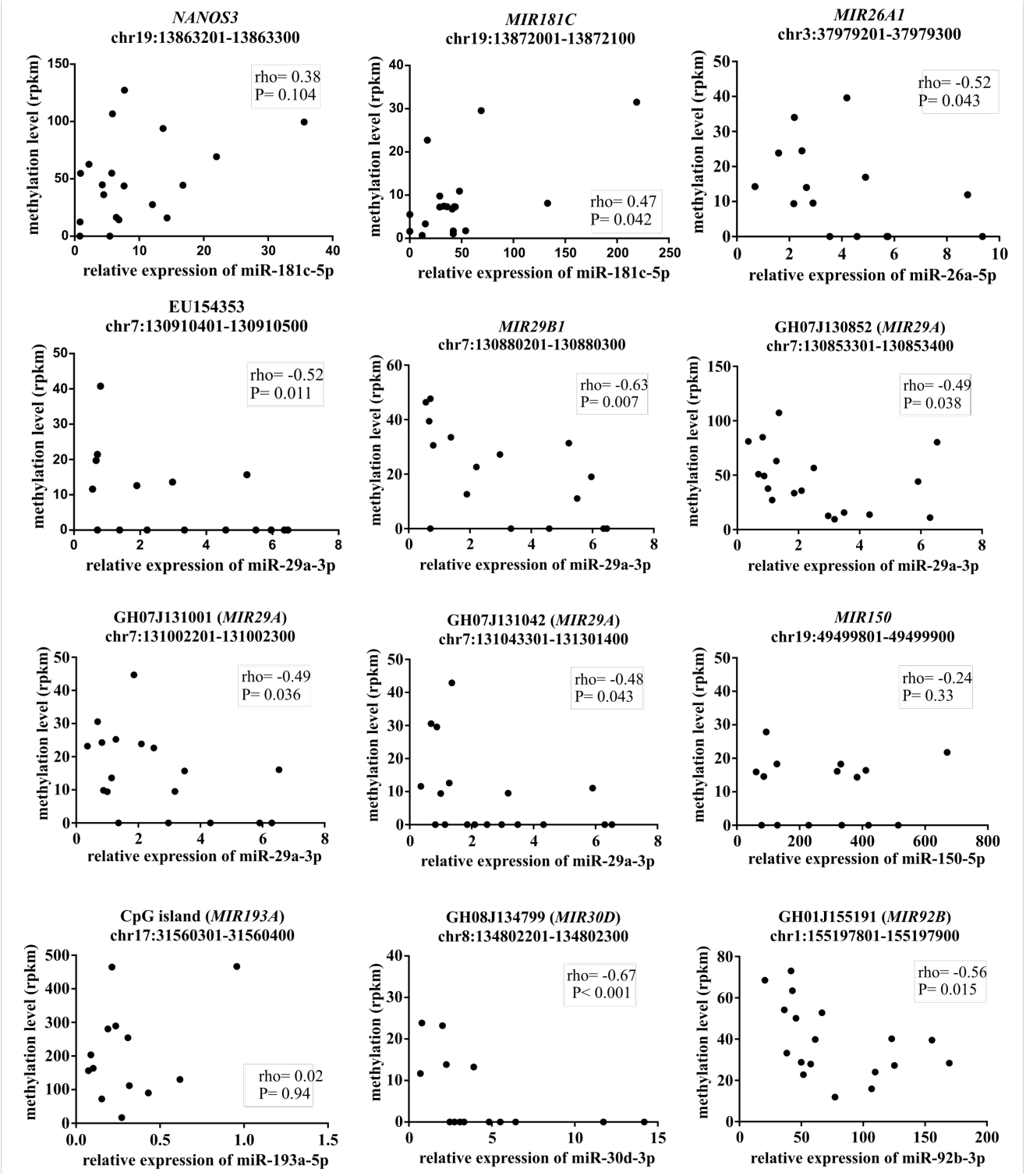

20. ANNEX XIII

List of miRNA targets common for miRDB and TargetScan databases.

miR-181c-5p
ADAM11, ADRA1A, AGO4, AKIRIN1, ATMIN, ATP1B1, ATXN7, BAG4, BEND3, BLOC1S6, C14orf28, CDH8, CREB1, DNAJC13, E2F7, EYA3, FAM160A1, FIGN, FNDC3B, GHITM, GOLGA1, GRM5, HCN2, IL1A, KAT2B, KIAA1549L, KIF3B, LIN28A, LRRC8D, OSBPL8, PHF3, PLCL2, POU2F1, PTPN4, RASSF1, RIMKLB, RLF, RPS6KB1, SIK3, SIPA1L2, SPP1, SSX2IP, ZDHHC3, ZDHHC7, ZFP1

miR-150-5p
ADAM19, ADIPOR2, AIFM2, BASP1, BSN, C6orf120, CAMK2G, CBL, CERS3, CHD2, CMTM6, CPD, DCAF6, DENND4A, ELOVL3, ENSA, EPHB2, FBXW11, FTO, GABRG2, GDI1, GGNBP2, HILPDA, HNRNPH3, HSP90B1, IPO9, KCNIP1, LRRC58, MBD6, MBTD1, MDM4, MTCH2, MYB, NDC1, NKX2-4, NR1D2, PAPPA, PAX5, PDE7A, PIK3AP1, PKP4, PLP2, POM121C, PRKAR1A, PRKCA, PTGFR, PURA, RAD23B, RC3H1, RORB, SLC30A5, SP1, SZRD1, TADA1, TSPYL5, UST, VPS53,WTAP, ZBTB4, ZEB1, ZFP91

miR-193a-5p
ACVR1, C18orf25, CEP57, DNTTIP2, DSCAML1, NETO2, SLC30A5, SLC4A10, UBE2D2

miR-26a-5p
ADAMTS19, ALS2, ANKS1B, APCDD1, ATPAF1, ATXN7, B4GALT4, BAG4, BBX, BEND4, BHLHE40, BLOC1S2, C16orf70, CCND2, CDK2AP1, CDK8, CELF2, CELSR1, CEP350, CHD1, CNTNAP3B, COL10A1, CPPED1, CREBRF, CREBZF, DAPK1, DLG5, EIF5, EP400, EPC1, ERC2, FAM172A, FBXO28, INHBB, KCNQ4, LSM11, LTBP1, MAP2, MAT2A, MDN1, MMP16, MTM1, NACC2, NEK1, NIPA1, PALM3, PEX13, PHTF2, PPP1R3D, PPP3R1, PRR5L, PTPRD, RB1, RHD, RNF6, SACS, SFPQ, SH3PXD2A, SHANK2, SLC16A6, SLC1A1, SLC22A23, SMAD1, SOCS7, SRSF6, STRADB, TANC2, TMCC1, TMEM86A, TNNT1, TNRC6B, TNRC6C, TRANK1, UBE2G1, UBE2K, USP25, USP3, USP37, WNK3, ZCCHC24, ZFHX4, ZNF469

miR-29a-3p
ABCE1, ADAMTS10, ADAMTS17, AKAP13, AKAP5, AKT3, AMER1, ANKRD13B, ANKRD13C, ANTXR2, ARHGEF10, ARPP19, ARVCF, ASAP2, ATAD2B, ATP1B4, ATP2B4, ATRN, B3GNT5, BACH2, BAK1, BTG2, C5orf15, CCNJ, CCSAP, CCSER2, CDC42, CDC42BPA, CDK6, CEP97, CHSY1, CNR1, COL11A1, COL19A1, COL1A1, COL1A2, COL25A1, COL4A2, COL4A4, COL5A1, COL5A2, COL5A3, COL6A3, COL9A1, CPEB3, CPS1, CPSF7, CRISPLD1, CSRNP2, CUEDC1, DAAM1, DAAM2, DCUN1D4, DCX, DDX3X, DENND6A, DGKD, DGKH, DICER1, DIO2, DLG2, DOLPP1, DPYSL3, DTWD2, DTX4, EFNA5, EIF3J, EIF4E2, ELF2, ELMSAN1, ELOVL4, EML4, EML6, ENHO, ENPP2, EOMES, ERCC6, ERLIN2, ETV6, FAM13B, FAM167A, FAM168B, FAM57B, FBN1, FBXW7, FEM1B, FERMT2, FGD4, FOXJ2, FRAT2, FREM2, FSTL1, GAB1, GID8, GNB4, GPCPD1, GPR37, GRIP1, GXYLT2, HAPLN3, HIF3A, HRK, ICOS, IFFO1, IFI30, IGF1, IL1RAP, ING2, IREB2, ISG20L2, JARID2, JAZF1, JMY, KCTD20, KCTD5, KDELC1, KDM4B, KIAA0895, KIAA1549, KIF26A, KIF26B, KLF4, KLHL28, KNOP1, LAMA2, LASP1, LDLRAD3, LIF, LIN7A, LOXL2, LOXL4, LPL, LSM11, LYSMD1, MAP4K4, MAPKBP1, MAPRE1, MAPRE2, MARCH1, MBTD1, MCL1, METAP2, MEX3B, MFAP3, MGA, MLXIP, MOB1A, MORF4L1, MTMR4, MYBL2, MYCN, N4BP2L1, NAPB, NASP, NAV3, NCKAP5, NFAT5, NFIA, NLRX1, NOTCH2, NPAS3, NSD1, NUP160, OSTC, OTUD4, PALM, PAN2, PAPOLG, PARG, PCDHA1, PCDHA10, PCDHA11, PCDHA12, PCDHA13, PCDHA2, PCDHA3, PCDHA4, PCDHA5, PCDHA6, PCDHA7, PCDHA8, PCDHA9, PCDHAC1, PCDHAC2, PCGF3, PDIK1L, PGAP1, PGAP2, PIK3R1, PLP1, PMP22, PPM1E, PPP1R15B, PRKAB2, PRKG1, PRKRA, PRPF40A, PRR14L, PTBP3, PTEN, PTPRK, PXDN, RAB30, RAP1A, RAP1GDS1, RAPGEFL1, RBAK, REL, REST, REV3L, RLF, RMND5A, RNF138, RNF19A, RNF39, SAMD4A, SERINC5, SESTD1, SETDB1, SGK1, SGMS2, SH3BP5L, SH3GLB1, SH3PXD2B, SHPRH, SIDT1, SIDT2, SIRT1, SLC16A14, SLC30A3, SLC5A8, SLC6A14, SLC7A6, SMIM17, SMPD3, SMS, SMTNL2, SNX24, SP1, SPARC, STMN2, STRN4, STX16, STX17, TAF5, TCF4, TDG, TET1, TET2, TET3, TFEC, TIMM8B, TLL1, TMEM178B, TMEM183A, TMEM236, TMEM65, TMOD3, TMTC3, TNFAIP3, TNFRSF1A, TNRC18, TRAF4, TRIB2, TRIM63, TTC9, TUBB2A, UBFD1, USP34, USP37, USP6NL, VASH1, VEGFA, WBP1L, WDFY1, XKR4, XKR7, YBX3, ZBTB10, ZBTB20, ZBTB34, ZDHHC21, ZFX, ZMIZ1, ZNF282, ZNF469, ZNF512B, ZNF704

miR-30d-3p
BRWD3, DLG5, KCTD5, KLF9, MCF2L, SBF1

miR-92b-3p
N/A